Dissecting the cellular effects of antimicrobial agents: The spatio-temporal impact of peptidoglycan synthesis inhibiting antibiotics in *Staphylococcus aureus* and mechanism of action elucidation of epilancin A37

Dissertation

zur

Erlangung des Doktorgrades (Dr. rer. nat.)

der

Mathematisch-Naturwissenschaftlichen Fakultät

der

Rheinischen Friedrich-Wilhelms-Universität Bonn

vorgelegt von

Jan-Samuel Puls

aus

Oberhausen

Bonn, März 2024

Angefertigt mit Genehmigung der Mathematisch-Naturwissenschaftlichen Fakultät
der Rheinischen Friedrich-Wilhelms-Universität Bonn

Gutachterin/Betreuerin: Prof. Dr. Tanja Schneider
Gutachterin: Priv.-Doz. Dr. Christiane Dahl

Tag der Promotion: 25.06.2024
Erscheinungsjahr: 2024

Acknowledgements

First and foremost, I want to thank Tanja Schneider for giving me the opportunity to research at the Institute of Pharmaceutical Microbiology. I highly value the degree of scientific freedom that I was able to enjoy there and the abundance of possibilities her management provided for me to pursue my ideas. I am further thankful for her being the 1st supervisor of this thesis. In this regard, I express my appreciation of Christiane Dahl, Lukas Schreiber and Ulrich Kubitscheck for agreeing to be part of my thesis committee.

I am especially thankful for all members and students of the Grein lab for their exceptional companionship and support throughout the years. Particularly, I appreciate Benjamin Winnerling for his amazing work on purification and characterization of A37 and his impressive courteousness throughout the years on this excitingly tedious project and beyond. I also thank Thomas Fließwasser for his energizing spirit and contagious fascination for biology, that never fails to motivate. Furthermore, I thank all the members of the Institute of Pharmaceutical Microbiology for all the help, inspiration, and joviality I experienced throughout the years. I would feel honored to know that I was able to return that sense of companionship, be it to the smallest extent. Especially, I want to thank Kevin Ludwig for the fruitful and productive cooperative work on DCAP and Lisa Fritz for her complementary work on the Lcp inhibition by moenomycin. I further appreciate Melina Arts for the cheerful camaraderie in tackling the technical and emotional challenges that accompanied our work in TRR261. Special thanks go to Stefania de Benedetti and Isabel Bodenstein for their heartful and motivated commitment to uphold a productive lab environment throughout all daily struggles. I thank the Kubitscheck lab for their amazing scientific work throughout the years on challenging and fascinating projects. I thank Ulrich Kubitscheck for sharing his calm intellectual brightness on countless occasions. Special thanks go to Dominik Brajtenbach, with whom I had the honor to work on the cellular impact of antibiotics on the cell division of *S. aureus* in close collaboration. I thank Jan-Peter Siebrasse and Annika Marie Krüger for all their constructive input in innumerable meetings. Working with all of you was an intellectual delight. Furthermore, I want to thank the Heilbronner lab for the collaborative work on IsdF, especially Lea Adolf, who did great work on characterization of the enzyme and provided the strains needed for my contribution to this project. Furthermore, I like to thank Jeffrey John Power for his diligent work on A37. In this regard, I also thank Debnath Ghosal and Matthew Johnson for their cryo electron tomography work on A37 treated cells. Thanks to all of you for the reliably accurate scientific work on highest standards. I thank all colleagues and collaborators for providing useful tools, compounds, and strains. I highly appreciate the students that agreed to be supervised in the lab by me. Their trust and willingness to learn was great inspiration and I certainly learned a lot from teaching them. Thank you, Gina Marke, Aynur Mancoglu, Yen Ly, Kai Wallerang and Marc Gregor Mohr.

Ultimately, my deepest gratitude is reserved for Fabian Grein for his exceptional guidance and supervision, which is driven by an uplifting sincerity towards science and people that is worthy of aspiration.

List of publications

Parts of this work have already been published and are here reproduced with permission.

Lead author(s) and the **author of this work** are highlighted.

Peer-reviewed publications:

Puls, Jan-Samuel; Winnerling, Benjamin; Power, Jeffrey John; Krüger, Annika Marie; Brajtenbach, Dominik; Johnson, Matthew; Bilici, Kevser; Camus, Laura; Fließwasser, Thomas; Schneider, Tanja; Sahl, Hans-Georg; Ghosal, Debnath; Kubitscheck, Ulrich; Heilbronner, Simon; Grein, Fabian (2024): *Staphylococcus epidermidis* bacteriocin A37 kills natural competitors with a unique mechanism of action. *The ISME Journal,* wrae044, DOI: https://doi.org/10.1093/ismejo/wrae044

Puls, Jan-Samuel; Brajtenbach, Dominik; Schneider, Tanja; Kubitscheck, Ulrich; Grein, Fabian (2023): Inhibition of peptidoglycan synthesis is sufficient for total arrest of staphylococcal cell division. *Science Advances,* 9 (12), eade9023, DOI: https://doi.org/10.1126/sciadv.ade9023

Deisinger, Julia Patricia; Arts, Melina; Kotsogianni, Ioli; **Puls, Jan-Samuel**; Grein, Fabian; Ortiz-López, Francisco Javier; Martin, Nathaniel I.; Müller, Anna; Genilloud, Olga; Schneider, Tanja (2023): Dual targeting of the class V lanthipeptide antibiotic cacaoidin. *iScience*, 26 (4), 106394, DOI: https://doi.org/10.1016/j.isci.2023.106394

Adolf, Lea Antje; Müller-Jochim, Angelika; Kricks, Lara; **Puls, Jan-Samuel**; Lopez, Daniel; Grein, Fabian; Heilbronner, Simon (2023): Functional membrane microdomains and the hydroxamate siderophore transporter ATPase FhuC govern Isd-dependent heme acquisition in *Staphylococcus aureus*. *eLife,* 12, e85304, DOI: https://doi.org/10.7554/eLife.85304

Book contributions:

Brajtenbach, Dominik; **Puls, Jan-Samuel**; Matos de Opitz, Cruz L.; Sass, Peter; Kubitscheck, Ulrich; Grein, Fabian (2023): Quantitative Analysis of Microscopy Data to Evaluate Bacterial Responses to Antibiotic Treatment. In: *Antibiotics. Methods in Molecular Biology*, *(MIMB, volume 2601),* pp. 231-257, DOI: https://doi.org/10.1007/978-1-0716-2855-3_12

Selected talks:

International Conference TRR261 “Cellular Mechanisms of Antibiotic Action and Production” 2023, title: “Impact of antibiotics on the spatio-temporal organization of the cell wall biosynthesis machinery and cell division”

Gordon Research Conference “Bacterial Cell Surfaces” 2022, short talk, title: “The novel epilancin A37 destabilizes bacterial membranes and induces intracellular vesicle formation”

Selected posters:

International Conference “Controlling Microbes to Fight Infections” 2023, title: “Characterization of the potentially microbiome-shaping epilancin A37 reveals a unique mechanism of action”. **Jan-Samuel Puls**, Benjamin Winnerling, Jeffrey Power, Annika Marie Krüger, Dominik Brajtenbach, Kevser Bilici, Matthew Johnson, Tanja Schneider, Hans-Georg Sahl, Debnath Ghosal, Ulrich Kubitscheck, Simon Heilbronner, Fabian Grein.

International Conference TRR261 “Cellular Mechanisms of Antibiotic Action and Production” 2023, title: “Characterization of the potentially microbiome-shaping epilancin A37 reveals a unique mechanism of action”. **Jan-Samuel Puls**, Benjamin Winnerling, Jeffrey Power, Annika Marie Krüger, Dominik Brajtenbach, Kevser Bilici, Matthew Johnson, Tanja Schneider, Debnath Ghosal, Simon Heilbronner, Ulrich Kubitscheck, Fabian Grein.

Gordon Research Conference “Bacterial Cell Surfaces” 2022, title: “The novel epilancin A37 destabilizes bacterial membranes and induces intracellular vesicle formation”. **Jan-Samuel Puls**, Benjamin Winnerling, Annika Marie Krüger, Dominik Brajtenbach, Jeffrey Power, Matthew Johnson, Tanja Schneider, Debnath Ghosal, Simon Heilbronner, Ulrich Kubitscheck, Fabian Grein.

Annual conference of the Association for General and Applied Microbiology 2022, title: “Effects of the novel epilancin A37 on bacterial and artificial membranes”. **Jan-Samuel Puls**, Dominik Braijtenbach, Annika Krüger, Benjamin Winnerling, Jeffrey Power, Stefania De Benedetti, Tanja Schneider, Simon Heilbronner, Ulrich Kubitscheck, Fabian Grein.

List of Content

List of abbreviations and units

Knowledge of standard units of measurement, common chemical formula notation and IUPAC chemical notation nomenclature is assumed. Amino acids were abbreviated according to IUPAC amino acid single letter or three letter code.

Abbreviation or unit	full notation
ABC	ATP-binding cassette
AMP	ampicillin
ATCC	American Type Culture Collection
ATP	adenosine triphosphate
BCA	bicinchoninic acid
BODIPY	dipyrrometheneboron difluoride
CAMP	cationic antimicrobial peptide
CAO	cacaoidin
CAP	convolved average projection
CCCP	carbonylcyanid-m-chlorphenylhydrazone
CFU	colony forming units
CLOV	clovibactin
CLP	cyclic lipopeptide
CWBM	cell wall biosynthesis machinery
Da	Dalton
DCAP	dichlorocarbazol hydroxypropyl aminohydroxymethyl propanediol
$DiBAC_4(3)$	bis-(1,3-dibarbituric acid)-trimethine oxanol
$DiSC_3(5)$	3,3-dipropylthiadicarbocyanine iodide
DMF	dimethyl formamide
DMSO	dimethyl sulfoxide
DNA	desoxyribonucleic acid
DSMZ	German Collection of Microorganisms and Cell Cultures
EDTA	ethylene diamine tetraacetate
ERY	erythromycin
Fig.	figure
FMM	fluid membrane microdomains
FOS	fosfomycin
FPLC	fast protein liquid chromatography
GFP	green fluorescent protein
GlcNAc	N-acetylglucosamine
GTP	guanosine triphosphate
HADA	3-[[(7-Hydroxy-2-oxo-2H-1-benzopyran-3-yl)carbonyl]amino]-D-alanine hydrocholoride
HiLo	highly inclined and laminated optical sheet
HPLC	high pressure liquid chromatography
HYP	hypeptin
IPTG	isopropyl-β-D-thiogalactopyranoside
Isd	iron-regulated surface determinant
(k)bp	(kilo)base pairs
LB	lysogeny broth/Luria–Bertani
LP	lipoprotein
LPS	lipopolysaccharide
LTA	lipoteichoic acid
MH	Müller-Hinton
MIC	minimal inhibitory concentration
MOE	moenomycin

MRS	mersacidin
MRSA	methicillin resistant *Staphylococcus aureus*
MSSA	methicillin-susceptible *Staphylococcus aureus*
MurNAc	N-acetylmuramic acid
NEAT	near iron transporter
NHS-ester	N-hydroxy succinimide ester
NIS	nisin
OD	optical density
OMP	outer membrane protein
OXA	oxacillin
PBP	penicillin binding protein
PCC	pearson coefficient of correlation
PGS	peptidoglycan synthesis
PI	propidium iodide
PP	pentapeptide
PPi	pyrophosphate
px	pixel
RFU	relative fluorescence unit
rpm	rounds per minute
SAR	structure-activity-relationship
SD	standard deviation
SEDS	shape, elongation, division and sporulation
SIA	siamycin
Tab.	table
TEIX	teixobactin
TGase	transglycosylase
THCz	tetrahydrocarbazole
TLC	thin layer chromatography
TPase	transpeptidase
UDP	uridine diphosphate
UK	United Kingdom
USA	United States of America
VAL	valinomycin
VAN	vancomycin
VISA	vancomycin-intermediate *Staphylococcus aureus*
VRE	vancomycin-resistant enterococcus
VRSA	vancomycin-resistant *Staphylococcus aureus*
WHO	World Health Organization
WTA	wall teichoic acid
YFP	yellow fluorescent protein

Summary

The increasing threat of antibiotic resistance requires innovation in antibiotic research and development. However, the knowledge of how antimicrobial agents kill bacteria is still limited, even for clinically relevant antibiotics. Bacterial cell wall biosynthesis is the target of many important antibiotics. Its spatiotemporal organization is closely coordinated with cell division. However, the roles of the cell wall biosynthesis machinery (CWBM) and peptidoglycan synthesis (PGS) within cell division are not fully understood. Even less is known about the impact of antibiotics on the coordination of these two essential processes.

In this work, the cellular effects of clinically used PGS-targeting antibiotics on *Staphylococcus aureus* were investigated to construct a model of how PGS inhibition impacts the spatio-temporal organization of the CWBM and cell division. Blocking the ultimate PGS substrate lipid II with the glycopeptide antibiotics vancomycin or telavancin caused a complete inhibition of septum constriction. The beta-lactam oxacillin stopped cell division by preventing recruitment of the major peptidoglycan synthase PBP2 to the septum. Accordingly, this work identifies cell division as a main cellular target of PGS-targeting antibiotics. It further provides evidence that PGS is the essential driving force of septum constriction throughout cell division of *S. aureus* and reveals PBP2 as being crucial for septum closure. Inhibition of PGS was found to ultimately cause total arrest of *S. aureus* cell division. This newly established framework was subsequently used to investigate the cellular effects of the PGS-inhibiting natural product moenomycin and the small synthetic molecule DCAP on the CWBM and cell division. Moenomycin was found to impair cell splitting independent from its PGS-inhibiting action, indicating an additional target of moenomycin, which is involved in cell separation. DCAP was found to interfere with septum formation and CWBM organization, suggesting a PGS-inhibiting mechanism of action. Additionally, the impact of several PGS-targeting antibiotics on the transmembrane potential was investigated and the interaction of the *S. aureus* heme-transporter and virulence factor IsdF with the fluid membrane microdomain scaffold protein FloA was examined.

Similar to the knowledge gap for how antibiotics kill pathogens, not much is known about the mechanisms of action and ecological roles of the many antimicrobial agents produced by members of the human microbiome, despite its clearly established role in health and infection. In this work, cellular effects of the epilancin A37 from a human nasal *Staphylococcus epidermidis* isolate were investigated using the model organism *Corynebacterium glutamicum*. Staphylococci and corynebacteria constitute key genera of the nasal microbiome, and production of A37 was found to convey an advantage to *S. epidermidis* in this inter-species competition. A37 was found to enter the corynebacterial cytoplasm without impairing the cell membrane in a partially transmembrane dependent manner. Upon cytoplasmic accumulation, A37 was found to induce the formation of intracellular membrane vesicles, which were found to be linked to antibacterial activity. Thus, this work provides evidence for a microbiome shaping effect of epilancin A37 and reveals that A37 kills corynebacteria with an intricate and unique mechanism of action.

1. Introduction

1.1. The antibiotic resistance crisis

Antibiotics are essential for human health and fundamental for modern medicine (WHO 2021). Using antibiotics to treat bacterial infections saves millions of lives every year (Laxminarayan *et al.* 2013; Murray *et al.* 2022; Van Boeckel *et al.* 2014). Beyond this, antibiotics enable otherwise highly dangerous medical measures with increased risk of infection and/or required immunosuppression, e.g., cancer therapies, invasive surgeries, organ transplantations and many more procedures, which contribute to health in major ways and are themselves constitutive for modern medicine (Brown and Wright, 2016). Despite their critical role at the center of human health, antibiotic development has arrived at a low after decades of constant decline only 80 years after inception of the antibiotic era (Hutchings *et al.* 2019; Walesch *et al.* 2023). Meanwhile, antibiotic resistance is on a constant rise, threatening to annihilate the inestimable value of antibiotics for human health worldwide (Ikuta *et al.* 2022; Murray *et al.* 2022).

The first mass produced antibiotic penicillin was introduced in US and european markets in the 1940s. Within the next two decades, the complementary expertise of microbiological, biochemical, and pharmaceutical research brought a total of 27 different classes of antibiotics to market (Figure 1A). This diverse set of compound classes included natural products from bacteria and fungi as well as semi-synthetic or nature-inspired derivatives and also fully synthetic chemicals. Due to the unrivalled success of antibiotic development in the thirty years of 1940-1970, this time is often referred to as the “golden age of antibiotics” (Hutchings *et al.* 2019; Cook and Wright, 2022). Beyond the immediate beneficial impact on human health during that time, the accomplishments of this period lay the foundation for present antibiotic chemotherapy. The most used antibiotics today still belong to classes discovered during the “golden age” (Figure 1B, Klein *et al.* 2018; Van Boeckel *et al.* 2014; WHO 2021). Unfortunately, antibiotic development has seen a drastic decline in the following decades. Exhaustive mining of the natural product repertoire of a single group of actinomycetes led to increasing number of rediscoveries and financial failures, subsequently diverting efforts away from natural product discovery. Instead, focus of pharmaceutical development shifted towards increasingly artificial methods for identification of new antibiotic classes and concentrated more on adapting the chemical structures around already established pharmacophores to improve pharmacological parameters and counter resistance developments (E. D. Brown *et al.* 2016). Because of this change in focus, merely nine new classes of antibiotics were introduced in the five decades since (Hutchings *et al.* 2019; Stennett *et al.* 2022; Walesch *et al.* 2023). Today, most antibiotics in clinical (WHO, 2022a) and pre-clinical (WHO, 2022b) development are either permutations upon or in close structural proximity to already existing pharmacophores.

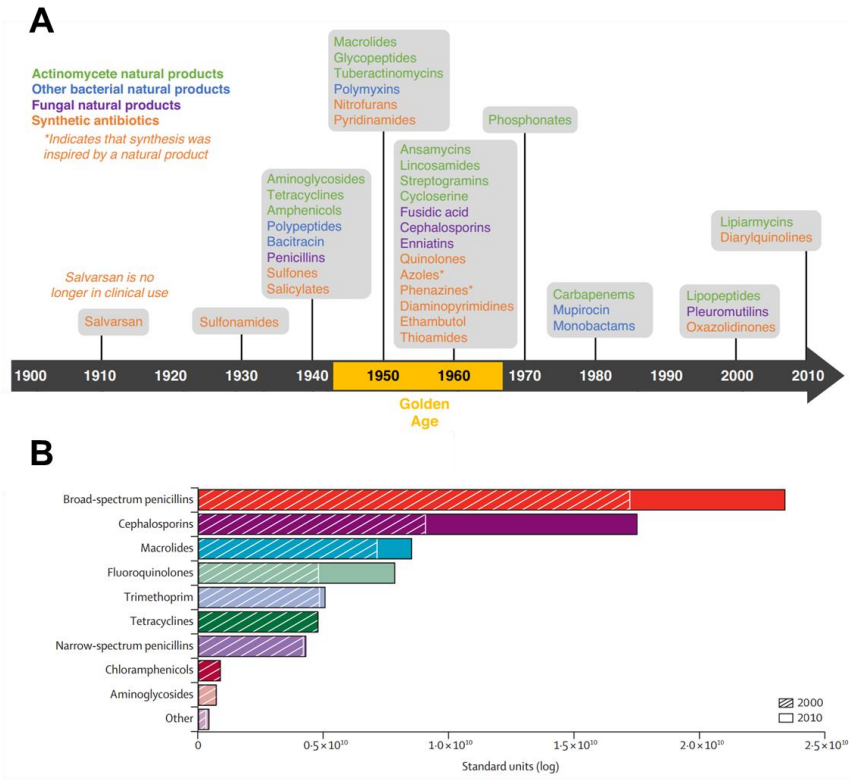

Figure 1: History of development and use of antibiotics worldwide. (A) Timeline of new antibiotic classes reaching clinical approval each decade. Antibiotic classes are color-coded for their source. Adapted from Hutchings *et al.* (2019). **(B)** Global human antibiotic consumption of the ten most consumed antibiotic classes in 2000 and 2010. Note, that the beta-lactams on this list are differentiated into subclasses (broad-spectrum and narrow-spectrum penicillins, cephalosporins). Standard unit = single dose, regardless of amount and delivery form. From Van Boeckel *et al.* (2014) with permission from Elsevier.

From a long-term public health perspective, this is undesirable, as evolutionary principles dictate the development of resistance against all classes and compounds that are actively deployed against bacteria (Bryson and Demerec, 1955; Davies and Davies, 2010; Richmond, 1969). Accordingly, the emergence of resistance was observed for every clinically used antibiotic, typically within a few years after introduction (Figure 2A, Stennett *et al.* 2022; Walesch *et al.* 2023). Over the years, this threat of antibiotic resistance consistently grew into a “silent pandemic”, which has become a leading cause of death worldwide and threatens the foundations of modern medicine on a global scale (Cars *et al.* 2021; Laxminarayan 2022). In 2019, nearly five million deaths were associated with resistant bacteria. 1.27 million of these deaths were attributable exclusively to the fact of antibiotic resistance in the infecting pathogen. This means that these 1.27 million deaths likely could have been avoided if effective antibiotics against the respective pathogen would have been available (Figure 2B, Murray *et al.* 2022). With the trend continuing upwards, it has been estimated, that antibiotic resistance could be responsible for up to 10 million deaths in the year 2050 (O’Neill 2014). Importantly, there are no substantial differences between low and high-income countries (Murray *et al.* 2022). This signifies the global scale of the problem, which cannot be solved by individualistic efforts that rely on capital investment into local healthcare. Substantial change is needed in the approaches to contain and treat antibiotic resistant pathogens worldwide.

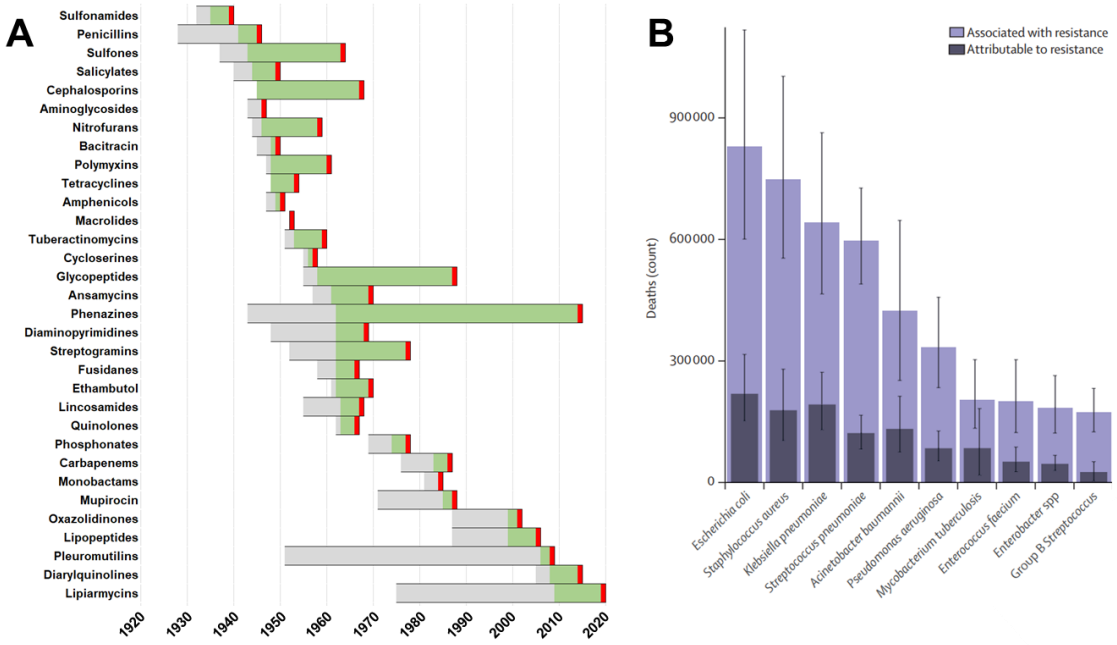

Figure 2: Antibiotic resistance development and associated cost of human lives. (A) Timeline of development (grey) to year of clinical introduction and "resistance-free window" (green) until the year of first report of clinical resistance (red) for several antibiotic classes. Created using data compiled by Stennett *et al.* (2022). **(B)** Estimated global deaths 2019 associated with and attributable to antibiotic resistance. The ten pathogens responsible for the most deaths are shown. Error bars show 95% uncertainty intervals. Adapted from Murray *et al.* (2022).

Most importantly, new antibiotic classes are needed to improve treatment options and combat resistance. However, the failed approaches of antibiotic research and development in recent decades culminated to a substantial deficit in new antibiotics reaching the patient. In stark contrast to the success of the *in vivo* based approaches during the "golden age" (Lewis 2013; Waksman *et al.* 1946), various high-throughput *in vitro* compound screening programs of subsequent decades did not deliver new antibiotic classes to the patient (Payne *et al.* 2015; Tommasi *et al.* 2015). This lay bare a critical shallowness in approaching the task to selectively kill the complex, self-regulating and rapidly adapting living systems that are bacteria. Meanwhile, it is still not comprehensively understood, how even decades-old, clinically successful antibiotics kill bacteria. To foster innovation in antibiotic development, a new paradigm of antibiotic action is required, which focuses on elucidating the cellular impact of antibiotic compounds that lead to cell death (E. D. Brown *et al.* 2016; Lewis 2013; Walesch *et al.* 2023). From molecular target inhibition emerge complex cascades of cellular effects, which can extent to substantial changes in the chemical composition and integrity of key cellular structures (Cho *et al.* 2014; Gardete *et al.* 2006; Łęski *et al.* 2005; Salamaga *et al.* 2021) and the rearrangement of metabolic and biosynthetic pathways (Belenky *et al.* 2015; Dörries *et al.* 2014; Gardete *et al.* 2006; Schelli *et al.* 2017). Key aspects of these cellular effects remain unknown, for new and old antibiotics alike. Fundamental knowledge of the complex net of cellular processes and how they enhance or diminish antibiotic impact is essential for understanding what makes antibiotics effective and how resistance develops.

1.2. The global health threat *Staphylococcus aureus*

In 2019, the gram-positive *Staphylococcus aureus* was associated with over one million deaths, constituting it as the leading cause of infection-related deaths worldwide (Ikuta *et al.* 2022). In the same year, *S. aureus* furthermore was the 3rd most cause of deaths attributable to antibiotic resistant infections globally, following only *Escherichia coli* and *Klebsiella pneumoniae* (Murray *et al.* 2022). In contrast to these other two pathogens, the problem with antibiotic resistant *S. aureus* can be attributed to one single pathogen-drug combination. Methicillin-resistant *S. aureus* (MRSA) is a phenotype resulting from an acquired resistance against nearly all clinically available beta-lactams, which constitute the most used group of antibiotics[1] with approximately 60% of all antibiotic doses given to patients (Figure 1B, Klein *et al.* 2018; Van Boeckel *et al.* 2014). Due to the resistance against this most critical group of antibiotics, MRSA caused over 100.000 lost lives worldwide. Notably, MRSA alone was responsible for over 26% of resistance-attributable deaths in high-income countries, illustrating that the extent of this problem cannot be countered by the means of currently available medicine (Murray *et al.* 2022).

As of now, MRSA constitutes the most common antibiotic resistant nosocomial pathogen (Murray *et al.* 2022). The high pathogenic potential of *S. aureus* and particularly MRSA is caused by two factors, the opportunistic nature of *S. aureus* and the closely associated problem of nosocomial infections. Under normal conditions, *S. aureus* is a typical member of the human microbiome and can be found in the upper respiratory tract of approximately 30% of the human population (Mainous 2006; Sollid *et al.* 2014). Proliferation of *S. aureus* is usually limited by the immune system and therefore of communalistic nature (Krismer *et al.* 2017). However, due to a range of pathogenicity and virulence factors[2] (amongst others the iron scavenging Isd system, see chapter 1.4), *S. aureus* has the potential to quickly establish serious infections, especially if the human immune system is compromised, e.g., due to illness, allergies, pregnancy or age. Importantly, this is also the case under conditions of immunosuppression, e.g., treatment of cancer or autoimmune diseases. These opportunistic and often nosocomial infections account for the significant danger *S. aureus* poses for human life worldwide (Ikuta *et al.* 2022; Kluytmans *et al.* 2005; Murray *et al.* 2022). Nonetheless, they can often be effectively suppressed by antibiotics. However, the pathogenicity of MRSA is not compromised by usage of the most common beta-lactam class of antibiotics. Thus, the MRSA phenotype substantially improves the pathogenic potential of *S. aureus* especially in conditions of increased patient instability, where susceptible *S. aureus* strains

[1] Beta-lactam antibiotics include the classes of penicillins (also referred to as penams), cephalosporins, monobactams and carbapenems, as well as the penems, cephamycins and carbacephems (Lima *et al.* 2020).

[2] *S. aureus* strains can produce a variety of hemolytic exotoxins (Dinges *et al.* 2000) as well as multiple other host-damaging enzymes (Lowy 1998), coagulating, clumping and fibronectin-binding factors, and other adhesins (A. G. Cheng *et al.* 2010; T. J. Foster 2019; T. J. Foster *et al.* 2014; Moreillon *et al.* 1995; Que *et al.* 2005), antibody-binding and thereby -inactivating proteins (Atkins *et al.* 2008; Moks *et al.* 1986; E. J. Smith *et al.* 2011) and other virulence factors improving in-host survival (Clauditz *et al.* 2006; Jenul *et al.* 2019; Koch *et al.* 2017; Sheldon *et al.* 2015), and sometimes poly-saccharide capsules (Kuipers *et al.* 2016; Nilsson *et al.* 1997; Portolés *et al.* 2001; Rausch *et al.* 2019; Thakker *et al.* 1998).

could be effectively contained with typical medical procedures (Gordon and Lowy 2008; Ippolito *et al.* 2010; Murray *et al.* 2022). Given these circumstances, it is necessary to find new treatment options for *S. aureus*, especially MRSA. Currently, clinical treatment of MRSA relies on few last-resort antibiotics, most importantly glycopeptides like vancomycin and the lipodepsipeptide daptomycin (Geriak *et al.* 2019; Jorgensen *et al.* 2020; Rieg *et al.* 2017). Resistance to these last-in-line defenses becomes increasingly more common in clinical MRSA isolates (Appelbaum 2006; Chambers *et al.* 2009; L. C. Chan *et al.* 2016; Chang *et al.* 2003; Haaber *et al.* 2017; Hayden *et al.* 2005; Hirschwerk *et al.* 2006; Mangili *et al.* 2005; Sieradzki *et al.* 1999; Wilson 2003). Thus, the effort to discover and develop potent new antibiotics against MRSA needs to be re-kindled.

1.3. The cell wall biosynthesis machinery of *S. aureus* as an antibiotic target

The peptidoglycan cell wall is a macromolecular structure unique to bacterial life and essential for survival and proliferation of virtually all bacteria. Accordingly, the bacterial cell wall biosynthesis machinery (CWBM) is a most prominent target pathway for antibiotics (Grein *et al.* 2019; Schneider and Sahl 2010). While gram-negative species have an additional outer membrane layer providing biophysical protection for their cell wall, the cell wall constitutes the most distal cell layer of gram-positive bacteria and is therefore the most exposed to external factors (Figure 3). Essential components of the CWBM as well as the cell wall structure itself are located on the outer layer of the cytoplasmic membrane and therefore outside of the biophysically more protected inner compartment of the gram-positive cell (Egan *et al.* 2017; Schneider and Sahl 2010; Silhavy *et al.* 2010). This enables a wide range of molecules to reach and interfere with these essential structures. Consequently, CWBM targeting antibiotics against gram-positive bacteria such as *S. aureus* are chemically and functionally diverse. Critical last-resort antibiotics as well as multiple pre-clinical (WHO 2022b) and clinical candidates (WHO 2022a) against *S. aureus* in general and MRSA in particular are directed against key components of the cell wall biosynthesis, illustrating its high relevance as antibiotic target to this day.

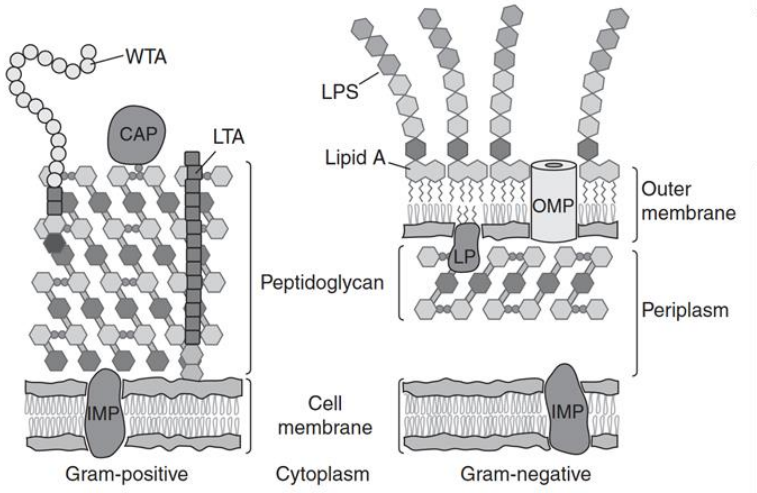

Figure 3: Schematic overview of the cell envelopes of gram-positive (left) and gram-negative (right) bacteria. WTA: Wall teichoic acid, CAP: covalently attached protein, l: Lipoteichoic acid, IMP: integral membrane protein, LPS: lipopolysaccharide, OMP: outer membrane protein, LP: lipoprotein. From Silhavy *et al.* (2010) with permission from Cold Spring Harbor Laboratory Press.

The main function of the bacterial cell wall is to provide essential stability against physical stresses, most importantly osmotic pressure (Mitchell and Moyle 1957; Scheffers and Pinho 2005; Vollmer *et al.* 2008). Gram-negative species regularly produce thin cell walls of only few nm and 1-3 layers of peptidoglycan and rely on their outer membrane as initial barrier against external factors. In contrast, gram-positive cell walls like that of *S. aureus* are significantly thicker and made of substantially more layers of peptidoglycan to provide protection (Giesbrecht *et al.* 1998; Scheffers *et al.* 2005; Vollmer *et al.* 2010; X. Yao *et al.* 1999). Furthermore, the *S. aureus* cell wall serves as a scaffold for a multitude of different proteins and attachments to regulate cellular functions and interact with the surrounding. E.g., wall teichoic acids (WTA) fulfil numerous important functions, as they modulate adherence (Aly *et al.* 1980; Heptinstall *et al.* 1970; Weidenmaier *et al.* 2004, 2005, 2008), cell cycle regulation (Atilano *et al.* 2010; Hammond *et al.* 2022; Y. Lu *et al.* 2023), autolysis (Biswas *et al.* 2012; Peschel *et al.* 2000; Schlag *et al.* 2010) and more. Many of these functions are closely associated with pathogenesis and virulence and are critical factors in antibiotic resistance (Kohler *et al.* 2009; Y. Lu *et al.* 2023; Misawa *et al.* 2015; van Dalen *et al.* 2020). As such, WTA alanylation regulates the cell envelope charge and thereby plays an important role in the bacteria's defense against cationic antimicrobial peptides (CAMPs) and Ca2+ complexing antibiotics like daptomycin (Bertsche *et al.* 2011, 2013; Müller *et al.* 2018; Peschel *et al.* 1999; Weidenmaier *et al.* 2008). Furthermore, WTA synthesis and modification were shown to play key roles in susceptibility to vancomycin (Hort *et al.* 2021; Peschel *et al.* 2000) and the virulence and beta-lactam resistance of MRSA (S. Brown *et al.* 2012; Campbell *et al.* 2011; Ersoy *et al.* 2022; Farha *et al.* 2013; Y. Lu *et al.* 2023). Components of nutrient acquisition systems like the ion scavenging Isd system are embedded into the cell wall and constitute significant factors for in-host survival (see chapter 1.4, Sheldon *et al.* 2015). The main *S. aureus* autolysin Atl as well as other cell wall hydrolyses like Sle1, LytH and LytN regulate cell wall recycling, cell growth and division (Biswas *et al.* 2006; Bose *et al.* 2012; Do *et al.* 2020; Frankel *et al.* 2012; Kajimura *et al.* 2005; Nega *et al.* 2020; Thalsø-Madsen *et al.* 2019; Veiga *et al.* 2023; Yamada *et al.* 1996). They are closely associated with susceptibility and resistance to multiple antibiotics, including beta-lactams, vancomycin and daptomycin (Cafiso *et al.* 2012; Homma *et al.* 2016; Maki *et al.* 1994; Müller *et al.* 2018; Peschel *et al.* 2000; Sakoulas *et al.* 2005; Salamaga *et al.* 2021; Sieradzki *et al.* 1997; Xu *et al.* 2023). Furthermore, the cell wall serves as anchor for capsular polysaccharides produced by some strains of *S. aureus*, which contribute substantially to virulence (Kuipers *et al.* 2016; Misawa *et al.* 2015; Portolés *et al.* 2001; Rausch *et al.* 2019). Beyond providing a scaffold for all these and more factors, the cell wall itself can play a vital role in antibiotic resistance, as a thickening of the structure confers reduced susceptibility to the last-resort antibiotic vancomycin by providing false binding sites for the antibiotic in vancomycin intermediate *S. aureus* (VISA, Cui *et al.* 2000, 2003; Hanaki 1998; Sieradzki *et al.* 2003).

Biosynthetic steps of cell wall construction

Chemically, the cell wall is a multi-layered, the whole cell encompassing macromolecule, built out of crosslinked peptidoglycan strands. Cell wall biosynthesis is the central pathway of constructing the peptidoglycan building blocks, which consist of a disaccharide glycan unit with a short peptide attached. These building blocks are subsequently integrated into the cell wall mesh in peptidoglycan synthesis

(PGS). While the principles of cell wall construction are the same in all bacteria, substantial differences exist in both the precise chemical constitution of the peptidoglycan units as well as the set of proteins in the CWBM and their spatio-temporal organization (Pinho *et al.* 2013; Scheffers *et al.* 2005). In *S. aureus*, PGS is spatially focused to the cell division septum and temporally coordinated with cell division (Monteiro *et al.* 2018). Furthermore, the species lacks an elongasome and has a comparably small set of CWBM components (see below, Pinho *et al.* 2013; Reed *et al.* 2015; Monteiro *et al.* 2018). Besides its value for antibiotic research and clinical relevance, this simplicity makes *S. aureus* an optimal model-organism for understanding core principles governing PGS. The cell wall biosynthesis pathway of *S. aureus* (Figure 4) can be divided into three parts:

1. Cytoplasmic construction of a MurNAc-pentapeptide (MurNAc-PP), which begins with the enzymatic conversion of UDP-GlcNAc to UDP-MurNAc by MurA and MurB (Gunetileke and Anwar 1966). Afterwards, the L-Ala-D-Glu-L-Lys-D-Ala-D-Ala pentapeptide chain is added to the acetyl-moiety in a stepwise manner by the enzymes MurC-MurF (Ito *et al.* 1973; Neuhaus 1962; Neuhaus *et al.* 1965; Walsh 1989).Notably, the final D-Ala-D-Ala is peptidated as a dipeptide, which is previously formed under ATP-consumption by DdlA (Neuhaus 1960, 1962).

2. Construction of the final peptidoglycan building block at the inner leaflet of the cytoplasmic membrane. Therefore, the UDP-MurNAc-PP is bound to the membrane spanning carrier lipid bactoprenol-phosphate ($C_{55}P$) through pyrophosphate ester formation, creating the membrane-bound precursor lipid I (C_{55}PP-MurNAc-PP, Anderson *et al.* 1965; Bouhss *et al.* 2004; Higashi *et al.* 1967). The ester formation is catalyzed by MraY via UMP condensation. Subsequently, the enzyme MurG catalyzes the glycosylation of the MurNAc-4'-Position with a GlcNAc, resulting in the ultimate peptidoglycan precursor lipid II (C_{55}PP-MurNAc-GlcNAc-PP, Anderson *et al.* 1967). In *S. aureus*, lipid II is further modified by the addition of a pentaglycine bridge to the ε-aminogroup of the pentapeptide L-Lys. This addition is catalyzed by by FemX (1st Gly), FemA (2nd-3rd Gly) and FemB (4th-5th Gly, Schneider *et al.* 2004). Subsequent amidation of the pentapeptide D-Glu, catalyzed by the enzymes MurT and GatD (Münch *et al.* 2012) yields the *S. aureus* specific version of the membrane-bound precursor lipid II (Figure 4C, C_{55}PP-MurNAc-GlcNAc-L-Ala-D-Gln-L-Lys-D-Ala-D-Ala-Gly_5). The pentaglycine bridge has significant impact on the crosslinking degree of *S. aureus*, as the specifics of enzymatic activity of peptidoglycan crosslinking enzymes are dependent on its length (Srisuknimit *et al.* 2017). It has been shown that the glycine bridge is important for *S. aureus* survival, and only few strains are adapted to growth with shortened or missing glycine bridges under special conditions (Monteiro *et al.* 2019).

3. Transport of lipid II through the cytoplasmic membrane bilayer to the outer leaflet and extracellular incorporation of the individual building blocks (MurNAc-GlcNAc-PP-Gly_5) into the peptidoglycan network. The translocation of lipid II to the outer leaflet of the cell membrane is performed by specific flippases. Currently, MurJ is the only known lipid II flippase of *S. aureus* (Monteiro *et al.* 2018; Rubino *et al.* 2018, 2020; Sham *et al.* 2014), with FtsW suggested to also fulfil that role due to the observation of *in vitro* flippase activity (Mohammadi *et al.* 2011). Despite successes in elucidating the structural conformations of MurJ and their putative role in lipid II translocation, the precise

mechanism is still unclear (Kohga *et al.* 2022; Kuk *et al.* 2017, 2019; Rubino *et al.* 2018, 2020). Following flipping to the outer leaflet of the membrane, the building blocks are incorporated into the cell wall structure by two peptidoglycan synthesis (PGS) reactions (Figure 4B, Figure 5):

1. Transglycosylases (TGases, sometimes referred to as glycosyltransferases) form glycosidic bonds between the MurNAc-GlcNAc disaccharides of two building blocks, thereby also releasing the carrier lipid as C_{55}PP from the donor strand (Figure 5A,C). Multiple iterations of this processive polymerization reaction result in long glycan strands (Huang *et al.* 2012; Lovering *et al.* 2007; Yuan *et al.* 2007). *S. aureus* comprises multiple TGases with different roles in cell division, cell shape and antibiotic resistance, most importantly the essential proteins FtsW (Meeske *et al.* 2016; Reichmann *et al.* 2019; Taguchi *et al.* 2019) and PBP2 (Barrett *et al.* 2005; Lovering *et al.* 2007) as well as the non-essential RodA (Emami *et al.* 2017) and the (also non-essential) monofunctional TGases SgtA and SgtB (also referred to as MGT, Huang *et al.* 2012; Reed *et al.* 2011, 2015; Q. M. Wang *et al.* 2001).

2. Transpeptidases (TPases) crosslink different glycan chains through synthesis of a peptide bond between the pentaglycine bridge terminus and the D-Ala-D-Ala-terminus of two different glycan chains (Figure 5A,B). In *S. aureus*, this reaction is performed by a set of four penicillin-binding proteins (PBPs[3], PBP1 to PBP4), of which PBP1 and PBP2 are essential (Memmi *et al.* 2008; S. F. F. Pereira *et al.* 2007, 2009; Pinho, De Lencastre *et al.* 2001; Pinho *et al.* 2000; Pinho, Filipe *et al.* 2001; Reed *et al.* 2015; Sieradzki *et al.* 1999). PBP2 is the only bifunctional PBP of *S. aureus*, catalyzing both TGase and TPase reactions. Accordingly, it has been described as the species' main peptidoglycan synthase (Monteiro *et al.* 2018). MRSA strains have an additional PBP named PBP2a (with co-incidental similar naming to PBP2), which shows drastically decreased beta-lactam binding affinities and is the defining factor of nearly all MRSA resistance phenotypes (Lim *et al.* 2002; Otero *et al.* 2013; Pinho, De Lencastre *et al.* 2001; Pinho, Filipe *et al.* 2001)[4]. This decrease in beta-lactam binding is achieved by a regulatory allosteric site, which binds to glycan moieties of peptidoglycan without TGase activity (Mahasenan *et al.* 2017; Otero *et al.* 2013).

[3] Beta-lactams, such as Penicillin, mimic the D-Ala-D-Ala moiety, thereby binding to and inhibiting TPases (see below). Thus, enzymes catalyzing TPase reactions were historically identified by their interaction with penicillin, hence the name.

[4] There are instances of MRSA, where increased expression and/or mutation of PBP4 conveys beta-lactam resistance (Alexander *et al.* 2018; Basuino *et al.* 2018; L. C. Chan *et al.* 2016; Greninger *et al.* 2016; Hamilton *et al.* 2017; Lahiri *et al.* 2016; Maya-Martinez *et al.* 2019; Memmi *et al.* 2008).

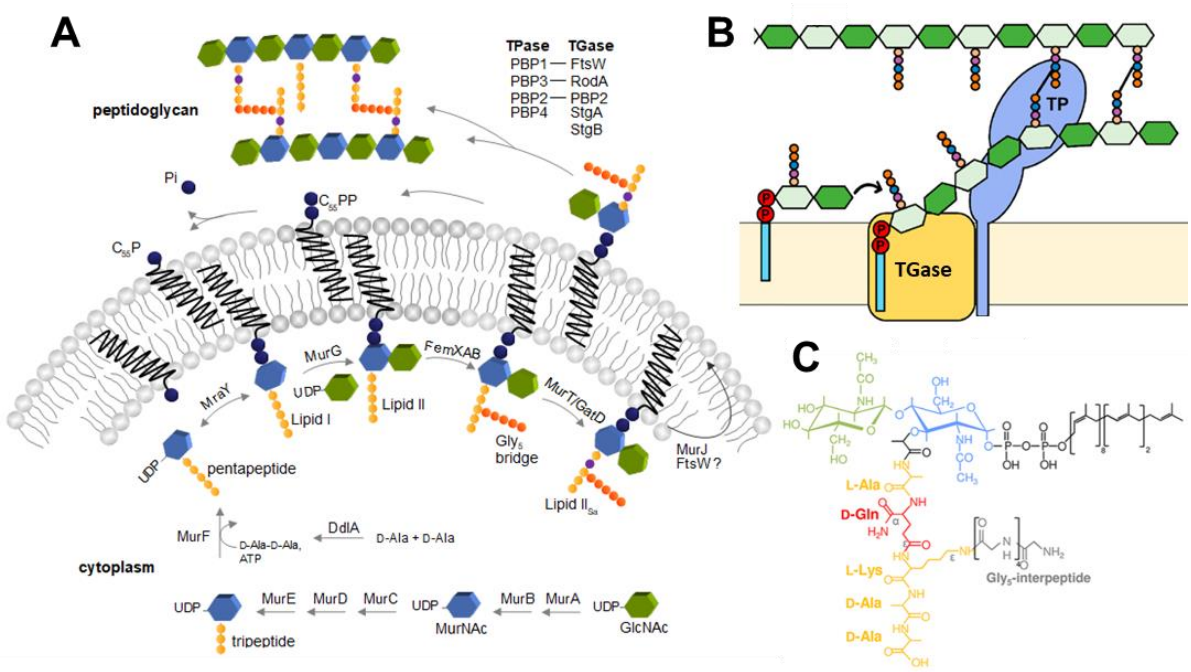

Figure 4: The *S. aureus* cell wall biosynthesis pathway. (A) Schematic overview of the cell wall biosynthesis pathway in *S. aureus*. MurA-F catalyze the construction of the soluble precursor UDP-MurNAc-pentapeptide, which is subsequently used as substrate for intracellular, membrane-bound synthesis of lipid II by MraY and MurG. FemXAB and MurT/GatD catalyze Gly_5-addition and Glu-amidation, yielding a *S. aureus* species-specific lipid II. This ultimate precursor is flipped to the outer leaflet by MurJ and putatively also by FtsW. Incorporation of the building block into the peptidoglycan network is catalyzes by transglycosylases (TGases) and transpeptidases (TPases). Adapted from Schneider and Sahl (2010) with permission from Elsevier. **(B)** Schematic overview of the processive polymerization of peptidoglycan strands by TGases and the subsequent crosslinking by TPases (TP). In *S. aureus*, PBP1-FtsW and PBP3-RodA form cognate pairs, where PBPs constitute the TPases, while FtsW/RodA catalyze the preceding transglycosylation. The bifunctional PBP2 comprises both functions within one protein (see Figure 5). Adapted with permission from S. Kumar *et al.* (2022). Copyright 2022 American Chemical Society. **(C)** Chemical structure of *S. aureus* lipid II. Green: GlcNAc, blue: MurNAc, black: C_{55}PP, yellow: Unmodified pentapeptide amino acids, red: Amidated pentapeptide D-glutamine, grey: Gly_5-interpeptide bridge. Adapted from Ulm and Schneider (2016) with permission from Springer Nature.

The first two parts of cell wall biosynthesis depend on relatively abundant substrates that are localized in the diffusive environment of the cytoplasm, and they catalyze a stepwise synthesis of small molecule building blocks. In contrast, the final steps of peptidoglycan synthesis (PGS) must ensure the formation of a highly ordered macromolecular structure with functional integrity. Accordingly, the molecular organization of the final TGase and TPase reactions is precisely coordinated, either by combining both enzymatic functions within one protein (PBP2, Figure 5) or by the formation of the interacting cognate pairs PBP1-FtsW and PBP3-RodA[5] (Martínez-Caballero *et al.* 2021; Reichmann *et al.* 2019; Taguchi *et al.* 2019). This enables a conveyer-belt-like biosynthesis of newly polymerized and rapidly crosslinked peptidoglycan strands, sometimes referred to as nascent peptidoglycan. These nascent peptidoglycan

[5] As FtsW and RodA belong to the shape, elongation, division and sporulation (SEDS) protein family, these cognate pairs are sometimes referred to as PBP-SEDS pairs (Reichmann *et al.* 2019).

strands are further matured by secondary crosslinking activity (mostly by PBP4, Gautam *et al.* 2015; Łęski *et al.* 2005; Lund *et al.* 2018; Monteiro *et al.* 2015), attachment of WTA by the enzymes LcpA – LcpC (Schaefer *et al.* 2017), and incorporation of cell wall associated proteins.

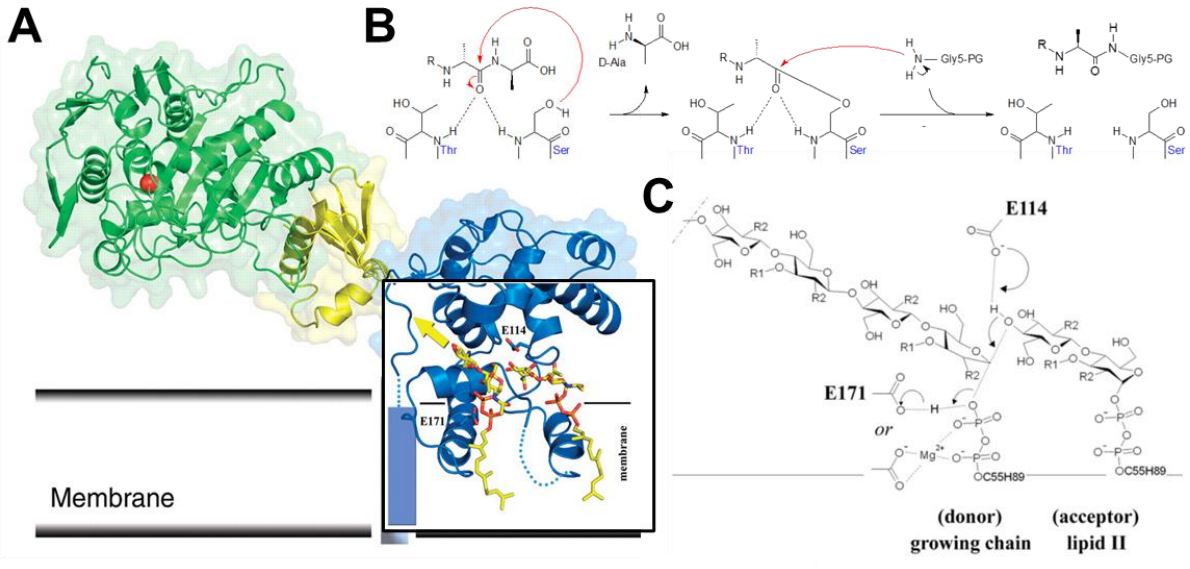

Figure 5: Structure and molecular mechanisms of enzymatic catalysis of the *S. aureus* main peptidoglycan synthase PBP2. (A) Crystal structure of *S. aureus* PBP2. Green: C-terminal transpeptidase domain with highlighted catalytic serine (red). Yellow: Linker domain. Blue: N-terminal transglycosylase domain with superimposed model of lipid II molecules (sticks) bound to the donor and acceptor sites for transglycosylation. Catalytic glutamate residues E114 and E171 are also shown as sticks. Yellow arrow denotes direction of the growing glycan chain during processive polymerization, funneling the new peptidoglycan strand towards the C-terminal transpeptidase domain. Blue bar denotes the N-terminal membrane anchor. Regions of the protein and lipid II molecules inserted into the cytoplasmic membrane are depicted accordingly. Adapted from Lovering, *et al.* (2007) with permission from AAAS. **(B)** Transpeptidase reaction mechanism. The catalytic SxxK motif forms a Michaelis complex with the amide bond of a growing glycan chains D-Ala-D-Ala terminus. The catalytic Ser acts as a nucleophile and forms a covalent ester bond with the penultimate D-Ala under condensation of the ultimate D-Ala. This ester bond is subsequently attacked by the nucleophilic ultimate amino group of the neighboring peptidoglycan strands Gly_5 bridge. This establishes an amide bond crosslink between the two peptidoglycan strands and releases the catalytic motif for the next transpeptidase reaction. H^+ ion activities and transient intermediate states not shown for simplicity. R: newly polymerized peptidoglycan strand. PG: peptidoglycan macromolecule. TPase reaction illustrated as described in Ghuysen (1991). **(C)** Transglycosylation reaction mechanism. E114 deprotonates the 4-OH group of a lipid II GlcNAc moiety. The deprotonated, nucleophilic 4-O^- group substitutes the pyrophosphate bond with the MurNAc-C1-atom of the donor peptidoglycan strand. This substitution releases the carrier lipid $C_{55}PP$ and establishes a covalent β-1,4 glycosidic bond, resulting in an elongation of the peptidoglycan strand. E171 assists the reaction via pyrophosphate protonation or stabilization of the $C_{55}PP$ leaving group. R1: OAc. R2: NHAc. Adapted from Lovering *et al.* (2007) with permission from AAAS.

Antibiotics targeting cell wall biosynthesis

The ubiquitous essentiality of cell wall biosynthesis in nearly all bacteria combined with the high number of steps, enzymes and substrates involved, and the exposed nature of its final steps (especially in gram-positive bacteria) make the CWBM one of the most relevant targets of antibiotics (Figure 6). Many natural products targeting the pathway are known, including bacterial, fungal, and human antibacterial molecules.

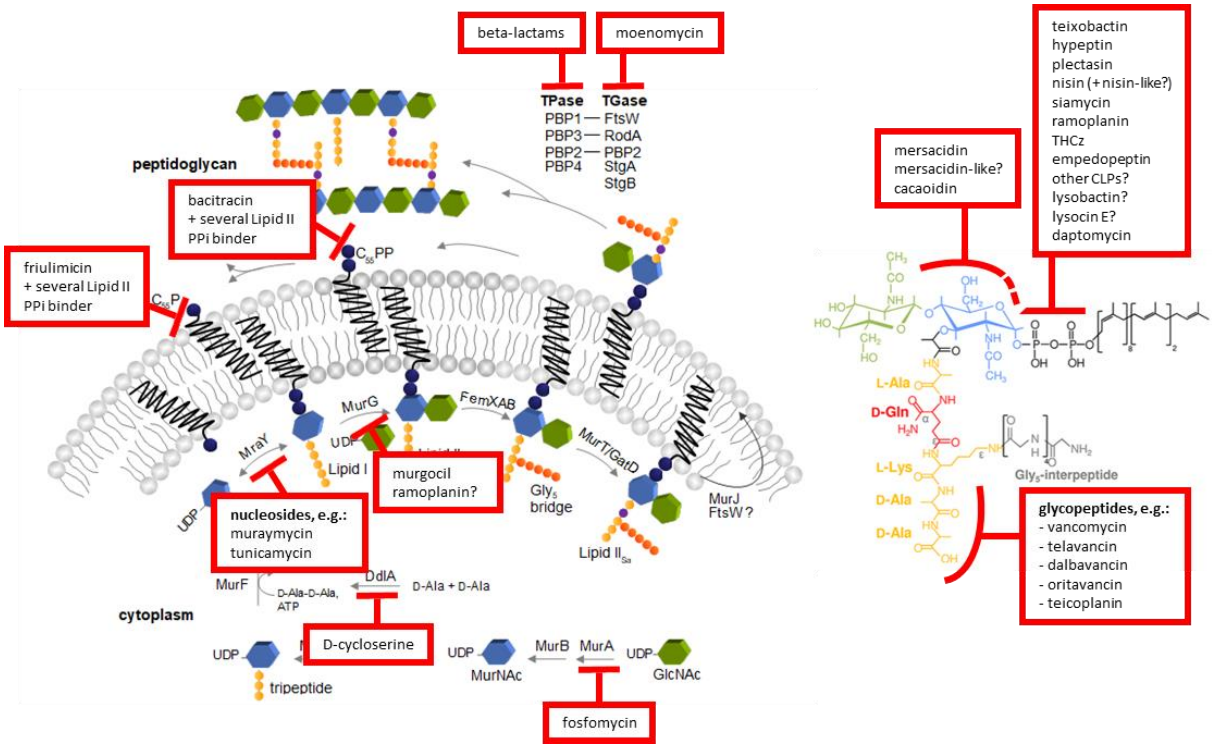

Figure 6: Schematic overview of the molecular interaction targets of antibiotics inhibiting the cell wall biosynthesis. Adapted from Schneider and Sahl (2010) with permission from Elsevier and Ulm and Schneider (2016) with permission from Springer Nature. PPi: Pyrophosphate.

Due to the biophysical protection of the cytoplasmic membrane, the intracellular synthesis steps leading up to lipid II is target to relatively few and primarily small molecule (≤ 1kDa) antibiotic classes. Fosfomycin (Figure 7A) inhibits the initial step of the pathway by irreversibly binding to the active center of MurA, leading to UDP-GlcNAc accumulation and depletion of all other cell wall precursors (Kahan *et al.* 1974; Mengin-Lecreulx *et al.* 1990). D-cycloserine (Figure 7A) inhibits DdlA, the enzyme that catalyzes the formation of the terminal D-Ala-D-Ala of the peptidoglycan pentapeptide, as well as the D-Ala producing alanine racemase Alr (Lambert and Neuhaus, 1972; Neuhaus and Lynch, 1964). MraY-mediated lipid I formation is inhibited by the class of nucleoside antibiotic compounds (Figure 7A), most prominently muraymycin and caprazamycin as well as tunicamycin[6], which acts primarily as a TarO

[6] Muraymycins, caprazamycins and tunicamycins are groups of structurally highly similar nucleoside natural products. They naturally occur in mixtures and share a common mechanism of action (Nakaya *et al.* 2022). For

inhibitor (a WTA biosynthesis protein, Campbell *et al.* 2011; Nakaya *et al.* 2022). MurG, the enzyme catalyzing the formation of lipid II from lipid I and UDP-GlcNAc, in inhibited by the steroid-like compound murgocil (Figure 7B, Mann *et al.* 2013). Additionally, the lipoglycodepsipeptide ramoplanin was suggested to bind to lipid I, thereby inhibiting lipid II formation, although this has been criticized due to a missing rationale for cell membrane crossing of the large compound (Figure 7C, X. Fang *et al.* 2006; Lo *et al.* 2000; Somner *et al.* 1990).

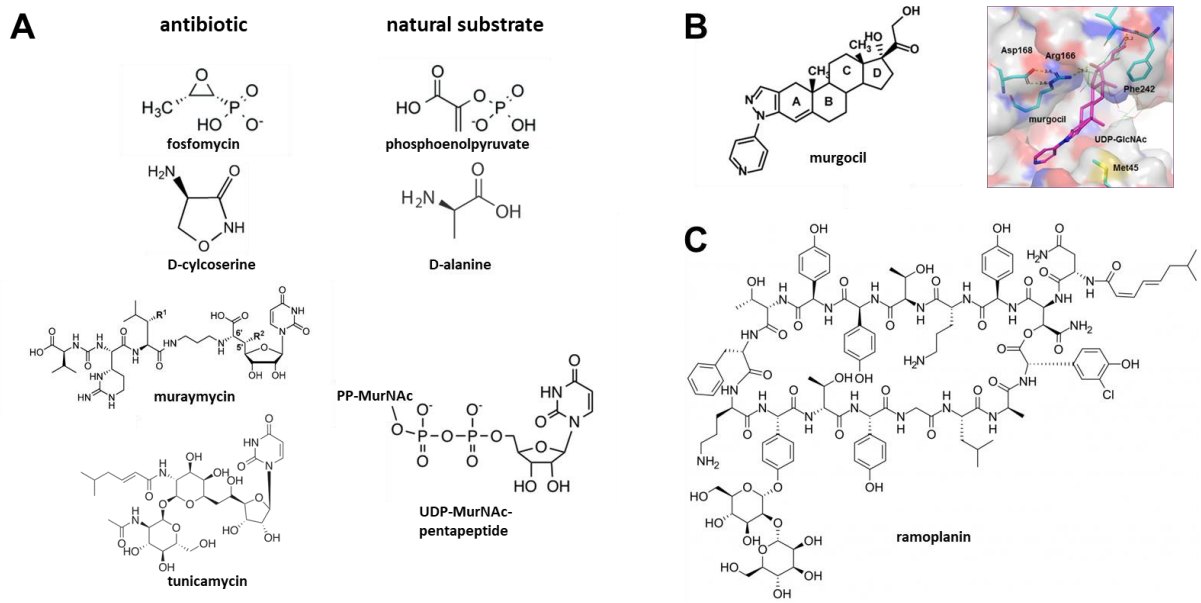

Figure 7: Overview of CWBM inhibitors acting on intracellular targets. (A) Chemical structures of intracellular, substrate-mimicking antibiotics and their respective natural substrate counterparts. **(B)** The steroid-like, intracellular acting murgocil does not directly mimick a natural substrate of MurG. Instead, it likely occupies the catalytic site via unique non-covalent interactions, competitively inhibiting access of the substrate UDP-GlcNAc. Left: Chemical structure of murgocil. Right: Molecular modelling of murgocil and UDP-GlcNAc binding to the active site of MurG. Adapted with permission from Mann *et al.* (2013). Copyright 2013 American Chemical Society. **(C)** The large glycolipodepsipeptide ramoplanin was proposed to inhibit MurG by binding to the intracellular lipid I. However, it was suggested that the large structure is unable to traverse the cytoplasmic membrane barrier (X. Fang *et al.* 2006; Lo *et al.* 2000; Somner *et al.* 1990).

In contrast to this relatively small set of intracellular acting antibiotics, a remarkable variety of compounds inhibits the final steps of the extracellular PGS in *S. aureus*. Without the protective barrier of the cell membrane, the range of suitable chemical structures and molecule sizes is substantially broadened, ranging from small molecules like beta-lactams to heavily modified and bulky peptides. PGS inhibiting antibiotics can be functionally divided into protein- and substrate-binding compounds.

purpose of intelligibility, this work refers to these mixtures as “muraymycin”, “caprazamycin” and “tunicamycin” for each respective group of natural products.

Protein-binding antibiotics interact with the active center of the enzymes that catalyze PGS. Moenomycin[7] inhibits TGase reactions by occupying the donor strand site and thereby prevents the initiation of the processive glycan strand polymerization (Figure 8A,B, Bury *et al.* 2014; Gampe *et al.* 2011; Heaslet *et al.* 2009; Lovering *et al.* 2007; Van Heijenoort *et al.* 1980). This active site binding is non-covalent, but of high affinity, which results in potent antibiotic activity (Boes *et al.* 2020; Gampe *et al.* 2011, 2013). The large and most significant group of beta-lactam antibiotics inhibits TPase reactions by chemical mimicry of the D-Ala-D-Ala amide bond, which leads to a covalent binding of the antibiotic to the TPase active site and nearly irreversible inhibition of enzymatic activity (Figure 8C,D, Blumberg *et al.* 1971; Eagle 1954; J. M. Ghuysen 1991; J.-M. Ghuysen 1994; Kuzin *et al.* 1995).

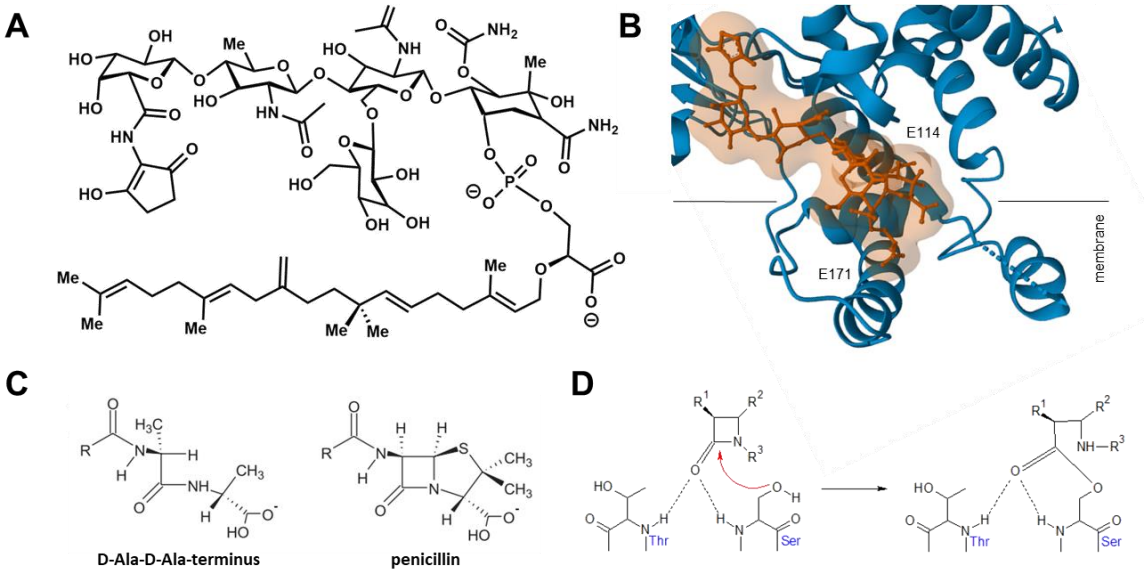

Figure 8: Molecular mechanisms of PGS inhibition via enzyme interaction by moenomycin and beta-lactam antibiotics. (A) Chemical structure of moenomycin A. **(B)** Crystal structure of moenomycin A (orange) bound to the N-terminal transglycosylase domain of PBP2 (blue, see Figure 5), thereby occupying the donor site of the domain. Illustration built using PDB entry 2OLV from Lovering *et al.* (2007). **(C)** Structural similarity of the peptidoglycan pentapeptide D-Ala-D-Ala terminus (R: peptidoglycan/lipid II) and the core of beta-lactam antibiotics, represented by the general penicillin structure (R: specimen-specific penicillin rest). **(D)** Mechanism of beta-lactam inhibition of transpeptidation. The core beta-lactam motif mimics the D-Ala-D-Ala amide bond (see Figure 5). The cyclic amide group is opened by the nucleophilic attack of the catalytic Ser, establishing a covalent ester bond between enzyme and antibiotics. In contrast to the natural substrate version, this covalent bond is highly stable and cannot be cleaved (except for very slow hydrolysis), thus inhibiting the transpeptidase. R^1-R^3: specimen-specific beta-lactam rests. Illustrated as described in J. M. Ghuysen (1991), J.-M. Ghuysen (1994) and Kuzin *et al.* (1995).

[7] Moenomycins are a group of structurally highly similar phosphoglycolipids, which naturally occur in mixtures and share a common mechanism of action (Ostash *et al.* 2010). For purpose of intelligibility, this work refers to these mixtures as “moenomycin”.

Complementary to these enzyme-targeting antibiotics, a large variety of compounds inhibit PGS by binding to the reaction substrates. Due to its central role as ultimate precursor, lipid II is a most prominent target structure (Figure 6, Grein *et al.* 2019; Schneider and Sahl 2010). As a product of a complicated biosynthesis involving multiple proteins in different cellular compartments, its structure is highly conserved. Changes in the chemical moieties of lipid II for resistance development are rare to non-existent. This and the exposed location outside the cell membrane have led to the description of lipid II as the "Achilles' heel" of bacteria and presumably explains at least partially its role as the target of many natural product antibiotics (Breukink *et al.* 2006; Schneider and Sahl 2010). A wide and structurally diverse range of antibiotic compounds utilize the binding to lipid II to achieve their antibiotic activity through different modes of molecular interaction with the ultimate peptidoglycan precursor.

The (to present knowledge) immutable pyrophosphate (PPi) moiety is the central interaction target of multiple antibiotic classes of diverse origin. Teixobactin complexes the PPi via a four-membered amino acid ring motif (Figure 9A, Ling *et al.* 2015; Shukla *et al.* 2020, 2022). The structurally similar hypeptin likely interacts with lipid II in a comparable manner (Wirtz *et al.* 2021). The lantibiotic nisin (see also chapter 1.6) forms a complex with the lipid II PPi via a two-ring system in a binding pattern referred to as pyrophosphate-cage (Figure 9B, Hsu *et al.* 2004). Multiple other lantibiotics with a similar binding motif were shown to also interact with lipid II and are therefore often categorized as nisin-like (Bonelli *et al.* 2006; Münch *et al.* 2014; Paiva *et al.* 2011; Parisot *et al.* 2008; L. Smith *et al.* 2008). Multiple peptide defensins, most prominently plectasin, achieve high affinities to the PPi moiety via specific folds of their unmodified amino acid sequence (Figure 9C, Essig *et al.* 2014; Oeemig *et al.* 2012; T. Schneider Kruse *et al.* 2010). Additionally, lipid II-binding capabilities have been confirmed for a range of other fungal (copsin, eurocin), invertebrate (Cg-Defh1, Cg-Defh2, and Cg-Defm) and also human (hNP1 and hBD3) defensins (Gueguen *et al.* 2006; Leeuw *et al.* 2010; Schmitt *et al.* 2010; V. Sass *et al.* 2010; Oeemig *et al.* 2012; Essig *et al.* 2014). Furthermore, the lassopeptide Siamycin (S. Tan *et al.* 2019) as well as the synthetic compound class of THCz (Reithuber *et al.* 2021) were also found to bind to the PPi of lipid II via biochemical elucidation of the minimal binding motif. However, structural data for these interactions are not yet available. In contrast, crystallographic structures of ramoplanin dimers suggests PPi as likely interaction moiety of this antibiotic, but structures of ramoplanin:lipid II complexes or biochemical evidence for this hypothesis are still missing (Hamburger *et al.* 2009; Hu *et al.* 2003). Additionally, the cyclic peptide antibiotics lysobactin and lysocin E bind to lipid II, likely via PPi interactions (W. Lee *et al.* 2016; Santiago *et al.* 2018). Similarly, guanidine-containing cyclic lipopeptides (CLPs, empedopeptin, plusbacins, tripopeptins) were also suggested to interact with lipid II. They all inhibit peptidoglycan synthesis and share a high structural similarity (Hashizume *et al.* 2011; S. J. Kim Singh *et al.* 2013; Maki *et al.* 2001; Müller *et al.* 2012). As of now, binding to lipid II was shown only for empedopeptin, which interacts with the PPi moiety, most likely as a dimerized Ca^{2+} complex (Müller *et al.* 2012). Elucidation of the structural features of this interaction as well as an extensive investigation of the differences and similarities of the different specimen of the CLPs has not been described as of now.

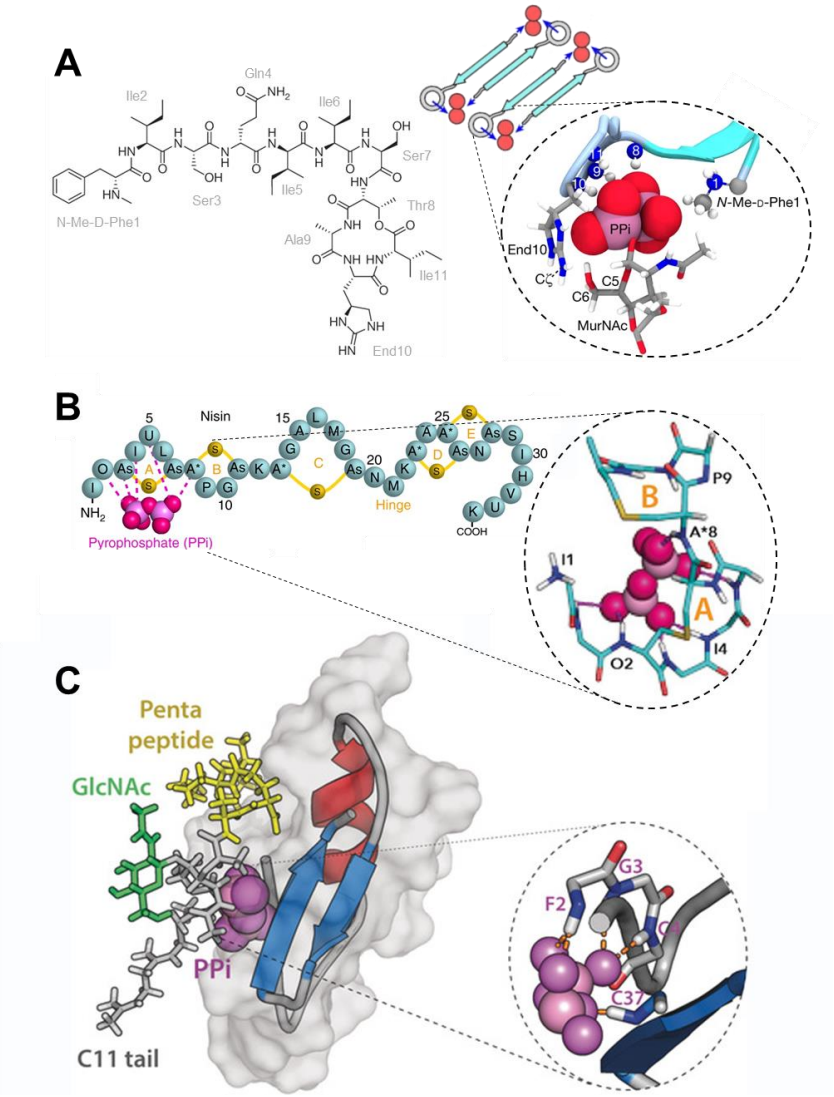

Figure 9: Molecular mechanisms of interaction with the lipid II PPi moiety. (A) Chemical structure of teixobactin (left) and schematic representation of antiparallel β-sheets formed by teixobactin:lipid II complexes with a detailed solid-state NMR structure of the PPi binding (right). The End10 interacts with the MurNAc sugar and coordinates the PPi together with the amino acid backbone of Ser8 – Ile11 and the N-terminus of a second antiparallel teixobactin molecule. Adapted from Ling *et al.* (2015) with permission from Springer Nature and Shukla *et al.* (2022). **(B)** Amino acid sequence of the post-translationally modified lantibiotic nisin interacting with the lipid II PPi moiety (left). The NMR structure (right) shows, how the lanthionine rings A – B enable a highly structured complex formation coordinated by Ile1 – Pro9, encaging the PPi group. Adapted from Medeiros-Silva *et al.* (2019). **(C)** NMR structure showing the complex formation of plectasin with a shortened C_{11} lipid II (left). The N-terminus coordinates the PPi moiety together with the C-terminal β-strand (right). Adapted from Medeiros-Silva *et al.* (2019).

Notably, some of these compounds also interact with the C_{55}PP and/or C_{55}P carrier intermediates, albeit with often reduced affinity. Thus, while most of the PPi interacting antibiotics show the highest affinity towards lipid II, the additional binding capabilities to other carrier intermediates likely modulates and even increases the antibacterial activity of these compounds (Grein *et al.* 2020; Homma *et al.* 2016; W. Lee *et al.* 2016; Ling *et al.* 2015; Reithuber *et al.* 2021; K. Scherer *et al.* 2013; S. Tan *et al.* 2019; Wirtz *et al.* 2021). Interestingly, multiple compounds also target the bactoprenol carrier lipids exclusively, e.g.,

bacitracin (binds C_{55}PP, Economou *et al.* 2013; Stone *et al.* 1971) and friulimicin (binds C_{55}P, Schneider *et al.* 2009). This was also suggested as potential mechanism of action for the CLP tripropeptin C (Hashizume *et al.* 2011), although the lipid II interaction of the structurally similar empedopeptin suggests lipid II as the primary target of all CLPs (see above).

In addition to this variety of PPi interacting compounds, the group of mersacidin-like lantibiotics also interact with the headgroup of lipid II (Böttiger *et al.* 2009; Brötz, Bierbaum *et al.* 1998; Brötz *et al.* 1997; S.-T. D. Hsu *et al.* 2003; Martínez *et al.* 2008; Oman *et al.* 2009; Wiedemann, Böttiger *et al.* 2006, 2006). However, mersacidin was shown to strictly require presence of the first sugar and the pentapeptide moieties to establish binding (Deisinger *et al.* 2023). Similar holds true for the recently discovered, first-in-class lanthidin antibiotic cacaoidin, which also requires a phosphate-sugar moiety, but not the pentapeptide of lipid I/ lipid II for interaction with the precursors (Deisinger *et al.* 2023; Ortiz-López *et al.* 2020). Without structural elucidation, it remains unclear how exactly these compounds bind to the ultimate cell wall precursor and what precise role the PPi moiety plays in this interaction.

The second critical binding moiety of lipid II is the pentapeptide, as it is the target moiety of glycopeptide antibiotics, which are clinically very relevant due to their status as reserve-antibiotics against MRSA (Geriak *et al.* 2019; Rieg *et al.* 2017). The overwhelming majority of glycopeptides with known antibiotic activity acts by binding to the D-Ala-D-Ala terminus of the peptidoglycan building block[8] (Blaskovich *et al.* 2018; Reynolds 1989). The general mechanism of the interaction is highly conserved within the glycopeptide antibiotics and best researched for vancomycin. The compound binds to the amino acid backbone of the D-Ala-D-Ala terminus with extremely high affinity and specificity (Figure 10A). The resulting complex (Figure 10B) prevents utilization of the peptidoglycan building block as substrate for TGase or TPase reactions in a highly effective manner (Figure 10C, Anderson *et al.* 1965; Bordet *et al.* 1970; McCormick *et al.* 1955). This is further improved by dimerization of the vancomycin:target complexes, increasing the binding strength substantially (Beauregard *et al.* 1995; Jia *et al.* 2013; Nitanai *et al.* 2009).

[8] Notable exceptions are complestatin and corbomycin, which bind to the peptidoglycan network, thereby interfering with autolysis regulation (Culp *et al.* 2020).

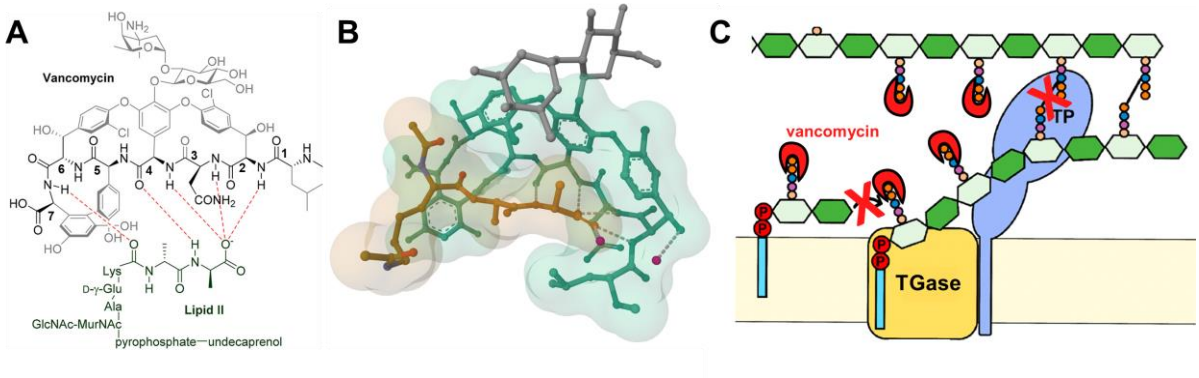

Figure 10: Molecular mechanism of action of vancomycin. (A) Chemical structure of vancomycin and the lipid II D-Ala-D-Ala terminus. A total of five hydrogen bonds establishes a strong binding between the vancomycin peptide backbone and the terminal dipeptide of lipid II. Adapted from Blaskovich *et al.* (2018). **(B)** Crystal structure of vancomycin (peptide in green, disaccharide in grey) binding to the shortened lipid II pentapeptide analogue Di-Ac-Lys-D-Ala-D-Ala (orange). The cross-linked, rigid three-ring system of residues 2, 4 and 6 facilitates the precise coordination of the target moiety by the antibiotics amino acid backbone. Illustration built using using PDB entry 1FVM from Nitanai *et al.* (2009). **(C)** Schematic representation of peptidoglycan biosynthesis inhibition by vancomycin (red). Binding to lipid II and nascent peptidoglycan strands inhibit both transglycosylase and transpeptidase reactions. Adapted with permission from S. Kumar *et al.* (2022). Copyright 2022 American Chemical Society.

Notably, the target motif of vancomycin is found in lipid II, nascent peptidoglycan strands and furthermore in uncrosslinked pentapeptides within the cell wall mesh. However, the effective peptidoglycan synthesis inhibition of glycopeptides is primarily governed by interaction with lipid II (and additionally the nascent peptidoglycan, Figure 10C). The “off-target” binding to uncrosslinked pentapeptides within the mature cell wall reduces the overall efficacy of vancomycin. Some *S. aureus* strains utilize this phenomenon to reduce susceptibility to the glycopeptide by cell wall thickening and decreased crosslinking activity in the vancomycin-intermediate *S. aureus* (VISA) phenotype (Cui *et al.* 2000, 2003, 2006; P. M. Pereira *et al.* 2007). To counteract this disadvantage, semi-synthetic derivates of natural vancomycin-like glycopeptides were developed to increase the specificity towards lipid II, primarily by addition of lipophilic appendages, which led to the class of lipoglycopeptides (Figure 11).

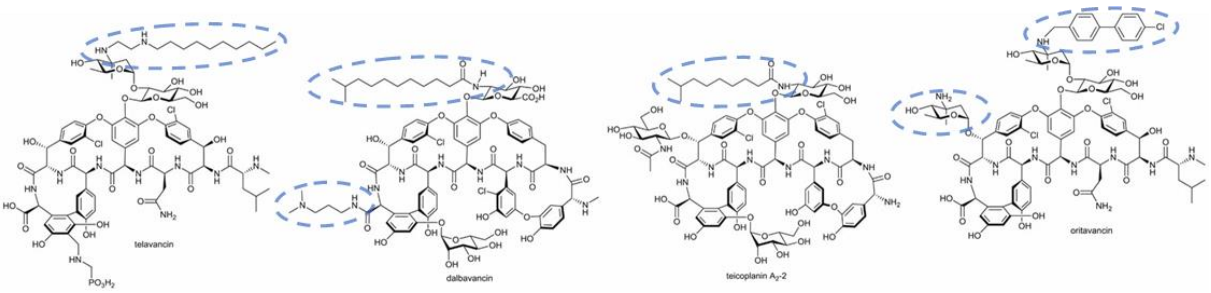

Figure 11: Chemical structures of (from left to right) telavancin, dalbavancin, teicoplanin A_2-2 and oritavancin. Critical moieties for modulating the antibacterial activity of the glycopeptide scaffold are highlighted. Adapted from Butler *et al.* (2014), reproduced with permission from SNCSC.

As such, telavancin and dalbavancin both utilize acyl-chains for hydrophobic interaction with lipid II and the cytoplasmic membrane, which translates to an improved binding to the ultimate peptidoglycan precursor both *in vitro* and *in vivo* (M. Cheng, Ziora *et al.* 2014; Higgins *et al.* 2005; Lunde *et al.* 2009, 2010; Song *et al.* 2012; Treviño *et al.* 2014). The naturally occurring lipoglycopeptide teicoplanin[9] was shown to act similarly *in vitro* (Kim *et al.* 2013; Treviño *et al.* 2014). Furthermore, oritavancin, another vancomycin-derived lipoglycopeptide with a chlorophenyl-benzyl- and a separate aminosugar-appendage, also shows substantially improved lipophilic interaction as well as improved dimerization capabilities (Allen *et al.* 1997). Additionally, oritavancin was found to interact with the interpeptide bridges of *S. aureus* and *Enterococcus faecium* (S. J. Kim *et al.* 2008, 2009; Kimi *et al.* 2006; Münch *et al.* 2015; Patti *et al.* 2009). Apart from these prominent examples, numerous other vancomycin-like glycopeptides exist (Blaskovich *et al.* 2018).

The glycopeptide scaffold was proven to be highly effective for antibiotic treatment and very accessible for semi-synthesis. This resulted in an extraordinary variety of approaches to improve upon the scaffold, with the lipophilic appendages being the most successful so far to increase antibiotic activity (Blaskovich *et al.* 2018). This is especially relevant due to the resistance developments against vancomycin (see chapter 1.2). Beyond the VISA phenotype, vancomycin-resistant *S. aureus* (VRSA) and vancomycin-resistant enterococci (VRE) can produce lipid II variants with structural substitutions at the glycopeptides target moiety. These strains produce a set of enzymes that catalyze the substitution of the terminal D-Ala with D-Lactate or D-Serine, which drastically reduces glycopeptide binding (Billot-Klein *et al.* 1994; Boyd *et al.* 2008; Bugg *et al.* 1991; Healy *et al.* 2000; Reynolds *et al.* 1994; Z. Wu *et al.* 1995). However, the increased affinities of the lipoglycopeptides towards lipid II can counteract these resistance mechanisms at least partially or sometimes completely, depending on the specificities of the resistance type and glycopeptide structure (Allen *et al.* 1997; Butler *et al.* 2014; C. M. Hill *et al.* 2010; R. N. Jones *et al.* 2013; Karlowsky *et al.* 2015; Kosowska-Shick *et al.* 2009; Patti *et al.* 2009; Pfaller *et al.* 2010; Roberts *et al.* 2015; Zhanel *et al.* 2010). Furthermore, approaches to optimize the glycopeptide scaffold for binding to these vancomycin-resistant lipid II variants are discussed and evaluated (Blaskovich *et al.* 2018).

Apart from the structural variety of lipid II binders, the functional effects of these interactions also vary substantially. Vancomycin, mersacidin-like lantibiotics, plectasin, siamycin and THCz reportedly reach their antibacterial activity exclusively by preventing the utilization of lipid II as PGS substrate (see above). In contrast to that, nisin shows substantial membrane interaction following lipid II complexation and forms large aggregates consisting of membrane-disrupting lipid II:nisin complexes. Formation of these lead to substantial membrane damage, resulting in rapid cell death (Jensen *et al.* 2020; Medeiros-Silva *et al.* 2018; K. Scherer *et al.* 2013; K. M. Scherer *et al.* 2015; Tol *et al.* 2015). In a comparable mechanism, the unique depsipeptide daptomycin forms tripartite complexes with cell wall precursors

[9] In fact, teicoplanins are a family of structurally highly similar phosphoglycolipids, which naturally occur in mixtures and share a common mechanism of action (Barna *et al.* 1984; Butler *et al.* 2014; Chmara *et al.* 1991). For purpose of intelligibility, this work refers to these mixtures as “teicoplanin”.

and anionic phospholipids, leading to massive membrane disarrangements and cell death within minutes of treatment (Grein *et al.* 2020; Müller *et al.* 2016). Less drastic membrane effects have been reported for lipoglycopeptides, where higher concentrations were observed to induce membrane depolarization and permeabilization (Belley *et al.* 2009, 2010; Domenech *et al.* 2009, 2010; Higgins *et al.* 2005; Lunde *et al.* 2009). Teixobactin was also suggested to act membrane-disruptive, as the formation of beta-sheet fibrils consisting of antiparallel teixobactin:lipid II complexes was observed to have membrane thinning consequences using atomic force microscopy and solid-state NMR. However, information on the *in vivo* relevance of this effect for the antibacterial activity is still limited (Shukla *et al.* 2020, 2022). Additionally, membrane thinning and membrane potential disrupting effects were also suggested to play a role in the mechanism of action of the CLP plusbacin A_3 (O'Connor *et al.* 2017). Still, the lipid II-binding capability of the structurally similar empedopeptin suggests substrate blocking as a primary mechanism of action for CLPs (see above).

Ambiguities like these exemplify a common problem. To date, the central paradigm of an antibiotics mechanism of action is the compound-target interaction. Mechanism of action studies and descriptions of new antibiotic compounds regularly focus on the molecular basis of antibiotic activity and suffice with the observation of growth inhibition (or some variant thereof, e.g., time-kill kinetics) for the cellular effects. Consequently, there is a remarkable body of knowledge on the biomolecular details of antibiotic action, as described above. The interactions between antibiotics and the enzymes, they are inhibiting, or the substrates, they are binding, are elucidated to the utmost details down to the atomic level with structural methods like crystallography and NMR. Kinetic and thermodynamic parameters of these interactions are well-researched and subjected to elucidation of critical moieties in antibiotics and targets alike. However, this level of understanding is rarely achieved beyond the molecular level. Strikingly, the most immediate cellular effects on the structural-functional integrity of biosynthetic machineries or the cytoplasmic membrane remain unclear to fully elusive for many well-established antibiotics. Likewise, impact of target inhibition on cellular homoeostasis, e.g., transcriptomic, proteomic, and metabolic changes as well as the regulatory mechanisms governing these responses are seldom well characterized, especially on a temporal axis. Extensive work on elucidating the minimal binding motifs of lipid II-binding antibiotics revealed, that these compounds often interact with multiple membrane bound precursors, which includes C_{55} carrier lipids, but in some cases also precursors of other pathways like WTA or capsule biosynthesis (Homma *et al.* 2016; Reithuber *et al.* 2021; Wirtz *et al.* 2021). Likewise, some antibiotics interact with multiple enzymatic steps of the same (cycloserine) or different pathways (tunicamycin). The cellular impact of these "multi-targeting compounds" and how the interaction with individual targets enhances or diminishes overall antibiotic activity remains largely hypothetical to date. Consequentially, this complicates the evaluation of individual aspects of antibiotic action for future drug development. This is despite singular advances, e.g., regarding the "dual-targeting" of teixobactin being closely associated with cell lysis (Homma *et al.* 2016). Similar problems apply to the multifaceted binding modes of glycopeptide antibiotics and the role of different target sites (lipid II variants, nascent peptidoglycan, mature cell wall) for their differential activity. Despite the high structural resemblance within this antibiotic class, the impacts on TGase/TPase activity, precursor accumulation and cell lysis differ substantially (Chmara *et al.* 1991; Homma *et al.* 2016; Lunde *et al.* 2009; Münch *et al.* 2015; Patti

et al. 2009; Qiao *et al.* 2017; Sidders *et al.* 2023; Song *et al.* 2012). Correspondingly, underlying mechanisms governing different resistance mechanisms against glycopeptides and how some of the antibiotics circumvent certain types of resistance is not well understood (Blaskovich *et al.* 2018; Butler *et al.* 2014). Furthermore, the large group of beta-lactam antibiotics show substantially diverse affinities towards PBPs (Asli *et al.* 2016; Farha *et al.* 2013; Georgopapadakou *et al.* 1986, 1980; Hayes *et al.* 1981; Kosowska-Shick *et al.* 2010; Ono *et al.* 2005; Sauvage *et al.* 2008; Shahid *et al.* 2009; Varghese *et al.* 2021). Additionally, the set of PBPs and their respective cellular roles are highly species-specific (Egan *et al.* 2017; Pinho *et al.* 2013; Sauvage *et al.* 2008). As a results, the full scope of differential target affinities and their influence on the cellular impact of these clinically most important antibiotics is still not fully elucidated after decades of continuous research and development. These open questions reveal striking deficits in the knowledge of how antibiotic activity translates from molecular target binding to growth inhibition and killing. This becomes even further apparent, once the cellular consequences of antibiotic target inhibition on affiliated and highly coordinated processes are considered.

Coordination of cell wall biosynthesis and cell division of *S. aureus*

In many species including *S. aureus*, the cell division septum is the main region of PGS (Figure 12A,B, Lund *et al.* 2018; Monteiro *et al.* 2018; Pinho *et al.* 2013). Cell wall biosynthesis is closely coordinated with cell division. This ensures accurate construction of new cell wall material along the division plane during septum constriction and closure, which ultimately results in daughter cell separation and cell splitting (Barrows *et al.* 2021; Lund *et al.* 2018; Monteiro *et al.* 2018; Pazos *et al.* 2018; Pinho *et al.* 2013). Both processes share a deeply integrated structural-functional organization. This is illustrated by the tight spatio-temporal connection between PGS and cell division machineries and the high degree of interaction between their components. This includes multiple proteins that unify essential roles for both processes within one structure. Furthermore, cell wall biosynthesis and maturing are intertwined with cell division and cell cycle progression via multiple regulatory systems. (Atilano *et al.* 2010; Lund *et al.* 2018; Martínez-Caballero *et al.* 2021; Monteiro *et al.* 2015, 2018, 2019; S. F. F. Pereira *et al.* 2007, 2009; Pinho *et al.* 2005; Reichmann *et al.* 2019; Steele *et al.* 2011; Veiga *et al.* 2023; Wacnik *et al.* 2022). Accordingly, the CWBM components responsible for lipid II translocation and incorporation of peptidoglycan building blocks into the cell wall are all almost exclusively localized at the septum of *S. aureus* (Figure 12A,B, Monteiro *et al.* 2018).

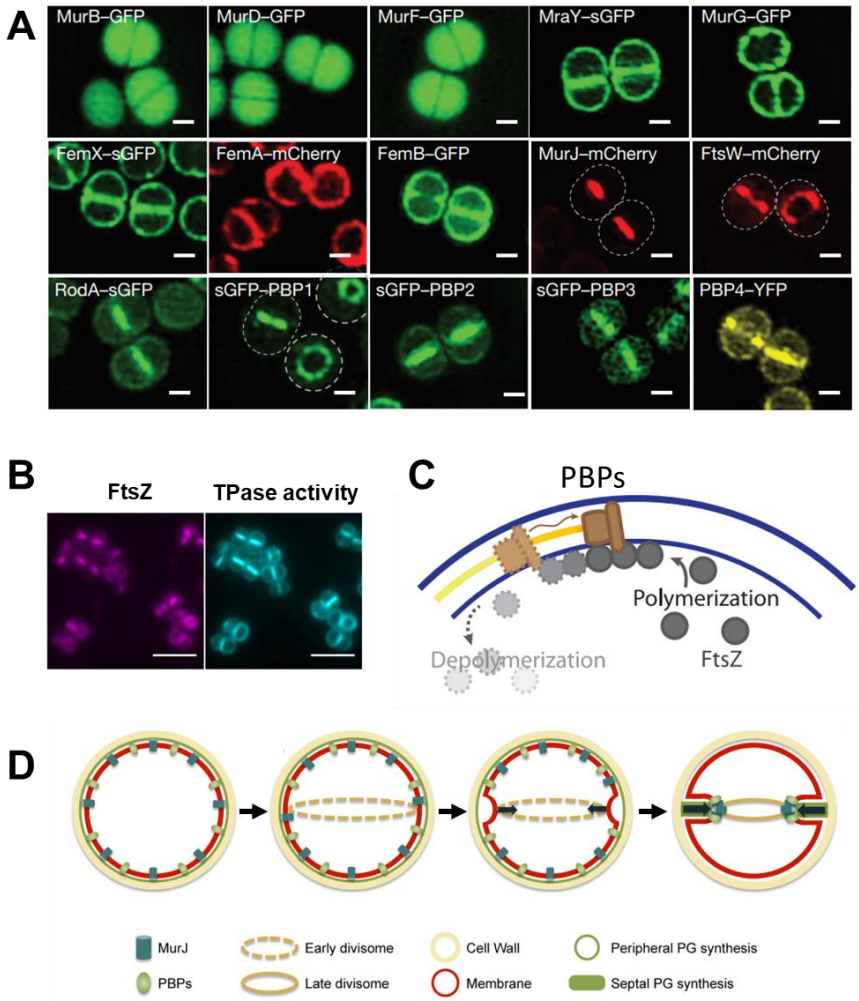

Figure 12: *S. aureus* cell wall biosynthesis is highly coordinated with cell division. (A) Fluorescence microscopy micrograph of fluorescently labelled cell wall biosynthesis proteins in *S. aureus*. Proteins that catalyze cytoplasmic steps of the pathway show homogenous cytoplasmic localization. Proteins that catalyze membrane-bound intracellular steps of the pathway show unspecific membrane-associated localization. The lipid II flippase MurJ and all enzymes that catalyze the extracellular PGS show a distinct septal focus in their localization pattern. Scale bars 0.5 µm. From Monteiro *et al.* (2018), reproduced with permission from SNCSC. **(B)** The co-localization of FtsZ-SNAP and TPase activity (visualized with the fluorescent D-amino acid HADA, see chapter 3.4.4) in cells of *S. aureus* illustrates the spatial coordination of cell division and cell wall biosynthesis. Scale bars 3 µm. Adapted from Lund *et al.* (2018). **(C)** The cytoplasmic cell division protein FtsZ forms treadmilling filaments via front-end polymerization and back-end depolymerization. Condensed FtsZ filaments serve as scaffold for the processive septal peptidoglycan synthesis machinery. Adapted from Yang *et al.* (2017) with permission from AAAS. **(D)** Model of the spatio-temporal organization of cell wall biosynthesis throughout the cell cycle of *S. aureus*. If no division site is present, CWBM components localize unspecifically within the cytoplasmic membrane and enable peripheral PGS. Upon formation of the early divisome, a first constriction phase is initiated. This constriction is driven by early divisome components and is dependent on FtsZ treadmilling. Recruitment of MurJ constitutes the turning point for late divisome formation, which includes the recruitment of CWBM components (including PBPs) to the septum. This leads to an increase in septal PGS and further septum constriction independent of FtsZ treadmilling. Adapted from Monteiro *et al.* (2018), reproduced with permission from SNCSC.

The key protein of bacterial cell division is the cytoplasmic protein FtsZ. GTPase activity of individual FtsZ molecules enables polymerization into filaments. The dynamic front-assembly and end-disassembly of these filaments leads to a net circular motion of FtsZ filaments along the mid-cell circumference, which is referred to as treadmilling. This process enables mid-cell condensation into a dense Z-ring, which subsequently provides a scaffold for septal cell wall biosynthesis (Figure 12C, Baranova *et al.* 2020; Bisson-Filho *et al.* 2017; Monteiro *et al.* 2018; Pazos *et al.* 2018; Squyres *et al.* 2021; Whitley *et al.* 2021). To ensure accurate Z-ring construction, a large cell division machinery governs placement, maintenance, and spatio-temporal organization of FtsZ, its GTPase activity and filament formation behavior. This complex regulatory system includes at least 17 proteins in *S. aureus*, which ensure functional cell division, cell shape maintenance, and play roles in pathogenesis and antibiotic susceptibility (Lund *et al.* 2018; Myrbråten *et al.* 2022; Pinho *et al.* 2013; Tinajero-Trejo *et al.* 2022; Veiga *et al.* 2023). The regulation of divisome formation and concomitant cell division progression also governs recruitment and localization of key CWBM components (Figure 12D). E.g., the cognate pairs PBP1-FtsW and PBP3-RodA are recruited to the septum very early in cell division. The activity of the essential PBP1-FtsW pair was proven to be crucial for Z-ring placement and cell cycle progression to the phases of septum constriction (S. F. F. Pereira *et al.* 2007, 2009; Reichmann *et al.* 2019; Wacnik *et al.* 2022). This example illustrates, that core CWBM proteins also have key roles in the sophisticated early divisome regulation, which essentially revolves around Z-ring formation as the central factor in early cell division. Accordingly, the FtsZ treadmilling enabling this Z-ring formation is essential in early cell division in *S. aureus.* Importantly, this extents to a first phase of septum constriction, corroborating hypotheses that propose treadmilling as a driving force of septum constriction (Coltharp et al. 2016; Erickson et al. 2010; McQuillen et al. 2020; Nguyen et al. 2019, 2021; Osawa et al. 2013; Szwedziak et al. 2014). However, treadmilling was shown to be redundant in *S. aureus* after septal recruitment of the CWBM component MurJ. The lipid II flippase localizes to the septum in direct dependence on the divisome sub-complex DivIB-DivIC–FtsL. Importantly, its septal lipid II translocation activity significantly increases PGS activity at the division site, which enables further septum constriction and subsequent cell separation even without active FtsZ treadmilling (Monteiro *et al.* 2018).

The multiple key roles, essential proteins of the CWBM play in cell division clearly illustrate how integrated these two essential processes of bacterial life are. However, the precise roles of PGS throughout cell division remain indistinctly defined. Even less is known about the impact of antibiotics on the spatio-temporal organization of the CWBM and the coordination of PGS and cell division. This is especially relevant due to the diversity of targets and molecular mechanisms of antibiotics targeting the cell wall biosynthesis pathway. It is not well investigated, if and how this variety translates into differential consequences of treatment on a cellular level. The level of molecular interaction is often precisely understood, and long-term impact on the culture level are also commonly addressed (bacteriostatic, bactericidal, bacteriolytic etc.). However, a substantial knowledge gap exists between these different levels of antibiotic action. Understanding how complex cellular effects emerge from molecular target interaction and how they impact the organization of deeply integrated cellular processes (such as CWBM and cell division) is a prerequisite for a comprehensive theory of how antibiotics work and what distinguishes effective from ineffective drugs. Achieving this knowledge is critical for an innovative and

rational drug design. A comprehensive understanding of the cellular impact as part of an antibiotics mechanism of action is urgently needed to fill this gap.

1.4. The *S. aureus* iron-regulated surface determinant (Isd) heme acquisition system

The *S. aureus* cell wall is not only highly relevant as antibacterial target itself, it also serves as scaffold for multiple physiologically relevant pathway components, which themselves constitute targets of anti-infective strategies. One promising approach is reduction of pathogenicity, thereby assisting the human immune system in infection containment. Part of this category is the strategy to prevent the pathogens access to essential resources for growth within the host-infection environment. This aims to decrease pathogenic proliferation, giving the immune system the necessary advantage to contain and eradicate the infection. Iron is one of the best subjects for such a strategy. The trace element is vital for virtually all biological life as it is an essential redox factor within multiple essential processes ranging from DNA replication to respiration and beyond. The combination of its high relevance and low abundance constitutes iron as a scarce and valuable resource for both host and pathogen. Accordingly, the human immune system harbors multiple systems to limit iron availability for potential intruders, a process termed nutritional immunity (Murdoch *et al.* 2022). However, pathogens circumvent these lines of defense with sophisticated strategies for iron-scavenging, most importantly the capture of iron from heme groups, which is the prominent complexation of iron in hemoglobin proteins for transport within the human blood (Farrand *et al.* 2013; Le Maréchal *et al.* 2011; Pishchany *et al.* 2014; Skaar and Schneewind 2004; Torres *et al.* 2006; Visai *et al.* 2009; Yeung *et al.* 2016).

S. aureus harbors an elaborate heme acquisition machinery named named iron-regulated surface determinant (Isd) system (Figure 13). It consists of nine components (IsdA-I), which funnel the iron-containing heme through multiple cellular compartments from the outermost surface of the cell wall (IsdA, IsdB, IsdH), through the peptidoglycan mesh (IsdC), and over the cell membrane into the cytoplasm (IsdE, IsdF and potentially IsdD), where the iron is made available for the bacterial cell (IsdG, IsdI). The sortases SrtA and SrtB anchor IsdA-C and -H to the cell wall structure (Hazmanian *et al.* 2003; Marraffini *et al.* 2004; Mazmanian *et al.* 2002; Zong *et al.* 2004), where IsdB and -H capture hemoglobins from the surrounding medium and remove the heme groups (Dickson *et al.* 2014; Pishchany *et al.* 2014; Sheldon *et al.* 2015; Torres *et al.* 2006). IsdA was suggested to assist this heme removal and has been shown to relay the heme groups through the peptidoglycan mesh in concert with IsdC, which serves as central conduit to funnel the scavenged heme to the membrane-associated lipoprotein IsdE (Muryoi *et al.* 2008; Tiedemann *et al.* 2012). The heme is then transported through the membrane by an IsdF homodimer into the cytoplasm (Adolf *et al.* 2023; Grigg *et al.* 2007; Mazmanian *et al.* 2002; Pluym *et al.* 2007). There, the monooxygenases IsdG and -I degrade the heme structure which results in the release of ferric iron (Fe^{3+}) to the cytosol (Skaar, Gaspar *et al.* 2004; R. Wu *et al.* 2005).

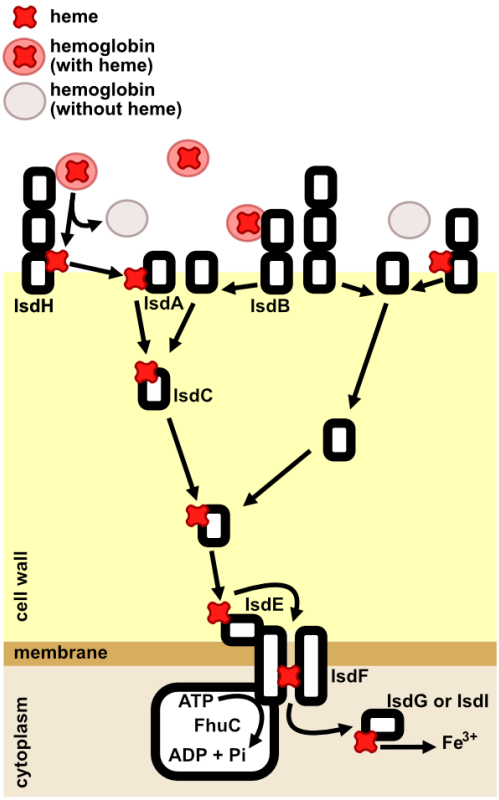

Figure 13: Schematic overview of the heme- scavenging Isd system in *S. aureus.* Hemoglobins are captured by IsdH and IsdB, which also extract the heme groups from the carrier proteins. Heme is then funneled from the distal IsdA through the cell wall via the IsdC to the celsdE. Homodimers of IsdF transport the heme from IsdE over the membrane into the cytoplasm. The reaction is energized by FhuC. The cytoplasmic IsdG and IsdI release ferric iron from the heme, producing staphylobilins and formaldehyde as side products (not shown for simplicity). Boxes correspond to the number of near iron transporter (NEAT) domains in the respective proteins (one: IsdA, IsdC, two: IsdB, three: IsdH, see Sheldon *et al.* 2015). Arrows denote the flux of heme through the cell wall and membrane.

While the principles of the Isd system are well described, many details are still not understood. Questions remain concerning the precise mechanism of heme removal from hemoglobin or the energization of heme membrane transport. IsdEF form an ATP-binding cassette (ABC) transporter, but the ATPase responsible for energizing the heme transport was only recently identified to be the iron-responsive ATPase FhuC (Adolf *et al.* 2023). Beyond this, it is currently unclear how the funneling of heme through immobile, cell-wall attached proteins is spatio-temporally coordinated with the membrane transporters, which localize in the significantly more mobile environment of the cytoplasmic lipid membrane. It is neither known, if a specific localization of the membrane-integrated IsdEF complex is necessary to ensure handover from the IsdA-C funnel, nor, how such a control of localization would be achieved.

1.5. The role of human microbiota in health and disease

In their natural environments, bacteria live in large communities that contain a multitude of species across different phyla, called microbiota (Debray *et al.* 2021; Groussin *et al.* 2021; Koopman 2004; L. Liu *et al.* 2012; Lloyd-Price *et al.* 2017; Segura Munoz *et al.* 2022; Sitaraman 2018; Tap *et al.* 2023). The human body is host for a variety of such microbiota, members of which are specifically adapted to the diverse regions of microbial growth, e.g., nose, gut, and skin. Each of these body sites harbors multiple ecological niches for bacterial life (Costello *et al.* 2012; Gilbert *et al.* 2018; Lloyd-Price *et al.* 2016, 2017; Proctor *et al.* 2019; B. Wang *et al.* 2017). Importantly, these different microbiota are known to significantly influence each other by species dispersal and horizontal gene transfer. Accordingly, due to the multitude of distinct microbiota contained within the human body, the overall human microbiome can be categorized as a metacommunity (Costello *et al.* 2012). Its different regions and niches are largely colonized by diverse sets of commensal bacteria (Gilbert *et al.* 2018; Lloyd-Price *et al.* 2017), but they also constitute niches for opportunistic pathogens like *S. aureus* (Conway *et al.* 2015; Krismer *et al.* 2017; Laux *et al.* 2019; Severn *et al.* 2022; Weyrich *et al.* 2015). Especially the disruption of microbiome homoeostasis (dysbiosis, e.g., through illness, malnutrition, immunosuppression, or antibiotic treatment) can lead to serious infections of these opportunistic pathogens or invasion of obligate pathogenic bacteria, as niches become vulnerable for alien colonization and pathogen proliferation. Thus, the human microbiome plays a key role in disease prevention and infection containment.

The compositions of human microbiota are highly individual and dynamic and depend on a multitude of factors, like bacterial and host genetics, species exposure and dispersal rate, host fitness and immune system, colonization order, host hygiene, nutrition, medical history, geographic location and more (De Filippo *et al.* 2010; Debray *et al.* 2021; DiGiulio *et al.* 2015; Goh *et al.* 2015; E. W. Jones *et al.* 2022; Sitaraman 2018; Warren *et al.* 2018; Yatsunenko *et al.* 2012). However, general principles governing the species composition of the respective microbiota can be devised. Identification of key species, which significantly influence and shape a microbiome is central for building foundational understanding of a microbiome. Efforts to categorize different key species and compositions of gut (Falony *et al.* 2016; Lloyd-Price *et al.* 2017; Schloissnig *et al.* 2012), vaginal (Gajer *et al.* 2012) and nasal (C. M. Liu *et al.* 2015) microbiota led to the definition of “community state types”. While this approach earned criticism for underrepresenting the huge diversity and temporal variation in species composition and density between individuals, the results of these and other studies helped to identify relevant core species of healthy human microbiota. Likewise, a range of medical conditions from obesity (Barlow *et al.* 2015; Hartstra *et al.* 2015), malnutrition, over a range of bowel, vaginal, dental (Deo *et al.* 2019) and skin diseases to diabetes (Barlow *et al.* 2015; Hartstra *et al.* 2015), Alzheimer (Askarova *et al.* 2020), depression (J. A. Foster and McVey Neufeld, 2013; Peirce and Alviña, 2019) and cancer (Garrett 2015) are closely associated or directly caused by certain microbiota states or pathogenic invasion of the microbiome (see also Wade 2013; C. Petersen *et al.* 2014; Qin *et al.* 2014; Trompette *et al.* 2014; B. Wang *et al.* 2017). Given this long and diverse list of serious harms to health and wellbeing, understanding the factors for resilience and vulnerability of microbiomes, i.e., gaining insight into the

details of microbiome ecology, are critical for human health. In this regard, the potential of microbiome ecology to control and prevent infections has sparked interest in recent years. Investigating the capability of some microbiome members to produce natural products that inhibit the growth of (potentially) pathogenic bacteria is a promising approach to find ways to shape the human microbiota in beneficial ways and combat pathogen colonization (Claesen *et al.* 2020; S. G. Kim *et al.* 2019; Kommineni *et al.* 2015; Nakatsuji *et al.* 2017; Sassone-Corsi *et al.* 2016; Sekirov *et al.* 2009; Zipperer *et al.* 2016). Still, the mechanisms, bacteria and chemical substances governing the complex microbiome dynamics and microbiome-host-relationships need to be understood to eventually enable targeted, productive, and long-term advantageous interventions in the future. The comprehensive elucidation of individual factors that shape microbiota is essential to build a foundational body of knowledge about the key principles, that influence the human microbiome and its role in human health (Hardy and Merrell 2020).

1.6. The epilancin group of lantibiotics

To ensure proliferation within the highly competitive environments of microbiomes, many microorganisms produce bacteriocins, which are a large and broadly defined group of primarily small molecule peptides (< 4 kDa) that kill or inhibit the growth of other bacteria. These compounds and their production are critical for the competitive fitness of producer and target, resulting in a significant microbiome shaping impact. Bacteriocins regularly target competitors of the producer strain specifically (Heilbronner *et al.* 2021). However, there are also bacteriocins with relatively broad-spectrum activity and rather general antibacterial targets such as the ultimate cell wall biosynthesis precursor lipid II (see chapter 1.3). Studying the production and action of bacteriocins therefore promises insight into how these compounds impact microbiota (Heilbronner *et al.* 2021). The characterization of antibacterial mechanisms of action helps to elucidate the ecological role of bacteriocins and contribute to the general understanding of antibiotic action and targets. It furthermore has the potential to provide new ways to treat pathogens that colonize or invade the different human microbiota, thereby expanding the range of potential anti-infective treatment options. Substantial progress in understanding the microbiome shaping roles of bacteriocins has been made by identifying interaction pairs of producer and target(s), the mechanism of action and the resulting impact of production on competitive fitness of both species in direct competition or within their natural environment. Application of this knowledge enabled successful pathogen exclusion from gut (Claesen *et al.* 2020; S. G. Kim *et al.* 2019; Kommineni *et al.* 2015; Sassone-Corsi *et al.* 2016), skin (Nakatsuji *et al.* 2017) and nasal microbiota (Bitschar *et al.* 2019). Within the large and diverse group of bacteriocins, lantibiotics constitute a most prominent subgroup with well over 80 described compounds (van Staden *et al.* 2021). Lantibiotics are ribosomally synthesized peptides, which are post-translationally modified by introduction of the defining structural motif of *meso*- or *3-methyl*-lanthionine groups (Figure 14A). The formation of these lanthionine cross-links via amino acid dehydration and thioether-linked ring formation is catalyzed by specific lanthionine synthetases (Schnell *et al.* 1988; Weil *et al.* 1990). Depending on the structural and functional features of these enzymes, lantibiotics are divided into four classes (I – IV, Figure 14B, Hegemann *et al.* 2020; Repka *et al.* 2017).

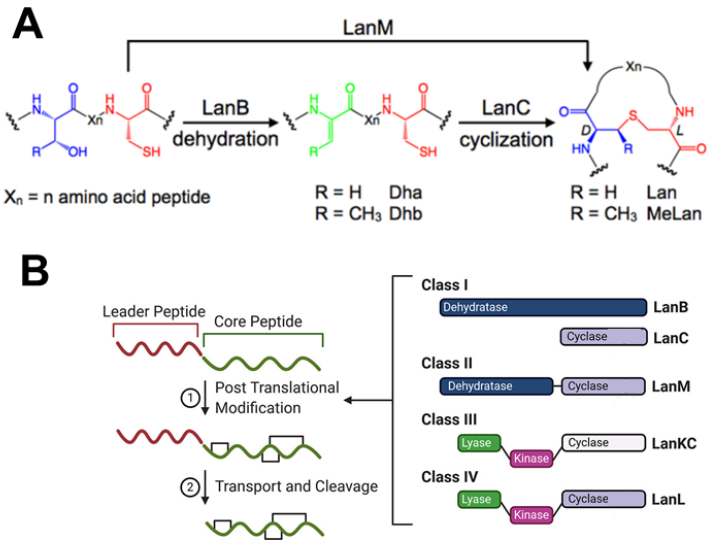

Figure 14: Classification of lantibiotics. (A) Reaction catalyzed by lanthionine (Lan) synthetases. A hydroxy-group containing amino acid (Thr, Ser) is dehydrated (catalyzed by a dehydratase) and a sulfide-crosslink is established through nucleophilic attack of a Cys thiol-goup (catalyzed by a cyclase). Adapted from Goto *et al.* (2010). **(B)** Schematic representation of the post-translational maturation process of lantipeptides. Lanthionine cross-links and other modifications are introduced, followed by cleavage of the leader peptide and transport across the cell membrane. Four different types on Lan synthetases serve as defining factors for lantipeptide classification. Adapted from van Staden *et al.* (2021) with permission from American Society for Microbiology.

Due to a large diversity in primary peptide sequences and a multitude of options for cyclization as well as additional posttranslational modifications, lantibiotics constitute a structurally highly diverse group. However, virtually all lantibiotics with a known mechanism of action kill bacteria by binding to cell wall biosynthesis precursors (see chapter 1.3) or by disrupting cytoplasmic membrane function, e.g., via pore formation. (Bierbaum and Sahl 2009; Draper *et al.* 2015; X. Wang *et al.* 2020; Cao *et al.* 2021; van Staden *et al.* 2021; Ongpipattanakul *et al.* 2022). Still, the precise mechanism of antibacterial activity is still unclear for many lantibiotics, including some well-characterized and -investigated specimen (X. Wang *et al.* 2020). Beyond that, the ecological function and relevance of the majority of lantibiotics remains unknown.

The first discovered and best researched lantibiotic nisin (produced by *Lactococcus lactis*) combines both cell wall precursor binding and membrane disruption. It uses lipid II as a high-affinity membrane target to facilitate formation of large pores formed via nisin:lipid II complex aggregation (see chapter 1.3). Due to its early discovery, its relevance as an industrially produced food preservative and the potential for medical use, the structural-functional relationship of the nisin has been extensively researched (van Staden *et al.* 2021). Nisin features 5 thioether ring systems, of which the N-terminal rings A-B are essential for binding of the cell wall precursor lipid II (Figure 15, Hsu *et al.* 2004; Medeiros-Silva *et al.* 2018, see also chapter 1.6, Figure 9). The three rings C-E were shown to interact with and penetrate the cytoplasmic membrane and facilitate aggregation of the nisin:lipid II complexes, causing pore formation, membrane disintegration and ultimately cell death (Jensen *et al.* 2020; Medeiros-Silva *et al.* 2018; K. Scherer *et al.* 2013; K. M. Scherer *et al.* 2015; 'T Hart *et al.* 2016; Tol *et al.* 2015).

Epilancins are a subgroup of lantibiotics produced by staphylococci with close structural similarity to nisin. The C-terminal and middle regions display nearly identical ring system configurations, albeit with a smaller middle region ring and alterations in the overall amino acid sequence. However, the N-terminal two-ring motif responsible for the lipid II-binding of nisin is completely absent in epilancins (Figure 15, Ekkelenkamp *et al.* 2005; Van De Kamp *et al.* 1995). Instead, a linear amino acid sequence of similar length is present. Accordingly, epilancins show no indications of a specific interaction with lipid II and are subject to ongoing speculations about the mechanism of action (Brötz Josten *et al.* 1998; X. Wang *et al.* 2020). As the membrane interacting C-terminal part is strikingly similar to that of nisin, membrane damaging mechanisms have been proposed and there are reports of epilancins impacting membrane potential and integrity at higher concentrations (Knerr *et al.* 2012; Velásquez *et al.* 2011). However, the precise mechanism of action and the consequences of epilancin treatment for the target cell remain largely unknown. Structure-activity-relationship (SAR) studies showed that presence of the linear N-terminal sequences is critical for antibiotic activity, but the precise function of this region for antibacterial action was not elucidated (Knerr *et al.* 2012). Beyond that, the role of epilancins in microbial communities were not addressed yet, leading to speculations about a potential microbiome-shaping function (Heilbronner *et al.* 2021; Severn *et al.* 2022). Currently, there are two structurally elucidated specimen of the epilancin group produced by *Staphylococcus epidermidis*, K7 (Bierbaum 1996; Van De Kamp *et al.* 1995) and 15X (Ekkelenkamp *et al.* 2005), and a third member produced by *Staphylococcus warneri,* SWLP1 (J. Petersen *et al.* 2009), has been described.

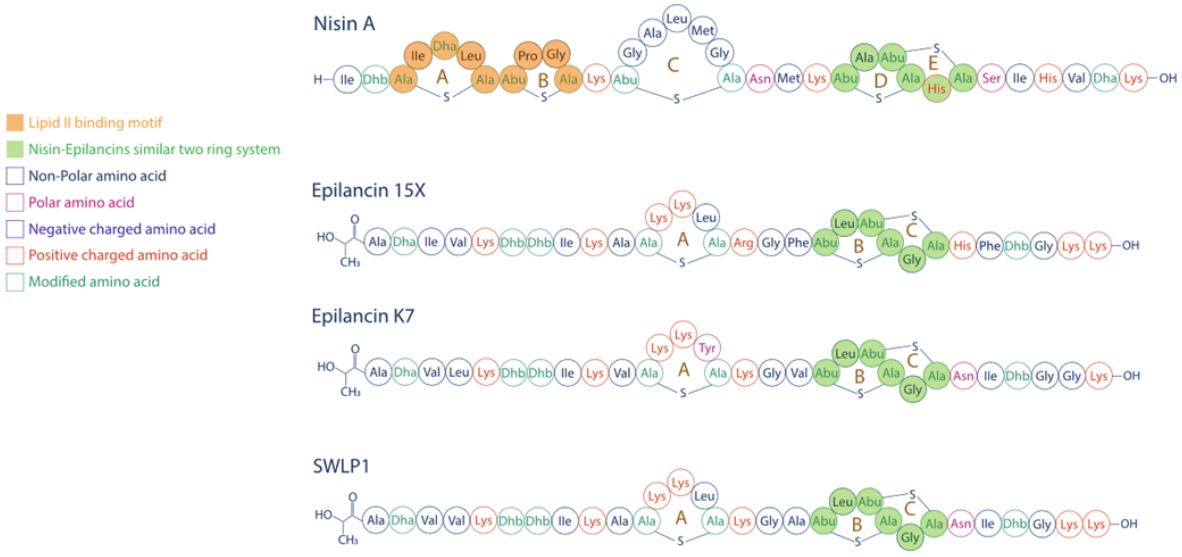

Figure 15: Schematic representation of nisin A and the epilancins 15X, K7 and SWLP1. Importantly, epilancins lack the N-terminal lipid II-binding two-ring motif of nisin. Apart from this key distinction, the two groups are very similar in structure. Epilancins show a slightly smaller middle ring motif than nisin and an almost identical C-terminal motif of two intertwined four-membered rings followed by six linear amino acids. Adapted from Wang *et al.* (2020).

2. Aims of this work

A central aim of this work was to investigate the cellular impact of antibiotic compounds, that target the bacterial cell wall biosynthesis machinery (CWBM), on the gram-positive pathogen and model organism *Staphylococcus aureus*. To systematically approach the complex cellular impact of CWBM targeting antibiotics, the aim of this work was to elucidate the first and most striking cellular effects directed towards the CWBM and the closely coordinated cell division. The methodological objective of this work was to utilize state-of-the-art fluorescence microscopy for in-depth investigation of the cellular impact of antibiotics *in vivo*. Therefore, it was aimed to develop and apply microscopic methods and coherent quantitative analyses scaling from the individual cell to samples of hundreds of cells. Using these techniques, the aims were to

1. use the antibiotics vancomycin, telavancin and oxacillin, which target the final steps of peptidoglycan synthesis (PGS), to identify a core paradigm for the initial cellular impact of PGS inhibition on CWBM and cell division (Chapter 4.1),
2. identify similarities and variations in the cellular effects to understand, how the molecular mechanisms of PGS substrate binding (vancomycin, telavancin) and transpeptidase enzyme inhibition (oxacillin) translate to the observed cellular effects (Chapter 4.1),
3. contextualize the cellular impact of PGS inhibition with the reported cytoplasmic membrane disrupting effect of telavancin and other lipid II-binding antibiotics (Chapter 4.2),
4. evaluate the cellular effects of the PGS inhibiting natural product moenomycin within the established paradigm of antibiotic impact on CWBM and cell division (Chapter 4.3),
5. investigate the cellular effects of the membrane-depolarizing synthetic small molecule DCAP on septum formation and CWBM organization (Chapter 4.4),
6. apply the established microscopic methods and analysis capabilities in an orthogonal approach to investigate the localization pattern of the iron-scavenging component IsdF (Chapter 4.5).

Furthermore, a central aim of this work was to investigate the epilancin A37, a lantibiotic bacteriocin that was recently found as a natural product from a human nasal *Staphylococcus epidermidis* isolate. Activity of A37 was observed to be especially high against corynebacteria, which constitute some of the most abundant human nasal commensals. Accordingly, an objective of this work was to investigate how A37 production contributes to competitiveness of *S. epidermidis* against corynebacteria (Chapter 4.6). Beyond this, the aim was to elucidate the mechanism of action of A37. By combining biochemical and microbiological approaches with quantitative and super-resolution fluorescence microscopy, the aim of this work was to investigate, how A37 impacts corynebacterial cells (Chapter 4.7). Special focus was on the effects of A37 on the cytoplasmic membrane, as membrane disruption is a common feature of many lantibiotics and was proposed as potential mechanism of action for epilancins.

3. Materials & Methods

3.1. Materials

3.1.1. Chemicals

If not stated otherwise, chemicals used in this work were purchased from Carl Roth (Karlsruhe, Germany), Merck KGaA (Darmstadt, Germany), Thermo Fischer Scientific (Waltham, USA), VWR (Radnor, USA) or their respective subsidiaries. All chemicals used in this work were of chemical purity grades appropriate for the respective experiments and at least of *pro analysis,* if available. Otherwise, the highest available purity grade was purchased.

3.1.2. Antibiotics

All antibiotic compounds used in this work are listed in Table 1.

Table 1: Antibiotic compounds used in this work, their respective abbreviations as used in this work, notes on purity, purification method and/or chemical formulation (if applicable) and the vendors/reference.

Compound	Abbreviation	Notes	Vendor/Reference
A37	A37	FPLC + C_{18}-RP-HPLC + C_4-RP-HPLC	Benjamin Winnerling
Ampicillin	AMP	≥97 %	Carl Roth
Cacaoidin	CAO	HPLC	Deisinger *et al.* 2023
Carbonylcyanid-m-chlorphenylhydrazone	CCCP	≥97 % (TLC)	Sigma-Aldrich
Clovibactin	CLOV	-	Shukla *et al.* 2023
2-((3-(3,6-dichloro-9H-carbazol-9-yl)-2-hydroxypropyl)amino)-2-(hydroxymethyl)propane-1,3-diol	DCAP	≥95% HPLC	Sigma-Aldrich
Erythromycin	ERY	≥93 %	Carl Roth
Fosfomycin	FOS	≥95 %	Sigma-Aldrich
Hypeptin	HYP	C_{18}-RP-HPLC	Wirtz *et al.* 2021
Mersacidin	MRS	-	Hoechst GmbH (Frankfurt am Main, Germany)
Moenomycin	MOE	Moenomycin complex, ≥95%	Cayman (Ann Arbor, USA)

Nisin	NIS	HPLC	Michaele Josten
Oxacillin	OXA	Na^+ salt, ≥95 %	Sigma-Aldrich
Siamycin	SIA	-	S. Tan *et al.* 2019
Teixobactin	TEIX	HPLC	Ling *et al.* 2015
Valinomycin	VAL	≥98 % (TLC), ≥90 % (HPLC)	Sigma-Aldrich
Vancomycin	VAN	Vancomycin HCl	Hikma (London, UK)

3.1.3. Bacterial strains

All bacterial strains used in this work are listed in Table 2.

Table 2: Bacterial strains used in this work and the selective antibiotic for their genotype (if applicable).

Species	Strain	Selective antibiotic	Reference
S. aureus	HG001	-	Herbert *et al.* 2010
	SA113	-	Herbert *et al.* 2010
	SG511	-	Dietrich *et al.* 2021
	RN4220	-	Herbert *et al.* 2010
	RN4220 pCQ11-MurJ-mNeongreen	10 µg/mL ERY	Puls *et al.* 2023
	RN4220 pCQ11-FtsZ-SNAP	10 µg/mL ERY	Lund *et al.* 2018
	RN4220 pCQ11-WalK-GFP	10 µg/mL ERY	Patrick Hardt
	RN4220 FtsW-GFP	10 µg/mL ERY	Grein *et al.* 2020
	RN4220 FtsW-GFP pCQ11-FtsZ-SNAP	10 µg/mL ERY	Puls *et al.* 2023
	RN4220 rodA-GFP	-	Puls *et al.* 2023
	RN4220 RNpPBP2-31	10 µg/mL ERY	Pinho *et al.* 2005
	RN4220 pCQ11-FtsZ-mCherry	10 µg/mL ERY	Puls *et al.* 2023
	RN4220 pCQ11-PknB-GFP-FtsZ-mCherry	10 µg/mL ERY	Hardt *et al.* 2017

	RN4220 pCQ11-PBP4-YFP	10 µg/mL ERY	Puls *et al.* 2023
	Newman FloA-SNAP pCQ11-IsdF-mNeongreen	10 µg/mL ERY	Adolf *et al.* 2023
	Newman *ΔfloA* pCQ11-IsdF-mNeongreen	10 µg/mL ERY	Adolf *et al.* 2023
	Newman *ΔfloA:floA* pCQ11-IsdF-mNeongreen	10 µg/mL ERY	Adolf *et al.* 2023
C. glutamicum	DSM 20300	-	DSMZ
	A37/8	-	Benjamin Winnerling
S. epidermidis	A37	-	Fabian Grein
	ATCC 14990	-	ATCC
E. coli	Stellar™ pCQ11-IsdF-mNeongreen	100 µg/mL AMP	Puls *et al.* 2023

3.1.4. Plasmids

All plasmids used in this work are listed in Table 3.

Table 3: Plasmids used in this work.

Plasmid	Reference
pCQ11-IsdF-mNeongreen	Puls *et al.* 2023

3.1.5. Primer

All primers used in this work are listed in Table 4.

Table 4: Primers used in this work, their sequences and the amplicon of each primer pair.

Primer	Sequence	Amplicon
pCQ11-seq2-for	GTTGACTTTATCTACAAGG	Insert of pCQ11
pCQ11-seq2-rev	TCTCGAAAATAATAGAGGG	

3.1.6. Buffers and Media

All buffers and media used in this work are listed in

Table 5. For preparation of agar plates, the respective medium was supplemented with 1.5 % w/w agar-agar Kobe I. If necessary, pH was adjusted with appropriate solutions of HCl or NaOH, if not stated otherwise.

Table 5: Buffers and media used in this work.

Buffer/Medium	Ingredients
Müller-Hinton (MH)	21g/L dehydrated Oxoid™ MH Broth
MH CLSI	MH + 34.63 g/L $CaCl_2$ (25 mg/L Ca^{2+}), 52.27 g/L $MgCl_2 \cdot 6\ H_2O$ (12.5 mg/L Mg^{2+})
Lysogeny Broth/Luria–Bertani (LB)	10 g/L Tryptone, 5g/L yeast extract, 10 g/L NaCl
Phosphate buffered saline (PBS), pH 7.4	8 g/L NaCl, 0.2 g KCl, 1.42 g Na_2HPO_4, 0.27 g KH_2PO_4
TAE	40 mM Tris, 1 mM EDTA, 0.114 % (v/v) acetic acid pH 8
Buffer A	50 mM MES pH 5.5
Buffer B	50 mM MES pH 5.5 + 1 M NaCl

3.1.7. Fluorescent proteins and dyes

All fluorescent proteins and dyes used in this work are listed in Table 6. Fluorescent proteins were fused to the C-terminus of the respective protein of interest, except for PBP2-GFP, PknB-GFP and RodA-GFP, which are N-terminal fusion proteins.

Table 6: Fluorescent proteins and chemical dyes used in this work, their abbreviation in this work, their excitation and emission maxima wavelengths and their application in this work.

Protein/Dye	Abbreviation	Ex/Em [nm]	Application
Green fluorescent protein mut2	GFP	485/508	Labeling of FtsW, RodA, PBP2, PknB, WalK
Yellow fluorescent protein	YFP	513/527	Labeling of PBP4
mNeongreen	-	506/517	Labeling of MurJ, IsdF
mCherry2	mCherry	589/610	Labeling of FtsZ

BODIPY™-FL	-	503/512	Labeling of A37, Vancomycin
3-[[(7-Hydroxy-2-oxo-2H-1-benzopyran-3-yl)carbonyl]amino]-D-alanine hydrocholoride	HADA	405/450	TPase activity
Bis-(1,3-Dibarbituric acid)-trimethine oxanol	$DiBAC_4(3)$	493/516	Membrane Depolarization
3,3-Dipropylthiadicarbocyanine iodide	$DiSC_3(5)$	622/670	Membrane Depolarization
SNAP-Cell® TMR Star	-	554/580	SNAP-tag® labeling (FtsZ-SNAP, FloA-SNAP)
SNAP-Cell® 505-Star	-	504/532	SNAP-tag® labeling (FtsZ-SNAP)
CellBrite® Fix 640		638/667	Membrane stain
Nile red	-	559/635	Membrane stain
GelRed®	-	279/593	DNA Stain
Propidium Iodide	PI	537/618	Membrane disruption

3.1.8. Devices

For a detailed description of the microscopes used in this work, see chapter 3.4.1.

For microplate measurements, a Tecan Spark 10M (Tecan, Männedorf, Switzerland) or a Tecan Infinite F Plex were used. If not performed in a microplate, an Implen NanoPhotometer® NP80 (Implen, München, Germany) or a NanoPhotometer® Classic were used were used for photometric measurements. For detailed descriptions, see the respective experiment methods in chapter 3.2.

For weighing, Sartorius Universal (Sartorius, Göttingen, Germany), Sartorius Analytic or Sartorius Micro balances were used, depending on the target weight of the substance weighed in.

Centrifugation was carried out in a VWR MicroStar12 centrifuge if not stated otherwise.

Liquid cultures were incubated in Infors HT ecotron incubators (Infors HT, Bottmingen, Switzerland), agar plates were incubated in Thermo Scientific Heratherm incubators.

Other Devices and equipment used for individual experiments are described in the respective experiment method (see chapters 3.2 - 3.5).

3.1.9. Software

All software used in this work is listed in Table 7.

Table 7: Software used in this work.

Software	Version(s)	Reference
Office 365	-	Microsoft (Redmond, USA)
SnapGene	6.1.2	Dotmatics (Boston, USA)
FIJI (ImageJ)	2.0.0-rc-69/1.52p; Java 1.8.0_172 [64-bit]	Schneider *et al.* 2012
Zen	Blue 2.0, Blue 3.6, Black 2.3 SP1	Carl Zeiss (Oberkochen, Germany)
Prism	8.0.2	Dotmatics

3.2. Microbiological methods

3.2.1. Bacterial strain maintenance

Bacterial strain stock cultures were kept frozen at -80°C in a 50 % v/v glycerol solution. Stock cultures were plated on MH agar plates (*S. aureus*, *S. epidermidis, Corynebacterium glutamicum*) or LB agar plates (*E. coli*) supplemented with the appropriate selective antibiotic, if applicable (see Table 2). Agar plates were incubated over night at 37°C and then stored at 4°C for a maximum of 4 weeks.

3.2.2. Cultivation of bacteria

Strains of *S. epidermidis* and *C. glutamicum* were cultivated in MH medium. Strains of *S. aureus* were cultivated in MH CLSI medium. Strains of *E. coli* were cultivated in LB medium. If applicable, selective antibiotics were added to the medium in the concentration given in Table 2. Main cultures were inoculated with 1 % v/v of an overnight culture. Both main and overnight cultures were grown at 37°C and 120 rpm agitation.

3.2.3. Bacterial growth measurements

Bacterial growth was quantified by measuring the optical density at 600 nm (OD_{600}). For control of culture density, 1 mL of the culture were measured in Semi-Micro cuvettes (Sarstedt, Nümbrecht, Germany) against sterile medium in a photometer. If necessary, cultures were pre-diluted for accurate OD_{600} measurements according to manufacturer specifications. For growth curves, 100 µL of culture were measured in sterile 96-well plate with u-shaped wells (Greiner Bio-One, Kremsmünster, Austria) over time in 15 min intervals.

3.2.4. Minimal inhibitory concentrations

Determination of minimal inhibitory concentrations (MICs) were performed according to CLSI Standards (Patel 2015). Briefly, 100 µL of a 1:2 serial dilution of the respective antibiotic was prepared in a sterile 96-well plate with u-shaped wells. 100 µL of a main culture grown as stated above to OD_{600} = 0.3 and diluted 1:100 in identical medium were added to each well. Plates were sealed and incubated at 37°C. The MIC was determined as the well with lowest antibiotic concentration, where no visible growth was observable after 20 h of incubation. MICs were confirmed in a total of three biologically independent experiments. To evaluate MICs with an increased inoculum, the identical procedure was applied to cultures grown to OD_{600} = 1 and diluted 1:50.

3.2.5. Time-kill kinetics

Cultures were grown as stated above to OD_{600} = 0.5 and diluted 1:100 in identical medium. 100 µL of each culture were transferred into a sterile 96-well plate with u-shaped wells and diluted in a 1:10 dilution series in identical medium. 50 µL of each dilution was streaked on the half area of an agar plate. Antibiotic was added to the culture and the plate was sealed. For the untreated control, no antibiotic was added prior to sealing. After 1 h, 2 h, 4 h and 24 h after addition of the antibiotic, dilution and streaking of all cultures was repeated. Agar plates were incubated for 24 h at 37°C after culture streaking. Colony forming units (CFU) were counted for each dilution. CFU/mL were calculated for each dilution with total CFU between 20 and 300. Final CFU/mL of each sample was determined as the mean of all dilutions, where a CFU/mL was calculated.

3.2.6. Plasmid purification

Plasmid purification was performed using the Monarch® Plasmid Miniprep Kit (New England Biolabs, Ipswich, USA) according to manufacturer specifications.

3.2.7. $DiSC_3(5)$ release assay

To measure membrane depolarization using $DiSC_3(5)$, a bacterial culture was grown as stated above to OD_{600} = 0.3. Then, $DiSC_3(5)$ (Biomol, Hamburg, Germany) was added to a final concentration of 1 µM and DMSO concentration was adjusted to 1 % v/v. 200 µL of the culture were transferred into a Greiner Bio-One flat bottom black polystyrene 96-well plate. $DiSC_3(5)$ fluorescence was measured in a Tecan Spark 10M equipped with a monochromator with 610 nm excitation and 660 nm emission every min until the signal remained stable for 5 min, indicating maximal uptake and auto-quenching of the dye. Antibiotic was added and $DiSC_3(5)$ fluorescence was measured for at least 30 min.

3.2.8. Propidium iodide influx assay

Culture was grown as stated above to OD_{600} = 0.25. 100 µL of the culture were transferred into a Greiner Bio-One flat bottom black polystyrene 96-well plate. Additional 100 µL culture were added to well 1. Antibiotic was added to well 1 and diluted in a 1:2 dilution series. The plate was sealed and incubated

at 37°C and 120 rpm. For the last 5 min of incubation, PI was added in a final concentration of 10 µg/mL. At the end of incubation, the plate was centrifuged in a Heraeus Megafuge 40R (Heraeus, Hanau, Germany) at 4,500 rpm for 10 min. Cells were resuspended in sterile PBS pH 7.4 and PI fluorescence was measured in a Tecan Spark 10M equipped with a monochromator with 530 nm excitation and 620 nm emission.

3.3. Biochemical methods

3.3.1. Agarose gel DNA separation

Size-separation of DNA fragments was achieved by agarose gel electrophoresis. DNA fragments were separated in a 1 % w/w agarose gel using an Advance Mupid® One Electrophoresis System (Advance, London, UK) with 100V for 1 h in TAE buffer. DNA was loaded to the gel using New England Biolabs Purple gel loading dye. Thermo Scientific™ GeneRuler 1 kb DNA Ladder was used for fragment size reference. DNA visualization was achieved by addition of GelRed® nucleic acid stain to the agarose gel in a 1:10,000 dilution prior to solidification. GelRed® was visualized in a Bio-Rad Gel Doc™ XR+ (Bio-Rad, Hercules, USA).

3.3.2. Fluorescent labeling of purified A37

Labeling of A37 was performed using purified A37 (kindly provided by Benjamin Winnerling). A37 was solved in dimethylformamide (DMF) to a final concentration of 5 mg/mL. BODIPY™-FL-NHS-Ester (Thermo Fischer Scientific) was solved in DMSO to a final concentration of 10 mg/mL. Both solutions were mixed in a ratio of 5:1 v/v (A37: BODIPY™-FL) to achieve a ratio of approx. 2.5:1 w/w (A37: BODIPY™-FL), which corresponds to a molar ratio of approx. 1:3 (A37: BODIPY™-FL). The mixture was vortexed for 2 h at room temperature and then purified via FPLC using a Bio-Rad NGC Chromatography System equipped with a HiTrap SP HF 1 mL column. After loading, the sample was washed with 20 column volumes (one column volume = 0.96 mL) with 100 % Buffer A, followed by a linear gradient elution to 100 % Buffer B over 15 column volumes (see

Table **5** for Buffer A and Buffer B). Elution from the column was quantified by constantly measuring absorption A_{280} (Figure 16A). Antibacterial activity of the elution fractions was assessed by applying 10 µL of each fraction to a plate with *C. glutamicum* DSM20300. After incubation at 37°C for 24 h, only fractions 28 and 29 showed antibacterial activity, indicating presence of active A37 in these samples. A37 concentration of these fractions was determined using a Pierce™ BCA Protein Assay Kit in a Greiner Bio-One transparent 96-well microplate with flat wells against a A37 standard curve (Figure 16B). Determined concentrations were 121.1 µg/mL (40.6 µM) for fraction 28 and 186.2 µg/mL (62.4 µM) for fraction 29. BODIPY™-FL concentrations of the fractions were determined photometrically by measuring the absorbance at 503 nm of 1:80 dilution in diH_2O and BODIPY™-FL concentration was calculated using the extinction coefficient of BODIPY™-FL at 503 nm [80,000 cm^{-1} M^{-1} in ddH_2O, manufacturer information, consistent with Fishkin (2015) and Zlotnick *et al.* (2007)] as 7.99 µM for fraction 28 and 7.36 µM for fraction 29. The degree of labeling was calculated as the quotient of

BODIPY™-FL and A37 concentration as 19.7 % for fraction 28 and 11.8% for fraction 29. Percentages indicate the abundance of BODIPY™-FL labels relative to the total number of A37 molecules. The degree of labeling was adjusted in both fractions with unlabeled A37 to a 10 % final degree of labeling. The antibacterial activity of the resulting 10 % A37- BODIPY™-FL / 90 % A37 mixture (A37FL) was confirmed via MIC against *C. glutamicum*. Both A37FL samples showed MICs of 1 µg/mL, identical to an unlabeled A37 control.

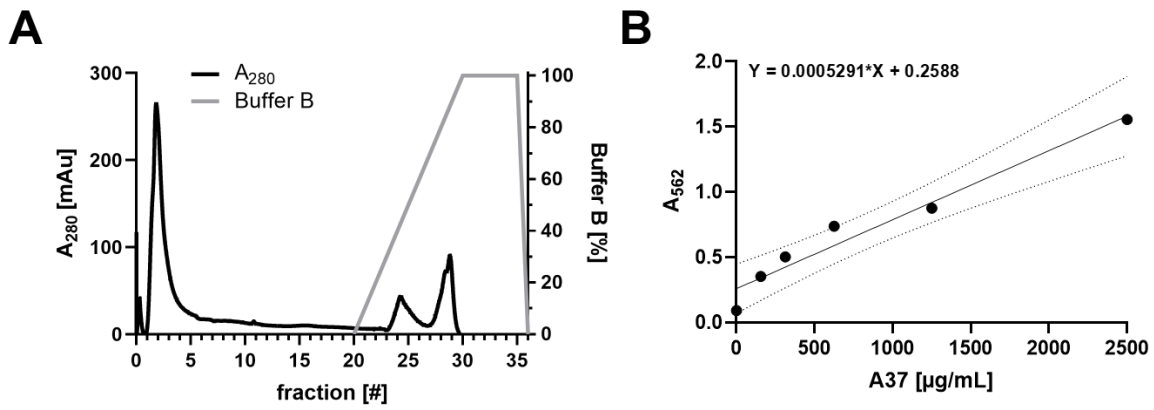

Figure 16: **Purification of A37FL. (A)** FPLC purification of the A37-BODIPY™-FL labeling reaction. Black line shows the absorption at 280 nm (A_{280}), grey line shows the applied Buffer B gradient. Fractions 20 – 35 were tested for antibacterial activity against *C. glutamicum* DSM20300, only fractions 28 and 29 showed activity. **(B)** BCA Assay standard curve of A37. A solution of A37 was diluted in diH_2O to the concentrations used for the standard curve and Absorption at 562 nm (A_{562}) was measured in a microplate reader. Line graph shows the linear regression curve ± 95% Confidence interval with the equation given on the upper left. Linear regression was calculated using Prism 8.

3.4. Microscopic methods

3.4.1. Microscopic setups

Widefield microscopy

Widefield fluorescence microscopy of A37FL, Van-FL, FtsZ-SNAP, FtsW-GFP, HADA (with the exception of moenomycin experiments), MurJ-mNeongreen, $DiBAC_4(3)$, PknB-GFP (with the exception of oxacillin experiments), FtsZ-mCherry and PBP2-GFP (with the exception of cacaoidin, mersacidin and siamycin experiments) was performed on a Carl Zeiss AxioObserver Z1 equipped with a HXP 120 C lamp, an Carl Zeiss αPlan-APOCHROMAT 100×/1.46 oil immersion objective and an Carl Zeiss AxioCam MRm camera. The setup was controlled using the Carl Zeiss Zen Blue 2.0 Software. Widefield fluorescence microscopy of FloA-SNAP, HADA (moenomycin experiments), IsdF-mNeongreen, Nile red, PknB-GFP (oxacillin experiments), RodA-GFP, PBP4-YFP, WalK-GFP, PBP2-GFP (cacaoidin, mersacidin and siamycin experiments) and widefield phase contrast microscopy of *S. epidermidis* and *C. glutamicum* were performed on a Carl Zeiss AxioObserver Z1 equipped with a X-Cite Xylis LED Lamp (Excelitas, Waltham, USA), an Carl Zeiss αPlan-APOCHROMAT 100×/1.46 oil immersion objective and

an Teledyne Photometrics Prime BSI express camera (Teledyne Photometrics, Tucson, USA). The setup was controlled using the Carl Zeiss Zen Blue 3.6 Software. In either setup, visualization of HADA was achieved using Carl Zeiss filter set 49 (335-390 nm excitation, 395 nm beam splitter, 420-470 nm emission), visualization of A37FL, $DiBAC_4(3)$, FtsW-GFP, IsdF-mNeongreen, MurJ-mNeongreen, PBP2-GFP, PBP4-YFP, PknB-GFP, RodA-GFP, Vancomycin-FL or WalK-GFP was achieved using Carl Zeiss filter set 38 (450–490 nm excitation, 495 nm beam splitter and 500–550 nm emission) and visualization of CellBrite® Fix 640, FtsZ-mCherry, nile red or SNAP-Cell® TMR-Star (used for labeling of FtsZ-SNAP or FloA-SNAP, see 3.4.3) was achieved using Carl Zeiss filter set 43 (538–562 nm excitation, 570 nm beam splitter and 570-640 nm emission).

HiLo live-cell widefield microscopy

All HiLo live-cell widefield microscopy micrographs shown in this work were imaged by Dominik Brajtenbach. Conceptualization, data analysis and conclusions drawn from analysis were done by the author of this work with technical support from Dominik Brajtenbach. Usage of representative micrographs in this work was permitted by Dominik Brajtenbach.

Briefly, HiLo live-cell widefield microscopy was performed on a Nikon Eclipse Ti (Nikon, Tokyo, Japan) equipped with a Nikon CFI Apo TIRF 100x/1.49 oil immersion objective, a Teledyne Photometrics Prime BSI and a Nikon external phase contrast with 100x PH4. Fluorescence was excited using a 488 nm laser (Cobalt 06-MLP 488 nm, 120 mW) and a 561 nm laser (Cobalt 06-DPL 561 nm, 100 mW) employing a quadband filter set (ET 405/488/561/640nm Laser Quad Band Set by Chroma). Live-cell images were deconvoluted with synthetic point spread functions (PSFs) using the FIJI plugin deconvolutionlab2 (Sage *et al.* 2017). PSFs were generated with the FIJI plugin PSFGenerator (Kirshner *et al.* 2013) for the corresponding emission wavelengths.

Confocal Airyscan microscopy

All Confocal Airyscan micrographs shown in this work were imaged by Dominik Brajtenbach. Conceptualization, data analysis and conclusions drawn from analysis were done by the author of this work with technical support from Dominik Brajtenbach. Usage of representative micrographs in this work was permitted by Dominik Brajtenbach.

Briefly, confocal Airyscan microscopy was performed using a Carl Zeiss LSM 880 equipped with a Carl Zeiss Plan-Apochromat 63x/1.4 oil immersion objective and a Carl Zeiss Airyscan detector. The setup was controlled using the Carl Zeiss Zen Black 2.3 SP1 Software. Excitation was achieved using 488 nm for SNAP-Cell® 505-Star and A37FL and 640 nm for CellBrite® Fix 640 and nile red.

3.4.2. Visualization of fluorescent fusion proteins

Strains with fusion proteins were grown as stated above. If fusion proteins were encoded on a pCQ11 plasmid, main cultures were supplemented with 0.1 mM Isopropyl-β-D-thiogalactopyranosid (IPTG). Main cultures were grown for a total of 4 h, including incubation time with antibiotic compounds. Density

was adjusted to OD_{600} = 0.5 in identical medium immediately before addition of antibiotics. Cultures were washed three times in identical medium (2 min, 13,000 rpm), mounted on 1% w/w agarose slides and microscopically visualized as described above.

3.4.3. Visualization of SNAP-Tag® fusion proteins

Strains with SNAP-Tag® fusion proteins were grown as stated above. Main cultures were supplemented with 0.1 mM Isopropyl-β-D-thiogalactopyranosid (IPTG). Main cultures were grown for a total of 4 h, including incubation time with antibiotic compounds. Density was adjusted to OD_{600} = 0.5 in identical medium immediately before addition of antibiotics. For the last 20 min of incubation, SNAP-Tags® were chemically labelled by addition of 200 nM of SNAP-Cell® TMR-Star or SNAP-Cell® 505-Star. Cultures were washed three times in medium (2 min, 13,000 rpm), mounted on 1% w/w agarose slides and microscopically visualized as described above.

3.4.4. Visualization of fluorescent chemical probes

CellBrite® Fix 640

CellBrite® Fix 640 is a chemical fluorescent dye, that covalently stains outer cell membranes of bacteria (manufacturer information). The dye itself poorly penetrates cytoplasmic membranes, thereby ensuring exclusive labeling of the cell membrane (manufacturer information). To label bacterial cells with CellBrite® Fix 640, cultures were grown as stated above for a total of 4 h, including incubation time with antibiotic compounds. Density was adjusted to OD_{600} = 0.5 in identical medium immediately before addition of antibiotics. For the last 20 min of incubation, CellBrite® Fix 640 was added to a final dilution of 1:100. Cultures were washed three times in medium (2 min, 13,000 rpm), mounted on 1% w/w agarose slides and microscopically visualized as described above.

$DiBAC_4(3)$

To quantify membrane depolarization using $DiBAC_4(3)$, cultures were grown as stated above for a total of 4 h, including incubation time with antibiotic compounds. Density was adjusted to OD_{600} = 0.5 in identical medium immediately before addition of antibiotics. For the last 15 min of incubation, $DiBAC_4(3)$ was added to a final concentration of 10 µM. Cultures were washed three times in medium (2 min, 13,000 rpm), mounted on 1% w/w agarose slides and microscopically visualized as described above.

HADA

To microscopically investigate HADA incorporation, cultures were grown as stated above to OD_{600} = 0.5. Antibiotics were added to the desired concentration and cells were incubated at 37°C and 120 rpm. Immediately after treatment, cultures were washed three times in medium (2 min, 13,000 rpm) and resuspended in identical medium. HADA was added to a final concentration of 250 µM and cultures were incubated for 15 min. Cultures were washed three times in medium (2 min, 13,000 rpm), mounted on 1% w/w agarose slides and microscopically visualized as described above.

Nile red

For nile red staining, cultures were grown as stated above for a total of 4 h, including incubation time with antibiotic compounds. Density was adjusted to OD_{600} = 0.5 in identical medium immediately before addition of antibiotics. Cultures were washed three times in medium (2 min, 13,000 rpm) and mounted on 1% w/w agarose slides. 20 nM nile red in 1% v/v DMSO was applied directly on the mounted cells immediately prior to microscopic visualization as described above.

3.4.5. Visualization of fluorescent compounds

A37FL

For visualization of A37FL, cultures were grown as stated above to OD_{600} = 0.5. A37FL was added to a final concentration of 4 µg/mL, if not stated otherwise. Cultures were incubated for 15 min at 37°C and 120 rpm, then washed three times in medium (2 min, 13,000 rpm), mounted on 1% w/w agarose slides and microscopically visualized as described above.

Vancomycin-FL

To visualize BODIPY™-FL labelled vancomycin (Van-FL, Thermo Fischer Scientific), cultures were grown as stated above for a total of 4 h, including incubation time with antibiotic compounds. Density was adjusted to OD_{600} = 0.5 in identical medium immediately before addition of antibiotics. For the last 15 min of incubation, 0.5 µg/mL Van-FL and 4.5 µg/mL unlabeled vancomycin were added to the cultures. Cultures were washed three times in medium (2 min, 13,000 rpm), mounted on 1% w/w agarose slides and microscopically visualized as described above.

3.5. Data Analysis

3.5.1. Image processing

If not stated otherwise in the respective method, all image data analysis was performed using raw, unprocessed micrograph images.

Brightness and contrast adjustments

For representative micrograph images and for the manual evaluation of cell characteristics (see below), brightness and contrast (B/C) were individually adjusted for the respective image by using the FIJI B/C adjustment auto function. If B/C was adjusted to a control, all samples were adjusted to the values determined for the control.

z-Projections and Deconvolution

z-Projections of stacks were created using the FIJI Z project function. Deconvolution of z-stacks acquired via widefield microscopy was performed using the Carl Zeiss Zen Blue 3.6 direct processing optimized for quality. Deconvolution procedures of HiLo live-cell micrographs and Airyscan superresolution micrographs are described in chapter 3.4.

3.5.2. Individual cell detection and analysis

Detection of individual bacterial cells was achieved using the FIJI plug-In MicrobeJ (Ducret *et al.* 2016). The plug-in was used to algorithmically detect and segment individual cells based on the phase contrast image, thus enabling unbiased cell recognition with respect to the fluorescent signals. Parameters for cell recognition and segmentation were adjusted for each species to optimize for minimal false positive recognitions, while enabling detection of cells within a range of cell morphologies (e.g. cell size, length:width ratio) to include cells with phenotypic changes due to antibiotic treatment in an unbiased way. Binary mask settings were optimized for each micrograph to optimize for maximum cell area coverage. Unsharp and artifact-rich regions were always excluded from the analysis.

3.5.3. Convolved average projections

Convolved average projections (CAPs) were generated from all individual cells of a sample detected with MicrobeJ (see chapter 3.5.2). All single cell images were stacked using the FIJI images to stack function with bicubic interpolation to scale (smallest) after automated rotation of the longer cell axis into a vertical orientation. Stacked images were convolved to increase contrast, emphasize fluorescence maxima and minimize unspecific background, using the FIJI convolve process with the convolution Kernel {-1 -1 -1 -1 -1; -1 -1 -1 -1 -1; -1 -1 24 -1 -1; -1 -1 -1 -1 -1; -1 -1 -1 -1 -1}. The convolved cell image stacks were projected using the Fiji average projection function to a single average image. An overview of the process is shown in Figure 20 (see chapter 4.1.2).

3.5.4. Medial:lateral and septal:peripheral measurements

Quantification of intensity values along either the septal axis (medial:lateral measurements) or the medial axis (septal:peripheral measurements) was achieved by measuring intensity values along the respective axis using the FIJI line plot profile function with a line width of around 190 nm in cells (exact values depended on image-specific px to nm conversion). This procedure was identical for both individual cells and CAPs with a line width of 3 px.

Ratios of medial:lateral measurements were determined by first normalizing the obtained intensity values to the medial maximum value of the plot, which was determined within a 3-pixel (px) range around the center px of the measurement. Lateral maxima were determined from the relative numbers as the highest values outside the range used for determination of the medial maximum. Two lateral maxima were determined per plot, one for the px value smaller and one for the px value higher than the medial maximum, yielding a left and a right lateral maximum. The two lateral maximum values were used to

calculate a mean lateral maximum value. Medial:lateral ratios were calculated as the quotient of the mean lateral maximum and the medial maximum. Ratios of septal:peripheral measurements were determined likewise with septal and peripheral maxima, respectively.

3.5.5. Relative abundance of morphologies

Relative abundance of morphologies (e.g., cells with septal signal of the proteins of interest) was determined by manually assessing 200 cells of a sample (if not stated otherwise) after individual B/C adjustment for each single cell image (see chapter 3.5.1). Images were manually sorted for the distinctive visual appearance of the morphologic phenotype and the relative abundance was calculated.

Septal signal

A distinctive septal signal was defined as a visible septum morphology in any stage of septum progression with any orientation to the visual axis. If a potentially septal signal orthogonal to the visual axis could not be distinguished form an unspecific membrane signal, cells were handled as not showing a septal signal.

Aberrant septum formation

Cells with aberrant septa were defined as cells, where a distinctive septal signal was apparent, but the morphologic features of that septum were misshapen in any way (e.g., bent septum). Similarly, if multiple septa were visible in a single cell, this was also counted as aberrant septum formation. Additionally, cells with impaired daughter cell separation and irregular septum placement according to the definition of assembly state (see below) were also included.

Assembly state

Assembly state was defined as the visibility of septal signal in the daughter cells prior to cell separation of the parent cell following the model of *S. aureus* septum placement in sister cells described by Saraiva *et al.* (2020).

Cytoplasmic localization

Cytoplasmic localization was defined as the disappearance of any ordered localization, resulting in an apparently unspecific, cytoplasmic signal.

Cell cycle phase distribution

The distribution of cell cycle phases was determined using single cell images of cells stained with nile red (see chapter 3.4.4). Cells were manually assessed and classified according to a previously described model of staphylococcal cell membrane morphology throughout the cell cycle (Monteiro *et al.* 2015). Briefly, three cell phases were distinguished: Phase 1; where no distinctive septal signal was

visible, Phase 2; where a clearly open septum was observed and Phase 3; where a septum with visibly continuous septal signal was observed.

3.5.6. Z-ring diameter of cells imaged with Airyscan superresolution microscopy

To quantify the Z-ring diameters of cells imaged with Airyscan superresolution microscopy, medial:lateral plots were measured for 150 cells per sample (see chapter 3.5.4), if not stated otherwise. Z-ring diameters were determined as the distance between the left and right fluorescence maximum of each plot with a lower threshold of 300 nm.

3.5.7. Z-ring diameter over time

The progression of Z-ring size over time was analyzed using deconvoluted HiLo live-cell microscopy data. To determine the behavior of Z-ring diameter throughout one cell cycle in *S. aureus*, ~ 30 cells at the start of a cell division cycle (Z-ring in assembly state, prior to division of the parent cell) were chosen randomly at t = 0 min. Assembly state was defined via visibility of a newly formed Z-ring prior to parent cell division (see chapter 3.5.5). To analyze Z-ring dynamics during antibiotic treatment, cells were chosen randomly at t = 0 min until ~ 30 cells per category (assembly state, early-, mid- and late-stage cell division state) were found. Early-, mid- and late-stage cell division state of cells was determined by measuring the Z-ring diameter at t = 0 min (early: ≥780 nm, mid: 585 - 715 nm, late: ≤ 520 nm, increments corresponding to px size). For each individual cell, the Z-ring diameter was measured every 10 min from t = -20 min to t = 70 min with pixel-size accuracy (65nm). The Z-ring diameter was defined as the distance between the left and right fluorescence maximum of each plot with a lower threshold of 325 nm. To determine the relative abundance of division stage categories at t = 0 min, cells were chosen randomly and categorized as described above. Z-ring diameter was always denoted 0 nm if the Z-ring diameter was below the lower threshold and a cell division event was observed in the phase contrast channel. Septum closure was achieved if the Z-ring diameter was decreased to 0 nm according to this definition. The time needed for septum closure was measured from t = 0 min or from the time where a septal Z-ring was imaged first. The time of active septum constriction was defined as the interval between the first time point, where a decrease in Z-ring size compared to the time point before was observed, and septum closure. Active septum progression was defined as ≥ 130 nm decrease of Z-ring size compared to t = 0 min.

3.5.8. PBP2-GFP septal localization over time

The localization of PBP2-GFP over time was analyzed using HiLo live-cell microscopy data. For each replicate, a total of 30 cells was chosen randomly at t = -20 min and assessed qualitatively for a septal PBP2 localization signal every 10 min from t = -20 min to t = 70 min. If cells divided, one of the daughter cells was chosen randomly for analysis of the subsequent time points. Fluxes between each time point were classified into four categories:

- cell division, septal PBP2 becomes non-septal in the daughter cell,
- PBP2 recruitment, PBP2 localization changes from non-septal to septal,
- PBP2 localization remains non-septal,
- PBP2 localization remains septal.

A theoretical 5th category, where PBP2 localization becomes non-septal without division, was not needed as no cells behaved this way in the analyses carried out for this work.

3.5.9. Fluorescence Intensities

Fluorescence intensities of individual cells were determined with the mean fluorescence per cell function in MicrobeJ. If necessary, background correction was performed using the MicrobeJ mean_c function. Population mean values were calculated as the mean of all determined cell mean values of a sample.

3.5.10. Fluorescence maxima

Fluorescence maxima were determined on the individual cell level using the MicrobeJ maxima detection process. Maxima were defined as a px of highest local fluorescence (MicrobeJ “point” function). Maxima detection was limited to three (HADA) or five (FloA, IsdF, A37FL) maxima per cell to ensure that only the maxima with highest fluorescence intensities relative to the cell mean intensity were detected (MicrobeJ “CutOff” function). Lower threshold (MicrobeJ “tolerance” function) was set to 10 % of the population mean intensity to detect maxima even in cells with comparably low intensity, while excluding potential artifacts and outliers with negligible fluorescence intensity. Location coordinates of all maxima were recorded relative to the individual cell center as origin and normalized for the individual cell dimensions to enable a normalized plotting of all detected maxima of a population in a cartesian coordinate system. Plotting the mean contour of all straightened cells as measured in absolute values (µm) over the plotted, normalized maxima using the contour center as origin enabled conversion of the relative coordinates to absolute coordinates given in µm. Thus, final plots show an integrated localization map of all detected maxima within the mean cell dimensions.

3.5.11. Co-localization analysis

Co-localization analysis on the individual cell level was determined as the Pearson product-moment correlation coefficient (PCC) between two micrograph channels. The PCC was determined using the MicrobeJ intensity correlation function. PCC calculates the correlation between px intensity values resulting in values of -1 and 1. Negative values correspond to negative correlation (high intensity of a px in channel A is likely to show a low intensity in channel B) an positive values correspond to positive correlation (high intensity of a px in channel A is likely to show a high intensity in channel B). Therefore, positive PCC values represent co-localization of the two fluorescent signals, while negative PCC values represent an exclusionary localization of the two fluorescent signals.

3.5.12. A37 spots per cell

To quantify the Spots of A37 in cells of *C. glutamicum*, the sum of visible spots in all cells of a sample was determined after individual B/C adjustment for each single cell image (see chapter 3.5.1). The mean number of spots per cell was calculated as the quotient of the sum of spots and the number of cells.

3.5.13. Statistical analysis

All statistical analysis in this work was performed using GraphPad Prism 8.0.2 (263). Statistical significance was determined in unpaired two-tailed students t-tests with a 95% confidence interval, if not stated otherwise. Statistical significance was denoted as ns, not significant; *, p = 0.05 to 0.01; **, p = 0.01 to 0.001; ***, p = 0.001 to 0.0001; ****, p ≤ 0.0001. All experiments in this work were repeated three times with biologically independent replicates, if not stated otherwise. Statistical analysis was always performed on either the population mean values of the independent replicates, or the convolved average projection data, if not stated otherwise.

If data analysis required data normalization, all data was normalized to the replicate mean of the respective control.

Outlier exclusion was performed solely to improve data intelligibility in graphs. All statistical analysis was performed on the full data sets. All conclusions drawn from the results presented in this work were based on the full data sets. Thus, outlier exclusion had no impact on any statistical analysis or the scientific reasoning of this work. Outlier exclusion was performed using Prism 8 robust regression and outlier removal (ROUT) with Q = 1% (Motulsky *et al.* 2006).

3.5.14. Data visualization

All graphs show the mean of all three population mean values with error bars denoting the standard deviation, if not stated otherwise. Distribution of individual cell values or population mean values were plotted either as superplots, insets or in another appropriate way to increase data intelligibility whenever applicable (Lord *et al.* 2020).

4. Results

4.1. Investigating the impact of peptidoglycan synthesis inhibition on *S. aureus* cell division

To examine the key cellular consequences of PGS inhibition for cell division of *S. aureus*, the effects of the glycopeptides vancomycin and telavancin as well as the beta-lactam oxacillin on the central cell division protein FtsZ and key CWBM components were investigated.

4.1.1. Determination of antibiotic treatment time and concentration

First, the appropriate antibiotic concentration and time range for observing the first and most relevant cellular effects of vancomycin, telavancin and oxacillin on cell division was determined. Therefore, the antibacterial activity of the three antibiotics was evaluated. MICs according to CLSI standards were determined against *S. aureus* RN4220 as 2 µg/mL (vancomycin), 0.25 µg/mL (telavancin) and 0.5 µg/mL (oxacillin). Due to reports of an inoculum effect for telavancin (Barcia-Macay *et al.* 2006), MICs were also performed with an increased inoculum and indeed, an increase in MIC was observed for telavancin. As further experiments were performed with cell densities closer to this increased inoculum than to the CLSI standard inoculum, this second set of MIC values was chosen as basis for further experiments. Using the adjusted MIC values of 2 µg/mL (vancomycin), 1 µg/mL (telavancin) and 0.5 µg/mL (oxacillin), time-kill kinetics for *S. aureus* were determined (Figure 17). For all three antibiotics, a concentration of 4 x MIC resulted in a long-term bactericidal effect, while having moderate impact on cell viability within the first hours of treatment. Importantly, complete growth inhibition was observed at these concentrations for all three antibiotics, as CFU/mL stagnated from the moment of antibiotic addition. It was concluded, that investigating the initial hour of treatment with 4 x MIC was suitable for the aim of this work to understand the key cellular consequences of PGS inhibition on cell division and the spatio-temporal organization of the CWBM prior the ultimate cell death.

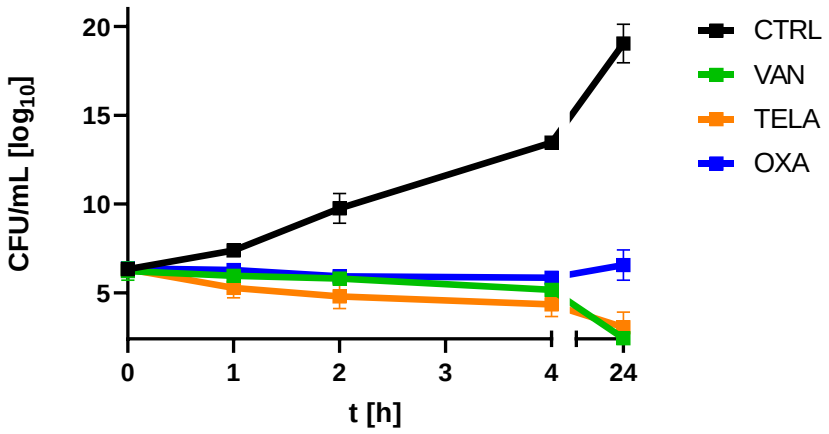

Figure 17: Time-kill kinetics of vancomycin, telavancin and beta-lactam oxacillin against *S. aureus* RN4220. Symbols show the mean of three independent biological experiments ± SD.

The PGS inhibiting impact of the three antibiotics under experimental conditions used for microscopic experiments was validated using the fluorescent dye HADA (HCC-amino-D-alanine). The amino acid derivative serves as alternative electron donor in the TPase reaction and is thereby incorporated into the cell wall by transpeptidases. Accordingly, the amount of HADA signal is proportional to the TPase activity and enables quantitative analysis of extent and localization of the final PGS step *in vivo* (Kuru *et al.* 2012, 2019). Treatment with 4 x MIC vancomycin, telavancin or oxacillin for 15 min significantly reduced the HADA signal, illustrating that rapid and effective PGS inhibition was achieved under the chosen conditions (Figure 18).

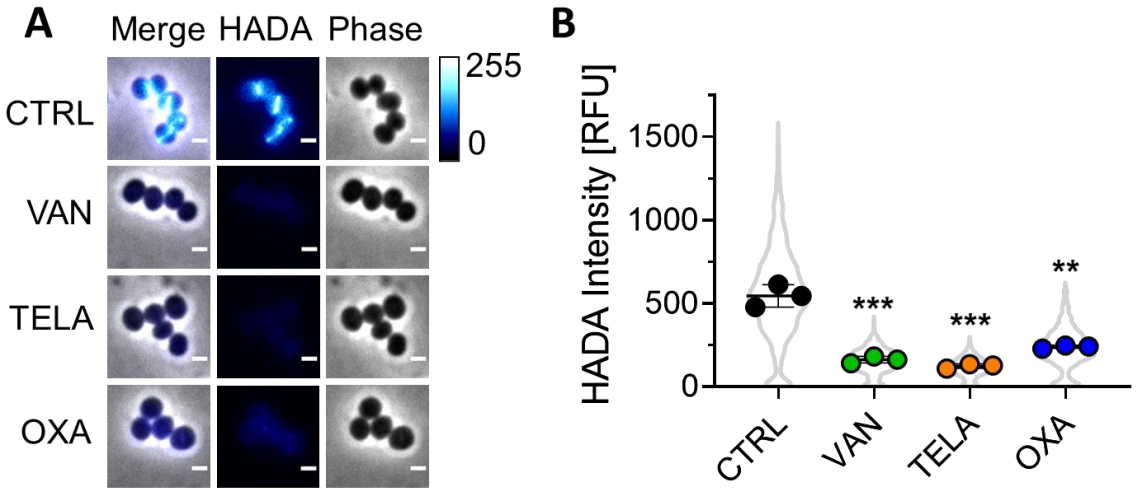

Figure 18: 4 x MIC of vancomycin, telavancin or oxacillin effectively inhibit HADA incorporation. (A) Representative micrographs of *S. aureus* RN4220 treated for 15 min with 4 x MIC, vancomycin, telavancin or oxacillin and stained with HADA. Brightness and contrast of the HADA channel was adjusted to the untreated control for all micrographs. Scale bar, 1 µm. **(B)** Quantification of HADA intensities of individual cells. Violin plots show the distribution of individual cell data after exclusion of outliers. Line and error bars show mean ± SD of three independent biological experiments. Symbols show mean of each independent replicate. n ≥ 275 per replicate and condition. RFU: Relative Fluorescence Unit. Statistical significance was determined against the untreated control using unpaired two-tailed students t-tests with a 95% confidence interval. Statistical significance was denoted as **, p = 0.01 to 0.001; ***, p = 0.001 to 0.0001.

4.1.2. Impact of antibiotics vancomycin, telavancin and oxacillin on cell division of *S. aureus*

Using the determined concentrations, the impact of vancomycin, telavancin and oxacillin on the cell cycle of *S. aureus* RN4220 was investigated. In a well-established approach, the membrane dye nile red can be used to distinguish between three cell cycle phases in *S. aureus* (Figure 19B, see Monteiro *et al.* 2015). The control population of untreated cells showed a cell cycle phase distribution of approximately 55% of cells without membrane invagination (Phase 1), 20% of the cells with initiated septum constriction (Phase 2), and the remaining 25% of the cells in the late stage of cell division (Phase 3), which is well in line with earlier reports (Monteiro *et al.* 2015). Treatment with either antibiotic had significant impact on these dynamics. For all three antibiotics, the proportion of cells in phase 3 was notably reduced from 25% to approximately 8%, while the proportion of cells in phase 1 increased

accordingly. Interestingly, the relative abundance of phase 2 cells remained stable with only minor differences to the untreated control. These results illustrated a significant effect of PGS inhibition on the cell cycle of *S. aureus*, which indicated an impairment of septum constriction and/or initiation of cell division.

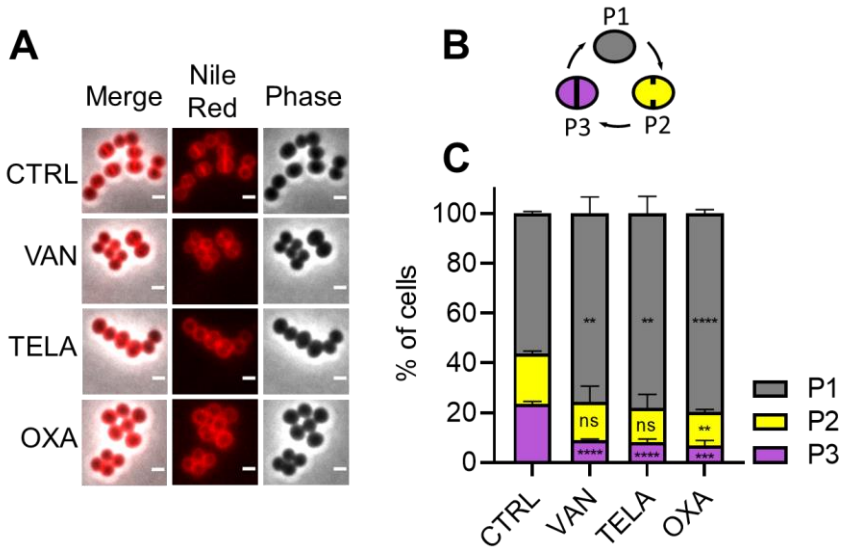

Figure 19: Treatment with PGS-targeting antibiotics leads to a pronounced shift in cell cycle phase distribution. (A) Representative micrographs of *S. aureus* RN4220 cells stained with the membrane dye Nile Red after 25 min of treatment with vancomycin, telavancin or oxacillin and an untreated control. Scale bar, 1 µm. **(B)** Schematic representation of the three distinctive morphologies of *S. aureus* throughout the cell cycle as visible in a membrane stain. Black lines represent the cell membrane. Grey: Phase 1 (P1) cells. Yellow: Phase 2 (P2) cells. Violet: Phase 3 (P3) cells. **(C)** Quantification of cell cycle phase distribution in *S. aureus* RN4220 after 25 min of treatment with vancomycin, telavancin or oxacillin and an untreated control. Grey: P1 cells. Yellow: P2 cells. Violet: P3 cells. Bars show the mean of three independent biological experiments ± SD. n ≥ 200 cells per replicate and condition. Statistical significance was determined against the untreated control using unpaired two-tailed students t-tests with a 95% confidence interval. Statistical significance was denoted as ns, not significant, $p > 0.05$; **, $p = 0.01$ to 0.001; ***, $p = 0.001$ to 0.0001; ****, $p \leq 0.0001$.

To further investigate this pronounced effect on the cell cycle, antibiotic impact on localization of the central cell division protein FtsZ was microscopically visualized. FtsZ localization is highly dynamic during the cell cycle, and the Z-ring formed by treadmilling FtsZ filaments is a structure constantly decreasing in size during cell division in the process of septum constriction (see chapter 1.3, Bisson-Filho *et al.* 2017; Monteiro *et al.* 2018; Yang *et al.* 2017). Therefore, FtsZ localization is very diverse within a population of *S. aureus* cells even under normal conditions, which had to be accounted for in developing a method for reliable detection of antibiotic impact on FtsZ localization. Additionally, typical high-throughput methods of subcellular localization analysis are unsuitable for the unique challenges of *S. aureus* morphology. Most model organisms (e.g., *E. coli, Bacillus subtilis* or *Streptococcus pneumoniae*) display some form of geometric asymmetry. This enables automated orientation of the image plane with respect to the cell morphology and therefore provides a geometric basis for analyzing the subcellular localization of fluorescence signals. However, *S. aureus* stays nearly spherical

throughout the cell cycle, and the minor elongation is not sufficient to precisely detect the medial axis automatically in diffraction-limited fluorescence microscopy (Monteiro *et al.* 2015). As a result, automated high-throughput methods of image analysis usually fail at the phenotypic variety of *S. aureus* cells. This phenomenon is further amplified by the multitude of possible viewing angles with respect to the cell division septum of the coccoid cells, which are not automatically oriented parallel to the image plane, as elongated cells generally do. More detailed approaches of manual single-cell assessment are also affected by these challenges and therefore require a precise parameter design to not introduce biases into the analysis, e.g., by excluding entire subpopulations from measurements due to method prerequisites, or by neglecting relevant patterns that cannot be quantified by the chosen method.

Combining the obtained microscopy images of all cells within a sample set into a comprehensive representation is a promising approach to visualize and analyze fluorescence localization patterns (and changes thereof) in an automated and unbiased way. Recent studies already used a similar approach by combining individual cells into average projections for analysis of *B. subtilis* and *E. coli* septum formation (Navarro *et al.* 2022; Squyres *et al.* 2021). Importantly, average projections require a precise alignment of the individual cells prior to projection. As a result of this prerequisite, simple average projections were unsuccessful for visualizing localization patterns in *S. aureus* due to the small size of the coccoid bacteria and the above-mentioned problems arising from the cell morphology and FtsZ localization dynamics. To solve this, the method of averaging was optimized by including a pre-processing convolution step of the individual cell images prior to the subsequent average projection. These convolved average projections (CAPs) were therefore established as a tool to comprehensively visualize the impact of antibiotic treatment on protein localization under consideration of the unique challenges of analyzing fluorescence localization patterns in *S. aureus* populations (Figure 20).

To generate a CAP from raw micrographs, first an automated cell recognition and segmentation is performed based on phase contrast image of the cells (Figure 20). This enables a cell recognition independent from the fluorescence signal. Then all cells are aligned along the automatically determined medial axis into a vertical orientation. To minimize the negative effects of the above-mentioned imprecise alignment, the individual cell images are pre-processed via convolution. The convolution kernel chosen for this correction heavily emphasizes local fluorescence maxima and drastically reduces the other signals. Consequently, unspecific background fluorescence is minimized, and the average projection is constructed from only the brightest fluorescence signals of each cell. All convolved and correctly oriented single cell images are then z-projected to one average image. This single “cell-like” image is effectively a condensed representation of the complete sample population. While CAPs have only limited informative value about individual cells (given their nature as averages), they visualize general localization patterns and trends in an automated, unbiased way.

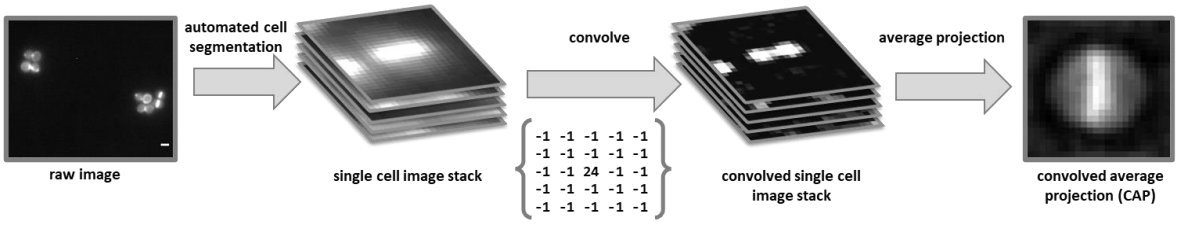

Figure 20: Schematic overview of the generation of convolved average projections. Automated cell segmentation and extraction of single cell images was performed using MicrobeJ (see chapter 3.5.2). Convolution, stack generation and average projection was performed using FIJI. The convolution kernel is shown in parenthesis. Scale bar, 1 µm.

To validate technical reproducibility of CAP generation (Figure 21), a set of 1292 imaged cells of *S. aureus* RN4220 pCQ11-MurJ-mNeongreen was subsampled by randomly choosing 400 cells from the set and combining them into a subset. This was repeated for a total of three times, thereby generating three technical subsamples from one biological replicate. Furthermore, the impact of the input cell number for CAPs was tested by stepwise subtraction of cells from each subsample stack. This process yielded a total of three technical replicates of multiple cell stacks with cell numbers ranging from 40 to 400 cells. CAPs were generated from each stack (Figure 21A) and relative brightness along septal and medial axes were determined for each generated CAP (Figure 21B,C). These measurements demonstrated that technical reproducibility of CAPs was reliable even at comparably low cell numbers below 100 cells. Furthermore, measurements did not significantly differ between CAPs generated from low cell numbers and CAPs generated from high cell numbers.

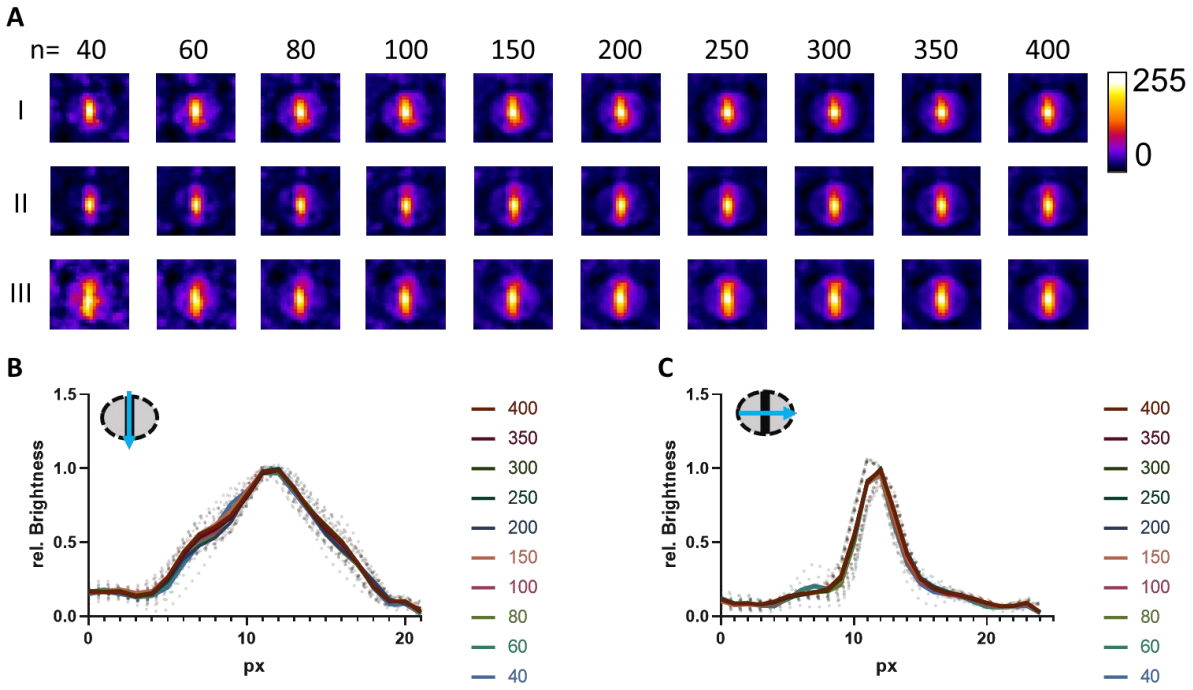

Figure 21: Technical reproducibility of CAPs and impact of cell number used for CAP generation. (A) Technical replicates I - III of CAPs were generated from a sample population of 1292 cells of *S. aureus* RN4220 pCQ11-MurJ-mNeonGreen. For each technical replicate, a subsample of 400 cells was randomly chosen via the MicrobeJ random selection function. To test impact of cell number on CAP appearance, cells were stepwise subtracted from the subsample stack, with n corresponding to the number of cells left in the subsample. The order of individual cells in each technical replicate subsample stack was determined according to the MicrobeJ name.ID image naming. **(B)** Quantification of CAP brightness of the technical replicates shown in A along the septal axis, plotted relative the medial brightness value. For each condition, the mean of three independent biological experiments is shown as thick line ± SD as dotted, semi-transparent lines. **(C)** Quantification of CAP brightness of the technical replicates shown in A along the medial axis, plotted relative the septal brightness value. For each condition, the mean of three independent biological experiments is shown as thick line ± SD as dotted, semi-transparent lines. E-F: Representation of different localization patterns in CAP appearance.

With the newly developed tool of CAPs, the impact with vancomycin, telavancin and oxacillin on FtsZ localization was investigated. FtsZ was visualized on a widefield microscope using the strain *S. aureus* RN4220 pCQ11-FtsZ-SNAP labelled with SNAP-Cell® TMR Star (Figure 22). CAPs of the untreated control showed a uniform distribution of brightness along the septal axis (Figure 22B,C). This observation is in line with the expected even distribution of cells with different Z-ring sizes due to the normal septum constriction over the course of cell division. Treatment with PGS inhibiting antibiotics, however, resulted in pronounced shifts of the CAP brightness towards the lateral edges of the septum, with a corroborating decrease in medial brightness. Quantifying this medial:lateral ratio revealed significant differences between the treated cells and the untreated control, indicating that more cells with large Z-rings were found after treatment with PGS inhibiting antibiotics (Figure 22D). Importantly, samples treated with either antibiotic still showed the same abundance of cells with septal FtsZ localization in distinctive ring-like formation after 25 min of treatment (Figure 22E). Thus, Z-ring integrity was clearly unaffected antibiotic treatment.

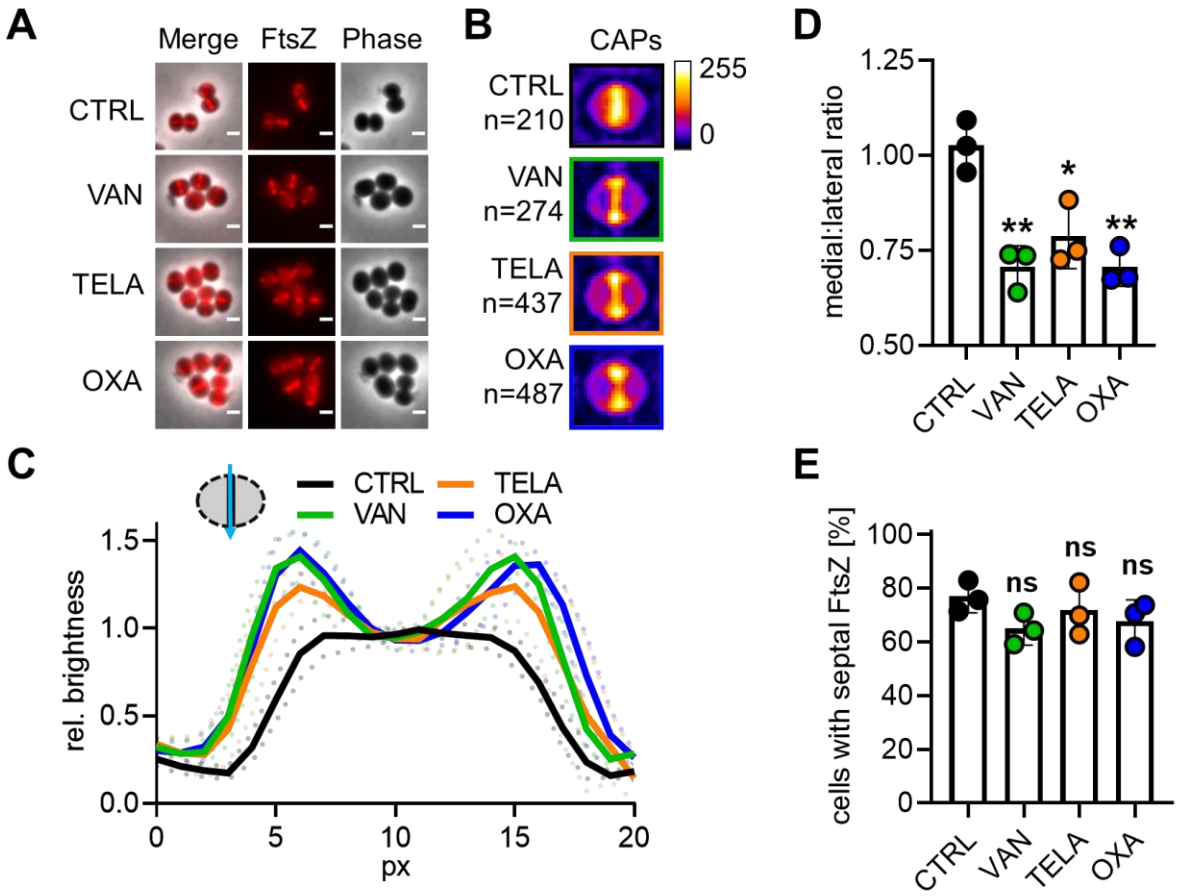

Figure 22: CAPs indicate significant impact of PGS inhibition on Z-ring size. (A) Representative micrographs of *S. aureus* RN4220 pCQ11-FtsZ-SNAP after 25 min of treatment with vancomycin, telavancin or oxacillin and an untreated control. SNAP-tags were labelled with SNAP-Cell® TMR Star. Scale bar, 1 µm. **(B)** CAPs of *S. aureus* RN4220 pCQ11-FtsZ-SNAP cells treated with vancomycin, telavancin or oxacillin and an untreated control. n corresponds to the number of individual cells used for CAP generation. Representative CAPs of three independent biological experiments. **(C)** Quantification of CAP brightness along the septal axis, plotted relative to the medial brightness value. The mean of three independent biological experiments is shown as thick line ± SD as dotted, semi-transparent lines. **(D)** Medial:lateral ratio of CAP brightness profiles. Bar graphs show the mean of three independent biological experiments ± SD, respectively. Symbols indicate the values of the individual replicates. **(E)** Relative abundance of cells with septal FtsZ localization as % of total population after 25 min of treatment with vancomycin, telavancin or oxacillin and an untreated control. Bar graphs show the mean of three independent biological experiments ± SD. Symbols indicate the values of the individual replicates, determined as the mean of n ≥ 161 individual cells per replicate and condition. Statistical significance was determined against the untreated control using unpaired two-tailed students t-tests (95% confidence interval) against the untreated control. Statistical significance was denoted as ns, not significant, $p > 0.05$; *, $p = 0.05$ to 0.01; **, $p = 0.01$ to 0.001.

The significant changes in CAP brightness indicated a higher abundance of cells with large Z-ring diameters after antibiotic treatment. To validate this, the impact of vancomycin, telavancin and oxacillin on Z-ring size was quantified on the individual cell level. Therefore, FtsZ was visualized on an Airyscan superresolution microscope using the strain *S. aureus* RN4220 pCQ11-FtsZ-SNAP labelled with SNAP-Cell® 505 Star (Figure 23). The improved resolution enabled high-quality 3D visualization of Z-rings in individual cells and precise manual measurements of Z-ring diameters. Additionally, cells were stained with the membrane dye CellBrite® Fix 640 for visualization of cell outlines. Measurements of individual Z-ring diameters were performed with a lower threshold of 300 nm.

This precise evaluation of the antibiotics impact on Z-ring size confirmed the indications of the CAP analysis. A notable shift in Z-ring diameters towards larger diameters was observed after treatment with PGS inhibiting antibiotics (Figure 23B). Mean Z-ring diameters were significantly increased by 30% (vancomycin), 41% (telavancin), and 44% (oxacillin), compared to the untreated control. Notably, diameters well above 1100 nm were measured in treated cells, while the FtsZ ring diameter of untreated cells did not exceed 893 nm, corroborating reports of cell swelling during treatment with either glycopeptides or beta-lactams (Salamaga *et al.* 2021; Wacnik *et al.* 2022).

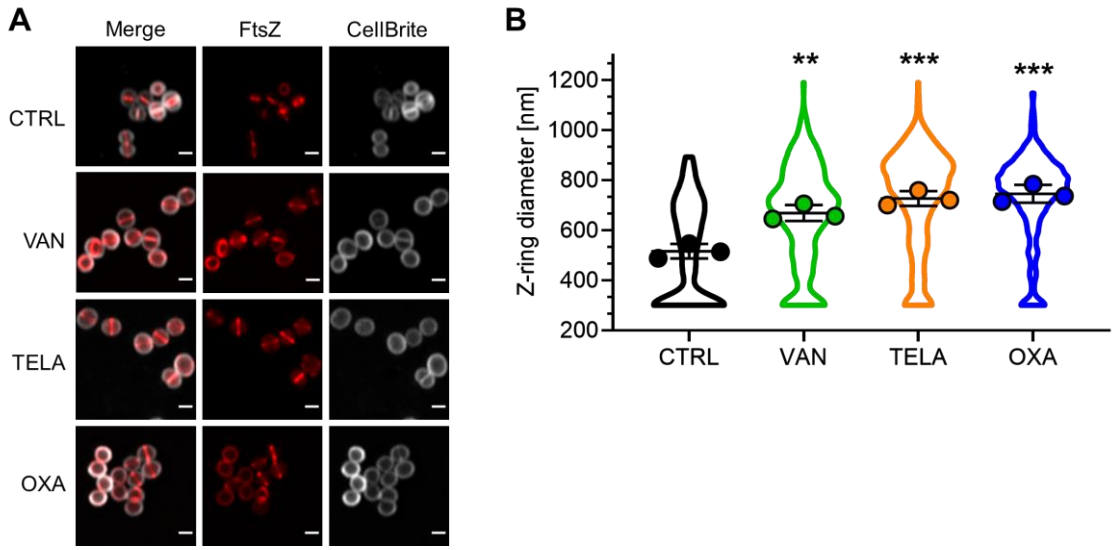

Figure 23: Z-ring diameters are significantly increased after treatment with PGS inhibiting antibiotics. (A) Representative AiryScan superresolution microscopy images of *S. aureus* RN4220 pCQ11-FtsZ-SNAP treated for 25 min with vancomycin, telavancin or oxacillin and an untreated control. SNAP-tag was labelled with SNAP-Cell® 505-Star. Cell membrane was stained with CellBrite® Fix 640. Scale bar, 1 µm. Imaging by Dominik Brajtenbach. **(B)** Z-ring diameter distribution after antibiotic treatment. Violin plots show individual cell data, symbols show replicate means. n ≥ 57 cells per replicate and condition. Statistical significance was determined against the untreated control using unpaired two-tailed students t-tests (95% confidence interval) against the untreated control. Statistical significance was denoted as **, p = 0.01 to 0.001; ***, p = 0.001 to 0.0001.

4.1.3. Analysis of live-cell Z-ring dynamics throughout the *S. aureus* cell cycle

The Z-ring size is a measure of septum progression (Bisson-Filho *et al.* 2017; Monteiro *et al.* 2018; Squyres *et al.* 2021; Whitley *et al.* 2021). The increase in Z-ring diameter and shift in cell cycle phases revealed a massive impact of PGS inhibition on cell division and suggested an impairment of septum constriction. To elucidate the extent and speed of this effect, the dynamics of Z-ring size in individual cells was visualized over time using live-cell microscopy with HiLo illumination. First, a comprehensive analysis of the Z-ring dynamics in an untreated control was performed (Figure 24). Interestingly, it was observed that Z-rings of daughter cells were frequently assembled prior to division of the parent cell (Figure 24A,B), a phenotype previously described (Saraiva *et al.* 2020), but not well characterized. Z-ring size dynamics over the course of one cell cycle were evaluated starting from this assembly state (Figure 24C). Within the first minutes, Z-ring diameters increased because of cell splitting and the resulting rapid transformation of the new cells into a spherical shape, which is a well-understood process in *S. aureus* (Monteiro *et al.* 2015). Subsequent cell division began with a short phase of stagnation, followed by a fast constriction resulting in septum closure and cell separation. The duration of one cell cycle was 44.6 min on average with 26.8 min of active septum constriction (see appendix 1), which is in line with reported growth rates of *S. aureus* in microscopic setups (Monteiro *et al.* 2015, 2018).

As the cultures were not synchronized, cells in different stages of the cell cycle were observed at every image acquisition. To enable comprehensive analysis of the generated data, individual cells were categorized into four categories depending to their phenotype at t = 0 min. Cells in assembly state constituted about 10% of the total population (Figure 24B) and were visually distinguished from cells in cell division state. Cells in the cell division state were further categorized depending on the Z-ring diameter into early (large Z-rings), mid (medium Z-rings) and late (small Z-rings) stage of cell division. For all three categories, rapid septum constriction and subsequent cell division were observed (Figure 24D).

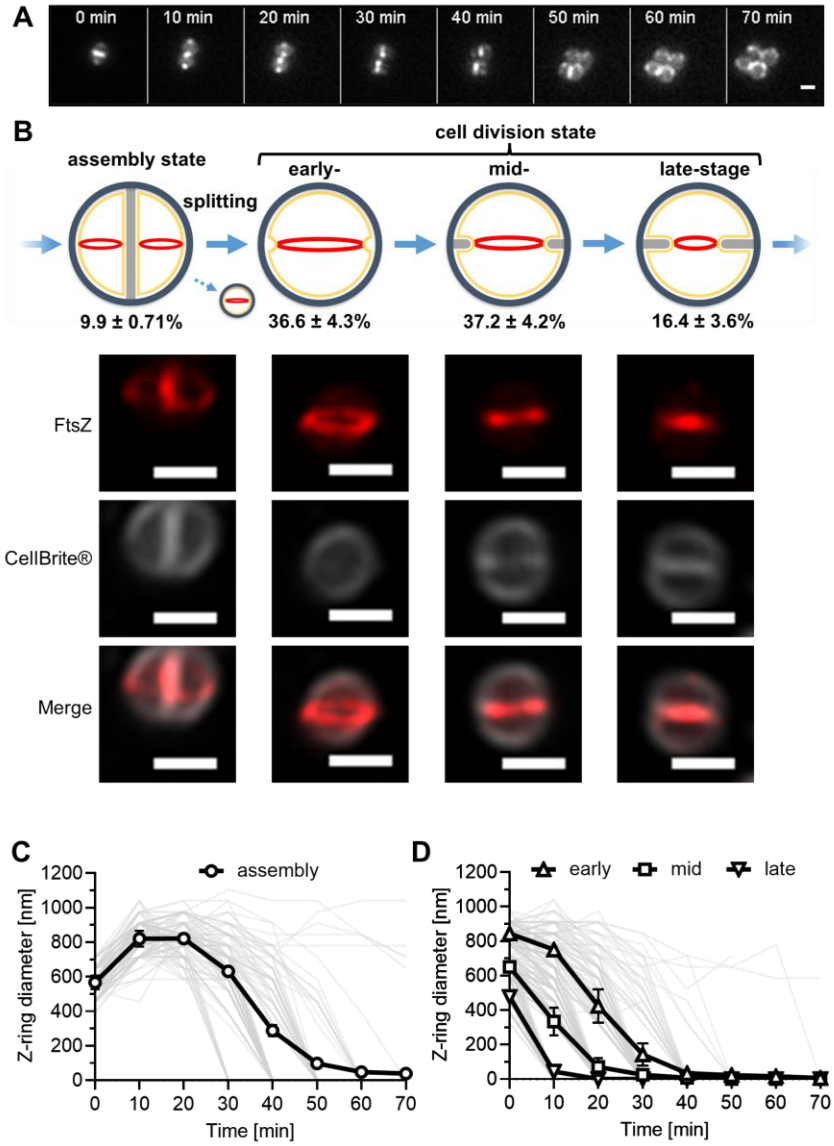

Figure 24: Live-cell dynamics of Z-ring size over time in *S. aureus*. (A) Representative HiLo microscopy images of Z-ring dynamics of *S. aureus* RN4220 pCQ11-FtsZ-mCherry over time. Scale bar 1 µm. Imaging by Dominik Brajtenbach. **(B)** Pictogram illustrating the cell cycle states and cell division stages in *S. aureus* with corresponding Z-ring phenotypes and representative Airyscan super-resolution micrographs of *S. aureus* RN4220 pCQ11-FtsZ-SNAP. Imaging by Dominik Brajtenbach. SNAP-tag was labelled with SNAP-Cell® 505-Star. Cell membrane was stained with CellBrite® Fix 640. Percentages show the relative abundance of each phenotype at t = 0 min as the mean of three independent biological experiments ± SD. n ≥ 131 cells per replicate. Coloring of the pictogram: red: Z-ring. Light grey: new cell wall. Dark grey: old cell wall. Yellow: cell membrane. Micrographs are z-stack maximum projections, scale bar 1 µm. **(C)** Quantification of Z-ring dynamics over the course of one complete cell cycle of *S. aureus*. Per replicate, 30 cells in the assembly state were chosen at t = 0 min and Z-ring size was quantified over 70 min. Individual cell data are plotted as thin semi-transparent lines. Thick black lines with open circles show the mean of three independent biological experiments ± SD. n ≥ 30 cells per replicate. **(D)** Quantification of Z-ring dynamics over time after classification of cells into cell division stages according to Z-ring size at t = 0 min. Individual cell data are plotted as thin semi-transparent lines. Thick black lines with open symbols show the mean of three independent biological experiments ± SD. n ≥ 29 cells per replicate and division stage.

4.1.4. Impact of vancomycin and telavancin on septum constriction

In contrast to the situation in the untreated control (see chapter 4.1.3), Z-ring dynamics were substantially altered in cells treated with vancomycin or telavancin (Figure 25). Both glycopeptides abolished septum constriction almost completely within minutes of treatment (Figure 25A,B). The percentage of cells with active septum progression (≥ 130 nm septum closure) was reduced from 48% in the control to less than 3% within the first 10 min of treatment (Figure 25C). The effect was independent of the cell division stage at the time point of the antibiotics application and resulted in a complete arrest of nearly all septum progression. Effectively, only 6% of cells treated with either vancomycin or telavancin showed active septum progression within 70 min of treatment (Figure 25C). In contrast, more than 98% of untreated cells showed active septum progression in this time. Remarkably, merely three out of the 735 analyzed cells were able to divide after addition of one of the glycopeptides, while 98% of untreated cells proceeded to cell division. These results clearly emphasize the rapid and massive impairment of cell division progress caused by the PGS inhibiting glycopeptides. Interestingly, treated cells that were in the assembly state at the time of exposure still showed parent cell splitting, demonstrating that divisome components responsible for daughter cell separation remained functional (Figure 25B). This result corroborated the reduced abundance of cells in phase 3 in the cell cycle dynamics analysis (see chapter 4.1.2). However, complete cell cycle arrest was subsequently observed in all daughter cells, as they were unable to perform septum constriction (Figure 25B).

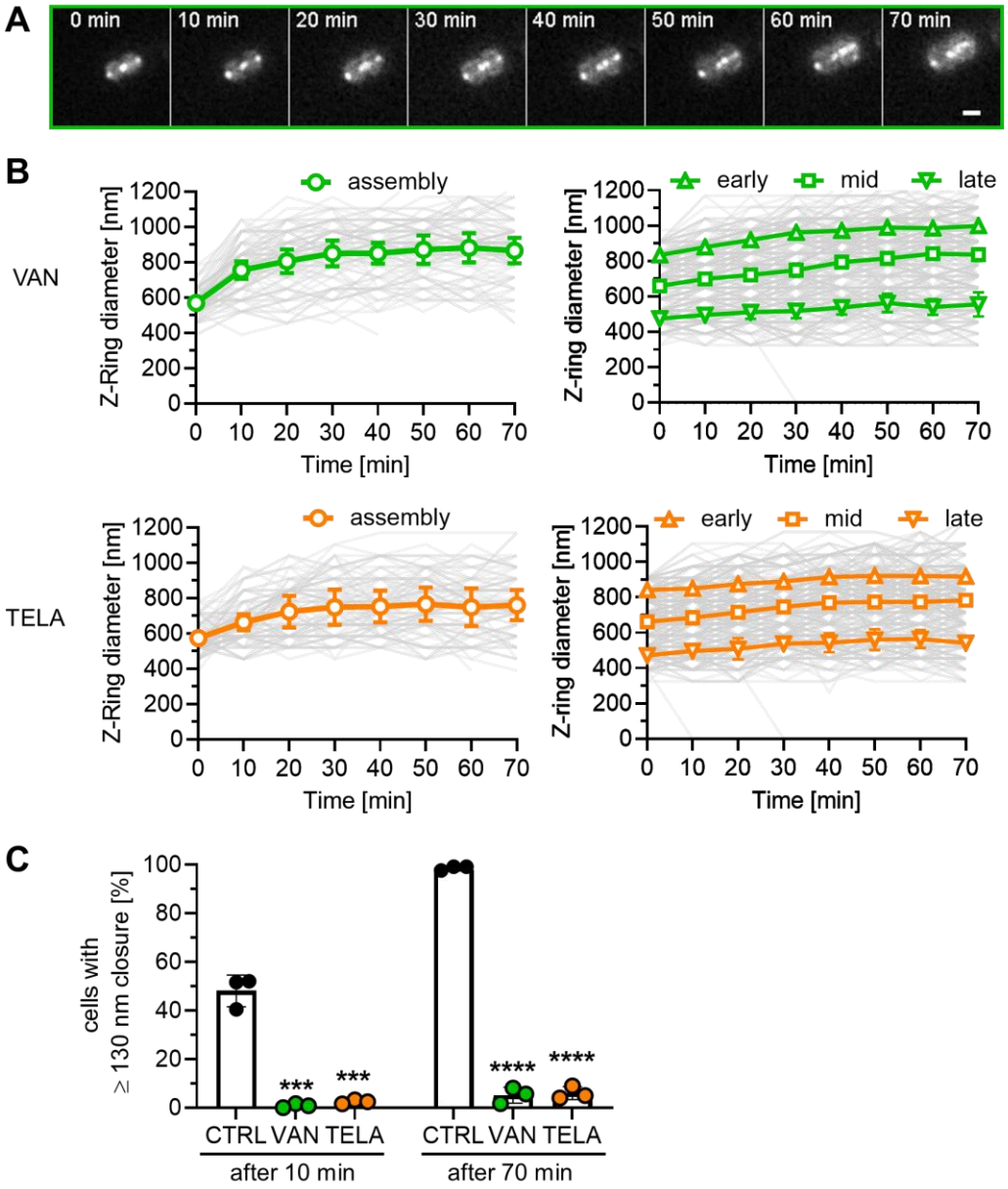

Figure 25: Glycopeptides vancomycin and telavancin lead to immediate arrest of septum progression. (A) Representative HiLo microscopy images of Z-ring dynamics of *S. aureus* RN4220 pCQ11-FtsZ-mCherry over time during vancomycin treatment. Scale bar 1 µm. Imaging by Dominik Brajtenbach. **(B)** Quantification of Z-ring dynamics over time, after classification of cells cycle states and cell division stages according to Z-ring size at t = 0 min. Green: Cells treated with vancomycin. Orange: Cells are treated with telavancin. Individual cell data are plotted as thin semi-transparent lines. Thick lines with open symbols show the mean of three independent biological experiments ± SD. Open symbols correspond to the time points when the cells were imaged. n ≥ 28 cells per replicate, condition, and division stage. **(C)** Quantification of active septum progression. Symbols correspond to values of individual replicates, bar shows the mean of three independent biological experiments ± SD. n ≥ 28 cells per replicate, condition, and division stage. Statistical significance was determined against the untreated control using unpaired two-tailed students t-tests with a 95% confidence interval. Statistical significance was denoted as ***, p = 0.001 to 0.0001; ****, p ≤ 0.0001.

4.1.5. Impact of oxacillin on septum constriction

Oxacillin likewise had drastic impact on septum constriction dynamics (Figure 26). However, in contrast to the glycopeptides, the effect was more intricate and depended on the cell division stage at the time of exposure (Figure 26A,B). As observed during glycopeptide treatment, cells in the assembly state still showed parent cell splitting, but subsequently stopped in the early stage of cell division with nearly complete arrest of septum progression. Similarly, constriction was almost completely inhibited in early-stage cells with large Z-rings at the time of oxacillin addition. Interestingly, mid- and late-stage cells were still able to perform septum closure and proceed to cell division (Figure 26B). The percentage of cells performing septum closure was determined as 95%, 63% and 15% for late-stage, mid-stage and early-stage cells, respectively (Figure 26C). Notably, a significant increase in the time needed for septum closure was observed in those cells still able to divide, demonstrating a reduction in septum constriction velocity (Figure 26D).

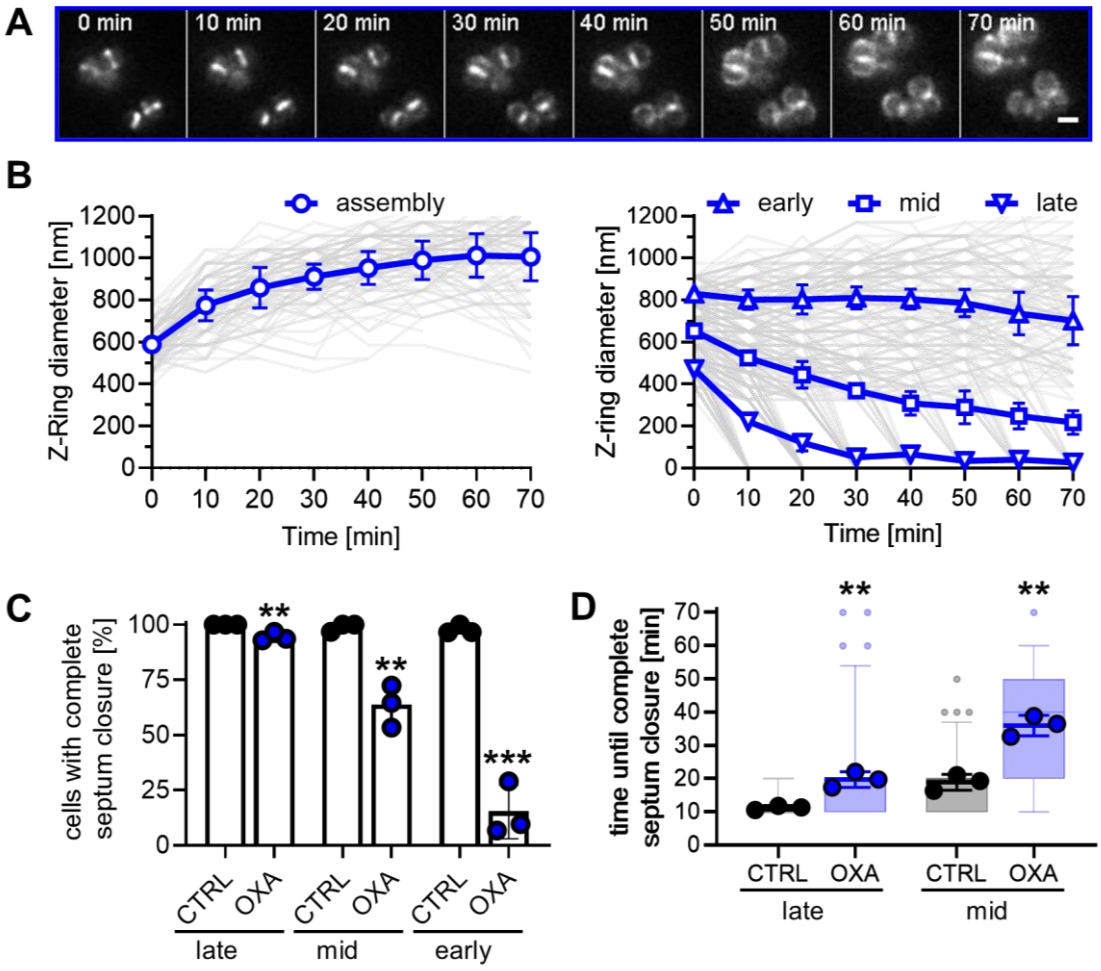

Figure 26: Oxacillin differentially affects septum constriction depending on the cell division stage. (A) Representative HiLo microscopy images of Z-ring dynamics of *S. aureus* RN4220 pCQ11-FtsZ-mCherry over time during oxacillin treatment. Scale bar, 1 µm. Imaging by Dominik Brajtenbach. **(B)** Quantification of Z-ring dynamics over time, after classification of cells into cycle states and cell division stages according to Z-ring size at t = 0 min. Individual cell data are plotted as thin semi-transparent lines. Thick lines with open symbols show the mean of three independent biological experiments ± SD. Open symbols correspond to the time points, when cells were imaged, and Z-ring sizes were analyzed. n ≥ 30 cells per replicate and cell cycle state. **(C)** Quantification of septum closure activity as % of cells with complete septum closure within 70 min of treatment. Symbols correspond to values of individual replicates, bars show the mean of three independent biological experiments ± SD. n ≥ 29 cells per replicate, condition, and division stage. **(D)** Quantification of the time needed for complete septum closure. For the category of early-stage cells, the sample size was too small for a reliable analysis, given the nearly complete halt of septum progression. Semi-transparent boxplots show the distribution of individual cell data with 95% confidence interval. Semitransparent small points represent outlier of individual cell data. Large symbols correspond to values of individual replicates, thick lines show the mean of three independent biological experiments ± SD. n ≥ 29 cells per replicate, condition, and division stage. Statistical significance was determined against the untreated control using unpaired two-tailed students t-tests with a 95% confidence interval. Statistical significance was denoted as **, p = 0.01 to 0.001; ***, p = 0.001 to 0.0001.

4.1.6. Impact of vancomycin, telavancin and oxacillin on subcellular localization of septal CWBM components

To investigate the relation between cell division arrest and structural integrity of the CWBM, the subcellular localization patterns of multiple key CWBM components were analyzed after antibiotic treatment. Strains of *S. aureus* RN4220 with fluorescently labelled proteins FtsW, RodA, MurJ, PBP4 and PBP2 were visualized on a widefield microscope (Figure 27). All visualized proteins are known to localize to the septum in *S. aureus* (see chapter 1.3, Monteiro *et al.* 2018). However, the mechanisms and timepoints of their septal recruitments differ as well as their respective molecular functions and structural roles for the CWBM:

- The two members of the SEDS protein family, FtsW and RodA, which are both localized to the septum in the early phase of cell division (Monteiro *et al.* 2018). Both proteins are TGases (Emami *et al.* 2017; Meeske *et al.* 2016; Reichmann *et al.* 2019; Taguchi *et al.* 2019). FtsW is essential for *S. aureus* growth and survival and a putative lipid II flippase (Mohammadi *et al.* 2011). RodA is non-essential, but has an important role in cell shape maintenance (Reichmann *et al.* 2019). Both proteins are known to form cognate pairs with monofunctional PBPs (PBP1-FtsW and PBP3-RodA, respectively, Reichmann *et al.* 2019).

- The essential lipid II flippase MurJ is recruited to the mid-stage cell division site by direct interaction with the divisome complex DivIB-DivIC-FtsL. The recruitment of MurJ represents a key turning point of *S. aureus* cell division, as it potentiates septal PGS activity and speeds up septum constriction (Monteiro *et al.* 2018).

- PBP4 is recruited to the septum following the redirection of WTA biosynthesis machinery to the divisome. Accordingly, the recruitment of the TPase was proposed to be organized by a direct or indirect interaction with WTA biosynthesis intermediates or proteins (Atilano *et al.* 2010).

- The main peptidoglycan synthase of *S. aureus*, PBP2, is known to localize to the septum via substrate interaction of its TPase active site (Monteiro *et al.* 2018; Pinho *et al.* 2005).

Despite the differences in structure, function and temporal localization, a general pattern was observed for all proteins, with the notable exception of PBP2. FtsW, RodA, MurJ and PBP4 all remained localized at the septum after antibiotic treatment without significant changes compared to the untreated control (Figure 27A,B). CAP analysis for all four proteins reproduced the pattern observed for FtsZ after treatment with vancomycin, telavancin or oxacillin (Figure 28C, see chapter 4.1.2). Overall, this demonstrated that the antibiotic treatment had no significant effect on the subcellular localization of these CWBM components. Interestingly, the impact of the antibiotics on PBP2 localization was more intricate. Vancomycin and telavancin had a moderate effect on the abundance of septal localization of PBP2. Oxacillin, however, effectively abolished septal PBP2 signal (Figure 27B: PBP2).

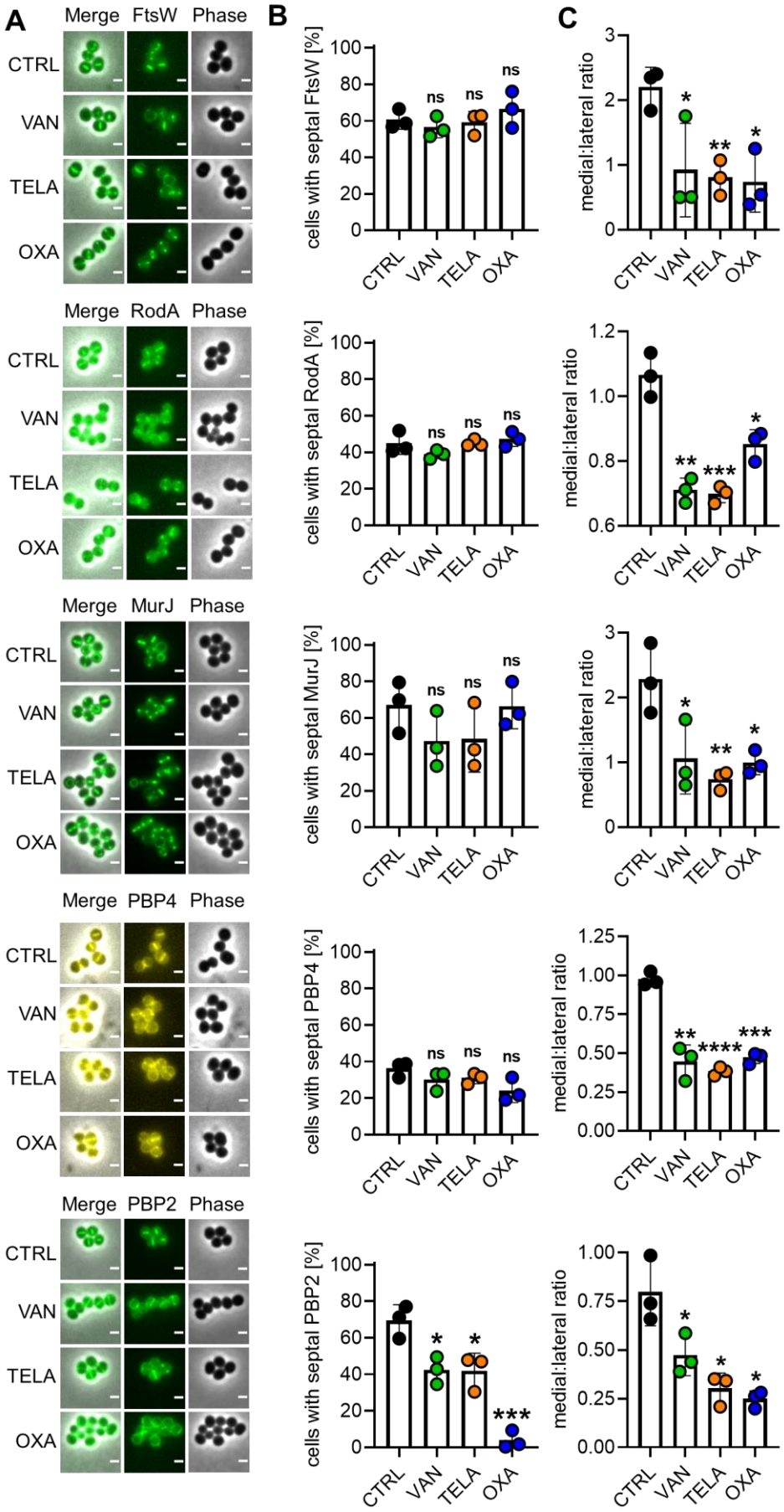
A
Merge FtsW Phase
CTRL
VAN
TELA
OXA
Merge RodA Phase
Merge MurJ Phase
Merge PBP4 Phase
Merge PBP2 Phase
B
cells with septal FtsW [%]
cells with septal RodA [%]
cells with septal MurJ [%]
cells with septal PBP4 [%]
cells with septal PBP2 [%]
ns
*
**
***
****
C
medial:lateral ratio
CTRL
VAN
TELA
OXA

Figure 27: Impact of antibiotic treatment on CWBM components, that localize to the septum. (A) Representative micrographs of *S. aureus* RN4220 FtsW-GFP, *S. aureus* RN4220 RodA-GFP, *S. aureus* RN4220 pCQ11-MurJ-mNeongreen*, S. aureus* RN4220 pCQ11-PBP4-YFP and *S. aureus* RN4220 RNpPBP2-31 after 25 min of treatment with vancomycin, telavancin or oxacillin and an untreated control. Scale bar, 1 µm. **(B)** Relative abundance of cells with septal FtsW, RodA, MurJ, PBP4 and PBP2 localization as % of total population after 25 min of treatment with vancomycin, telavancin or oxacillin and an untreated control. Bar graphs show the mean of three independent biological experiments ± SD. Symbols indicate the values of the individual replicates. **(C)** Medial:lateral ratios of CAP brightness profiles of FtsW, RodA, MurJ, PBP4 and PBP2 localization after 25 min of treatment with vancomycin, telavancin or oxacillin and an untreated control. Ratios were determined as the ratio of medial maximum to the mean of both lateral maxima. CAPs and brightness profiles are shown in appendix 2. Bar graphs show the mean of three independent biological experiments ± SD. Symbols indicate the values of the individual replicates**.** n ≥ 94 cells per replicate and condition. Statistical significance was determined against the untreated control using unpaired two-tailed students t-tests with a 95% confidence interval. Statistical significance was denoted as ns, not significant, $p > 0.05$; *, $p = 0.05$ to 0.01; **, $p = 0.01$ to 0.001; ***, $p = 0.001$ to 0.0001; ****, $p \leq 0.0001$.

4.1.7. Impact of oxacillin on PBP2 localization

The strikingly different effects on the localization of PBP2 were further investigated by analyzing PBP2 dynamics in individual cells using live-cell HiLo microscopy of *S. aureus* RN4220 with GFP-labelled PBP2 (*S. aureus* RN4220 RNpPBP2-31, Figure 28). Cells of an untreated control displayed a “biphasic” behavior of oscillation between septal and non-septal PBP2 localization (Figure 28A,B). Cells with PBP2 at the septum were able to divide within 22 min on average (see appendix 3). After cell splitting, the daughter cells showed non-septal PBP2 localization, with PBP2 signal distributed along the cytoplasmic membrane. After subsequent progression through the cell cycle, PBP2 was recruited to the new division septum, followed by septum closure and cell splitting. This resulted in an oscillation between the two states of septal and non-septal PBP2 localization over time (Figure 28B). As cultures were not synchronized in their cell cycle, subpopulations of both states (septal and aseptal PBP2) were observed at every time point. During treatment with oxacillin, this oscillatory dynamic was massively disturbed within minutes (Figure 28A,B). While cells with septal PBP2 still divided, cells were unable to recruit PBP2 to the septum from the moment oxacillin was added. In a total of 90 analyzed cells, only a single PBP2 recruitment event was observed after addition of oxacillin (Figure 28C). This lack of recruitment to the division site resulted in a constant decrease of cells with septal PBP2 localization (Figure 28B). Interestingly, oxacillin treatment did not delocalize PBP2 already localized at the septum at the moment of exposure. Loss of septal PBP2 localization without cell splitting was not observed. These results demonstrate an effective impairment of PBP2 recruitment.

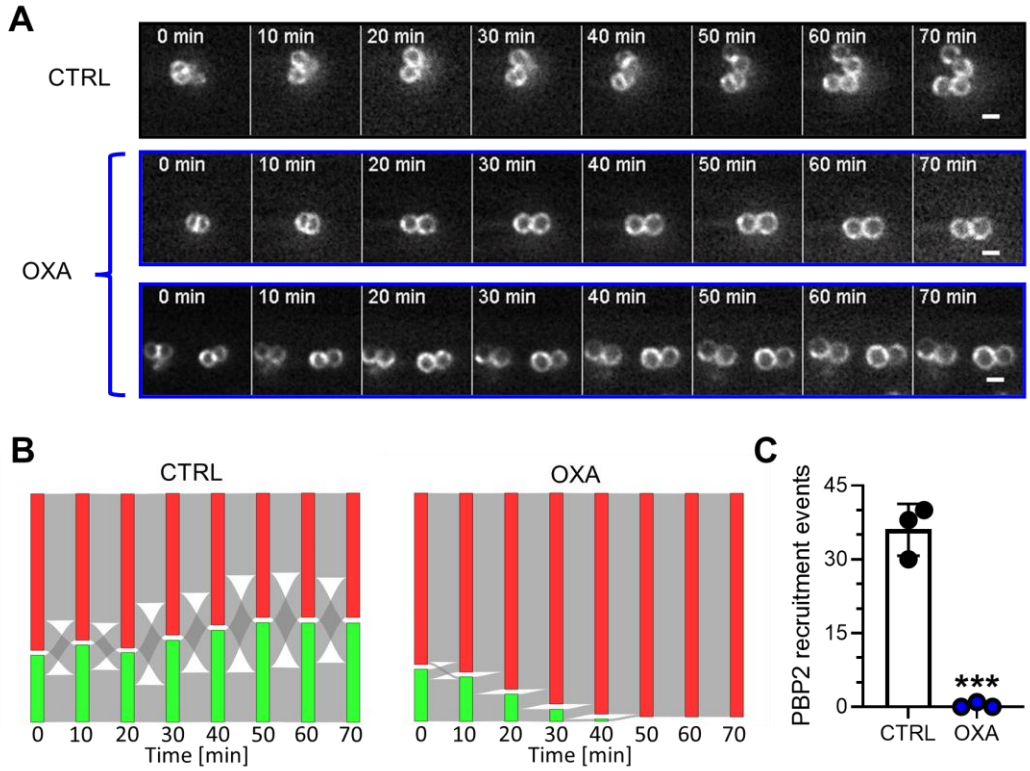

Figure 28: Oxacillin prevents PBP2 recruitment to the septum. (A) Representative HiLo microscopy images of PBP2 dynamics of *S. aureus* RN4220 RNpPBP2-31 over time during oxacillin treatment and an untreated control. Scale bar, 1 µm. Imaging by Dominik Brajtenbach. **(B)** Fluxes of cells with specific PBP2 localization as a function of time in an untreated control (left) and during oxacillin treatment (right). Red: cells without septal PBP2 localization, green: cells with septal PBP2 localization. Red-to-green fluxes indicate cells that recruit PBP2 to the septum. Green-to-red fluxes indicate cells that divide and thereby lose septal PBP2 localization in the daughter cells. Bar height represents relative abundance of cells with the respective PBP2 localization. Sum of both bars is always 100%. Mean of three independent biological experiments is shown. For each replicate and condition n = 30. **(C)** Total number of observed events of PBP2 recruitment to the septum, quantified from data shown in B. Symbols correspond to values of individual replicates, bars show the mean of three independent biological experiments ± SD. n = 30 cells per replicate and condition. Statistical significance was determined against the untreated control using unpaired two-tailed students t-tests with a 95% confidence interval. Statistical significance was denoted as ***, p = 0.001 to 0.0001.

4.1.8. Impact of vancomycin and telavancin on PBP2 localization

To understand the moderate effect of glycopeptides on PBP2 localization observed in CAPs, live-cell dynamics of the protein were also investigated during treatment with vancomycin or telavancin (Figure 29). In line with the arrest of septum constriction (see chapter 4.1.4), the oscillatory dynamic of PBP2 localization came to a complete stop after addition of the antibiotics (Figure 29A,B). However, in the first 20 min of treatment, division of individual cells and an according moderate loss in the relative number of cells with septal PBP2 signal was observed. This result corresponds with the observation of assembly-state cells, that are still able to perform cell splitting after addition of the glycopeptides (see chapter 4.1.4). It furthermore explains the moderate reduction in cells with septal PBP2 previously observed (see chapter 4.1.6).

Despite not having an effect on PBP2 localization like oxacillin, the substrate masking of the glycopeptides could still potentially impact PBP2 recruitment, albeit to a lesser degree than the beta-lactam. To investigate this hypothesis, septal:peripheral (S:P) ratios of fluorescent PBP2 signal in individual cells were determined after glycopeptide treatment (Figure 29C,D). Therefore, the fluorescence intensities of the peripheral cytoplasmic membrane and the septum are determined and the quotient of the two values was calculated. As the septum constitutes two cytoplasmic membranes in proximity of a few nm, the expected value for a protein localized unspecifically in the cell membrane is approximately 2, which has been experimentally validated numerous times (Atilano *et al.* 2010; Hardt *et al.* 2017; M. A. Hill *et al.* 2019; Lund *et al.* 2018; Monteiro *et al.* 2018; Reichmann *et al.* 2019; Tinajero-Trejo *et al.* 2022; Wacnik *et al.* 2022). Accordingly, membrane proteins specifically localizing at the divisome show S:P ratios > 2, with precise values depending on the molecular spatio-temporal organization of the specific proteins' septal localization as well as microscopic setup, labeling method and regulation of protein production. Accordingly, the untreated control displayed a PBP2 S:P ratio of 3.5 (Figure 29D), which is in line with reported values (Monteiro *et al.* 2018) and corresponds to the strong septal focus of PBP2 localization. In contrast, both glycopeptides significantly reduced this septal focus throughout the sample population, resulting in a notable shift towards lower ratios. Effectively, the mean S:P ratios were reduced to 2.41 (vancomycin) and 2.26 (telavancin), which corresponds to a considerable reduction in septal PBP2 localization (Figure 29D).

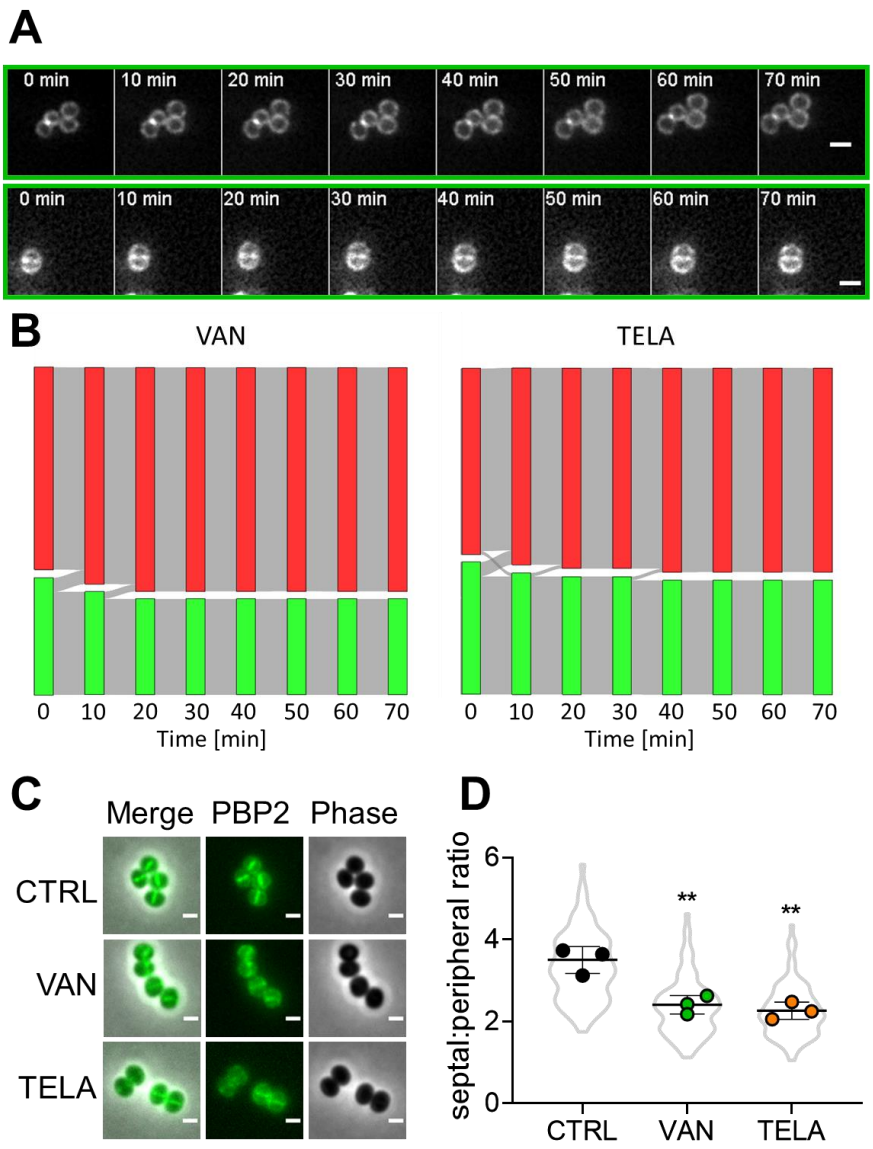

Figure 29: Glycopeptides vancomycin and telavancin reduce the septal focus of PBP2 localization. (A) Representative HiLo microscopy images of PBP2 dynamics of *S. aureus* RN4220 RNpPBP2-31 over time during vancomycin treatment. Scale bar, 1 µm. Imaging by Dominik Brajtenbach. **(B)** Fluxes of cells with specific PBP2 localization as a function of time during vancomycin (left) or telavancin treatment (right). Red: cells without septal PBP2 localization, green: cells with septal PBP2 localization. Red-to-green fluxes indicate cells that recruit PBP2 to the septum. Green-to-red fluxes indicate cells that divide and thereby lose septal PBP2 localization in the daughter cells. Bar height represents relative abundance of cells with the respective PBP2 localization. Sum of both bars is always 100%. Mean of three independent biological experiments is shown. n ≥ 29 cells per replicate and condition. **(C)** Representative micrographs of *S. aureus* RN4220 RNpPBP2-31 after 25 min of treatment with vancomycin or telavancin and an untreated control. Scale bar 1 µm. **(D)** Septal:peripheral ratios of PBP2 after 25 min of treatment with vancomycin or telavancin and an untreated control. Ratios were determined for individual cells with a visible continuous septal PBP2 signal. Violin plots show the distribution of individual cell data after exclusion of outliers. Line and error bars show mean ± standard deviation of three independent biological experiments. n = 30 cells per replicate and condition. Statistical significance was determined against the untreated control using unpaired two-tailed students t-tests with a 95% confidence interval. Statistical significance was denoted as **, p = 0.01 to 0.001.

4.1.9. Impact of vancomycin, telavancin and oxacillin on PknB localization

As substrate-binding by the glycopeptides had a considerable impact on the septal localization of PBP2, the possibility of a similar effect towards the serine-threonine kinase PknB was investigated. PknB has three PASTA (Penicillin binding proteins And Serine Threonine Associated) domains, which were proven to interact with lipid II *in vitro* and are crucial for the septal localization of the protein (Hardt *et al.* 2017). Compared to an untreated control, abundance of cells with septal localization of PknB was significantly reduced after treatment with the glycopeptides (Figure 30). Instead, the signal was unspecifically distributed along the cytoplasmic membrane in most cells. Notably, it was previously shown that PknB is not recruited to the cell division site in an early stage of cell division. Instead, unspecific cell membrane localization is observable up to a late-stage septal recruitment, alongside a relatively moderate septal focus upon recruitment (Hardt *et al.* 2017). Thus, the here observed result may be caused by substrate-masking by the glycopeptides, or alternatively be a downstream effect of the cell division arrest. To test this, impact of oxacillin treatment on PknB localization was also investigated, since the beta-lactam also induced cell division arrest without directly interfering with the interaction partner of PknB, lipid II. Indeed, oxacillin produced an effect similar to the glycopeptides, which suggested that the dislocation of PknB after treatment with the PGS inhibiting antibiotics is likely a downstream effect of cell cycle arrest, which is caused by the PGS inhibition (see chapters 4.1.2 - 4.1.8).

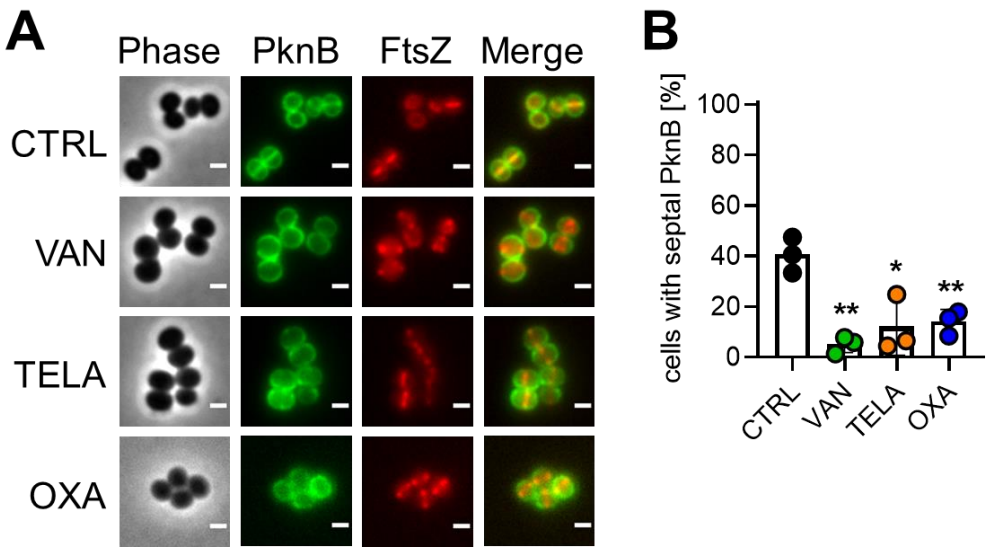

Figure 30: PGS inhibition prevents septal recruitment of PknB. (A) Representative micrographs of *S. aureus* RN4220 pCQ11-PknB-gfp-FstZ-mCherry after 25 min of treatment with vancomycin, telavancin or oxacillin and an untreated control. Scale bar, 1 µm. **(B)** Relative abundance of cells with septal PknB localization as % of total population after 25 min of treatment with vancomycin, telavancin or oxacillin and an untreated control. Bar graphs show the mean of three independent biological experiments ± SD. Symbols indicate the values of the individual replicates. n ≥ 187 cells per replicate and condition. Statistical significance was determined against the untreated control using unpaired two-tailed students t-tests with a 95% confidence interval. Statistical significance was denoted as *, p = 0.05 to 0.01; **, p = 0.01 to 0.001.

4.2. Investigating putative membrane depolarization by lipid II-binding antibiotics

4.2.1. Impact of telavancin on the transmembrane potential

For multiple lipoglycopeptides, including telavancin, a membrane depolarizing effect at higher concentrations has been previously reported. However, neither the underlying molecular mechanism nor its role in the antibacterial activity of telavancin was comprehensively analyzed (Higgins *et al.* 2005; Lunde *et al.* 2009; Song *et al.* 2012). To understand how this potential secondary mechanism of action of telavancin relates to the cellular effects caused by PGS inhibition (see chapter 4.1), the impact of the lipoglycopeptide on membrane function was investigated (Figure 31). Therefore, the experimental conditions were consistent with those, in which growth inhibition and complete cell division arrest were observed (see chapter 4.1.1). First, the impact on the transmembrane potential was tested by measuring the release of $DiSC_3(5)$, an autoquenching dye which accumulates in cells via the transmembrane potential due to its cationic charge. Efflux of the dye, e.g., due to membrane depolarization, can be quantified as a de-quenching of the fluorophore proportional to its release from the cells (te Winkel *et al.* 2016). The positive control 5 µM valinomycin+ 300 mM KCl [10] induced a rapid increase of $DiSC_3(5)$ fluorescence (Figure 31A). In contrast, treatment with telavancin or vancomycin did not result in any significant change of $DiSC_3(5)$ fluorescence in the medium. This indicated that both antibiotics had no effect on the transmembrane potential under the chosen conditions.

To validate this result on a single cell level, the transmembrane potential was quantitatively analyzed in individual cells using $DiBAC_4(3)$, an anionic dye whose intracellular fluorescence intensity increases proportional to membrane depolarization (te Winkel *et al.* 2016). Additionally, localization of FtsZ was visualized. After loss of the membrane potential, the GTPase activity of FtsZ is eliminated, resulting in depolymerization and disassembly of the Z-ring (Strahl *et al.* 2010). As no such effect was observed in the results shown above (see chapter 4.1), the association between $DiBAC_4(3)$ fluorescence and Z-ring integrity was determined (Figure 31B-D). Nisin was used as positive control for membrane disruption caused by lipid II interaction. A concentration of 1 x MIC (16 µg/mL) nisin caused a complete loss of Z-ring integrity in 82.7 % of cells and a significant increase in mean $DiBAC_4(3)$ fluorescence. Loss of Z-ring integrity and increase in $DiBAC_4(3)$ fluorescence clearly coincided in cells treated with nisin (Figure 31B). In contrast, treatment with telavancin or vancomycin had no significant impact on Z-ring integrity (corroborating results shown above, see chapter 4.1.2) and did not result in any significant increase of $DiBAC_4(3)$ fluorescence. Thus, neither vancomycin nor telavancin showed an impact on the transmembrane potential under the tested conditions and concentrations.

[10] Valinomycin is a ionophore, that selectively transports K^+ ions over the cytoplasmic membrane. A high extracellular K^+ concentration thus leads to abolishment of the transmembrane potential, as positive ions are transported into the cytoplasm (te Winkel *et al.* 2016).

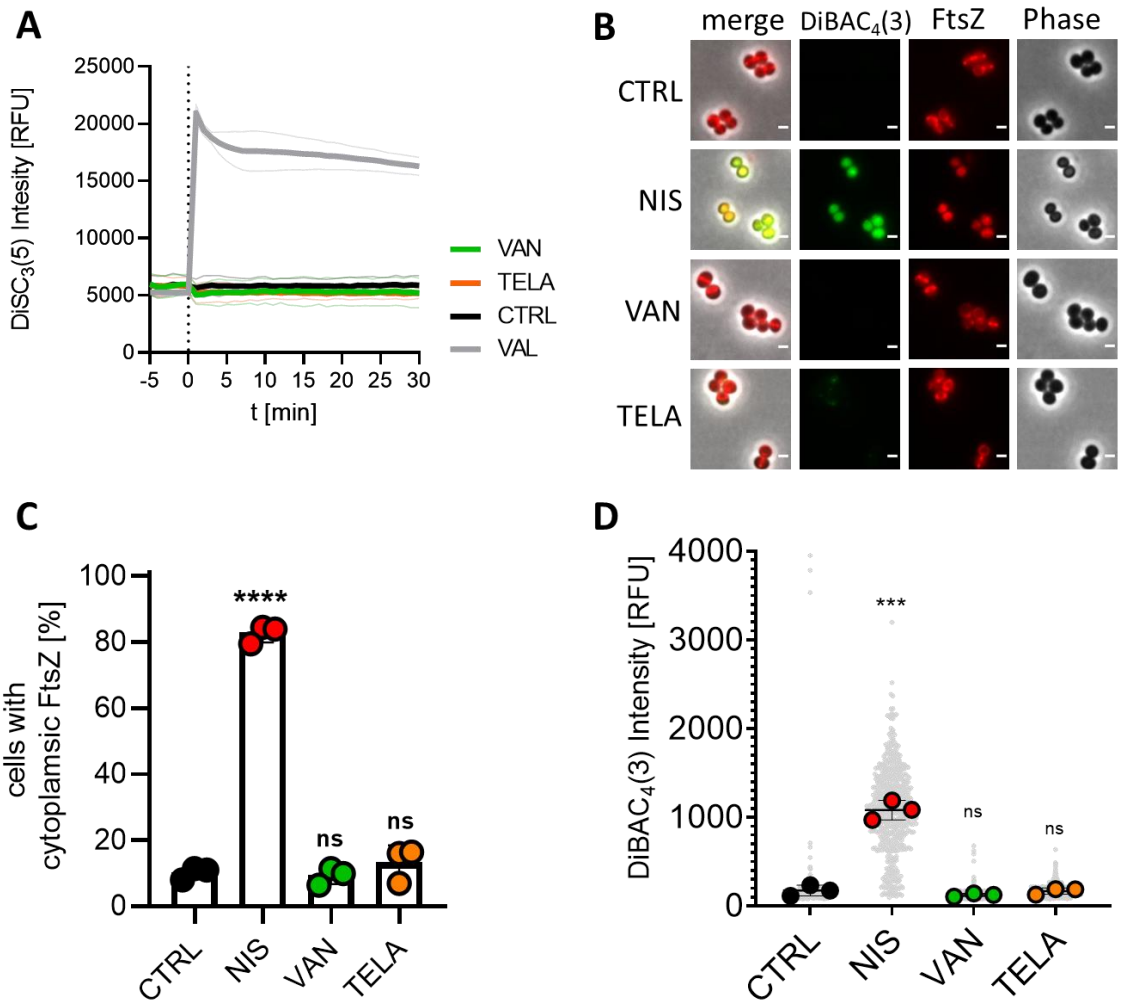

Figure 31 Glycopeptides vancomycin and telavancin do not affect the cytoplasmic membrane potential at 4 x MIC. (A) Quantification of $DiSC_3(5)$ fluorescence during treatment of *S. aureus* RN4220 with vancomycin, telavancin, and an untreated control. 5 µM valinomycin + 300 mM KCl was used as positive control. Mean of three independent biological experiments is shown as thick line ± SD as thin, semi-transparent lines. **(B)** Representative micrographs of *S. aureus* RN4220 pCQ11-FtsZ-SNAP treated with 1 x MIC nisin or 4 x MIC vancomycin or telavancin for 25 min. Red: FtsZ-SNAP, SNAP-tag labelled with SNAP-Cell® TMR Star. Green: fluorescent membrane depolarization probe $DiBAC_4(3)$, adjusted to the positive nisin control. Representative images of three independent biological experiments. **(C)** Relative abundance of cells with exclusively cytoplasmic FtsZ localization as % of total population after 25 min of treatment with vancomycin, telavancin or nisin and an untreated control. Bar graphs show the mean of three independent biological experiments ± SD. Symbols indicate the values of the individual replicates. n ≥ 175 cells per replicate and condition. **(D)** Quantification of $DiBAC_4(3)$ fluorescence intensities of individual cells. Small symbols show individual cell data. Line shows mean of three biologically independent experiments ± SD. Large symbols show the mean of each individual biological experiment. n ≥ 175 cells per replicate and condition. RFU: Relative Fluorescence Unit. Statistical significance was determined against the untreated control using unpaired two-tailed students t-tests with a 95% confidence interval. Statistical significance was denoted as ns, not significant, $p > 0.05$; ***, $p = 0.001$ to 0.0001.

4.2.2. Impact of teixobactin and structurally similar antibiotics on the transmembrane potential

Another recently described mechanism of lipid II-binding antibiotics to interfere with cytoplasmic membrane function is the fibril-formation by teixobactin. Teixobactin binds to the PPi moiety of lipid II and multiple of these teixobactin:lipid II complexes were shown to configurate into β-sheets and large fibril-like aggregates, that can have membrane-deforming effects (Shukla *et al.* 2020, 2022). The formation of similar aggregations was observed for the recently described clovibactin, which shares many structural and functional features with teixobactin (Shukla *et al.* 2023).

The potential impact of this fibril-formation on the cytoplasmic membrane function was investigated using DiBAC$_4$(3) as depolarization probe after 30 min of treatment with 5 x MIC of teixobactin as well as the structurally related antibiotics hypeptin and clovibactin (Figure 32). Treatment with 2 x MIC nisin resulted in a significant increase in DiBAC$_4$(3) fluorescence, which is in line with results shown above (see chapter 4.2.1). In contrast, none of the tested compounds impacted intracellular DiBAC$_4$(4) signal considerably. Clovibactin showed a significant, but negligible impact on the mean fluorescence intensity.

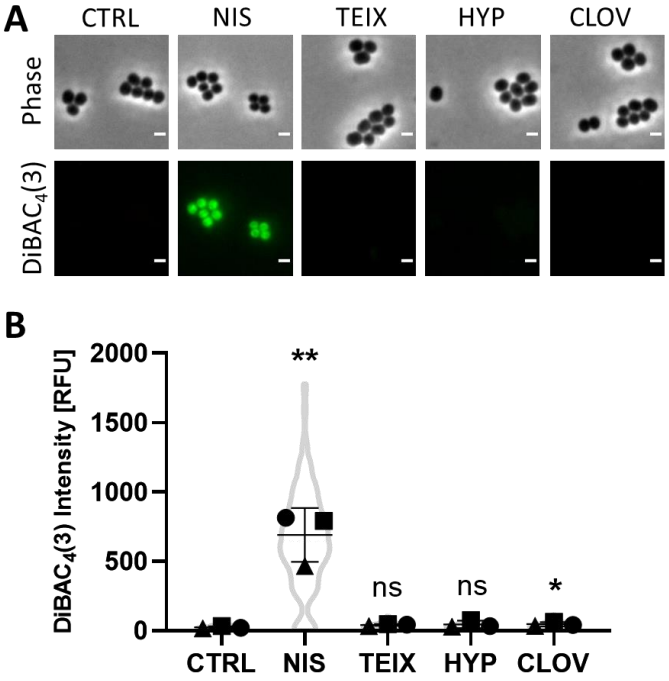

Figure 32: No observed increase in fluorescence intensity of the membrane depolarization probe DiBAC$_4$(3) after treatment with either teixobactin, hypeptin or clovibactin. (A) representative micrographs of *S. aureus* SG511 treated with 2 x MIC nisin or 5 x MIC of teixobactin, hypeptin or clovibactin for 30 min and stained with DiBAC$_4$(3). DiBAC$_4$(3) brightness and contrast adjusted to the positive nisin control. Representative images of three independent biological experiments. Scale bar, 1 µm. **(B)** Quantification of DiBAC$_4$(3) fluorescence intensities of individual cells. Violin plots show the distribution of individual cell data after exclusion of outliers. Line and error bars show mean ± SD of three independent biological experiments, symbols show the mean of each biological replicate. n ≥ 124 cells per replicate and condition. RFU: Relative Fluorescence Unit. Statistical significance was determined against the untreated control using unpaired two-tailed students t-tests with a 95% confidence interval. Statistical significance was denoted as ns, not significant, p > 0.05; *, p = 0.05 to 0.01; **, p = 0.01 to 0.001.

4.2.3. Impact of the lanthidin cacaoidin on the transmembrane potential

Many lantibiotics either directly interact with the cytoplasmic membrane by hydrophobic interactions or by binding to membrane-bound target structures (Bierbaum *et al.* 2009; Cao *et al.* 2021; Draper *et al.* 2015; Ongpipattanakul *et al.* 2022; X. Wang *et al.* 2020). Therefore, it is rational to assume and investigate a potential impact of lantibiotics on membrane function. The recently discovered first-in-class lanthidin cacaoidin shares structural features with lantibiotics (Ortiz-López *et al.* 2020) and was shown to interact with lipid II and the TGase site of PBP2 *in vitro* (Deisinger *et al.* 2023). To investigate a putative membrane function impairment, $DiBAC_4(3)$ fluorescence was quantified after 30 min of treatment with up to 5 x MIC cacaoidin or mersacidin (Figure 33), a lantibiotic which binds to lipid II without impairing the cell membrane (Böttiger *et al.* 2009; Brötz, Bierbaum *et al.* 1998; S.-T. D. Hsu *et al.* 2003; P. Sass *et al.* 2008). While the positive control nisin induced significant increase of intracellular $DiBAC_4(3)$ signal, neither mersacidin nor cacaoidin had notable impact on fluorescence of the depolarization probe in cells. A negligible, albeit statistically significant increase of $DiBAC_4(3)$ signal was observable for cacaoidin.

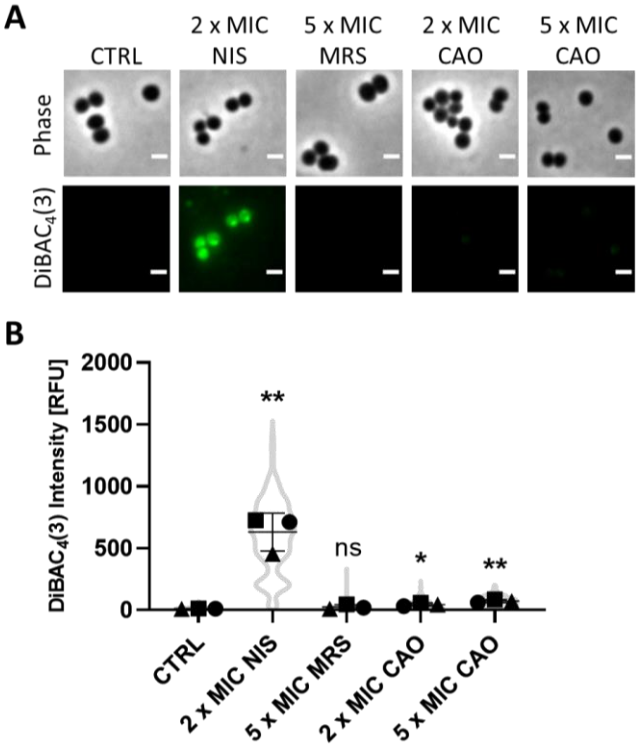

Figure 33: Cacaoidin has a negligible impact on fluorescence intensity of the membrane depolarization probe $DiBAC_4(3)$. (A) Representative micrographs of *S. aureus* SG511 treated with 2 x MIC nisin, 5 x MIC mersacidin, 2 x MIC cacaoidin or 5 x MIC cacaoidin for 30 min and stained with $DiBAC_4(3)$. $DiBAC_4(3)$ brightness and contrast adjusted to the positive nisin control. Representative images of three independent biological experiments. Scale bar, 1 µm. **(B)** Quantification of $DiBAC_4(3)$ fluorescence intensities of individual cells. Violin plots show the distribution of individual cell data after exclusion of outliers. Line and error bars show mean ± SD of three independent biological experiments, symbols show the mean of each biological replicate. n ≥ 71 cells per replicate and condition. RFU: Relative Fluorescence Unit. Statistical significance was determined against the untreated control using unpaired two-tailed students t-tests with a 95% confidence interval. Statistical significance was denoted as ns, not significant, $p > 0.05$; *, $p = 0.05$ to 0.01; **, $p = 0.01$ to 0.001.

4.3. Investigating the impact of moenomycin on *S. aureus* cell division

The results of how peptidoglycan synthesis inhibition interferes with septum constriction clearly demonstrated that a functioning CWBM is essential for maintaining the cell cycle homeostasis in *S. aureus* (see chapters 4.1 and 5.1). Using the framework established by these results, the impact of moenomycin on *S. aureus* CWBM and cell division was investigated.

4.3.1. Determination of antibiotic treatment time and concentration

Parallel to the approach chosen for investigating the impact of vancomycin, telavancin and oxacillin on cell division (see chapter 4.1.1), the appropriate antibiotic concentration and time range for moenomycin was evaluated. The MIC according to CLSI standards were determined against *S. aureus* RN4220 as 0.25 µg/mL. An increased inoculum had no effect on this value. Determination of time-kill kinetics revealed complete growth inhibition at 4 x MIC (Figure 34). Corresponding to the rationale for glycopeptides and beta-lactam, it was concluded that this concentration was suitable for investigating the key cellular effects of moenomycin, which are most closely associated with its antibacterial activity and a direct consequence of the antibiotics main molecular target(s).

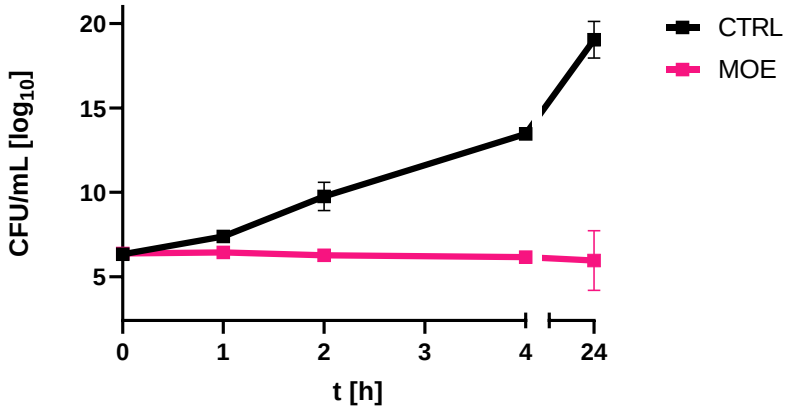

Figure 34: Killing kinetics of moenomycin against *S. aureus* RN4220. Symbols show the mean of three independent biological experiments ± SD

4.3.2. Impact of moenomycin on *S. aureus* cell division progress

To gain insight into a potential impact on cell division by moenomycin, the effect of treatment on the distribution of cell cycle phases was evaluated using nile red as a membrane stain (Figure 35). Moenomycin had considerable impact on the cell cycle progression of *S. aureus*. Unexpectedly, treatment increased the abundance of cells in the late phase of cell division significantly from 22 % to almost 42 %. This was in notable contrast to the effects of the other PGS-targeting antibiotics (see chapter 4.1.2), which indicated a considerable deviation in the activity of moenomycin from the expected PGS inhibition and subsequent septum constriction arrest. Instead, the effect seemed to be more directed towards the final steps of cell division, which include ultimate septum closure, assembly of the new daughter cell Z-rings and autolysis-mediated cell separation.

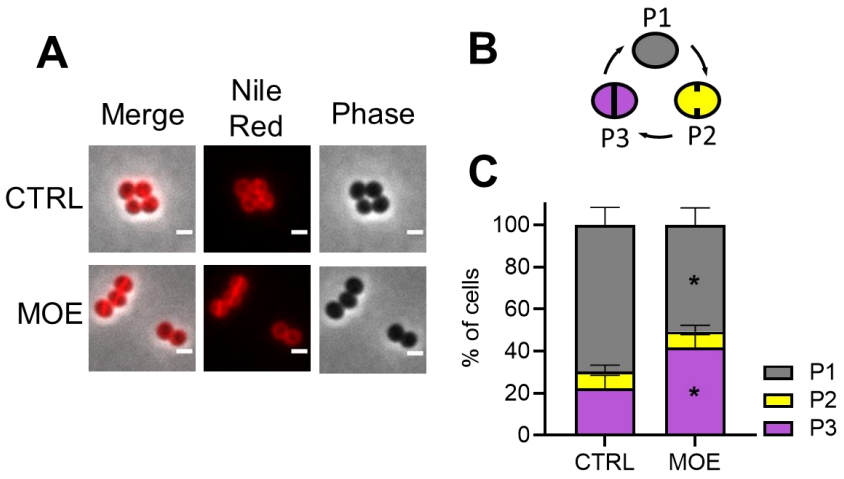

Figure 35: Moenomycin treatment impairs late-stage cell division progress. (A) Representative micrographs of *S. aureus* RN4220 cells stained with the membrane dye nile red after 25 min of treatment with moenomycin and an untreated control. Scale bar, 1 µm. **(B)** Schematic representation of the three distinctive morphologies of *S. aureus* throughout the cell cycle as visible in a membrane stain. Black lines represent the cell membrane. Grey: Phase 1 (P1) cells. Yellow: Phase 2 (P2) cells. Violet: Phase (P3) cells. **(C)** Quantification of cell cycle phase distribution in *S. aureus* RN4220 after 25 min of treatment with moenomycin and an untreated control. Grey: P1 cells. Yellow: P2 cells. Violet: P3 cells. Bars show the mean of three independent biological experiments ± SD. n ≥ 200 cells per replicate and condition. Statistical significance was determined against the untreated control using unpaired two-tailed students t-tests with a 95% confidence interval. Statistical significance was denoted as *, p = 0.05 to 0.01.

This was further substantiated by CAPs of FtsZ localization after treatment with moenomycin (Figure 36A-D), which showed a shift of brightness towards the center of the septal axis and an according increase in medial:lateral ratio (Figure 36C,D). This indicated a significant impairment of the final cell division stage, with less cells that show lateral fluorescence from large (early-stage) Z-rings, and simultaneously more cells with a focused FtsZ signal in the cell center (either from late-stage cells or assembly-state cells). Moenomycin had no impact on Z-ring integrity, as no significant change in the abundance of cells with septal FtsZ localization was observed (Figure 36E).

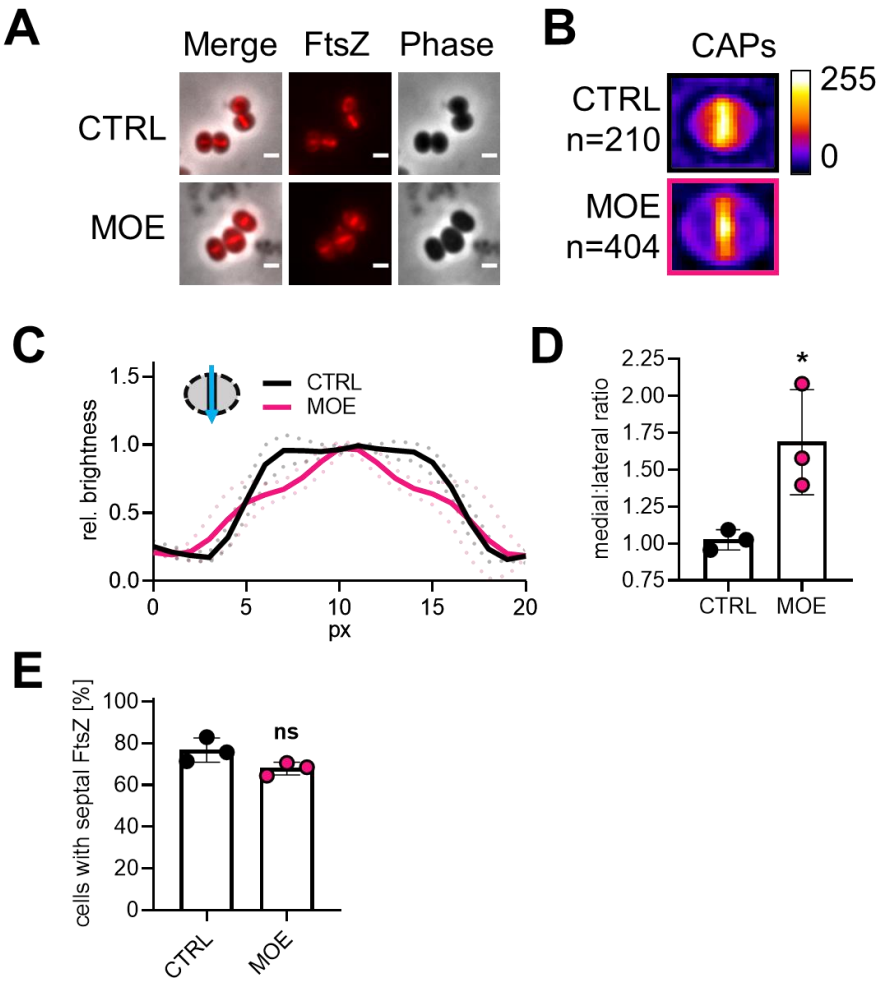

Figure 36: CAPs indicate that moenomycin impacts the final stages of *S. aureus* cell division leading to inhibition of cell splitting. (A) Representative micrographs of *S. aureus* RN4220 pCQ11-FtsZ-SNAP after 25 min of treatment with moenomycin and an untreated control. SNAP-tags were labelled with SNAP-Cell® TMR Star. Scale bar, 1 µm. **(B)** CAPs of *S. aureus* RN4220 pCQ11-FtsZ-SNAP cells treated with moenomycin and an untreated control. n corresponds to the number of individual cells used for CAP generation. Representative CAPs of three independent biological experiments. **(C)** Quantification of CAP brightness along the septal axis, plotted relative to the medial brightness value. The mean of three independent biological experiments is shown as thick line ± SD as dotted, semi-transparent lines. **(D)** Medial:lateral ratio of CAP brightness profiles. Bar graphs show the mean of three independent biological experiments ± SD, respectively. Symbols indicate the values of the individual replicates. **(E)** Relative abundance of cells with septal FtsZ localization as % of total population after 25 min of treatment with moenomycin and an untreated control. Bar graphs show the mean of three independent biological experiments ± SD. Symbols indicate the values of the individual replicates. n ≥ 161 cells per replicate and condition. Statistical significance was determined against the untreated control using unpaired two-tailed students t-tests (95% confidence interval) against the untreated control. Statistical significance was denoted as ns, not significant, p > 0.05; *, p = 0.05 to 0.01; **, p = 0.01 to 0.001.

To narrow down at which point moenomycin interferes with the final stage of cell division, FtsZ localization was visualized using Airyscan superresolution microscopy (Figure 37). After moenomycin treatment, significantly more cells were in assembly state than in the untreated control. The abundance of this phenotype increased from 16.6% to 24.3%. Thus, the result corroborated the observation of the

shift in cell cycle phase distribution and CAP visualizations. Cells were able to progress to the assembly state, but unable to perform the separation of the daughter cells. Thus, the mechanism of cell cycle interference seemed to be directed towards organization of the cell splitting event. In contrast, 4 x MIC vancomycin (MIC: 2 µg/mL) had the opposite effect on the abundance of assembly state cells (Figure 37). This was in line with the results shown above (see chapter 4.1) that cells in assembly state were still able to perform cell splitting one last time before entering complete cell cycle arrest caused by PGS inhibition.

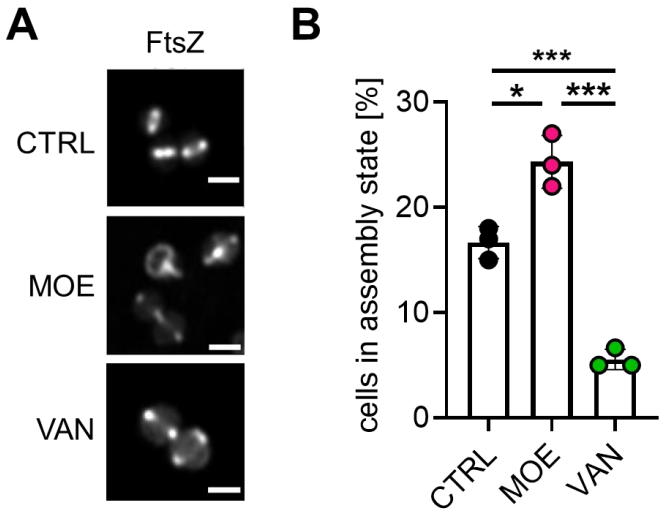

Figure 37: Moenomycin treatment partially arrests cells in the assembly state. (A) Representative Airyscan super-resolution microscopy images of *S. aureus* RN4220 pCQ11-FtsZ-SNAP treated for 25 min with moenomycin or vancomycin and an untreated control. SNAP-tag was labelled with SNAP-Cell® 505-Star. Scale bar, 1 µm. Imaging by Dominik Brajtenbach. **(B)** Relative abundance of cells in assembly state as % of total population after 25 min of treatment with moenomycin or vancomycin and an untreated control. Bar graphs show the mean of three independent biological experiments ± SD, respectively. Symbols indicate the values of the individual replicates. Statistical significance was determined using unpaired two-tailed students t-tests with a 95% confidence interval. n ≥ 57 cells per replicate and condition. Statistical significance was denoted as *, p = 0.05 to 0.01; ***, p = 0.001 to 0.0001.

To investigate the putative downstream impact of moenomycin-induced inhibition of cell splitting, localization of FtsW and MurJ were visualized using widefield microscopy (Figure 38). No significant differences in the number of cells with either protein present at the septum were observed, which indicated that divisome integrity stayed intact after moenomycin treatment (Figure 38B). Remarkably, a considerable fraction of moenomycin-treated cells showed FtsW in an assembly-state formation (7.7%), a morphology virtually absent in untreated or vancomycin-treated cells (Figure 38C). The abundance of this phenotype corresponded to the increase of assembly-state cells determined in Z-ring visualization, thus validating the result shown above. This demonstrated, that despite failure to divide, cells trapped in the assembly state aberrantly progressed in their cell cycle. This aberrant cell cycle progression reached the point of recruiting the early divisome protein and CWBM component FtsW to the aberrant septa. However, it did not reach the mid-stage turning point of MurJ recruitment, as no such phenotype was observed for the localization of MurJ (Figure 38C).

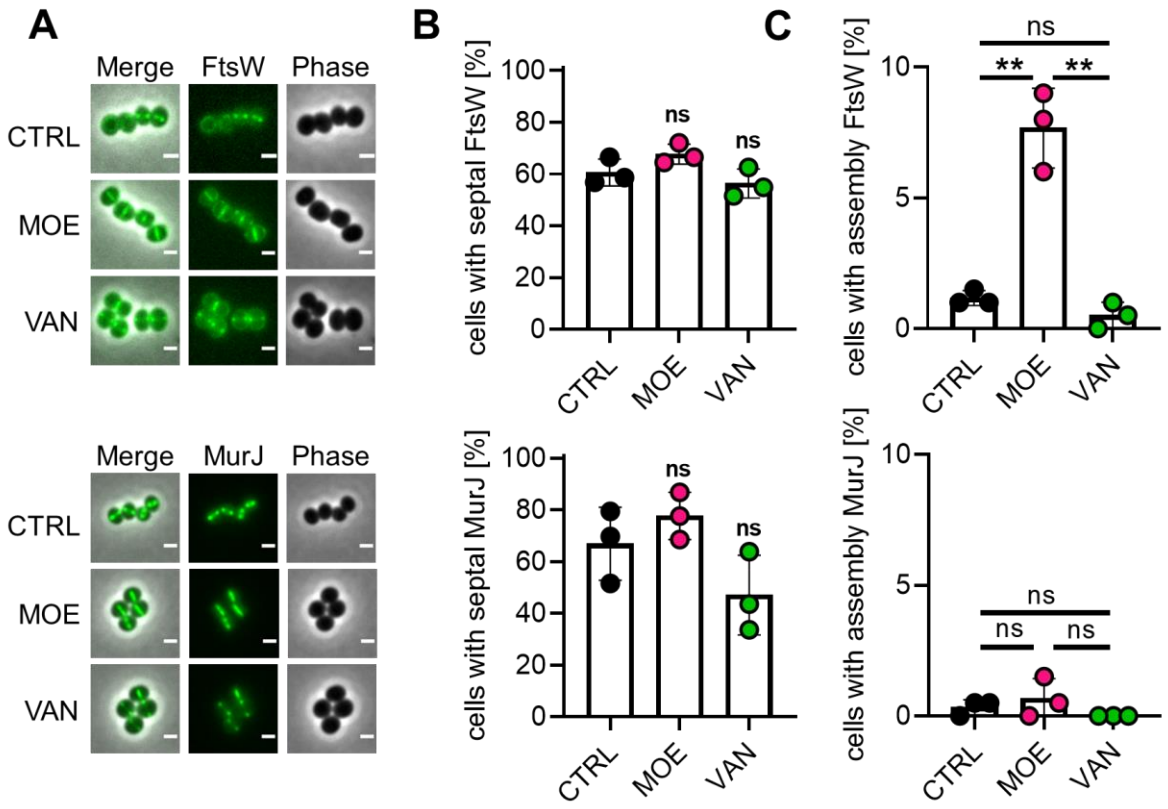

Figure 38: Cells trapped in assembly state by moenomycin progress to FtsW recruitment at the new divisomes, but do not reach the mid-stage marked by MurJ recruitment. (A) Representative micrographs of *S. aureus* RN4220 FtsW-GFP and RN4220 pCQ11-MurJ-mNeongreen after 25 min of treatment with moenomycin or vancomycin and an untreated control. Scale bar, 1 µm. **(B)** Relative abundance of cells with septal FtsW or MurJ localization as % of total population after 25 min of treatment with moenomycin or vancomycin and an untreated control. Bar graphs show the mean of three independent biological experiments ± SD, respectively. Symbols indicate the values of the individual replicates. **(C)** Relative abundance of cells with assembly state FtsW or MurJ localization as % of total population after 25 min of treatment with moenomycin or vancomycin and an untreated control. Bar graphs show the mean of three independent biological experiments ± SD, respectively. Symbols indicate the values of the individual replicates. n ≥ 185 cells per replicate and condition. Statistical significance was determined using unpaired two-tailed students t-tests with a 95% confidence interval. If not indicated otherwise, statistical significance was determined against the untreated control. Statistical significance was denoted as *, p = 0.05 to 0.01; ***, p = 0.001 to 0.0001.

4.3.3. Investigating the temporal relationship of cell division effects and peptidoglycan synthesis inhibition of moenomycin

The impact of moenomycin was observed to be drastically different from that of vancomycin. Both antibiotics are known to inhibit TGases, but via different molecular mechanisms. Moenomycin binds to the active site of TGases, while vancomycin blocks the substrate of both TGases and TPase, thereby inhibiting both final PGS reactions (see chapter 1.3). To contextualize the unexpected impact of moenomycin within the newly established framework of the role of PGS within *S. aureus* cell division (see chapter 4.1 and Discussion), the extent of PGS inhibition by moenomycin was visualized using HADA, a fluorescent amino acid which is incorporated into the peptidoglycan by TPases (Kuru *et al.* 2012, 2019).

Remarkably, when HADA incorporation was quantified after 30 min of treatment with moenomycin, no significant change in fluorescence intensity was observed (Figure 39A). Cells still showed active HADA incorporation, which was still primarily located at the septal region. Interestingly, no cells with an assembly-state phenotype of HADA fluorescence were found, showing that the aberrant progression of the assembly-state trapped cells did not proceed to the recruitment (or activation) of PBPs at the new divisomes.

As expected (and shown above, see chapter 4.1.1), treatment with vancomycin effectively abolished HADA incorporation within the same timeframe of 30 min. As an additional control, HADA signals of cells treated with fosfomycin were also quantified. Fosfomycin inhibits the first step of cell wall biosynthesis, leading to a depletion in peptidoglycan precursors (see chapter 1.3). Accordingly, fosfomycin-treated cells were used to control for a potential residual TPase activity (e.g., in secondary crosslinking events or by expenditure of TPase target moieties in newly polymerized peptidoglycan strands, that were synthesized prior to final loss of TGase activity). However, 4 x MIC fosfomycin (MIC: 16 µg/mL) resulted in the same outcome as vancomycin treatment, with nearly complete inhibition of all TPase activity within 30 min. This demonstrated, that the HADA incorporation observed for moenomycin was caused by a still functioning PGS after 30 min of treatment.

However, this was in stark contrast to the known inhibition of the TGase reaction by moenomycin. To rule out a general failure to capture this TGase inhibition via HADA incorporation, treatment time was prolonged to a total of 90 min (Figure 39B). This resulted in moenomycin significantly reducing HADA signal to nearly identical levels as vancomycin and fosfomycin. This demonstrated functionality of the method and that moenomycin was – as expected – able to ultimately inhibit PGS. However, this inhibition was established at a much slower pace than for vancomycin or fosfomycin.

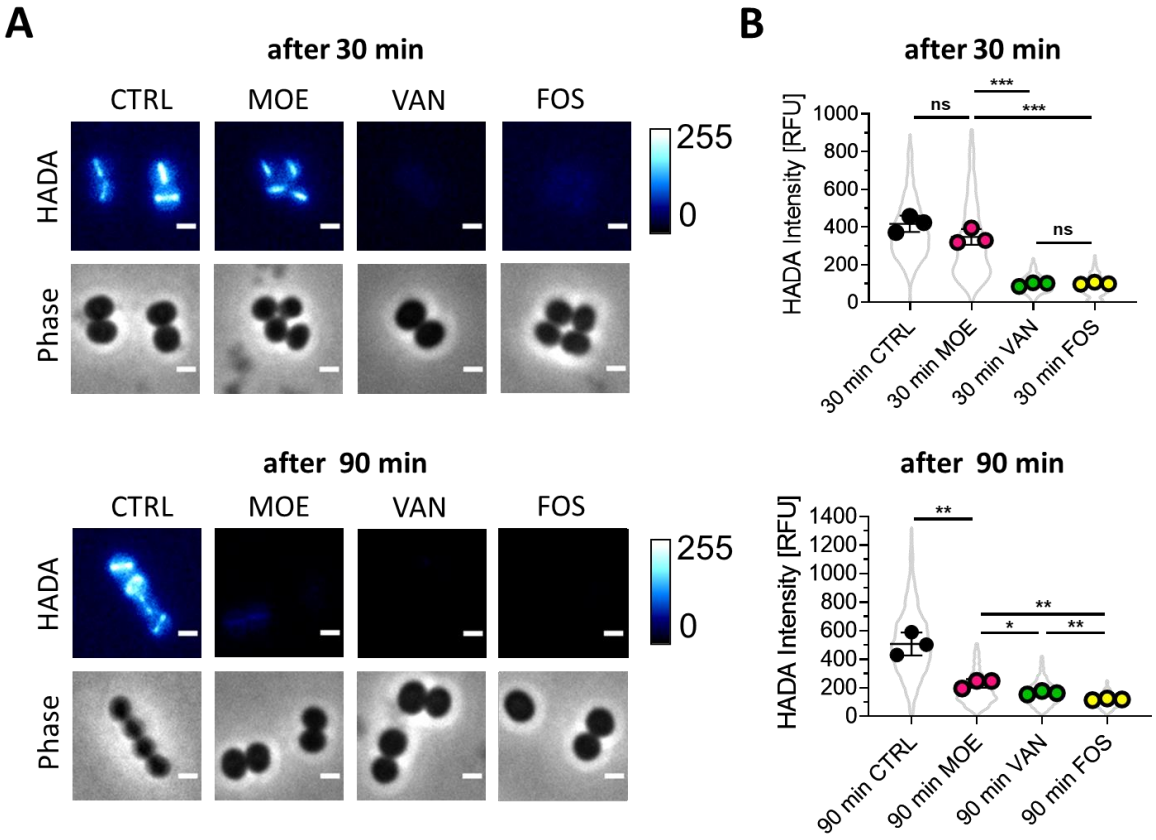

Figure 39: 30 min of moenomycin treatment are not sufficient for inhibition of peptidoglycan synthesis. (A) Representative micrographs of *S. aureus* RN4220 treated with 4 x MIC moenomycin, vancomycin or fosfomycin and stained with HADA. Upper panel: after 30 min treatment. Lower panel: after 90 min treatment. Brightness and contrast of the HADA channel was adjusted to the untreated control for all micrographs. Scale bar, 1 µm. **(B)** Quantification of HADA intensities of individual cells. Upper panel: after 30 min treatment. Lower panel: after 90 min treatment. Violin plots show the distribution of individual cell data after exclusion of outliers. Line and error bars show mean ± SD of three independent biological experiments. Symbols show mean of each independent replicate, n ≥ 282 cells per replicate and condition. RFU: Relative Fluorescence Unit. Statistical significance was determined against the untreated control using unpaired two-tailed students t-tests with a 95% confidence interval. Statistical significance was denoted as ns, not significant, p > 0.05; *, p = 0.05 to 0.01; **, p = 0.01 to 0.001; ***, p = 0.001 to 0.0001.

Interestingly, CAP analysis of the HADA signal after 30 min treatment revealed notable changes in the subcellular fluorescence distribution induced by moenomycin (Figure 40). In the untreated control, the signal was distributed along the septal axis with a clear focus at the lateral edges. This result was expected from the described mode of PGS in *S. aureus,* which leads to HADA incorporation throughout the septum (Lund *et al.* 2018; Monteiro *et al.* 2018). Moenomycin treatment drastically changed CAP appearance. A significant shift towards the cell center was observed, which corresponds to the observed impact on FtsZ localization (see chapter 4.3.2). This illustrated that despite not inhibiting PGS, moenomycins impact on cell division was visualizable with HADA and clearly already affecting cells after 30 min of treatment. Thus, visualization of HADA incorporation demonstrated that the effect of moenomycin on cell splitting was independent from and more immediate than ultimate inhibition of the cell wall biosynthesis.

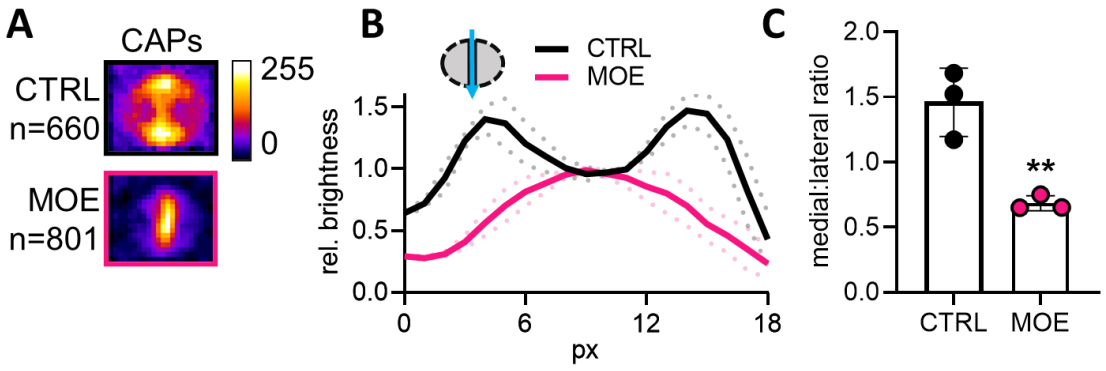

Figure 40: HADA CAPs show an impact of moenomycin on cell division independent of PGS inhibition. (A) CAPs of HADA fluorescence in *S. aureus* RN4220 cells treated for 30 min with moenomycin and an untreated control. n corresponds to the number of individual cells used for CAP generation. Representative CAPs of three independent biological experiments. **(B)** Quantification of CAP brightness along the septal axis, plotted relative to the medial brightness value. Mean of three replicates ± SD. **(C)** Medial:lateral ratio of CAP brightness profiles. Line and error bars show mean ± SD of three independent biological experiments. Symbols show mean of each independent replicate, n ≥ 282 cells per replicate and condition. Statistical significance was determined against the untreated control using unpaired two-tailed students t-tests with a 95% confidence interval. Statistical significance was denoted as **, p = 0.01 to 0.0 01.

4.4. Investigating the impact of DCAP on the organization of *S. aureus* cell division and cell wall biosynthesis machineries

The small synthetic molecule DCAP [2-((3-(3,6-dichloro-9H-carbazol-9-yl)-2-hydroxypropyl)amino)-2-(hydroxymethyl)propane-1,3-diol] was identified as an inhibitor of bacterial cell division in an *in vitro* high-throughput screening (Eun *et al.* 2012). Interestingly, the compound was determined as active against various gram-positive and -negative bacteria. Investigations of the molecular mechanism of action revealed membrane depolarization, membrane permeabilization and the delocalization of essential membrane-associated proteins. It was speculated that these effects were caused by interaction of DCAP with lipids or proteins of the cytoplasmic membrane. However, no specific target was identified (Eun *et al.* 2012; Hurley *et al.* 2015). To further elucidate the mechanism of action of DCAP and its effects leading up to cell death, the cellular impact of DCAP treatment on *S. aureus* was investigated.

4.4.1. Determination of antibiotic treatment time and concentration

To further characterize the multi-facetted mechanism of action of DCAP on a cellular level, the minimal inhibitory concentration of the compound against various strains of *S. aureus* was determined as 16-32 µg/mL, depending on the respective strain (Table 8, performed and kindly provided by Kevin Ludwig).

Table 8: Minimal inhibitory concentrations (MICs) of DCAP against a range of *S. aureus* strains (determined and kindly provided by Kevin Ludwig).

Strain	MIC DCAP [µg/mL]
Staphylococcus aureus RN4220	16
Staphylococcus aureus SG511	16
Staphylococcus aureus HG001	32
Staphylococcus aureus SA113	32

Time-kill kinetics showed a differential and concentration-dependent impact of DCAP on *S. aureus* viability (Figure 41). While 1 x MIC inhibited bacterial growth without significant decrease in CFU/mL, higher concentrations led to complete killing within the first hours of treatment. The rapid killing of 4 x MIC indicated that the bactericidal impact of DCAP at higher concentrations might be too fast for evaluation of the cellular effects leading up to cell death. Therefore, it was concluded to investigate the cellular consequences of DCAP treatment using concentrations of 1 – 2 x MIC.

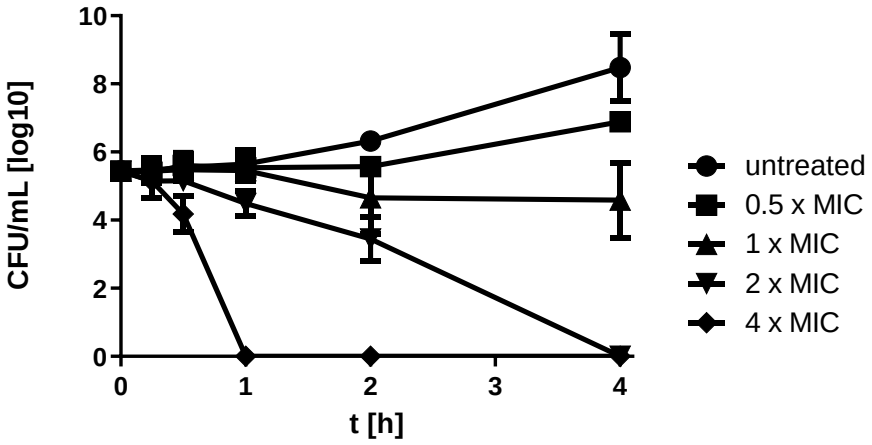

Figure 41: Killing kinetics of DCAP against *S. aureus* HG001. Symbols show the mean of three independent biological experiments ± SD.

4.4.2. Impact of DCAP on septum formation of *S. aureus*

To explore the distinct cellular effects of DCAP on *S. aureus*, impact of the compound on cell morphology was visualized using BODIPY-FL labelled vancomycin (Van-FL) as a cell wall stain (Figure 42). Previous descriptions of DCAP mechanism of action largely focused on the impact on transmembrane potential, which were directly compared and found to be similar to the ionophore CCCP (Carbonyl cyanide m-chlorophenyl hydrazone, Eun *et al.* 2012; Hurley *et al.* 2015). Therefore, CCCP was used as a control for the cellular effects arising from membrane depolarization alone. CCCP had no significant effect on cell morphology. In contrast, DCAP treatment resulted in a range of aberrations

in septum formation, including multiple septation, failed cell separation and a unique bent septum phenotype (Figure 42). Septum formation is an essential part of cell division and the closely coordinated cell wall biosynthesis. Thus, these results suggested a specific effect of DCAP on either of these processes, which was independent from the impairment of the transmembrane potential.

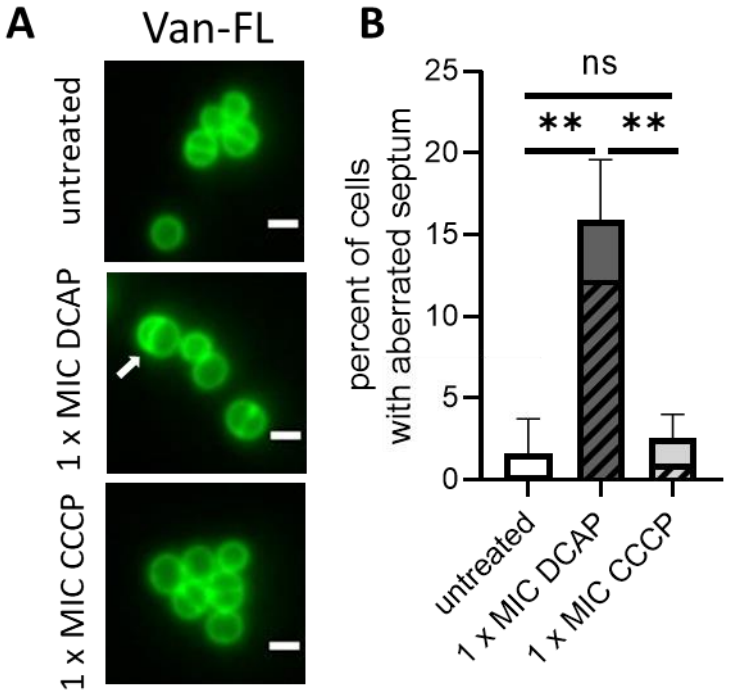

Figure 42: DCAP treatment induces aberrant septum formation. (A) Representative micrographs of *S. aureus* RN4220 treated for 1 h with 1 x MIC DCAP or 1 x MIC CCCP and an untreated control. Cell walls were stained with Vancomycin-FL (Van-FL). White arrow indicates a aberrated bent septum after DCAP treatment. Scale bar, 1 µm. **(B)** Relative abundance of cells with aberrant septum shape as % of total population after 1 h of treatment with 1 x MIC DCAP or 1 x MIC CCCP and an untreated control. Bar graphs show the mean of three independent biological experiments ± SD, respectively. Shaded areas indicate the relative abundance of aberrant septa with a bent septum phenotype, n ≥ 100 cells per replicate and condition. Statistical significance was determined using unpaired two-tailed students t-tests with a 95% confidence interval. Statistical significance was denoted as ns, not significant, $p > 0.05$; **, $p = 0.01$ to 0.001.

To analyze how DCAP impairs septum organization, the central cell division protein FtsZ and the early-divisome essential CWBM protein FtsW were visualized (Figure 43). 1 x MIC DCAP primarily affected the septum morphology, and only a minor fraction of cells showed delocalization of the proteins into an unspecific, cytoplasmic signal. Corroborating the observed cell wall morphologies, FtsZ and FtsW localized in misplaced and misshaped septa, most prominently the afore-mentioned bent septa and multiple divisome assemblies within one cell. With almost 40 % of cells displaying aberrant septa (Figure 43B), the multiple septum formation defects were even more pronounced than in the Van-FL strain. This difference is likely caused by the more precise visualization of the divisome, as it does not rely on substantial septal cell wall assembly to visualize misshaped septa. FtsZ and FtsW stayed highly co-localized, indicating that early divisome assembly itself was not drastically impaired by DCAP. Interestingly, both FtsZ and FtsW accumulated heavily in the crescent-shaped cells resulting from bent septum formation, indicating that these were not viable daughter cells.

In contrast, the CCCP control did not show significant effects towards septum morphology (Figure 43). Instead, 1 x MIC CCCP caused a significant decrease in cells with intact Z-rings. This is caused by the loss of FtsZ GTPase activity due to dissipation of the transmembrane potential (Strahl *et al.* 2010, see also chapter 4.2). Thus, both FtsZ and FtsW were both found delocalized in the cytoplasm. The same phenotype was also observed in cells treated with 1 x MIC DCAP, however, to a lesser degree than in the CCCP control. Interestingly, increasing the DCAP concentration to 2 x MIC considerably increased the abundance of cells showing exclusively cytoplasmic signals of both proteins, similar to the effect observed for CCCP. Meanwhile, it did not significantly alter the abundance of aberrant septa compared to 1 x MIC, indicating a higher hierarchization of targeted septum disorganization over transmembrane potential dissipation at low DCAP concentrations. This further suggested an additional, functionally independent effect of the compound directed towards cell division and/or cell wall biosynthesis.

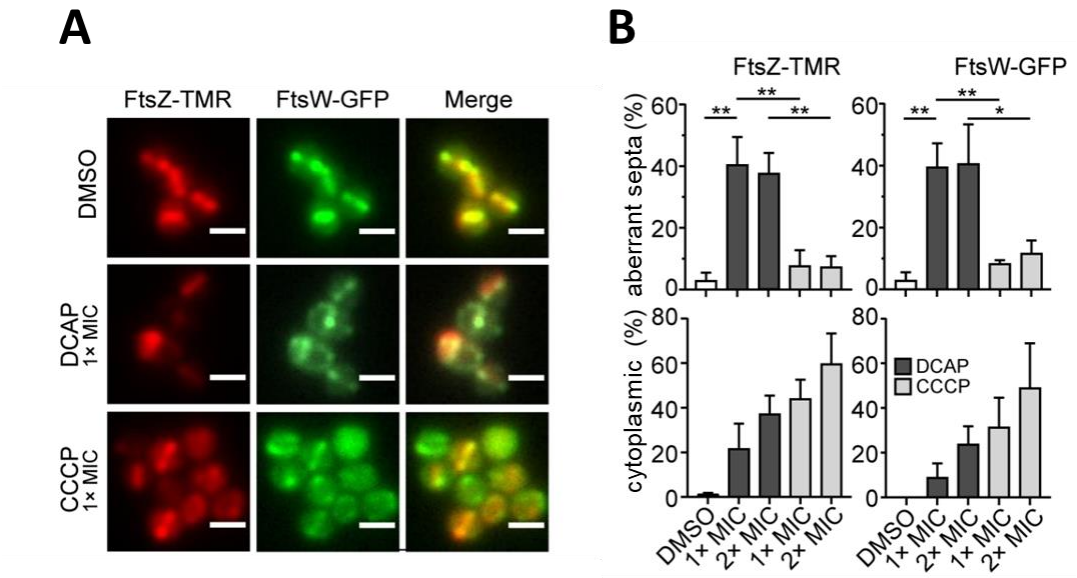

Figure 43: DCAP disrupts septum formation and impacts the localization of FtsZ and FtsW. (A) Representative micrographs of *S. aureus* RN4220 FtsW-GFP pCQ11-FtsZ-SNAP treated for 1 h with 1 x MIC DCAP or 1 x MIC CCCP and an untreated control. SNAP-tags were labelled with SNAP-Cell® TMR Star. Scale bar, 1 µm. **(B)** Relative abundance of cells with FtsZ and FtsW localizing in aberrant septa shape, or cytoplasmic localization, respectively, as % of total population after 1 h of treatment with DCAP or CCCP and an untreated control. Bar graphs show the mean of three independent biological experiments ± SD, respectively. n ≥ 100 cells per replicate and condition. Statistical significance was determined using unpaired two-tailed students t-tests with a 95% confidence interval. Statistical significance was denoted as ns, not significant, p > 0.05; *, p = 0.05 to 0.01; **, p = 0.01 to 0.001.

4.4.3. Impact of DCAP on the spatial organization of peptidoglycan synthesis

To evaluate, if the specific impact of DCAP on septum morphology was caused by interference with cell wall biosynthesis, the compound's effect on peptidoglycan synthesis was visualized on an individual cell level. Therefore, incorporation of HADA by transpeptidases was quantified and subcellular localization of transpeptidase activity foci was mapped via maxima analysis (Figure 44). CCCP and DCAP both reduced overall HADA fluorescence intensity to a similar extent (Figure 44B). However, DCAP remarkably caused complete dislocation of the signal resulting in homogenous fluorescence distribution across the cell. CCCP instead had significantly less effect on spatial organization of the transpeptidase activity with most of the HADA fluorescence remaining at the septum (Figure 44C). When analyzing the subcellular localization of TPase activity foci, both the untreated and the CCCP control showed the expected septal distribution of HADA maxima. In contrast, an unspecific maxima distribution was observed after DCAP treatment, which illustrated that virtually no directed septal peptidoglycan synthesis occurred under these conditions (Figure 44D). Accordingly, it was concluded that DCAP may impact cell wall biosynthesis organization in a targeted and direct way, rather than as an unspecific downstream result of transmembrane potential impairment.

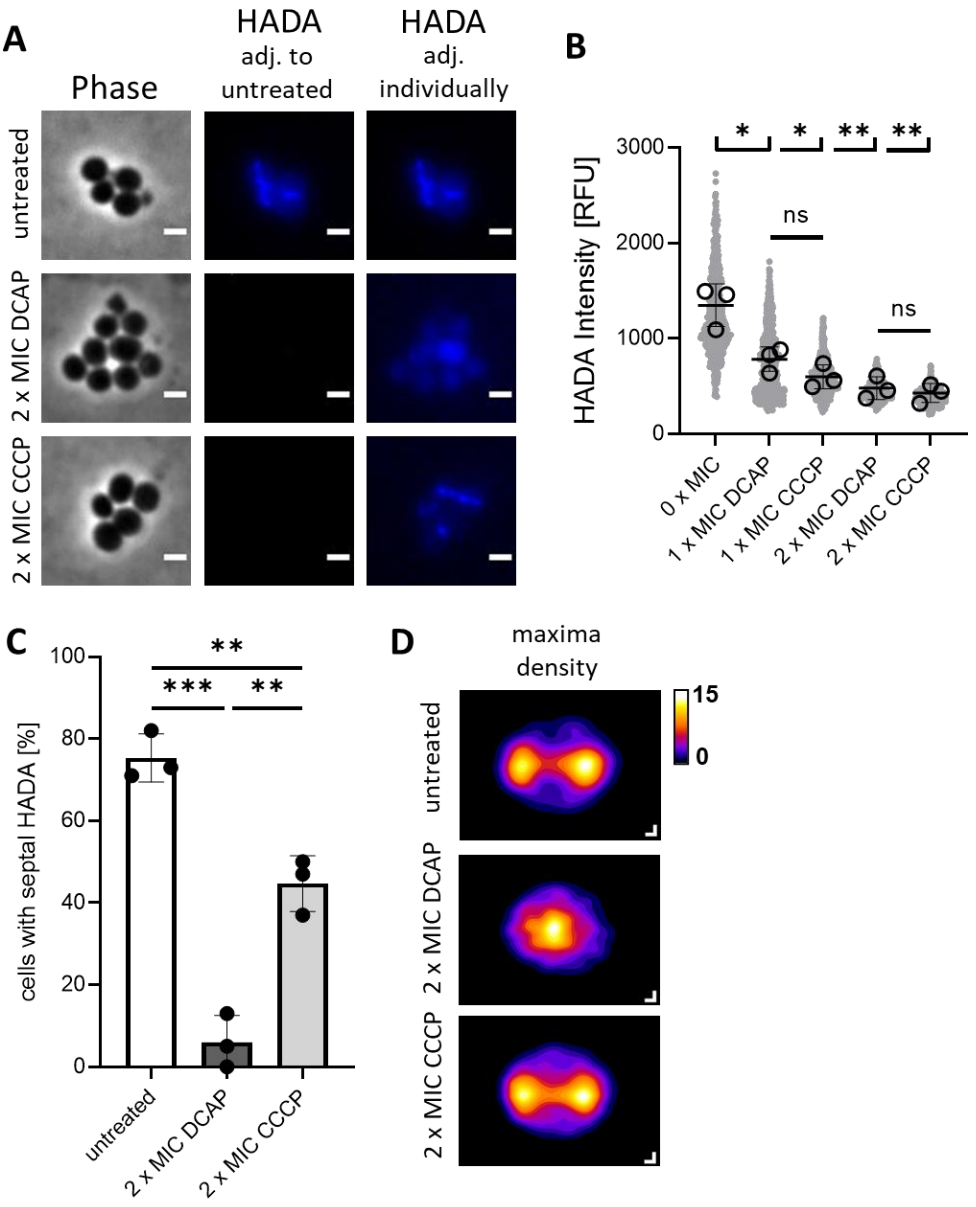

Figure 44: DCAP dislocates transpeptidase activity. (A) Representative micrographs of *S. aureus* SA113 treated with 2 x MIC DCAP or 2 x MIC CCCP for 1 h and an untreated control, stained with HADA. The HADA channel of each micrograph is shown twice. Middle: HADA channel with brightness and contrast adjusted to the untreated control. Right: HADA channel with brightness and contrast adjusted to the individual image. Scale bar, 1 µm. **(B)** Quantification of HADA intensities of individual cells. Grey small symbols indicate individual cell data. Line and error bars show mean ± SD of three independent biological experiments. Large symbols show means of each independent replicate, n ≥ 100 cells per replicate and condition. **(C)** Relative abundance of cells with septal HADA incorporation as % of total population after 1 h of treatment with 2 x MIC DCAP or 2 x MIC CCCP and an untreated control. Bar graphs show the mean of three independent biological experiments ± SD, respectively. **(D)** Distribution of HADA fluorescence intensity maxima. Maxima were identified in ≥ 100 individual cells from three independent biological experiments. X/Y coordinates of all maxima were plotted, and the density was calculated for each condition. Scale bar, 0.1 µm for X and Y, respectively. RFU: Relative Fluorescence Unit. Statistical significance was determined against the untreated control using unpaired two-tailed students t-tests with a 95% confidence interval. Statistical significance was denoted as ns, not significant, $p > 0.05$; *, $p = 0.05$ to 0.01; **, $p = 0.01$ to 0.001. ***, $p = 0.001$ to 0.0001.

To validate this, the impact of DCAP on the localization of the main peptidoglycan synthase PBP2 was investigated (Figure 45). Localization of the essential CWBM protein depends on its transpeptidation substrate and its septal localization is essential for cell division (Pinho *et al.* 2005, see chapters 4.1.7 and 4.1.8). Accordingly, PBP2 plays a major role in the spatio-temporal organization of cell wall biosynthesis and cell division. Visualizing PBP2 after DCAP treatment (Figure 45) revealed a significant decrease in both the abundance of cells with septally localized PBP2 (Figure 45B) and in the septal focus of PBP2 (in cells, where PBP2 still localized to the septum, Figure 45C). Similar to FtsZ and FtsW, PBP2 also accumulated in the crescent-shaped cell halves, further indicating failure of viable cell division in this phenotype (Figure 46A).

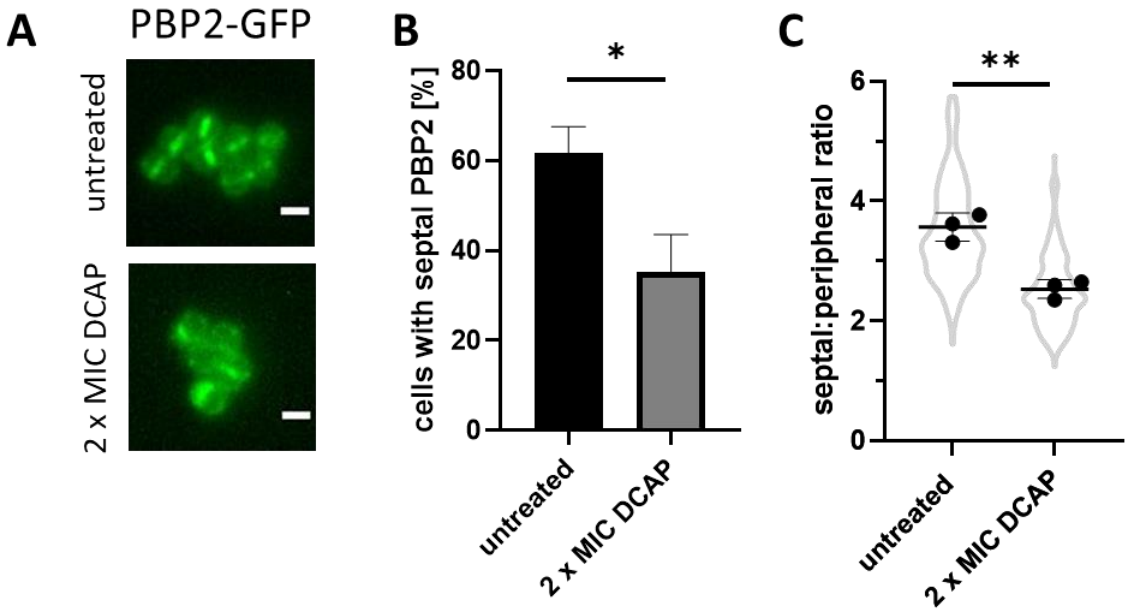

Figure 45: DCAP delocalizes the main peptidoglycan synthase PBP2. (A) Representative micrographs of *S. aureus* RN4220 RNpPBP2-31 after 1 h of treatment 2 x MIC DCAP and an untreated control. Scale bar, 1 µm. **(B)** Relative abundance of cells with septal PBP2 localization as % of total population after 1 h of treatment with 2 x MIC DCAP and an untreated control. Bar graphs show the mean of three independent biological experiments ± SD, respectively. n ≥ 100 cells per replicate and condition. **(C)** Septal:peripheral ratios of PBP2 after 25 min of treatment with 2 x MIC DCAP and an untreated control. Ratios were determined for individual cells with a visible continuous septal PBP2 signal. Violin plots show the distribution of individual cell data after exclusion of outliers. Line and error bars show mean ± SD of three independent biological experiments. Symbols show mean of each independent replicate, n ≥ 30 cells per replicate and condition. Statistical significance was determined against the untreated control using unpaired two-tailed students t-tests with a 95% confidence interval. Statistical significance was denoted as *, p = 0.05 to 0.01; **, p = 0.01 to 0.001.

4.5. Investigating the interaction of the *S. aureus* heme-acquisition system component IsdF with FloA *in vivo*

In *S. aureus*, targeting the iron-regulated surface determinant (Isd) heme-acquisition system may be a promising anti-infective approach due to the critical role of the scarce and essential resource iron (see chapter 1.4). Accordingly, impairment of the Isd system might contribute to reduce pathogenic proliferation of *S. aureus*, especially in often life-threatening bloodstream infections. IsdF, the membrane-integrated permease responsible for transferring captured heme into the cytoplasm, was

recently found to accumulate in the detergent-resistant membrane (DRM) fraction after non-ionic detergent treatment of isolated *S. aureus* cell membranes (Adolf *et al.* 2023). DRM contents correlate with and are therefore often associated to fluid membrane microdomains (FMMs, Adolf *et al.* 2023; Bach *et al.* 2013; Bramkamp *et al.* 2015; D. A. Brown 2002; Donovan *et al.* 2009; García-Fernández *et al.* 2017; H.-M. Zhang *et al.* 2005). Co-purification experiments showed a direct interaction of IsdF with FloA, the constituting scaffold protein of FMMs (Adolf *et al.* 2023).

To further investigate the interaction of the two proteins, both proteins were visualized in *S. aureus* with a chromosomally tagged FloA-SNAP and a plasmid-encoded IsdF-mNeongreen (Figure 46). FloA showed a heterogenous signal distribution along the cell surface, corresponding to the described aggregation of the protein in distinct patches within the cytoplasmic membrane (Figure 46A, García-Fernández *et al.* 2017; Koch *et al.* 2017). IsdF also localized in distinct foci along the membrane. Some of these foci co-localized with those of FloA. Additionally, some of the foci of either protein formed mutually exclusive patches in close proximity to each other. Accordingly, calculation of the co-localization as the Pearson product-moment correlation coefficient (PCC) for individual cells showed a distribution ranging from moderate positive correlation to non-correlative and even negative correlation for co-localization mean cell values (Figure 46B). This suggested a more complex interaction dynamic of IsdF and FloA (or FMMs, respectively).

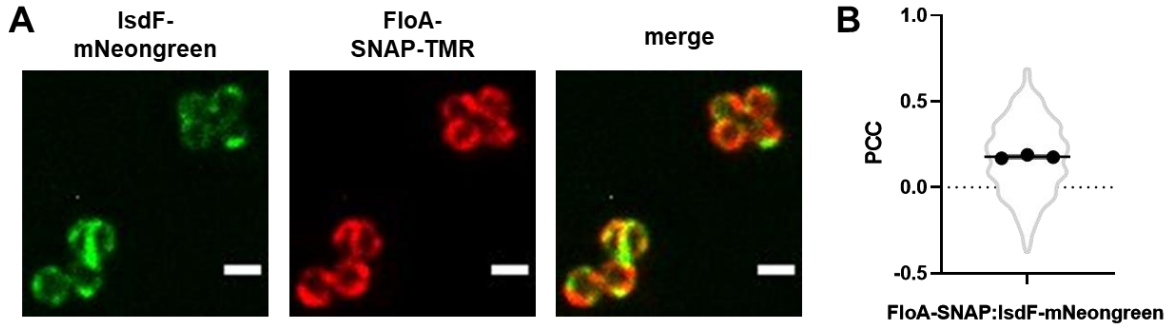

Figure 46: IsdF localizes in discrete foci in the cytoplasmic membrane in close proximity to and partially co-localizing with FloA foci. (A) Representative deconvolved micrographs of *S. aureus* Newman FloA-SNAP pCQ11-IsdF-mNeongreen. Scale bar, 1 µm. **(B)** Quantification of co-localization of IsdF-mNeongreen fluorescence and FloA-SNAP-TMR fluorescence, determined as Pearson correlation coefficient (PCC) in individual cells. Violin plot shows the distribution of individual cell data. Black symbols show mean values of three independent biological experiments, bar shows their mean ± SD. n ≥ 293 cells per replicate.

To further investigate the role of FloA in localization of IsdF, the plasmid encoding IsdF-mNeongreen was cloned into *S. aureus* Newman *ΔfloA* (provided by Lea Adolf) and visualized using widefield microscopy (Figure 47). Remarkably, no fluorescence signal significantly different the unspecific background fluorescence of an uninduced control was observed. A control clone harboring the same plasmid alongside a SNAP-tagged FloA showed a significant mNeongreen signal with the aforementioned IsdF localization pattern. Chromosomal complementation of *floA* in *S. aureus* Newman *ΔfloA* via allelic exchange (performed and provided by Lea Adolf) rescued the IsdF-mNeongreen

fluorescence, restoring both fluorescence signal intensity and localization pattern (Figure 47). This clearly demonstrated that FloA is essential for functional production of a stable and/or correctly folded and membrane integrated IsdF.

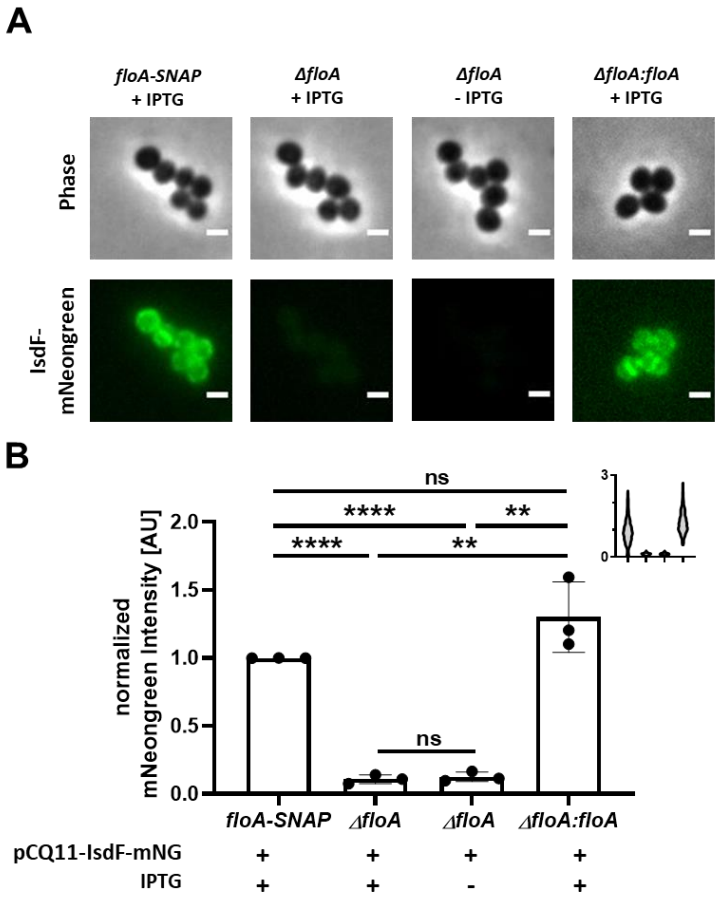

Figure 47: Production of functional IsdF-mNeongreen depends on presence of FloA. (A) Representative micrographs of *S. aureus* Newman FloA-SNAP pCQ11-IsdF-mNeongreen, *S. aureus* Newman *ΔfloA* pCQ11-IsdF-mNeongreen and *S. aureus* Newman *ΔfloA:floA* pCQ11-IsdF-mNeongreen. pCQ11-IsdF-mNG: pCQ11-IsdF-mNeongreen. For datasets labelled "+ IPTG", expression of IsdF-mNeongreen was induced with 0.1 mM IPTG for 6 h. Brightness and contrast of the mNeongreen channel were adjusted to the respective positive control. Scale bar, 1 µm. **(B)** Quantification of IsdF-mNeongreen fluorescence intensity of individual cells. Inset violin plot shows the distribution of individual cell data after exclusion of outliers. Bar shows the mean ± SD of three independent biological experiments. Large symbols show the mean of each replicate. n ≥ 718 cells analyzed per strain. Data was normalized to the respective FloA-SNAP replicate mean. AU: Arbitrary Unit. Statistical significance was determined using unpaired two-tailed student's t-test with 95% confidence interval. **** = $p < 0.0001$. ns = $p > 0.05$.

As an additional control, the plasmid pCQ11-IsdF-mNeongreen was purified from the defective strain *S. aureus* Newman *ΔfloA* pCQ11-IsdF-mNeongreen. In a PCR, an insert with the correct fragment size was successfully amplified, demonstrating that the genetic basis for IsdF-mNeongreen production was still present in the non-fluorescent strain (Figure 48).

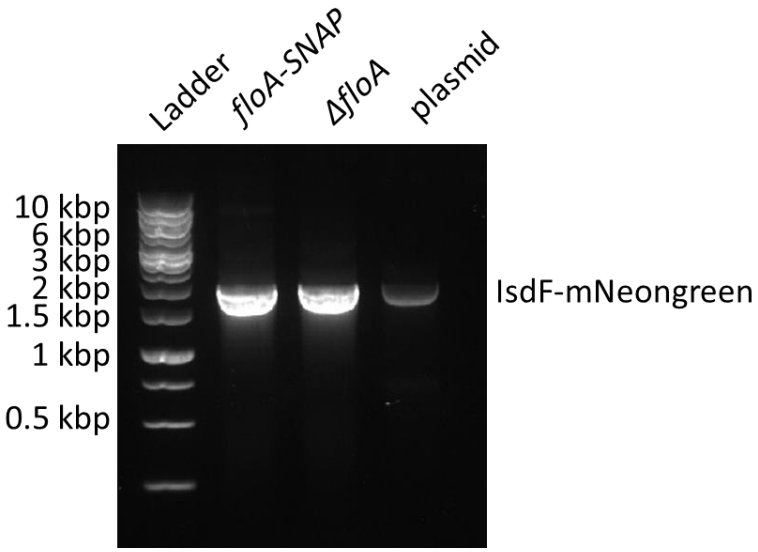

Figure 48: IsdF-mNeongreen insert is present in *S. aureus* Newman *ΔfloA* pCQ11-IsdF-mNeongreen. PCR Products of plasmids purified from *S. aureus* Newman FloA-SNAP pCQ11-IsdF-mNeongreen and *S. aureus* Newman *ΔfloA* pCQ11-IsdF-mNeongreen and a plasmid control of pCQ11-IsdF-mNeongreen purified from the *E. coli* shuttle strain. PCR Primers against the insert IsdF-mNeongreen, with a resulting product of 1.936 kilo base pairs (kbp). DNA Fragments were separated in a 1% agarose gel and visualized using GelRed. GeneRuler 1 kb DNA Ladder for fragment size reference.

4.6. Investigating the impact of A37 production on interspecies competition of *S. epidermidis* against *C. glutamicum*

The discovery of a new member of the epilancin family sparked interest in the potential of the compound to shape the natural environment of the producer strain, and to elucidate the mechanism of action against its natural target species. The compound was observed to be produced by the nasal isolate *S. epidermidis* A37 and was accordingly named epilancin A37. Genetic analysis predicted, that it featured the defining three-ring structure of the epilancin scaffold, with multiple differences to K7 and 15X in the primary sequence, revealing an overall amphiphilic, polycationic structure with a net charge of + 6 at pH 7.0 (Figure 49, genetic analysis performed and kindly provided by Jeffrey John Power and Benjamin Winnerling).

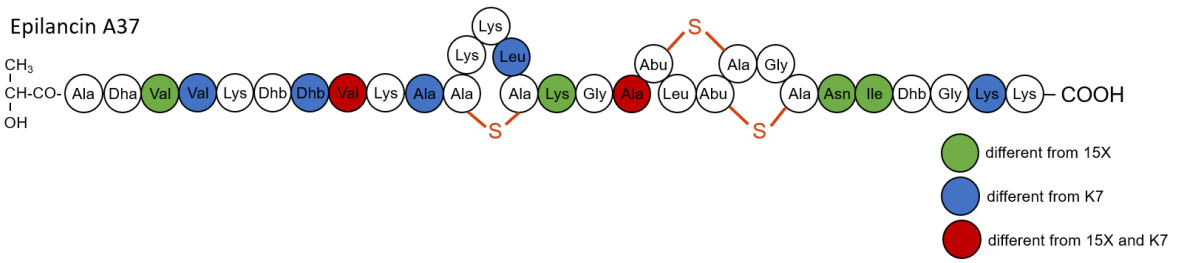

Figure 49: Structural prediction of epilancin A37 with highlighted differences to other structurally elucidated epilancins produced by *S. epidermidis*, 15X and K7. Figure kindly provided by Fabian Grein.

Purified A37 showed moderate activity against coagulase negative staphylococci and a particularly potent effect against corynebacteria (performed and kindly provided by Benjamin Winnerling). MICs against multiple species of this family ranged from 0.5 – 2 µg/mL, corresponding to growth inhibiting activity at nanomolar concentrations (molecular weight of A37: 2984 Da). The comparably well-characterized model organism *Corynebacterium glutamicum* was chosen for detailed analysis of the activity of A37 towards corynebacteria. Similar to other species of the family, the type-strain *C. glutamicum* DSM20300 (referred to as *C. glutamicum* wild type from here on) showed a high susceptibility to A37 with a MIC of 1 µg/mL. To further elucidate this competitive advantage of A37 production, *S. epidermidis* A37 and *C. glutamicum* wild type were co-cultivated and the relative abundance of *S. epidermidis* was determined via microscopy (Figure 50). Therefore, both strains were grown to mid-logarithmic phase and adjusted to OD_{600} = 0.05. These cell suspensions were mixed 99:1 (v/v, *C. glutamicum*:*S.epidermidis*), resulting in a relative *S. epidermidis* abundance of 1%. After 3 h of co-cultivation, a drastic increase in relative abundance of *S. epidermidis* A37 to 43.2% was observed (Figure 50A,B). As a control, the experiment was repeated using the type strain *S. epidermidis* ATCC14990, which does not produce an epilancin. In this experiment, the *S. epidermidis* strain only showed 7 % abundance after 3h of co-cultivation. This clear difference demonstrated that A37 production contributed to the competitiveness of *S. epidermidis* against *C. glutamicum*. As additional verification, a lab-generated *C. glutamicum* strain with 8-fold reduction in A37 susceptibility named *C. glutamicum* A37/8 (kindly provided by Benjamin Winnerling) was also co-cultivated with *S. epidermidis.* As expected, the relative abundance of the producer strain *S. epidermidis* A37 was significantly lower after 3 h of co-cultivation in this experiment. This validated that the susceptibility of *C. glutamicum* towards A37 played an important role in the competition with the producer strain *S. epidermidis* A37 (Figure 50A,B). Corroborating this, the abundance of the control strain *S. epidermidis* ATCC 14990 after 3 h of co-cultivation did not differ significantly between the two experimental setups, which showed that there was no generally improved competitiveness of *C. glutamicum* A37/8 against *S. epidermidis.* Heavy clumping of *C. glutamicum* cells unfortunately prevented quantitative analysis of abundances after longer co-cultivation times (Figure 50C). Thus, samples were assessed only semi-quantitatively by estimating the approximate abundance of *S. epidermidis* and *C. glutamicum* cells after 24 h of co-cultivation. Still, these approximations corresponded well to the quantitative results after 3 h of co-cultivation. In the experiments with *S. epidermidis* A37 and *C. glutamicum* wild type, cultures after 24 h appeared to consist almost exclusively of *S. epidermidis* cells (Figure 50D) in all three biologically independent replicates. When *C. glutamicum* A37/8 was used in co-cultivation with *S. epidermidis* A37, the *S. epidermidis* cells still constituted the majority of cells. However, multiple heavily aggregated cell-clumps of *C. glutamicum* were found in all three replicates. This indicated the presence of a small, but viable population of *C. glutamicum* A37/8 in these samples. These observations suggested, that *S. epidermidis* A37 displaced *C. glutamicum* wild type due to the production of A37, while being unable to displace *C. glutamicum* A37/8 due to this strains decreased susceptibility. This was further corroborated by the outcome of co-cultivating *S. epidermidis* ATCC 14990 with either of the two *C. glutamicum* strains for 24 h. In these setups, *C. glutamicum* wild type or *C. glutamicum* A37/8, respectively, were found in all samples after 24 h of co-cultivation.

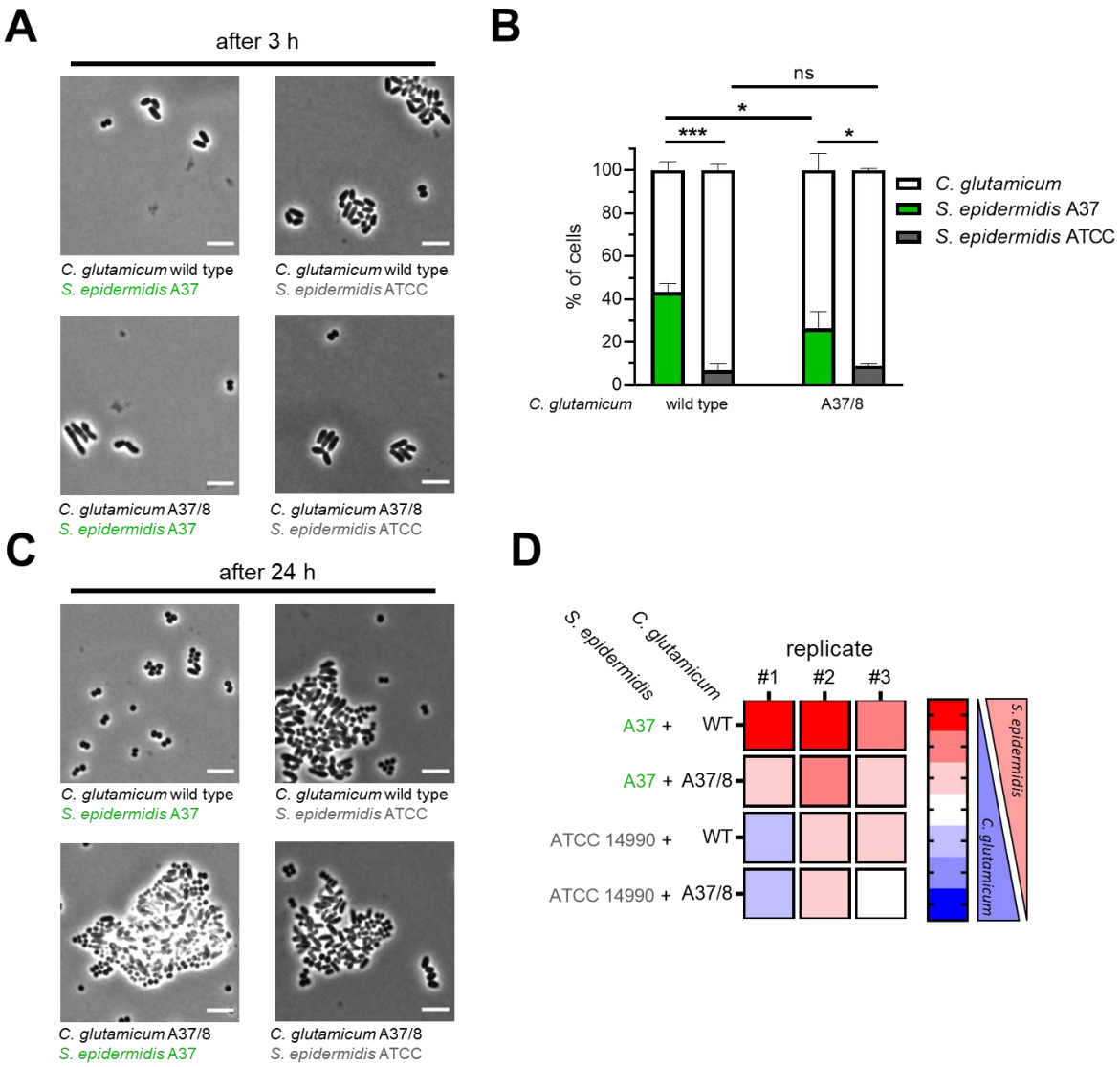

Figure 50: The producer strain *S. epidermidis* A37 has an increased competitive advantage against *C. glutamicum* wild type. Decreased susceptibility towards A37 in the lab-generated *C. glutamicum* A37/8 translates to an improved fitness against the producer strain. (A) Representative micrographs of cells of *S. epidermidis* A37 or *S. epidermidis* ATCC 14990 mixed with *C. glutamicum* wild type or *C. glutamicum* A37/8 after 3 h of co-cultivation. Mixture 99% *C. glutamicum* and 1% *S. epidermidis.* Scale bar, 5 µm. **(B)** Relative abundance of the *S. epidermidis* A37 or *S. epidermidis* ATCC 14990 subpopulation as % of total population after 3 h of co-cultivation with either *C. glutamicum* wild type or A37/8. Bar graphs show the mean of three independent biological experiments ± SD, respectively. n ≥ 204 cells per replicate and condition. **(C)** Representative micrographs of cells of *S. epidermidis* A37 or *S. epidermidis* ATCC 14990 mixed with *C. glutamicum* wild type or *C. glutamicum* A37/8 after 24 h of co-cultivation. Mixture 99% *C. glutamicum* and 1% *S. epidermidis.* Scale bar, 5 µm. **(D)** Semi-quantitative analysis of the relative abundance of *S. epidermidis* A37 or *S. epidermidis* ATCC 14990 mixed with *C. glutamicum* wild type or *C. glutamicum* A37/8 after 24 h of co-cultivation. Data for three independent biological experiments (Replicate #1 - #3) are shown. Statistical significance was determined against the untreated control using unpaired two-tailed students t-tests with a 95% confidence interval. Statistical significance was denoted as p > 0.05; *, p = 0.05 to 0.01; ***, p = 0.001 to 0.0001.

To investigate the potential impact of each strains growth dynamics on these results, all four strains used in the competition experiments were incubated separately with inoculum and conditions identical to the competition setup (Figure 51). The two *S. epidermidis* strains showed very similar growth dynamics, with a slightly longer lag phase in the A37 producer strain. The *C. glutamicum* wild type strain showed a lag phase similar to *S. epidermidis* A37, but a more linear growth phase, as expected from the linear *C. glutamicum* growth dynamics (Messelink *et al.* 2021). Importantly, while *C. glutamicum* wild type showed an OD_{600} increase only moderately different from the *S. epidermidis* strains, substantially slower growth was observed for *C. glutamicum* A37/8. OD_{600} increase of that strain showed notably irregularities both within and between biological replicates, which might be an artifact of the heavy clumping observed in microscopy. Importantly, while *S. epidermidis* exhibited faster growth than *C. glutamicum*, growth behaviour of the individual strains did not correspond to the population dynamics in the co-cultivation. *S. epidermidis* A37 grew slightly slower and with a longer lag phase than *S. epidermidis* ATCC14990 but showed substantially better competitive fitness against *C. glutamicum* in the co-cultivation. Furthermore, *C. glutamicum* A37/8 showed considerably slower growth than the *C. glutamicum* wild type, but still outperformed the wild type in competition against *S. epidermidis* A37. These results verified that the observations of the co-cultivation are not caused by the growth dynamics of the different strains.

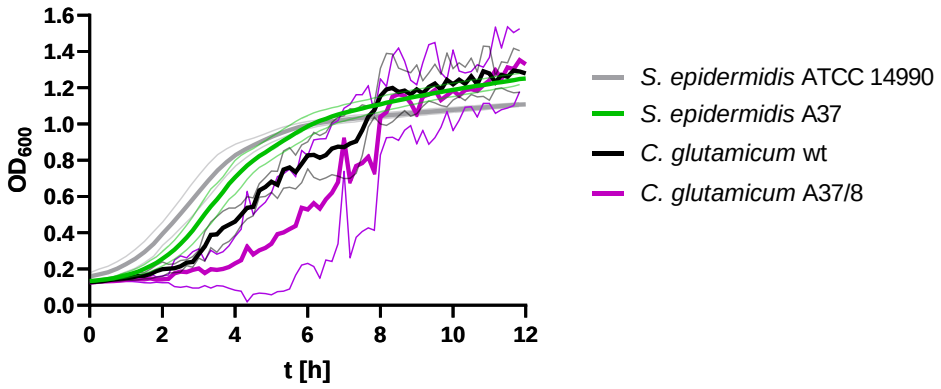

Figure 51: Growth curves of *S. epidermidis* ATCC 14990, *S. epidermidis* A37, *C. glutamicum* wild type and *C. glutamicum* A37/8. Lines show the mean of three independent biological experiments ± SD.

4.7. Investigating the mechanism of action of epilancin A37

4.7.1. Subcellular localization of A37 and impact on cytoplasmic membrane function

To investigate the cellular impact of A37 on *C. glutamicum* and gain an understanding of potential sites of action, binding of a BODIPY-FL labelled derivative A37FL to cells of *C. glutamicum* wild type was visualized using Airyscan superresolution microscopy (Figure 52). Therefore, a mixture of 10% labeled and 90% unlabeled A37 was used (see also chapter 3.3.2). Remarkably, A37 was found to be localized primarily in the cytoplasm after 15 min of treatment, with no membrane binding that was significantly distinguishable from the cytoplasmic signal (Figure 52A). Interestingly, distinct spots of accumulated

A37FL were frequently observed, typically associated to the inner cell boundaries. Mapping the subcellular localization of these fluorescent spots by maxima analysis illustrated that these spots were primarily localized near the septum and the cell poles (Figure 52B).

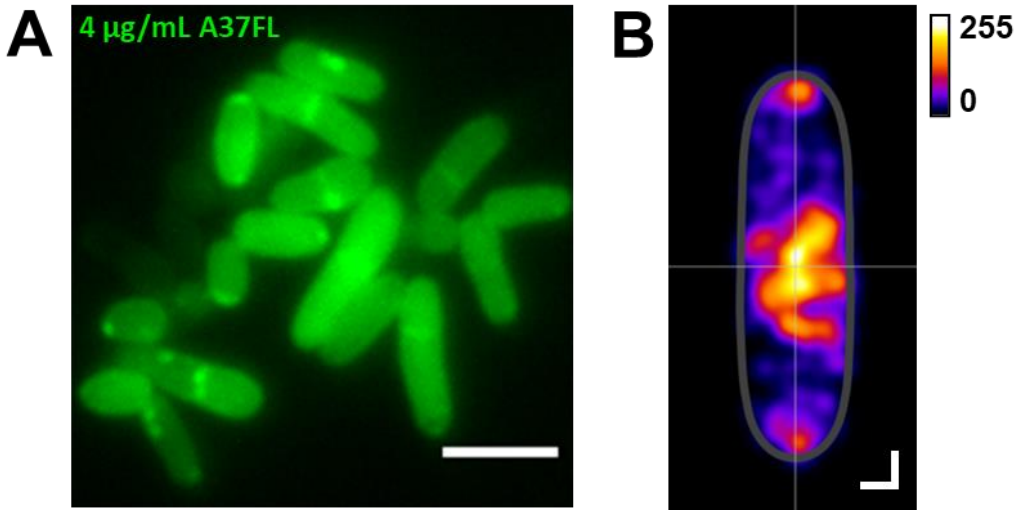

Figure 52: BODIPY-FL labelled A37 (A37FL) localizes into the cytoplasm of *C. glutamicum* and forms distinct intracellular accumulation spots. (A) Representative AiryScan superresolution micrograph of *C. glutamicum* wild type treated with 4 x MIC A37FL for 15 min. Scale bar, 2 µm. Imaging by Dominik Brajtenbach. **(B)** Distribution of A37FL fluorescence intensity maxima. Maxima were identified in n = 782 individual cells from three independent biological experiments. X/Y coordinates of all maxima were plotted, and the density of these coordinates was calculated and visualized. Scale bar, 0.2 µm for X and Y, respectively.

Intracellular localization of lantibiotics can be a result of massive membrane damage, leading to lysis and aggregation. However, this is typically accompanied by significant membrane binding of the lantipeptide to induce the necessary membrane integrity impairment (Omardien *et al.* 2018; Wenzel *et al.* 2014, 2018). This phenotype was not observed in cells treated with A37FL. Instead, all cells with A37FL signal showed a homogenous cytoplasmic localization of the compound, with one or more A37FL accumulation spots inside 32.6% of the cells. Importantly, cells with spots, but without a cytoplasmic localization were not found. This rendered it unlikely, that spots were a transient state of compound uptake prior to cytoplasmic dispersal. To investigate, whether the observed cytoplasmic localization was caused by a preceding event of membrane disruption, the effect of A37 treatment on propidium iodide (PI) influx was analyzed. PI is a DNA stain which cannot pass intact cytoplasmic membranes. However, if the membrane integrity is impaired, e.g. by pore formation, disintegration or lysis, PI can enter the cell and bind to the DNA, which results in a pronounced increase in quantum yield as well as a shift in the excitation and emission spectra. Thus, PI is an excellent probe to determine cytoplasmic membrane damage (Arndt-Jovin *et al.* 1989; Auty *et al.* 2001; Leuko *et al.* 2004; Stiefel *et al.* 2015; Stocks 2004). Quantification of PI fluorescence during treatment with 0.5 -16 x MIC of A37 resulted in no, or negligible, signal increase over 1 h (Figure 53). Only very high concentrations of the epilancin showed a moderate effect on PI signal. In contrast, treatment with 4 x MIC nisin (MIC: 16 µg/mL) induced rapid and massive PI within the first 5 min of treatment, which was even further elevated over time, which clearly demonstrated that the effect of A37 drastically differed from that of nisin. This result and the primarily

cytoplasmic cell binding strongly suggested, that membrane integrity impairment was not the primary mechanism of action of A37. Furthermore, it indicated, that A37 was able to penetrate and pass the cytoplasmic membrane without inducing membrane damage.

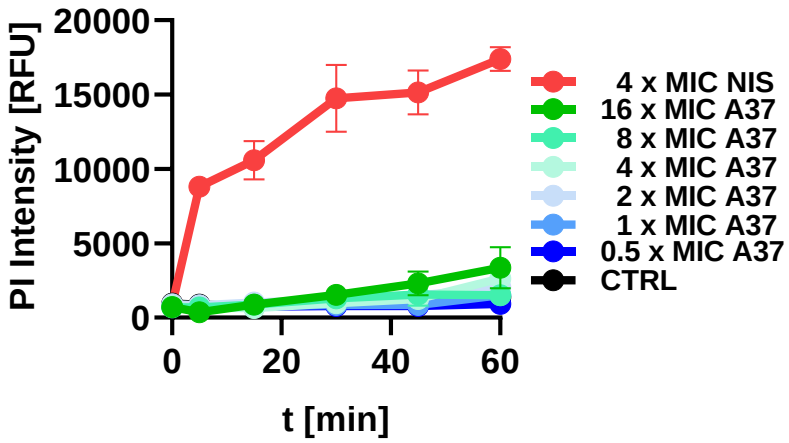

Figure 53: A37 does not impair cell membrane integrity within the first hour of treatment. Membrane disruption of *C. glutamicum* wild type was measured by quantifying the staining of cells with damaged membrane integrity by propidium iodide (PI) fluorescence over time. Lines Indicate the mean of three biologically independent experiments ± SD. Symbols indicate timepoints of measurement.

To narrow down possible mechanisms of action of A37, the effect of A37 treatment on the transmembrane potential of *C. glutamicum* was investigated. Membrane depolarization can be achieved without impairing membrane integrity (Strahl *et al.* 2010; te Winkel *et al.* 2016). To quantify the epilancins impact on the transmembrane potential on the individual cell level, $DiBAC_4(3)$ was used, an anionic dye whose intracellular fluorescence intensity increases proportional to membrane depolarization (te Winkel *et al.* 2016). However, no significant change in $DiBAC_4(3)$ signal was observed after 15 min of treatment with up to 16 x MIC of A37 (Figure 54A). In contrast, 4 x MIC nisin caused drastic increase of intracellular $DiBAC_4(3)$ fluorescence. This further confirmed the differences between the mechanisms of action of the two lantibiotics and showed that A37 had no membrane depolarizing effect on *C. glutamicum.*

The bacterial transmembrane potential is a sum of multiple biophysical effects, which result in a net negative potential between the outside and inside the bacterial cell (Benarroch *et al.* 2020). Accordingly, this potential energizes cation and H^+ uptake and can enable the intracellular aggregation of cationic molecules (Benarroch *et al.* 2020; Taber *et al.* 1987; te Winkel *et al.* 2016). The poly-cationic nature of A37 and the observation, that the epilancin had no impact on transmembrane potential homeostasis, congregated to a putative uptake mechanism driven by the negative potential, which could cause the cytoplasmic localization of the epilancin. To investigate this hypothesis, release of the fluorescent dye $DiSC_3(5)$ was quantified during A37 treatment. $DiSC_3(5)$ is a cationic self-quenching dye that accumulates in cells proportional to their membrane polarization (te Winkel *et al.* 2016). Accordingly, release of the dye from cells results in de-quenching and fluorescence proportional to the amount of released dye. 4 x MIC nisin lead to massive and rapid release of $DiSC_3(5)$ due to its ultimately membrane

disrupting mechanism of action (Figure 54B). When cells of *C. glutamicum* were treated with A37, a rapid and dose-dependent release of $DiSC_3(5)$ was observed (Figure 54B), which reached equilibrium within the first minutes of treatment (see appendix 5). Importantly, the extent of this release was considerably lower than in the nisin control, even at very high concentrations of A37 (Figure 54B). As PI and $DiBAC_4(3)$ experiments demonstrated that A37 has no significant impact on membrane functionality, this efflux could not be explained by an A37-facilitated depolarization. Instead, it indicated a transmembrane-potential driven uptake of the polycationic A37 into the cytoplasm, which triggered a dose-dependent exchange of the cationic $DiSC_3(5)$ molecules with the polycationic A37 peptides. Notably, even 16 x MIC A37 still caused significantly less dye efflux than nisin, further underlining that impairment of membrane function is not the defining factor in the antimicrobial action of A37.

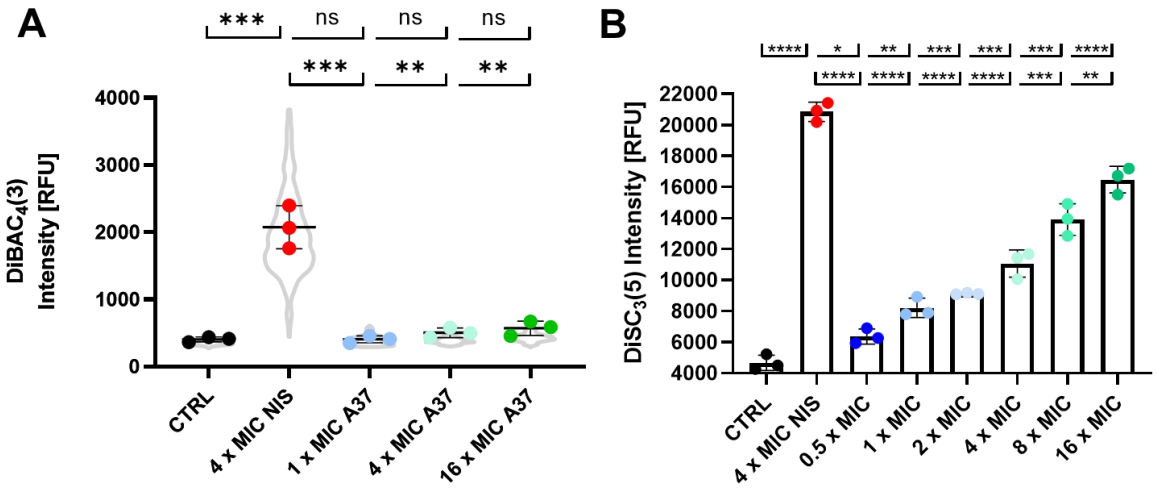

Figure 54: A37 does not induce membrane depolarization but causes a dose-dependent release of the cationic dye $DiSC_3(5)$. (A) Quantification of $DiBAC_4(3)$ fluorescence intensities of individual cells of *C. glutamicum* wild type after 15 min of treatment with 4 x MIC nisin or 1 – 16 x MIC A37 and an untreated control. Violin plots show the distribution of individual cell data after exclusion of outliers. Line shows mean of three biologically independent experiments ± SD. Symbols show the mean of each individual biological experiment. n ≥ 125 cells per replicate and condition. **(B)** $DiSC_3(5)$ release from cells of *C. glutamicum* wild type after 2 min of treatment with 4 x MIC nisin or 1 – 16 x MIC A37 and an untreated control. Bar graphs show the mean of three biologically independent experiments ± SD. Symbols show the mean of each individual biological experiment. RFU: Relative Fluorescence Unit. Statistical significance was determined using unpaired two-tailed students t-tests with a 95% confidence interval. Statistical significance was denoted as ns, not significant, $p > 0.05$; *, $p = 0.05$ to 0.01; **, $p = 0.01$ to 0.001; ***, $p = 0.001$ to 0.0001; ****, $p \leq 0.0001$.

To investigate the relevance of a transmembrane potential for A37 uptake, cells were pre-treated with 10 µg/mL of CCCP for 5 min (CCCP shock). It has been shown that the ionophore significantly and rapidly reduces the bacterial transmembrane potential (Jensen *et al.* 2020; Parsons *et al.* 2012; Rubino *et al.* 2020; Strahl *et al.* 2010). CCCP itself has no cationic character at physiological pH and does not impair membrane integrity (Jensen *et al.* 2020; Kasianowicz *et al.* 1984; Parsons *et al.* 2012; Strahl *et al.* 2010; Xing *et al.* 2014). Following the short CCCP shock, the cytoplasmic binding of A37FL was then quantified on the individual cell level and compared to a control with unaffected transmembrane potential (Figure 55). The CCCP shock significantly reduced the binding of A37FL, leading to a notable shift in fluorescence intensities of individual cells and an almost 50% reduction in mean A37FL binding (Figure 55A,B). This result illustrated that transmembrane potential is a significant, but not the exclusive factor in mediating the binding and translocation of A37 into the cytoplasm. Interestingly, the CCCP shock also caused a significant reduction in the number of A47FL spots inside the cells, indicating a correlation between A37FL binding and the formation of these spots (Figure 55C).

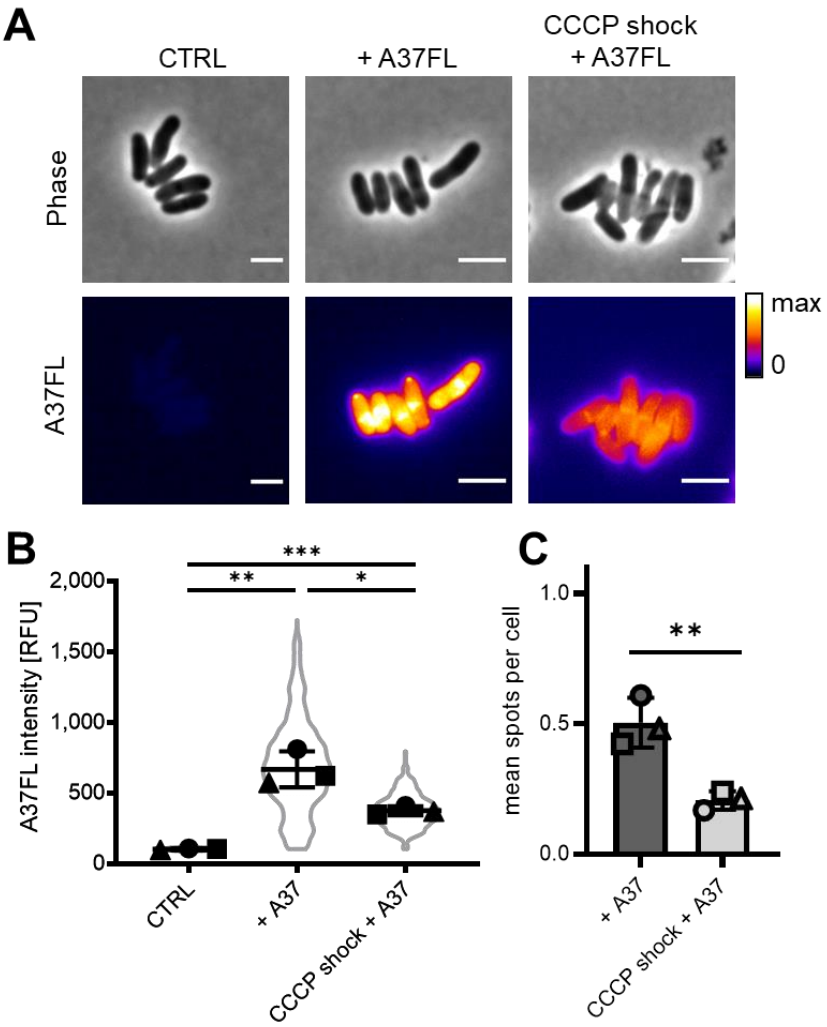

Figure 55: A37 enters the cytoplasm in a transmembrane potential dependent manner. (A) Representative micrographs of *C. glutamicum* wild type treated for 5 min with 10 µg/mL CCCP, followed by treatment with 4 µg/mL A37FL 15 min, and a positive control without CCCP treatment as well as an untreated control. Brightness and contrast of the A37FL channel were adjusted to the positive control. Scale bar, 2 µm. **(B)** Quantification of A37FL fluorescence intensities of individual cells. Violin plots show the distribution of individual cell data after exclusion of outliers. Line shows mean of three biologically independent experiments ± SD. Symbols show the mean of each individual biological experiment. n ≥ 108 cells per replicate and condition. **(C)** Quantification of the relative abundance of A37FL accumulation spots as mean spots per cell. Number of spots in n ≥ 108 cells per replicate and condition was counted and subtracted by the total number of cells. Bar graphs show the mean of three biologically independent experiments ± SD. Symbols show the mean of each individual biological experiment. RFU: Relative Fluorescence Unit. Statistical significance was determined using unpaired two-tailed students t-tests with a 95% confidence interval. Statistical significance was denoted as *, p = 0.05 to 0.01; **, p = 0.01 to 0.001; ***, p = 0.001 to 0.0001.

4.7.2. Investigating the role of intracellular accumulation in the mechanism of action of A37

To investigate the association of spot formation with antibiotic activity, binding of A37FL to cells of *C. glutamicum* wild type was compared to the lab-generated strain with 8-fold increased MIC *C. glutamicum* A37/8 (Figure 56). Despite the substantially decreased susceptibility in strain A37/8, no significant difference in the cytoplasmic concentration of A37FL was observed when both strains were treated with 4 µg/ml A37FL (4-fold wild type MIC, Figure 56A,B). However, a significant reduction in spot formation was apparent in cells of strain A37/8 (Figure 56A,C). Increasing the A37FL concentration to 32 µg/ml (i.e., adjusting for MIC to 4 x MIC of strain A37/8) resulted in spot formation of similar extent as observed for 4 µg/mL in the wild type strain (Figure 56A,C). Again, no significant difference in overall binding could be determined[11] (Figure 56B).

[11] Accordingly, dose dependent $DiSC_3(5)$ release was identical in both strains (see appendix 6), corroborating results shown above (see chapter 4.7.1).

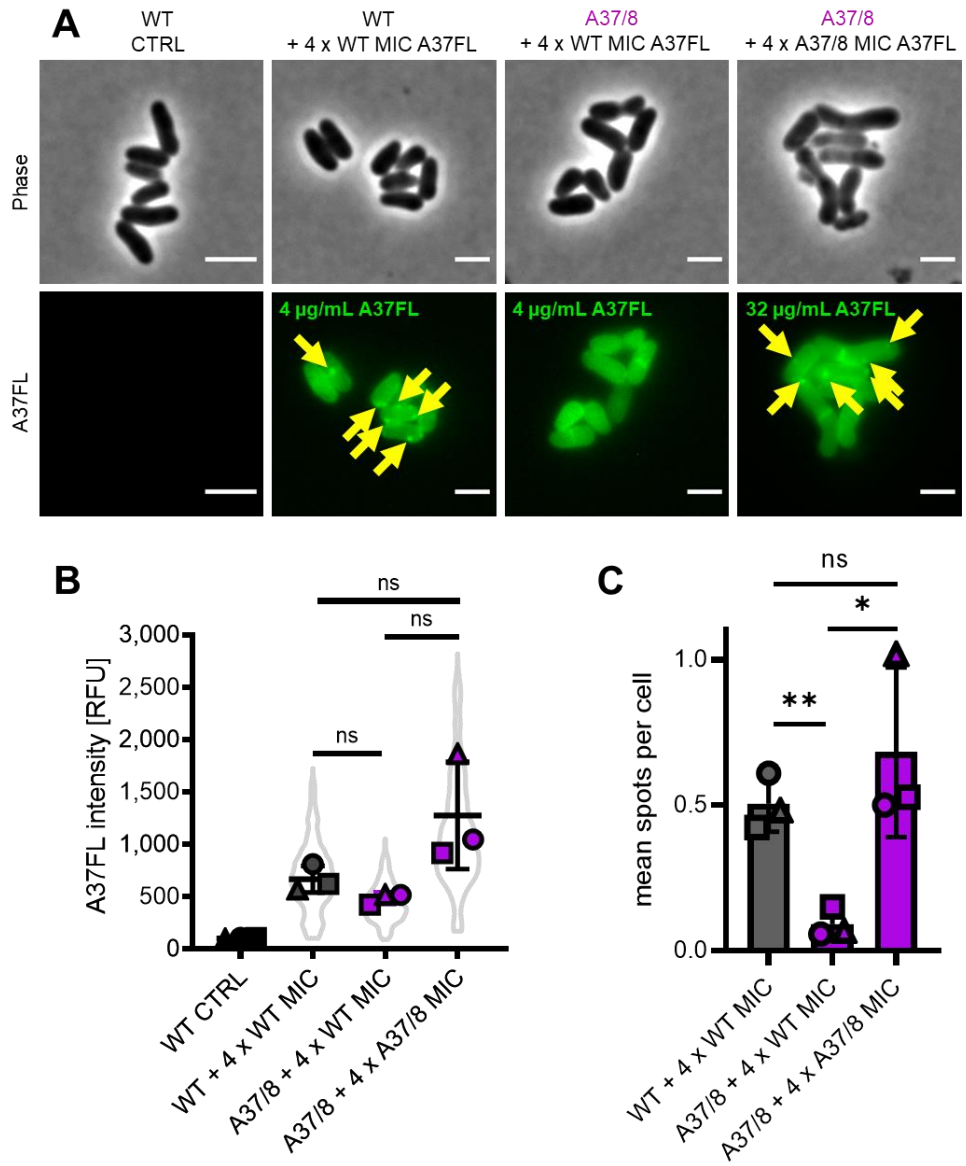

Figure 56: Formation of intracellular A37FL spots corresponds to antibacterial activity. (A) Representative micrographs of *C. glutamicum* wild type and *C. glutamicum* A37/8 treated with A37FL for 15 min and an untreated control. Left panel: untreated control. Middle panels: Cells of both strains treated with 4 µg/mL A37FL, corresponding to 4 x MIC of wild type and 0.5 x MIC of A37/8. Right panel: Cells of *C. glutamicum* A37/8 treated with 32 µg/mL A37FL, corresponding to 4 x MIC of the strain. Yellow arrows indicate A37FL accumulation spots. All images individually adjusted except for the negative control, which was adjusted to WT + 4 x WT MIC for clarity. Scale bar, 2 µm. **(B)** Quantification of A37FL fluorescence intensities of individual cells. Violin plots show the distribution of individual cell data after exclusion of outliers. Line shows mean of three biologically independent experiments ± SD. Symbols show the mean of each individual biological experiment. n ≥ 92 cells per replicate and condition. **(C)** Quantification of the relative abundance of A37FL accumulation spots as mean spots per cell. Number of spots in n ≥ 92 cells per replicate and condition. Per replicate, number of accumulation spots in all cells was determined and subtracted by the number of cells. Bar graphs show the mean of three biologically independent experiments ± SD. Symbols show the mean of each individual biological experiment. RFU: Relative Fluorescence Unit. Statistical significance was determined using unpaired two-tailed students t-tests with a 95% confidence interval. Statistical significance was denoted as ns, not significant, $p > 0.05$; *, $p = 0.05$ to 0.01; **, $p = 0.01$ to 0.001.

To characterize the A37 accumulation spots in detail, co-localization of A37FL with the membrane dye CellBrite Fix® 640 was visualized using Airyscan superresolution microscopy (Figure 57). This approach revealed the presence of intracellular lipophilic spots, which protruded from the cell membrane into the cytoplasm (Figure 57A). Strikingly, these spots strongly co-localized with the spots of accumulated A37FL (Figure 57B). This suggested that A37 leads to the formation of intracellular membrane vesicles, which are heavily loaded with the epilancin.

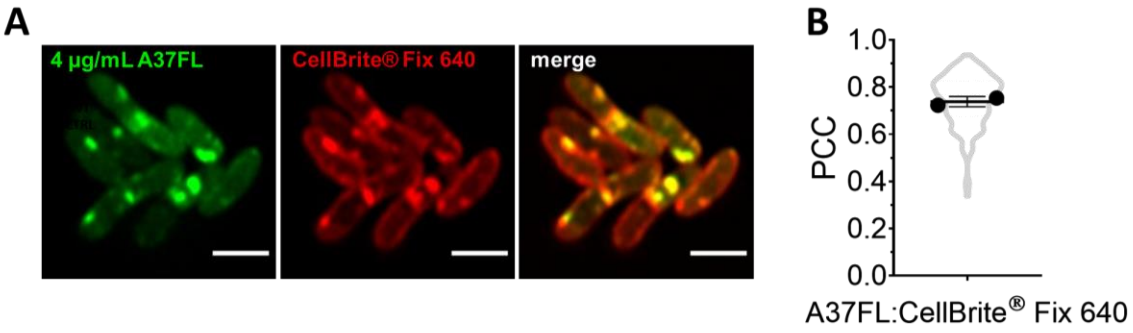

Figure 57: A37FL co-localizes with a membrane dye in intracellular lipophlic spots loaded with the fluorescently labelled epilancin. (A) Representative Airyscan super-resolution micrographs of *C. glutamicum* wild type treated with 4 µg/mL A37FL for 15 min and stained with the membrane dye CellBrite® Fix 640. Scale bar, 2 µm. Imaging by Dominik Brajtenbach. **(B)** Quantification of colocalization of A37FL fluorescence and CellBrite® Fix 640 fluorescence, determined as Pearson correlation coefficient (PCC) in individual cells. Violin plot shows the distribution of individual cell data. Black symbols show mean values of two independent biological experiments, bar shows their mean ± SD. n ≥ 42 cells per replicate.

To further elucidate details of spot formation by A37 and its consequences, native A37 and the bright and cell-penetrating dye nile red as membrane stain were used in the same microscopic setup (Figure 58). The high fluorescence intensity of nile red staining allowed for image deconvolution. The resulting increase in resolution unequivocally confirmed the nature of membrane vesicles (Figure 58A). Furthermore, z-stack acquisition allowed to study the impact on membrane geometry. The cell membrane displayed a negative curvature at locations were the vesicles protruded into the cytoplasm (Figure 58B). Notably, these effects were observed using conditions (4 x MIC and 15 min incubation time), that did not severely impair overall membrane integrity or potential (see chapter 4.7.1). In support with this, live-cell microscopy with nile red visualized vesicle formation within the first few minutes of A37 treatment (Figure 58C).

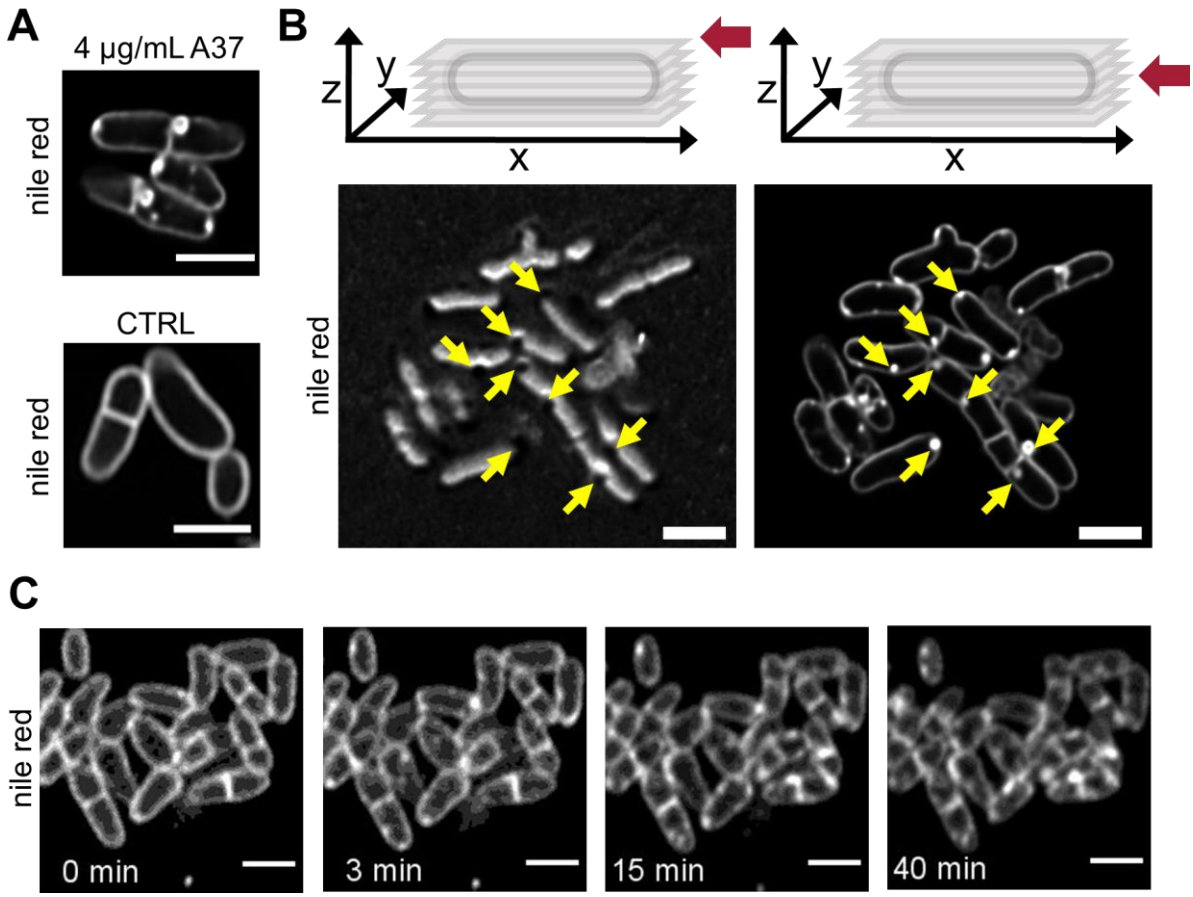

Figure 58: Vesicle formation by A37 deforms the cell membrane and occurs within minutes of treatment. **(A)** Representative deconvolved Airyscan super-resolution micrographs of *C. glutamicum* wild type treated with 4 µg/mL A37FL for 15 min and an untreated control, stained with the membrane dye nile red. Scale bar, 2 µm. **(B)** Deconvolved z-slices of *C. glutamicum* wild type treated with 4 µg/mL A37FL for 15 min and stained with nile red. Schemes above the images illustrate the z-positions. Yellow arrows indicate locations of intracellular vesicles and the corresponding membrane curvature. Representative Airyscan super-resolution micrographs. Scale bar, 2 µm. **(C)** Deconvolved micrographs of a time-series of *C. glutamicum* wild type treated with 4 µg/mL A37FL for 40 min and stained with nile red. Scale bar, 2 µm.

5. Discussion

5.1. Peptidoglycan synthesis inhibition is sufficient for total arrest of cell division in *S. aureus*

Given the rampant rise of antimicrobial resistance and the continuous deficit in new antibiotic classes reaching the market, innovation in research and development of antibiotics is critical to maintain the invaluable benefit, that antimicrobial chemotherapy provides for humanity (see chapter 1.1). To gain in-depth knowledge of how antibiotics work on a cellular level is fundamental for a comprehensive understanding of what makes antibiotics effective and how resistance develops. To contribute to this endeavor, a central aim of this work was to investigate the initial and most striking cellular impact of peptidoglycan synthesis (PGS) inhibiting antibiotics on cell wall biosynthesis machinery (CWBM, see chapter 1.3) and the closely coordinated cell division of *S. aureus* using state-of-the-art quantitative fluorescence microscopy. The gram-positive model organism *S. aureus* is the leading cause of infection-related deaths worldwide and the inability to treat methicillin-resistant *S. aureus* (MRSA) costs millions of human lives every year, which could be saved if effective antibiotic treatment were available (see chapter 1.1). The special concern of MRSA further increases the necessity for in-depth understanding of how PGS-targeting antibiotics, particularly beta-lactams and the reserve antibiotics like glycopeptides, act against this most problematic pathogen. Both beta-lactams and glycopeptides target the ultimate steps of PGS – transglycosylase (TGase) and transpeptidase (TPase) reactions – via different molecular mechanisms in highly specific fashion (see chapter 1.3), making them ideal candidates to elucidate the cellular impact of direct PGS inhibition.

5.1.1. Impact of vancomycin, telavancin and oxacillin on cell cycle and FtsZ localization pattern

Analysis of *S. aureus* cell cycle phase distribution showed that the glycopeptide vancomycin, the lipoglycopeptide telavancin and the beta-lactam oxacillin had significant impact on the cell cycle progress of *S. aureus* (see chapter 4.1.2). The shift in distribution towards cells in an early stage of cell division indicated that the CWBM-targeting antibiotics interfered with the progression of cell division. The effect of the antibiotics corresponds well with data from Salamaga *et al.* (2021), who visualized the impact of methicillin (another beta-lactam) and vancomycin on the *S. aureus* cell cycle using transmission electron microscopy (TEM). In line with the present work, they observed a decrease in cells with completed septum and an increase of cells without a septum. Additionally, they found a distinct septal plasmolysis after incubation with methicillin (see also chapters 5.1.5 and 5.1.9). Interestingly, while the data presented here and by Salamaga *et al* (2021). were generated using methicillin-sensitive *S. aureus* (MSSA) strains, oxacillin was reported to increase the abundance of cells in a late stage of septum constriction in the MRSA strain COL (Monteiro *et al.* 2018). This might be caused by secondary effects of the extremely high antibiotic concentrations needed to achieve MIC multiples of beta-lactams in MRSA and/or differences in the function of PBP1 in MSSA and MRSA (see chapter 5.1.8).

The indicated interference with cell division was confirmed by visualization of the core cell division protein FtsZ (see chapters 4.1.2 - 4.1.5). To this end, the here established method of condensing individual cell data into convolved average projections (CAPs, see chapter 4.1.2) proved to be a reliable tool for detection of significant changes in FtsZ localization caused by antibiotic treatment. Visualization of the condensed data in a 'cell-like' image further indicated changes towards larger Z-ring diameters, that are caused by antibiotic treatment. This was successfully verified via Airyscan superresolution microscopy, which revealed a drastic increase in cells with a large Z-ring diameter after treatment with vancomycin, telavancin or oxacillin. The fact, that state-of-the-art superresolution imaging of individual cells verified the indications provided by CAPs also confirmed the methods usability as a reliable indicator of localization patterns within whole sample populations.

Notably, no impact on Z-ring integrity was observed for vancomycin, telavancin or oxacillin. A range of antibacterial compounds are known to target FtsZ as integral part of their mechanism of action. By modulating the GTPase activity, diverse detrimental effects ranging from prevention of polymerization (Berberines, benzimidazoles, CCR-11; Adams *et al.* 2011; Awasthi *et al.* 2013; Boberek *et al.* 2010; Domadia *et al.* 2008; Park *et al.* 2014; Ray *et al.* 2015; P. Singh *et al.* 2012; N. Sun *et al.* 2014) or inhibition of treadmilling via hyperstabilization of polymers (PC190723, TXA709; Andreu *et al.* 2010; Elsen *et al.* 2012; Ferrer-González *et al.* 2017; Haydon *et al.* 2008; Kaul *et al.* 2015, 2016; D. Singh *et al.* 2014) to proteolytic degradation of FtsZ through hyperactivation of Clp proteases (ADEPs; B.-G. Lee *et al.* 2010; P. Sass *et al.* 2011; Conlon *et al.* 2013; Silber *et al.* 2020). Accordingly, targeting FtsZ is a promising approach for the development of new antibiotic classes, as the example of TXA709 shows, which is currently undergoing phase I clinical trials for treatment of *S. aureus* infections (WHO, 2022a, 2022b). In contrast to all these compounds, no evidence was found for a direct or indirect effect of vancomycin, telavancin and oxacillin towards Z-ring integrity. This is in line with earlier data for *S. aureus* (Monteiro *et al.* 2018) as well as for other species (Bisson-Filho *et al.* 2017; Whitley *et al.* 2021) which show that Z-ring integrity and treadmilling are maintained during treatment with beta-lactams. The data presented here provides further evidence, that the structural-functional integrity of the Z-ring is not severely disrupted by inhibition of PGS.

5.1.2. Antibiotic impact on Z-ring size dynamics and cell separation

The increased Z-ring sizes after antibiotic treatment suggested a massive impairment of cell division progress that was caused by the PGS-targeting antibiotics. This was further supported by the changes in cell cycle phase distribution (see chapter 5.1.1). To elucidate speed and extent of antibiotic impact, Z-ring dynamics over time were visualized using live-cell microscopy (see chapters 4.1.3 - 4.1.5). Analysis of Z-ring size dynamics at the individual cell level showed that vancomycin and telavancin rapidly arrested virtually all septum constriction (see chapter 4.1.4). This revealed an effective abolishment of the cell division progress caused by inhibition of PGS through substrate blocking. In contrast, oxacillin had a more intricate, cell-division-stage dependent effect (see chapter 4.1.5). The TPase inhibiting beta-lactam stopped cell division progress of cells in early-stage cell division. Meanwhile, the effect of oxacillin towards cells in mid- or late-stage cell division was not as drastic, as

the majority of these cells were still able to perform septum closure upon exposure. However, oxacillin still slowed down septum constriction speed considerably in these cells.

Interestingly, none of the antibiotics affected the splitting of cells in assembly state at the time of exposure, which suggests that divisome components responsible for daughter cell separation remain functional even with impaired PGS. This is in line with the results of the shift in cell cycle phase distribution shown above (see chapter 4.1.2). Interestingly, previous reports linked the TPase activity of PBP1 to cell separation events (S. F. F. Pereira *et al.* 2009; Reichmann *et al.* 2019), as an PBP1 active site mutation was observed to result in an increased number of cells with completed septum, that remained unseparated. Unfortunately, these observations were not quantified with respect to cell cycle phases. However, more recent, quantitative results from the same group in the identical strain background showe, that mutation of the PBP1 active site does not severely affect the abundance of cells with a completed septum (Schäper *et al.* 2023). Additionally, all these experiments were conducted in the MRSA strain COL. In this regard, a recent work demonstrated that the presence of the MRSA resistance cassette *mecA* confounds the role of PBP1 in *S. aureus* (Wacnik *et al.* 2022). The same work further establishes, that a loss of PBP1 TPase activity in MSSA has massive impact on septum formation, shape and progression, but not on cell separation. Since PGS inhibition via vancomycin, telavancin or oxacillin did not prevent cell splitting events, the present work corroborates that the TPase activity of PBP1 (or any PGS activity, for that matter) is indeed not essential for functioning cell separation in MSSA[12]. Currently, it remains unclear whether PGS inhibition would affect cell separation in MRSA.

5.1.3. Antibiotic impact on localization of key septal CWBM components

Localization of key CWBM components was analyzed after antibiotic treatment to evaluate the impact of the antibiotics on the organization of the septal CWBM machinery (see chapter 4.1.6). Remarkably, all of the proteins remained localized at the septum upon antibiotic treatment, with the notable exception of PBP2. Accordingly, localization patterns of all proteins (except PBP2 after oxacillin treatment, see chapter 5.1.4) followed that of FtsZ, with an increase in lateral CAP brightness corresponding to an increased septum diameter after antibiotic treatment. Apart from this expected effect, no confounding of the localization of RodA, FtsW, MurJ or PBP4 was observed. Strikingly, septal PBP2 localization was nearly completely lost after treatment with oxacillin. Vancomycin and telavancin had a more moderate impact, where a reduction of the abundance of cells with septal PBP2 was observed, but still a considerable fraction of cells with septal PBP2 was present in the samples. This revealed a crucial divergence in the cellular impact of the beta-lactam and the glycopeptides, that might explain the differences observed in the Z-ring dynamics (see above) and was therefore more thoroughly investigated by visualizing PBP2 dynamics using live-cell microscopy (discussed in chapter 5.1.4).

12 Note, that this only holds true for cells already in assembly phase at the time of exposure, where ultimate cell separation is imminent and not dependent on any penultimate septum closure, which is obstructed by PGS inhibition, as discussed above.

Apart from the special case of PBP2, these results illustrate the overall high degree of structural-functional integration of the CWBM into the divisome machinery and the robustness of its recruitment and localization mechanisms. As septal recruitment of MurJ is dependent on prior formation of the DivIB–DivIC–FtsL early divisome complex (Monteiro *et al.* 2018), the septal localization of MurJ suggests that divisome integrity is maintained during treatment with the antibiotics. This is further corroborated by the undisturbed localization of FtsW and RodA, which are known to localize to the septum from a very early stage of cell division site formation (Monteiro *et al.* 2018) and are also referred to as key early divisome components (Käshammer *et al.* 2023; Mohammadi *et al.* 2011; Monteiro *et al.* 2018; Perez *et al.* 2019; Pinho *et al.* 2013; Reichmann *et al.* 2019; Taguchi *et al.* 2019; Yang *et al.* 2021). These results further validate the observation, that antibiotic treatment did not impact Z-ring integrity (see chapter 5.1.1), which is dependent on an intact divisome (Baranova *et al.* 2020; Barrows *et al.* 2021; Bisson-Filho *et al.* 2017; Egan *et al.* 2017; Monteiro *et al.* 2018; Pazos *et al.* 2018; Pinho *et al.* 2013; Szwedziak *et al.* 2014; Whitley *et al.* 2021; Yang *et al.* 2017).

Recruitment of PBP4 to the septum is known to depend on a functional septal WTA biosynthesis (Atilano *et al.* 2010). Thus, the proteins septal localization upon antibiotic treatment indicates, that this important biosynthetic pathway is still functional and remains spatially integrated into cell division during treatment with glycopeptides or beta-lactams. This is relevant, as WTA are crucial for autolysis regulation and functional cell separation (see chapter 1.3, 5.1.9 - 5.1.10 and 5.3). Autolysin activity in turn is linked to the ultimate cell death of *S. aureus* following treatment with glycopeptides or beta-lactams, as deletion of specific autolysins significantly reduced antibiotic killing of methicillin (Atl) or vancomycin (SagB, Ledala *et al.* 2006; Salamaga *et al.* 2021). However, many questions concerning the role and regulation of autolysis during antibiotic treatment remain (see also chapter 5.1.9). The mechanisms, that are responsible for the disbalanced autolysis following PGS inhibition leading up to cell death, are not fully elucidated yet and is likely to involve complicated regulatory processes, e.g., phosphorylation activity and crosstalk of the two-component system WalKR and the Ser/Thr-kinase PknB (Dubrac *et al.* 2007; Hardt *et al.* 2017; Homma *et al.* 2016; Howden *et al.* 2011; Huemer *et al.* 2023; Ji *et al.* 2016; Ledala *et al.* 2006; McEvoy *et al.* 2013; Sharkey *et al.* 2023; S. Tan *et al.* 2022, see also chapter 5.1.6).

5.1.4. Antibiotic impact on PBP2 localization dynamics

The observed impact of the antibiotics on PBP2, especially oxacillin (see chapter 5.1.3), corroborates earlier results by Pinho *et al.* (2005), who described a loss of septal PBP2 localization after treatment of *S. aureus* with oxacillin or vancomycin. The authors also noted that some cells retained septal PBP2 localization after vancomycin treatment, which is in line with the results described in the present work. Unfortunately, no quantitative analysis of this was reported in that publication. However, the authors achieved to link this loss of localization to the activity of the PBP2 TPase site, showing that the TPase function of PBP2 plays an essential role in the protein's septal localization. This was concluded from the observation that blocking the TPase active site with oxacillin results in loss of septal PBP2 signal. However, it was not differentiated whether oxacillin delocalizes PBP2 from the septum or prevents accurate recruitment to the septum (Pinho *et al.* 2005).

To resolve this ambiguity as well as to find a coherent explanation for the differences between glycopeptide and beta-lactam action on PBP2 localization and Z-ring size dynamics (see chapters 5.1.1 - 5.1.5), PBP2 localization was visualized in live-cell timelapse microscopy (see chapters 4.1.7 and 4.1.8). The results clearly show that oxacillin massively disturbs the dynamics of PBP2 localization explicitly by inhibiting the recruitment of the main peptidoglycan synthase to the septum. Cells where oxacillin prevented septal PBP2 localization were unable to perform septum closure and cell separation. This distinctly demonstrates that septal PGS activity of PBP2 is crucial for the later stages of septum constriction and septum closure in *S. aureus*. This critical role of PBP2 for cell division is further validated by the observation, that all cells with septal PBP2 at the moment of exposure still proceeded to cell separation. Notably, oxacillin did not cause loss of PBP2 localization pattern in these cells. They only became trapped in the early cell division stage of the next cell cycle, as recruitment of PBP2 to the new septum became impossible due to oxacillin preventing the new septal recruitment. These results show that oxacillin inhibits the septal recruitment of PBP2, while having no qualitative effect on PBP2 already at the septum at the time of exposure. Thus, the TPase site is clearly crucial for PBP2 recruitment to the septum, but septal localization seems to be secured by a different mechanism (e.g., by protein-protein interactions with other divisome components, see Pinho *et al.* 2005; Reichmann *et al.* 2019; Steele *et al.* 2011; Wacnik *et al.* 2022). These results further explain the observation of Z-ring dynamics during oxacillin treatment shown above (see chapter 4.1.5). Oxacillin prevents septal recruitment of PBP2 specifically in early-stage cell division cells (with large Z-rings), which need to recruit the main peptidoglycan synthase in order to proceed in septum constriction. This is rendered impossible by binding of the beta-lactam to the TPase active site. In contrast, mid- and late-stage cells (with smaller Z-rings) already possess PBP2 at the septum upon exposure. These cells are still able to finalize one last round of cell division but are getting trapped in the subsequent early stage (by being unable to recruit PBP2 to the new division site). Thus, the targeted impairment of PBP2 septal recruitment by oxacillin is a sufficient cause of cell division arrest.

In contrast, the impact of glycopeptide activity on PBP2 localization is an emergent effect of the complete septum constriction stop, which is directly caused by the inhibition of PGS (see chapters 5.1.1 - 5.1.3). This complete arrest of septum constriction effectively “freezes” PBP2 localization dynamics[13] after a few minutes of treatment. Within these initial minutes, a few cells still perform a final cell separation event before subsequent cell cycle entrapment (see chapter 4.1.4 and 5.1.2). These first-minute effects corroborate the observations of Z-ring dynamics, where still effective cell splitting was observed (see chapter 5.1.2). This also explains the moderate reduction of septal PBP2 abundance (see chapters 4.1.6 and 5.1.3) on a temporal scale.

Interestingly, both vancomycin and telavancin significantly decreased the S/P ratio of PBP2, showing a quantitative impact of the antibiotic treatment on the septal focus of PBP2 localization. While this could be a technical artifact caused by the general increase in septum diameter (see chapter 4.1.2), it is also

[13] Note, that this refers only to the qualitative analysis of septal/aseptal PBP2 localization and is not a statement about dynamics of individual PBP2 molecules.

possible that the glycopeptides induce a PBP2 dislocation. Similar effects of antibiotic treatment have already been described numerous times for PBP2 (Pinho *et al.* 2005; Mann *et al.* 2013; S. Tan *et al.* 2019; Ferrer-González *et al.* 2021; Lu *et al.* 2023). Here, the effect may be caused by a reduction of recruitment signals due to masking of TPase substrates. In line with this, the lipid II depleting MurG inhibitor murgocil was observed to induce a similar reduction in septal PBP2 focus (Mann *et al.* 2013). Additionally, a loss of processive strand movement because of glycopeptides interfering with PGS strand synthesis could result in dislocation. A halting of processive PGS by vancomycin was recently observed for PBP1/FtsW. However, the authors did not describe a delocalizing impact resulting from this (Schäper *et al.* 2023). Alternatively, glycopeptides are known to induce massive accumulation of lipid II in the cell membrane (Qiao *et al.* 2017; Sidders *et al.* 2023), which may confound PBP2 and divert the protein into the periphery, especially as accumulated lipid II seems to be unbound by the glycopeptides for currently unknown reasons (personal communication Fabian Grein, unpublished data). Recent *in vitro* observations of the formation of a ternary vancomycin:lipidII:MurJ complex might explain this phenomenon (Ottonello *et al.* 2023, see also chapter 5.1.9). MurJ inhibition may cause accumulation of lipid II on the intracellular membrane leaflet, rendering the accumulated lipid II inaccessible for glycopeptides, which are not membrane permeable. Without further, detailed investigations, all this remains speculative. To elucidate the impact of glycopeptides on PBP2 localization more rigorously, the possibility of a technical limitation in the measurement of the PBP2 S/P ratio should be excluded, e.g., by repeating the experiment and analysis in a super-resolution setup, where fully closed septa are more easily distinguished. If the observation can be repeated in such a more precise setup, single molecule localization microscopy of PBP2 dynamics in different conditions of lipid II levels and PGS inhibition might shine light on the quantitative factors that influence for the protein's septal localization. Quantifying the impact of different lipid II-binding, lipid II-accumulating and lipid II-depleting antibiotics on PBP2 could help to further understand the mechanism governing localization of the main peptidoglycan synthase of *S. aureus* and its central role for antibiotic action. It would furthermore contribute to evaluate the role of precursor level modulation in antibiotic action (see also chapters 5.1.9 - 5.1.10).

5.1.5. The roles of PGS reactions and FtsZ treadmilling in septum constriction

The results presented in this work unequivocally demonstrate that inhibition of PGS in *S. aureus* has fast and drastic effects on cell division. The remarkable speed and extent, by which vancomycin, telavancin and oxacillin inhibit septum constriction and impair cell cycle progression reveals cell division interference as an essential part of these antibiotics' cellular action. The glycopeptides stopped all septum constriction within minutes of treatment, effectively trapping cells at the division stage they were in at the time of exposure. The rapid actualization of this effect constitutes a mechanism, where cell division arrest directly emerges from the glycopeptide's molecular mechanism of action, i.e., inhibition of both TGase and TPase reactions in PGS via substrate binding (Grein *et al.* 2019; Reynolds 1989). This is corroborated by the result, that no drastic effect on subcellular localization of key CWBM components or Z-ring integrity was observed, which could putatively indicate cell division impairment through an indirect effect (e.g. protein delocalization). The essentiality of PGS for septum constriction clearly demonstrates that FtsZ treadmilling alone cannot drive septum constriction without a functioning

PGS machinery. The treadmilling movement of FtsZ filaments has been discussed extensively and was proposed to act as driving force of septum constriction (Coltharp *et al.* 2016; Erickson *et al.* 2010; McQuillen *et al.* 2020; Nguyen *et al.* 2019, 2021; Osawa *et al.* 2013; Szwedziak *et al.* 2014). However, several studies have shown that FtsZ GTPase and therefore treadmilling function becomes nonessential for cell division after assembly of the septal peptidoglycan synthase complex (Bisson-Filho *et al.* 2017; Coltharp *et al.* 2016; Monteiro *et al.* 2018; Whitley *et al.* 2021; Yang *et al.* 2017). Concomitantly, a two-phase septum constriction model has been proposed for *S. aureus* (Monteiro *et al.* 2018, see chapter 1.3). In a first constriction phase, FtsZ treadmilling drives constriction up to the point of septal recruitment of the lipid II flippase MurJ. This enables septal lipid II translocation, which in turn recruits PBP2 to the septum. From this point onwards, PBP2 drives a second constriction phase via its peptidoglycan synthase activity.

The here presented observation of a complete stop of septum closure by glycopeptide antibiotics provides clear evidence that PGS is the essential driving force of septum constriction. Furthermore, the results of this work expand the abovementioned model as they demonstrate that PGS is essential not only in the second constriction phase, but throughout the entire process of cell division. This establishes PGS as the essential driving force of septum constriction in *S. aureus*. The essential SEDS-PBP pair FtsW/PBP1 (Reichmann *et al.* 2019) may drive septum constriction in the first phase, which is corroborated by recent findings that TPase activity of PBP1 is essential for cell division in *S. aureus* (Wacnik *et al.* 2022, see also chapters 5.1.2 and 5.1.8). Pre-print results from Schäper *et al.* (2023) expand on this by showing, that FtsW/PBP1 pairs perform processive septal PGS from the onset of *S. aureus* cell division. The authors also describe that the movement of this TGase/TPase cognate pair is independent of FtsZ-treadmilling and also argue that PGS drives septum constriction, thereby validating the results of this work in a complementary single-molecule-dynamics approach.

Importantly, the here presented conclusion of PGS driving septum constriction throughout cell division does not refute the clearly demonstrated essentiality of FtsZ treadmilling in the early phase of cell division in *S. aureus* (Monteiro *et al.* 2018). Instead, it is possible, that early stage of cell division depends on both factors to enable the initial septum constriction. Early cell division in *S. aureus* features the formation of thickened cell wall structure termed ‘piecrust’ (Lund *et al.* 2018; Santiago *et al.* 2018; Turner *et al.* 2010; Wacnik *et al.* 2022), which could reduce the inward driving force of PGS during that phase and make additional force from FtsZ treadmilling necessary. Beyond a direct participation in active septum constriction, FtsZ treadmilling is crucial for the structural-functional organization of the early divisome (Baranova *et al.* 2020; Barrows *et al.* 2021; Bisson-Filho *et al.* 2017; Monteiro *et al.* 2018; Whitley *et al.* 2021; Yang *et al.* 2017). Results from Monteiro *et al.* (2018) imply, that this is true up to the point of MurJ and subsequent PBP2 recruitment. This suggests a model, where treadmilling remains essential for providing the scaffolding function needed to proceed to full assembly of the septal CWBM, and not necessarily to provide an inward driving force.

Septum constriction was also massively disturbed by the beta-lactam antibiotic oxacillin. This consolidates the essential importance of functional PGS for cell division. In contrast to the glycopeptides, the effects of oxacillin were dependent on the cell division stage. Treatment led to a complete constriction stop only in cells in an early stage of cell division. Meanwhile, it slowed down septum constriction speed mid- and late-stage cells. This was shown to emerge from oxacillin preventing PBP2 recruitment to the septum, which revealed PBP2 as distinctly essential for the later stage of septum constriction and closure in *S. aureus* (see chapter 5.1.4). Interestingly, oxacillin also significantly slowed down the septum constriction speed of those cells, where PBP2 was already localized septally at the moment of exposure. This may indicate that TGase and TPase reactions both contribute to septum constriction. This is corroborated by pre-print results that show that septum constriction rate and FtsW/PBP1 processive movement velocity are significantly reduced upon loss of PBP1-TPase activity, either via beta-lactam inhibition or active site mutation (Schäper *et al.* 2023). Notably, these results along with the data presented here indicate, that TGase activity alone may be sufficient to drive septum constriction and is still occurring in situations of TPase inhibition/inactivation. This is further corroborated by the observation, that ^{14}C-GlcNAc is still incorporated into the *S. aureus* cell wall mesh during treatment with 10 x MIC methicillin (Salamaga *et al.* 2021), which shows that TGases remain active in conditions of TPase inhibition. The implications of TGase activity driving septum constriction alone during TPase inhibition are currently unclear. The impact of an inward driving force on an uncrosslinked septal cell wall structure might affect cellular integrity. Similarly, how such a build-up of unincorporated peptidoglycan strands would affect autolysis, cell wall and cell membrane integrity is still not fully understood. Oxacillin was observed to induce plasmolysis specifically at the septum, an effect that could be complemented by addition of vancomycin (Salamaga *et al.* 2021). It is possible that this relates to the accumulation of uncrosslinked peptidoglycan strands at the leading edge of septum constriction. Such an accumulation may induce critical disruption of the cell envelope, e.g., by direct physical impairment of cell wall/cell membrane integrity or by local deregulation of autolytic enzymes.

5.1.6. Loss of septal PknB localization during treatment with PGS-inhibiting antibiotics

Interestingly, both glycopeptides and oxacillin caused a substantial loss of septal PknB localization (see chapter 4.1.9). Importantly, this could not be exclusively attributed to the lipid II accumulation caused by the glycopeptides (see also chapter 5.1.4), as oxacillin also induced loss of septal PknB localization. It has been shown previously, that PknB localization depends on interaction of its PASTA domains with lipid II (Hardt *et al.* 2017). Furthermore, this interaction also governs activation of the Ser/Thr kinase function (Hardt *et al.* 2017; Kaur *et al.* 2019). Activity of PknB has been shown to be important for organization of cell division and autolysis regulation of *S. aureus*, which is likely caused by its phosphorylation of FtsZ filaments and elongation factors as well as crosstalk with the WalKR system (Hardt *et al.* 2017; Huemer *et al.* 2023; Sharkey *et al.* 2023). The latter is the critical expression control system for autolysis in *S. aureus* and an important resistance and virulence factor (Dubrac *et al.* 2007; Hardt *et al.* 2017; Homma *et al.* 2016; Howden *et al.* 2011; Huemer *et al.* 2023; Ji *et al.* 2016; Ledala *et al.* 2006; McEvoy *et al.* 2013; Sharkey *et al.* 2023; S. Tan *et al.* 2022). The loss of PknB localization upon antibiotic treatment suggests an effect on regulatory homeostasis in *S. aureus*. It is possible, that

la oss of localization corresponds with a loss of activity, as the activator molecule lipid II is most concentrated at the septum due to the septal location of the lipid II flippase MurJ (see chapters 4.1.6 and 5.1.3). Additionally, a loss of septal PknB localization may reduce phosphorylation activity on septally localized FtsZ, which may re-direct phosphorylation activity to cytoplasmically localized FtsZ molecules or even completely abolish FtsZ phosphorylation by PknB. While WalR is localized exclusively cytoplasmically and is likely to be less affected by a change in PknB localization, its close interaction partner WalK is also localized at the septum (Poupel *et al.* 2016), so there might be a loss of efficiency in the crosstalk between the systems. Since PknB is involved in tolerance and persistence phenomena (Huemer *et al.* 2023, see also chapter 5.1.10), the effect of antibiotics on its localization may be associated to the ultimate cause of cell death and the emergence of tolerance/persistence. However, this remains speculative. To understand the impact of the antibiotic-induced loss of septal PknB localization, the roles of the different PknB phosphorylation activities need to be determined and the effect of antibiotic treatment on its kinase action analyzed. This is also interesting with respect to MRSA, as inhibition of PknB was shown to increase beta-lactam activity against MRSA (Beltramini *et al.* 2009; Tamber *et al.* 2010).

5.1.7. Model of how PGS inhibition via vancomycin, telavancin and oxacillin impacts *S. aureus* cell division

Ultimately, the results of this work congregate to a following model of how the tested PGS-inhibiting antibiotics vancomycin, telavancin and oxacillin affect cell division (Figure 59). The glycopeptides inhibit TGase and TPase reactions of early divisome proteins (e.g., FtsW and PBP1, Monteiro *et al.* 2018; Reichmann *et al.* 2019; Schäper *et al.* 2023) by binding the reaction substrates, effectively stopping the first constriction phase. In contrast, oxacillin inhibits septal recruitment of PBP2 by TPase active site binding. The beta-lactam thereby prevents cells from transitioning to the second constriction phase, where PBP2 activity is essential for septum closure. Similar to the first phase, glycopeptides completely stop the second constriction phase by substrate blocking, preventing both PGS reactions catalyzed by PBP2. Oxacillin also considerably slows down the second constriction phase by TPase inhibition. This model identifies inhibition of cell division as key cellular effect of antibiotics targeting cell wall biosynthesis and provides a framework for further investigations of the cellular effects of CWBM targeting antibiotics.

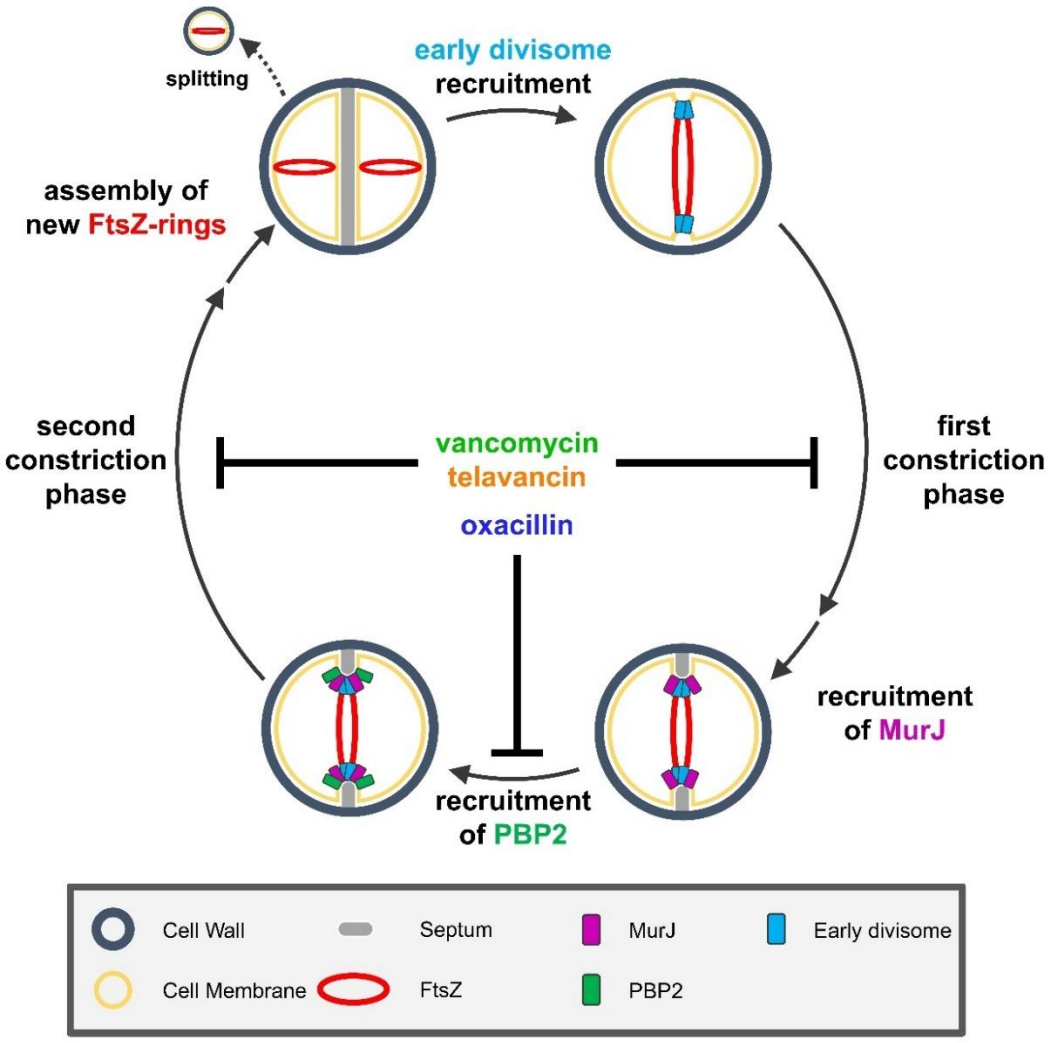

Figure 59: Model for cell cycle inhibition by the PGS-targeting antibiotics vancomycin, telavancin, and oxacillin.

5.1.8. Translation of the model to MRSA

Given the substantial differences in CWBM organization between MSSA and MRSA, it is desirable to evaluate how this model translates to MRSA. It has been shown previously, that PBP2a can functionally replace the TPase activity of PBP2 during antibiotic treatment (Pinho, De Lencastre *et al.* 2001; Pinho, Filipe *et al.* 2001). Accordingly, it has been suggested, that PBP2 and PBP2a form a TGase/TPase complex akin to the FtsW/PBP1 and RodA/PBP3 cognate pairs (Pinho, De Lencastre *et al.* 2001; Pinho, Filipe *et al.* 2001; Reichmann *et al.* 2019). How this impacts the enzymatic activity, localization principles and septal recruitment of PBP2 is currently unknown. If and how the septal recruitment of PBP2 during beta-lactam treatment is ensured in MRSA also remains to be investigated. Notably, it has been proven that the PBP2-TGase function becomes essential for survival in MRSA during beta-lactam treatment, while a loss of it can be compensated by other TGases under normal conditions (Pinho, De Lencastre *et al.* 2001; Pinho, Filipe *et al.* 2001). Thus, PBP2-TGase activity is clearly essential to beta-lactam resistance in MRSA, but not essential for growth, as long as other TGases are active. It is not clear, whether PBP2a-TPase activity directly depends on PBP2-TGase function and vice versa under conditions of beta-lactam treatment. The detrimental impact of TGase or TPase impairment on processive strand synthesis velocities of other TGase/TPase pairs suggest that this is the case (Bisson-Filho *et al.* 2017; Perez *et al.* 2019; Schäper *et al.* 2023; Whitley *et al.* 2021; Yang *et al.* 2021). Likewise, it is not known, if the PBP2-TGase function plays a role in securing the spatio-temporal organization of PBP2 and/or PBP2a in MRSA during beta-lactam treatment. Currently, the spatio-temporal and functional organization of PBP2a is almost entirely elusive. It is unknown, which mechanisms govern its septal recruitment and localization and how it is able to replace the different cellular roles of PBP2 (and also PBP1, see below) during beta-lactam treatment. It has been suggested that PBP2a maturation takes place in fluid membrane microdomains (FMMs), as it is part of the FMM protein cargo alongside the chaperone PrsA, which required for correct folding of PBP2a (García-Fernández *et al.* 2017; Koch *et al.* 2017). Accordingly, it has been demonstrated that beta-lactam resistance of MRSA depends on FMM integrity (García-Fernández *et al.* 2017). The same work also found PBP2 and RodA to be FMM cargo, which indicates a potential scaffolding role of FMMs in mediating an interaction of PBP2a with PBP2. Elucidating how PBP2a gets recruited from FMMs to the septum, and how its incorporation into the divisome/CWBM megamachinery is facilitated thus promises an important advance in understanding the cellular processes underlying MRSA resistance. In this regard, elucidating the relevance of FMMs for PBP2 (and also RodA) localization in both MRSA and in MSSA may be insightful as well.

Furthermore, the fact that PBP1-TPase activity is crucial during early-stage cell division (see chapters 5.1.4 and 5.1.7) implies, that PBP2a can replace the enzymatic activity of PBP1 during beta-lactam treatment to maintain essential TPase activity during that stage. However, if and how PBP2a is able to replace PBP1-TPase function and whether it therefore structurally interacts with the FtsW/PBP1 complex is unknown. Alternatively, MRSA could circumvent the essential role of PBP1-TPase by other, currently elusive means. The observation, that the cellular role of PBP1 is substantially altered in MRSA, rendering its TPase non-essential for survival, supports such a model (Wacnik *et al.* 2022). Additionally, for reasons not fully understood, structural presence of PBP1 is essential for *S. aureus* divisome

formation and cell division site selection, which remains so in MRSA (S. F. F. Pereira *et al.* 2007, 2009; Pinho, De Lencastre *et al.* 2001; Pinho, Filipe *et al.* 2001; Wacnik *et al.* 2022). Due to these many open questions, an in-depth characterization of the cellular roles of PBP1 in MRSA seems to be a prerequisite for detailed understanding of how PGS and cell division are coordinated in MRSA specifically.

Additionally, it has been established that PBP4 plays an important role in MRSA beta-lactam resistance. The non-essential TPase has its main role in secondary crosslinking, and loss of the gene has no impact on growth or cell shape of *S. aureus*, including MRSA (Gautam *et al.* 2015; Łęski *et al.* 2005; Lund *et al.* 2018; Monteiro *et al.* 2015, see chapter 1.3). However, deletion of the PBP4 gene *pbpD* (the gene encoding PBP4) caused a 16-fold reduction in beta-lactam MICs in some MRSA (Memmi *et al.* 2008). Reciprocally, upregulation of *pbpD* was observed to cause an increase in beta-lactam resistance and peptidoglycan cross-linking (Alexander *et al.* 2018; L. C. Chan *et al.* 2016; Hamilton *et al.* 2017; Henze *et al.* 1995, 1996; Lahiri *et al.* 2016). Notably, overproduction of PBP4 was shown to enable beta-lactam resistance of MRSA against the only two clinically used PBP2a-inhibiting beta-lactams ceftaroline and ceftobiprole[14] (Alexander *et al.* 2018; L. C. Chan *et al.* 2016; Hamilton *et al.* 2017; Lahiri *et al.* 2016), which further exemplifies the importance of PBP4 in MRSA. Why PBP4 is so relevant for beta-lactam resistance is currently not fully understood. A “cooperative-action” model has been proposed, which states that beta-lactam resistance relies on the cumulative activity of PBP2a and either PBP2 or PBP4 TPase activity for sufficient crosslinking (Farha *et al.* 2013; M. A. Hill *et al.* 2019; Reed *et al.* 2015). Thus, it might be possible that the cellular roles of PBP4 are modulated in MRSA to provide the necessary crosslinking at the correct location upon loss of PBP1-3 TPase activity during beta-lactam treatment.

These examples illustrate, how much fundamental knowledge about the mechanisms governing CWBM structure and function in MRSA is still missing. Consequently, investigation of the spatio-temporal organization of MRSA CWBM during treatment with PGS-targeting antibiotics (especially beta-lactams) promises to reveal key factors of MRSA resistance. This could be achieved using a methodology akin to that described in this work, given the availability of fluorescently labelled proteins in a MRSA strain. Beyond that, analyzing the impact of antibiotics and MRSA re-sensitization compounds on the CWBM organization could yield insights into the principles that govern their impact. This may help to identify new avenues to re-sensitize MRSA by disrupting the mechanism of MRSA CWBM organization. Disruption of septal PBP4 recruitment, either by inhibition of WTA biosynthesis (Farha *et al.* 2013) or by WTA blocking (Foxley *et al.* 2017; M. A. Hill *et al.* 2019), was previously shown to significantly increase beta-lactam activity against MRSA. Similarly, triggering FMM disassembly via inhibition of staphyloxanthin biosynthesis (through treatment with statins) led to a substantial improvement of MRSA beta-lactam treatment results in a mouse infection model (García-Fernández *et al.* 2017). These examples illustrate the potential of targeting MRSA resistance mechanisms on a cellular level, based on an in-depth understanding of the structural-functional organization of the MRSA CWBM.

[14] Mutations in the active site cleft of PBP4 were shown to contribute to this type of PBP4-governed resistance (Alexander *et al.* 2018; L. C. Chan *et al.* 2016; Greninger *et al.* 2016; Hamilton *et al.* 2017).

5.1.9. Translation of the model to other CWBM-targeting antibiotics

The results of this work present cell division arrest as a key cellular effect, that is integral to CWBM-targeting antibiotics. To this end, this has been experimentally shown by using vancomycin, telavancin and oxacillin, that target the final steps of PGS.

Lipid II-binding Glycopeptides

Both glycopeptides had a nearly identical impact in all experiments, and the increased affinity of telavancin towards lipid II did not significantly change the nature of the cellular effects. It is likely, that the complete stop of all septum constriction is a general cellular effect of lipid II-binding glycopeptides, since they all share their primary molecular mechanism of action and target. However, additional effects might influence the cellular consequences of glycopeptide treatment, such as membrane depolarization and lytic activity of lipoglycopeptides at higher concentrations (see chapter 5.2.1). Additionally, recent works describe the formation of ternary glycopeptide:lipidII:MurJ complexes, which forms with vancomycin, but not with synthetically bullvalene-linked vancomycin-dimers (Bolla *et al.* 2018; Ottonello *et al.* 2023). It is possible, that these and potentially other glycopeptides, that differ in the formation of such complexes, deviate from the cellular effects described here. Similarly, it has been previously suggested, that lipoglycopeptides may interact not only with lipid II, but also TGases. This could imply a formation of ternary glycopeptide:lipidII:TGase complexes or a dual mode of action directed at lipid II and TGases individually (Chen *et al.* 2003; Leimkuhler *et al.* 2005). Unfortunately, there is no *in vivo* evidence of the formation of any ternary complexes, so it is hard to estimate their role in glycopeptide activity.

Beta-lactams

Importantly, the effect of oxacillin was closely linked to inhibition of PBP2. Within the large group of beta-lactams, the affinities towards the four PBPs of *S. aureus* were reported to differ substantially between individual compounds (Dargis *et al.* 1994; Farha *et al.* 2013; Ferrer-González *et al.* 2017; Georgopapadakou *et al.* 1982, 1980; Wacnik *et al.* 2022). It is possible, that these differences modulate the impact on cell division. E.g., the beta-lactams imipenem or meropenem (with high reported specificity towards PBP1) might have a more drastic impact on the early stage of cell division, where the TPase activity of PBP1 was recently shown to be essential for correct septum placement (Wacnik *et al.* 2022). Similarly, cefoxitin (with high reported specificity towards PBP4) might have less effect on septum closure and cell division, but instead may cause aberrations in PBP4 localization or activity. Investigating the differential impact of beta-lactams on the CWBM and cell division of *S. aureus* promises a deeper understanding of both beta-lactam action and the roles of PBPs within growth and division of *S. aureus*, as the results of this work illustrate. Notably, it is likely, that such phenomena would be highly concentration-dependent, as they would emerge from differences in affinity, not absolute distinctions in molecular targets. Thus, a comprehensive elucidation of the differences in beta-lactam affinities towards the *S. aureus* PBPs is a prerequisite for comparing the specificities of their cellular effects. Additionally, it would be beneficial to visualize the full set of *S. aureus* PBPs to be able to quantify the impact of the

beta-lactams towards each PBP. It has recently been shown that beta-lactam treatment does not necessarily cause PBP delocalization but instead slows down processive strand synthesis velocity (Schäper *et al.* 2023, see also chapter 5.1.5). Accordingly, single molecule localization microscopy of PBPs would contribute substantially to the task of understanding the translation from molecular TPase inhibition to the emerging cellular effects.

Antibiotics targeting intracellular steps

A variety of antibiotics are known to target intracellular steps of the CWBM (see chapter 1.3), ranging from inhibition of soluble precursor synthesis by fosfomycin (inhibiting MurA, Kahan *et al.* 1974; Mengin-Lecreulx *et al.* 1990) or D-Cylcoserine (inhibiting DdlA and Alr, Lambert *et al.* 1972; Neuhaus *et al.* 1964) to blocking of MraY by nucleoside antibiotics (Campbell *et al.* 2011; Nakaya *et al.* 2022) and MurG by murgocil (Mann *et al.* 2013). It has been shown that inhibition of these earlier steps in CWBM leads to lipid II depletion (W. Lee *et al.* 2016; Y. Sun *et al.* 2023). The results of this work strongly suggest that this results in cell division arrest due to a loss of PGS substrate. Beyond that, numerous differences could lead to considerable divergence in cellular effects. Additionally, accumulation of different sets of soluble precursors may have variable impact WTA biosynthesis, which plays a central role in regulating autolysis and cell separation of *S. aureus* as well as in septal recruitment of PBP4 (see also chapters 5.1.3 and 5.1.8). E.g., inhibition of MurA by fosfomycin likely increases UDP-GlcNAc and $C_{55}P$ levels, which also constitute key substrates for WTA biosynthesis. In contrast, an inhibition of MurG by murgocil could induce an accumulation of lipid I, thereby depleting the precursor pool for WTA biosynthesis. Dual-targeting antibiotics like tunicamycin, which inhibits both MraY in cell wall biosynthesis and TarO in WTA biosynthesis, could exert even more complex effects (see also below). This illustrates, that effects of the different antibiotics on cell metabolism and precursor levels of CWBM and WTA biosynthesis need to be quantitatively analyzed and contextualized with their cellular effects. Understanding this could also reveal new weak points in the cellular response to these antibiotics and point towards new avenues for antibiotic action.

Other lipid II-binding antibiotics

In addition to glycopeptides, a diverse set of antibiotics bind to lipid II via a variety of interaction modes (see chapter 1.3). Many of these compounds interact with the pyrophosphate (PPi) moiety of the ultimate PGS precursor. Despite the high diversity of interaction mechanisms, all these antibiotics have in common, that they do not specifically interact with transglycosylated peptidoglycan, as their target moiety is not present after cleavage of the $C_{55}PP$ carrier lipid (see chapter 1.3). In this regard, PPi-interacting antibiotics differ from the D-Ala-D-Ala-interacting glycopeptides. Thus, PPi-interacting antibiotics inhibit PGS by TGase substrate blocking, with only indirect downstream impact on TPase activity caused by the depletion of newly polymerized glycan strands. How this affects the movement of TGase/TPase pairs, septum constriction speed and cell division is currently unknown. The model presented above indicates, that both TGase and TPase activity contribute to effective septum constriction (see chapter 5.1.5). However, it is hard to imagine, how TPase activity alone would drive the processive movement of a PGS synthase complex without prior TGase activity, which suggests that

glycan polymerization primarily drives the movement of peptidoglycan synthase complexes and thus septum constriction. In such a model, subsequent TPase activity would contribute to the efficient movement of the complex by preventing the build-up of uncrosslinked glycan strands. Investigating if PPi-binding antibiotics completely inhibit septum constriction and processive PGS synthase movement could help resolve this uncertainty.

Importantly, many of the compounds binding to the PPi moiety of lipid II also interact with other PPi-containing lipids, especially the carrier lipid C_{55}PP and the WTA precursor lipid III_{WTA} (C_{55}PP-GlcNAc, see chapter 1.3). The ability to bind different varieties of these lipids as well as affinities towards the different targets differ substantially between the compounds. This implies drastically different effects on the biosynthetic capacities of the affected pathways, especially as the inhibited reactions and substrate accumulation/depletion effects are likely to shift the balances in the shared precursor pools in compound-specific ways. How such effects impact antibiotic activity is still not well understood. It is likely, that additional targets modulate and improve the antibiotic effect of these compounds (Grein *et al.* 2020; Homma *et al.* 2016; W. Lee *et al.* 2016; Ling *et al.* 2015; Reithuber *et al.* 2021; K. Scherer *et al.* 2013; S. Tan *et al.* 2019; Wirtz *et al.* 2021). Comparing the cellular effects of different PPi-binding antibiotics, glycopeptides and other compounds interacting with lipid II could elucidate the role of multi-precursor targeting. To this end, the specific C_{55}PP binder bacitracin (Economou *et al.* 2013; Piepenbreier *et al.* 2019; Stone *et al.* 1971) and the specific C_{55}P binder friulimicin (T. Schneider *et al.* 2009) might prove to be useful tools to understand the impact of carrier lipid blocking on CWBM integrity and cell division. The lipid II depleting effect of bacitracin (Economou *et al.* 2013; W. Lee *et al.* 2016; Piepenbreier *et al.* 2019; Santiago *et al.* 2018) suggests a notable effect on septum constriction, based on the results of this work (see chapter 5.1.5). The low MICs, slow resistance development and promising mouse infection model activity of the recently described lipopeptide cilagicin (Z. Wang *et al.* 2022), which binds to both C_{55}P and C_{55}PP in highly specific manner, further illustrates the potential for antibiotics targeting the carrier lipid pool. Exploring the cellular effects of such antibiotics might help to improve the activity and effectiveness of other multi-targeting compounds, e.g., by optimizing the binding-behaviour of PPi-interacting compounds towards their putative targets in a rational manner. The effects of these different qualitative and quantitative effects on precursor pool levels in PGS and WTA biosynthesis pathways are key to comprehensively understand the antibiotic activity of these compounds. This is especially true given the importance of these pathways in cell division, autolysis, ultimate cause of cell death and tolerance/persistence development (see chapter 5.1.10).

Currently, it is not well understood how CWBM inhibition affects the amount of WTA precursors produced and the amount of WTA incorporated into the cell wall. It has recently been shown that gram-negative bacteria regulate allocation of UDP-GlcNAc between lipopolysaccharide biosynthesis and CWBM by a direct interaction of the committing enzymes LpxC and MurA (Hummels *et al.* 2023). Whether a similar mechanism regulates the expenditure of UDP-GlcNAc and C_{55}P for the two central biosynthetic pathways of CWBM and WTA biosynthesis is currently unknown and central to the question, how inhibition of either systems affects activity of the other. This open question is critical for a comprehensive understanding of antibiotic action, given the drastic cellular effects of CWBM inhibition

described in the present work and the key role of WTAs in governing cell separation and autolysis as well as spatio-temporal organization of CWBM components such as PBP4. A recent pre-print by Marmont *et al.* (2023) describes product inhibition of *Pseudomonas aeruginosa* MraY by excess lipid II, which suggests a model where coordination of cell wall and WTA biosynthesis is based on ultimate precursor availability (Marmont *et al.* 2023). However, this remains to be conclusively elucidated. Interfering with these processes might reveal new possibilities of antibiotic action, in a rationale informed by the understanding of how precursor pool levels and regulating principles govern the functionality of various vital systems of bacteria such as CWBM and autolysis.

To understand the relevance of WTA precursor interaction, the cellular effects of WTA biosynthesis inhibitors like targocil could be investigated. It has already been observed, that inhibition of WTA biosynthesis via targocil or tunicamycin interferes with cell separation (Hammond *et al.* 2022), which has been linked to the key role of WTA in the regulation of autolytic activity (see also chapter 5.3). It has been shown that newly formed WTA at the septum interacts with the main *S. aureus* autolysin Atl, thereby tethering its activity to the septal plane. In contrast, D-alanylated WTA in the matured cell wall reduces binding of Atl, which prevents autolysis of matured peptidoglycan (Büttner *et al.* 2014; Economou *et al.* 2013; Nega *et al.* 2020; Reichmann *et al.* 2013; Schlag *et al.* 2010; Turner *et al.* 2010; Z. Wang *et al.* 2022). As numerous PPi-binding antibiotics with lipid III_{WTA} binding capabilities were shown to induce substantial lysis (Homma *et al.* 2016; W. Lee *et al.* 2016; Ling *et al.* 2015; Reithuber *et al.* 2021; Shukla *et al.* 2022; Shukla *et al.* 2023; Wirtz *et al.* 2021), it may be possible that while singular WTA biosynthesis inhibition blocks autolytic activity, combinational inhibition of both CWBM and WTA biosynthesis in turn induces lytic activity. If and how this is established could be investigated by combining WTA and CWBM inhibiting antibiotics. In line with this hypothesis, it has been shown that high concentrations of tunicamycin, which inhibits both CWBM and WTA biosynthesis (Campbell *et al.* 2011; Hammond *et al.* 2022; Nakaya *et al.* 2022), lead to lysis of *S. aureus* (Homma *et al.* 2016; Zhu *et al.* 2018), while exclusive WTA biosynthesis inhibition via targocil reduces autolysis significantly (Campbell *et al.* 2012; Tiwari *et al.* 2018)[15]. Corroborating with this hypothesis, the lipid II and lipid III_{WTA} binding antibiotic teixobactin was shown to induce Atl-dependent lysis (Homma *et al.* 2016). Interestingly, the recently described clovibactin was reported to induce even stronger lysis, but in an Atl-independent mechanism not fully understood to date (Shukla *et al.* 2023). How this substantial difference is achieved despite the high similarity to teixobactin in structure and targets is unclear.

Oxacillin was also shown to induce Atl-dependent lysis, an effect that was complemented by the autolysis-inhibiting antibiotic complestatin, which binds to matured peptidoglycan (Cul *et al.* 2020, Salamaga *et al.* 2021). In a similar fashion, complestatin and the related compound corbomycin (Culp *et al.* 2020) could be used in future studies as tools to understand the relation between CWBM inhibition, WTA biosynthesis inhibition and lytic activity of PPi-binding antibiotics. Beyond that, only little is known

[15] The fact, that WTA biosynthesis inhibition via tunicamycin re-senzitizes MRSA to beta-lactams (Campbell *et al.* 2011) further adds to the importance of this. To date, this effect is not fully understood, however, PBP4 dislocation (see chapters 5.1.3 and 5.1.8) may contribute to it.

about how these two only recently described compounds kill bacteria and what cellular effects emerge from their unique molecular mechanism of action (Culp *et al.* 2020). This could be investigated by applying the methodology described in this work. Investigating clovibactins lytic activity with the same methodology could help elucidating the interesting particularities of its lysis induction. Furthermore, understanding how lysis is induced by CWBM-targeting antibiotics could reveal new approaches for antibiotic action via lysis induction and help to improve antibiotic activity and prevent persistence/tolerance formation (see chapter 5.1.10). The way by which these antibiotics interfere with autolysis seems to connect a key finding of the present work (that is cell division arrest as a key and immediate cellular effect) with ultimate cellular death.

5.1.10. Contribution of antibiotic-induced cell division arrest to tolerance/persistence development

Current models propose that PGS-inhibiting antibiotics ultimately kill cells by inducing a lethal malfunctioning in the homeostasis between PGS and cellular growth/autolysis regulation, while other cellular processes continue to function. At last, this decoupling results in lysis due to turgor pressure, cell swelling or substrate expenditure (Z. Yao *et al.* 2012; Cho *et al.* 2014; Homma *et al.* 2016; Wong *et al.* 2021; Lobritz *et al.* 2022). In line with this, it was recently observed that either PGS inhibition (and thus too much lytic activity) or a loss of lytic activity (and thus a loss of functional cell division) kills *S. aureus*, but an inhibition of both rescues cell viability (Salamaga *et al.* 2021). Other theories focus more on the production of reactive oxygen species during antibiotic treatment, claiming that ultimate cell death is caused by a failure to mitigate the accumulation of toxic byproducts of a deregulated metabolism (Kohanski *et al.* 2007, 2008, 2010; Z. Yao *et al.* 2012; Wong *et al.* 2022; Kawai *et al.* 2023). It is likely that a synthesis of both ideas comes closest to the complexity of describing actual cell death causes. Either way, ultimate cell death seems to not only depend on the failure to construct a functional cell wall but additionally relies on de-regulated autolytic and/or metabolic systems (Baquero *et al.* 2021; Cho *et al.* 2014; Kawai *et al.* 2019, 2023; Lopatkin *et al.* 2019; Salamaga *et al.* 2021; Stokes *et al.* 2019; Zheng *et al.* 2020, 2022). Accordingly, *per se* susceptible cells can become tolerant to antibiotic treatment, if metabolism and/or cellular growth is shut down, (Conlon *et al.* 2016; Huemer *et al.* 2020, 2021, 2023; Shan *et al.* 2017; Y. Wang *et al.* 2018; Zheng *et al.* 2020). Adaptions of autolysis rate have also been described, e.g., teixobactin treatment significantly decreases Atl expression in a cellular response to the lysis mediated by the autolysin (Homma *et al.* 2016). Examples like this illustrate, that bacterial cellular systems can identify and adapt to the mechanisms that eventually cause ultimate cell death during antibiotic treatment. The phenomenon of persistence arises, when some of the treated cells succeed in such an attempt to prevent killing, giving rise to a tolerant subpopulation (Balaban *et al.* 2019; Conlon *et al.* 2016; Huemer *et al.* 2021, 2023; Y. Wang *et al.* 2018; Zheng *et al.* 2022). Fully tolerant populations emerge, if all cells gain the ability to survive prolonged antibiotic treatment, often via mutational or environmental induction of a general growth restriction (Fridman *et al.* 2014; Haaber *et al.* 2015; Huemer *et al.* 2020; Ledger *et al.* 2022; Ronneau *et al.* 2021; Zheng *et al.* 2022). Tolerance and persistence are critical for clinical treatment, as they emerge during treatment from antibiotic susceptible genotypes, are therefore hard to detect and can cause life-threatening, difficult to treat infections (Dombrowski *et al.*

2008; Huemer *et al.* 2020; Kuehl *et al.* 2020; Westblade *et al.* 2020). Furthermore, they foster resistance development (Levin-Reisman *et al.* 2017; J. Liu *et al.* 2020; Windels *et al.* 2019) and thus play an important role in the effort to sustain effective antibiotic chemotherapy.

Antibiotics that are weakly dependent on an active metabolism are already known to be less prone to induce tolerance development, while antibiotics with high dependence on metabolism – like beta-lactams – lead to the fast evolution of tolerant subpopulations (Zheng *et al.* 2020, 2022). Effectively, the cellular effects of antibiotics and the ultimate causes of cellular death dictate, if and how tolerance/persistence can develop. This demonstrates, how critical an understanding of these effects is for rational antibiotic strategies. The results presented in this work contribute to this. The impact, vancomycin, telavancin and oxacillin have on cell cycle dynamics (and the behaviour of proteins) reveals a shutdown of cell cycle progression, which is caused by a PGS-inhibition induced arrest of septum constriction. However, the structural-functional integrity of the vital machineries of cell wall biosynthesis and cell division stayed largely intact, and no indication of significant complex disintegration of CWBM or divisome were found (see chapter 5.1.3). This may contribute to the development of cellular tolerance. It is likely, that cells can adapt to the enforced growth arrest by reducing metabolism and autolysis regulation more easily, when there is only little structural damage to biosynthetic machineries (and other vital systems). Combining beta-lactams with other, less metabolism-dependent antibiotics was observed to prevent evolution of tolerance in *E. coli* and *S. aureus* (Lázár *et al.* 2022; Zheng *et al.* 2020). E.g., combinations with the rapidly membrane-destructive daptomycin (Grein *et al.* 2020; Müller *et al.* 2016) were shown to prevent and break metabolism-dependent antibiotic persistence (Lázár *et al.* 2022; Mascio *et al.* 2007). Other membrane-targeting antibiotics could have similar beneficial impacts. The results of this work suggest that additional targeting of the integrity of divisome and/or CWBM may also contribute to the prevention of cellular tolerance development by increasing the antibiotic burden on the arrested cells beyond PGS inhibition. In this regard, synergistic effects[16] of combinations of FtsZ-targeting compounds and PGS inhibiting antibiotics have been described (Z. Fang *et al.* 2018; Ferrer-González *et al.* 2017, 2021; X. Lu *et al.* 2023), and are thus promising candidates to also reduce tolerance development. This might also apply to the dual targeting of CWBM and WTA biosynthesis and the use of autolysis-inducing antibiotic compounds (see chapter 5.1.9). Determining the effect of dual-targeting antibiotics such as teixobactin on persistence formation would help to answer this question. The apparent drastic and Atl-independent lysis induced by clovibactin (Shukla *et al.* 2023) could prove very favorable to this end. Combining the PGS-inhibiting potency of beta-lactams or glycopeptides with compounds to prevent persister formation might harbor great potential to improve clinical treatment outcomes. Persister formation might be effectively hampered by interfering with CWBM/divisome megamachinery organization (e.g., FtsZ-Inhibitors) or increasing autolytic activity (e.g., clovibactin) in addition to PGS inhibition.

[16] Importantly, evolution of tolerance/persistence does not substantially alter the MIC, but significantly increases the cells surviving during antibiotic treatment, which then can re-grow after antibiotic treatment has ended (Balaban *et al.* 2019). Therefore, combinations of antibiotics that do not act synergistically in a classical sense might still significantly decrease persistence development (Lázár *et al.* 2022; Zheng *et al.* 2022).

5.2. Inhibitory concentrations of different lipid II-binding antibiotics show no membrane depolarizing activity

5.2.1. Telavancin

Telavancin was previously reported to disrupt membrane potential and permeability of *S. aureus*. This was suggested to be part of a multi-targeting mechanism of action, that involves both PGS inhibition and membrane disruption (Higgins *et al.* 2005; Lunde *et al.* 2009). Notably, severe disruption of the transmembrane potential and integrity is known to lead to Z-ring disintegration, as the loss of respiratory activity decreases the amount of GTP substrate available to sustain the GTPase-dependent FtsZ filamentation (Strahl *et al.* 2010). However, in the present work, no effect of telavancin on Z-ring integrity was observed (see chapters 4.1.4 and 5.1). Therefore, the putative impact of telavancin on the transmembrane potential of *S. aureus* was quantified and related to the observed arrest of cell division (see chapter 4.2.1). To this end, release of the cationic, auto-quenching dye $DiSC_3(5)$ from cultures of *S. aureus* was measured. Furthermore, influx of the anionic fluorophore $DiBAC_3(4)$ into individual cells was quantified and compared with FtsZ localization. As expected, $DiBAC_4(3)$ influx corresponded with Z-ring disintegration, which was shown using the rapidly pore-forming, lipid II-binding lantibiotic nisin. However, no effect of telavancin treatment on membrane potential or Z-ring integrity of *S. aureus* was observed in either experiment. This difference to the reported membrane disrupting activity may be caused by differences in concentration or treatment time, as the authors report membrane depolarization beginning at 9 x MIC (with a MIC of 2 µg/mL). Importantly, the results of the present work clearly demonstrate, that telavancin has no significant influence on membrane function at a concentration, that is sufficient for total arrest of septum constriction via PGS inhibition (see chapters 4.1 and 5.1). Thus, it shows that the interaction with TGase and TPase substrates is substantially more relevant to the cellular effects and the antibacterial activity of this lipoglycopeptide and constitutes its primary molecular mechanism of action. In this regard, the membrane interaction of the lipophilic appendage likely has its main function in improving target affinity and specificity, thus reducing off-target binding in the cell wall mesh and fostering interaction with unprocessed lipid II. This has been clearly established by the enhanced activity of telavancin against VISA strains (Barcia-Macay *et al.* 2006; Hegde *et al.* 2010; Karlowsky *et al.* 2015; Kosowska-Shick *et al.* 2009; Krause *et al.* 2012; Madrigal *et al.* 2005; Marcos *et al.* 2010; Pfaller *et al.* 2010; K. Smith *et al.* 2013) as well as its improved binding to the septal region (compared to vancomycin, Lunde *et al.* 2009). The improved target interaction also reflects in the lower MIC of telavancin (compared to vancomycin) determined in the present work (see chapter 4.1.1). Still, secondary membrane impairing effects at higher concentrations may reduce the development of resistance and/or tolerance/persistence by enhancing cellular damage, thus improving the transition from growth inhibition to ultimate cell death (see chapter 5.1.10). How these results can be translated to other lipoglycopeptides is speculative. It has been shown previously, that teicoplanin does not induce membrane depolarization for concentrations up to 16 x MIC (with a MIC of 1 µg/mL, M. Cheng Huang *et al.* 2014), while oritavancin significantly affected the transmembrane potential of VISA at 8 x MIC and higher (with a MIC of 1 µg/mL, Belley *et al.* 2010) With these substantial differences in membrane activity and lipophilic appendage structure (see chapter 1.3), it might be necessary to perform comparative

studies of multiple lipoglycopeptides to elucidate the determinants, mechanisms and the role of their effect on the membrane.

5.2.2. Teixobactin and the structurally similar hypeptin and clovibactin

As $DiBAC_4(3)$ proved reliable to visualize membrane depolarization on the individual cell level and corresponded well with the associated cellular consequence of Z-ring disintegration (see chapters 4.2.1 and 5.2.1), it was used to determine the membrane depolarizing impact of teixobactin and the structurally similar antibiotics hypeptin (Wirtz *et al.* 2021) and clovibactin (Shukla *et al.* 2023). 30 min of treatment with either compound did not result in any substantial depolarization of *S. aureus* (see chapter 4.2.2). Clovibactin had a negligible, albeit statistically significant effect on the transmembrane potential. These results are in considerable contrast to recent reports, where teixobactin was shown to form fibrils of teixobactin:lipid II complexes arranged in β-sheets on *in vitro* model membranes (Shukla *et al.* 2020, 2022). These fibrils were observed to induce membrane deformation *in vitro* and the authors also described rapid depolarization and membrane damage using *Staphylococcus simulans* and *B. subtilis*. It is possible that the membrane-damaging impact of teixobactin is less pronounced in *S. aureus*. Alternatively, the discrepancy may be caused by differences in methodological setup. Shukla *et al.* (2022) reportedly measured both membrane potential and membrane integrity using 1 or 10 x MIC teixobactin on bacterial suspensions with an OD_{600} equivalent of 0.01 (1000-fold dilution of a culture adjusted to OD_{600} = 10) in Tris-NaCl Buffer. This experimental setup differs considerably from the one used in the present work, where both antibiotic treatment and the $DiBAC_4(3)$ visualization were carried out using OD_{600} = 0.5 cultures in MH medium. Interestingly, the more recently described clovibactin forms similar fibril structures but showed no indication of membrane disruption on *S. simulans* or *B. subtilis* (Shukla *et al.* 2023). For hypeptin, no reports on fibril formation or membrane interaction are available as of now. Further investigations into the cellular effects of these antibiotics are needed to elucidate the differences between their mechanisms of action, and to understand, how membrane interaction and fibril formation relate to the blocking of PGS and WTA biosynthesis (see also chapter 5.1.9) substrates.

5.2.3. Cacaoidin and mersacidin

The recently discovered cacaoidin represents the first-in-class compound of the lanthidins (Ortiz-López *et al.* 2020) due to its unique structure sharing characteristic features of the lanthipeptides (lanthionine ring, see chapter 1.6) and the linaridins (dimethylated N-terminus). Interestingly, cacaoidin was shown to bind to lipid II and additionally interact with TGases of *S. aureus*, constituting PGS inhibition as primary molecular mechanism of action (Deisinger *et al.* 2023). To also investigate a potential membrane activity, $DiBAC_4(3)$ fluorescence was visualized after treatment of *S. aureus* with up to 5 x MIC cacaoidin. Additionally, the similarly lipid II-binding mersacidin (see chapter 1.3) was evaluated. Mersacidin showed no depolarizing effect. Cacaoidin treatment caused a negligible, albeit statistically significant reduction in transmembrane potential (see chapter 4.2.3). Thus, membrane disruption can be excluded as a primary mechanism of action for cacaoidin.

5.3. Moenomycin interferes with the final stage of *S. aureus* cell division

The demonstration of fast and drastic arrest of septum constriction and cell division progress upon inhibition of PGS (see chapter 5.1) provides a framework for elucidating the cellular consequences of treatment with CWBM targeting antibiotics. This framework was applied to investigate the impact of moenomycin on CWBM and cell division of *S. aureus*. Moenomycin is known to bind with high affinities to the TGase donor region of PBP2 and monofunctional TGases in *S. aureus* and is therefore described as a potent inhibitor of the penultimate step in peptidoglycan synthesis (Bury *et al.* 2014; Gampe *et al.* 2011; Heaslet *et al.* 2009; Lovering *et al.* 2007; Van Heijenoort *et al.* 1980). However, neither the full range of its molecular targets (Arbeloa *et al.* 2004; Gampe *et al.* 2013; McPherson *et al.* 2003; Ostash *et al.* 2010; Qiao *et al.* 2014) nor the cellular consequences of treatment with moenomycin are well understood. There is a substantial lack of research on the cellular impact of moenomycin beyond the observation of lipid II accumulation upon TGase inhibition (Qiao *et al.* 2014, 2017). Therefore, the initial effects of moenomycin treatment were investigated to reveal previously unknown aspects of the antibiotics mechanism of action and provide a first detailed description of how it impacts the *S. aureus* CWBM and cell division cycle on a cellular level.

5.3.1. Moenomycin disrupts the temporal organization of cell division progress

Remarkably, the observed effects of moenomycin on cell cycle phase distribution (see chapter 4.3.2) differed substantially from those caused by vancomycin, telavancin and oxacillin (see chapters 4.1 and 5.1). Moenomycin treatment induced a significant increase in late-stage cell division cells, accompanied by a decrease of cells in an early stage of cell division. These results are diametrical to the ones observed after treatment with the glycopeptides and the beta-lactam. However, visualization of FtsZ localization on a population level (CAPs, compare chapter 4.1.2) and on an individual cell level (Airyscan superresolution microscopy) both corroborated the observations of cell cycle phase distribution (see chapter 4.3.2). CAP analysis showed a significant shift towards more cells with small Z-rings and Airyscan superresolution microscopy visualized, that moenomycin significantly increased the abundance of assembly state cells (compare chapter 4.1.3). These were found to aberrantly progress

to the recruitment of FtsW, a known component of the early divisome (Monteiro *et al.* 2018). These results clearly demonstrated, that moenomycin interferes with cell separation. The antibiotic was found to trap cells in the assembly state and induce a malfunction in the regulation of divisome construction in the daughter cells, which leads to newly formed division sites without prior cell splitting. These cellular effects closely resemble the recently described impact of WTA biosynthesis inhibitors tunicamycin and targocil on cell cycle phase distribution and septum formation in *S. aureus*. Using these two antibiotics, Hammond *et al.* (2022) found a substantially increased abundance in late-stage cell division cells. Additionally, they observed aberrated localization of the early divisome protein GpsB to new division sites in non-separated daughter cells. This closely resembles the effects of moenomycin described in the present work. This suggests, that moenomycin interferes with WTA biosynthesis, which is crucial for regulating cell-splitting autolysins (see also chapters 5.1.3, 5.1.6, 5.1.9 and 5.1.10). In line with this, moenomycin was found to bind to and inhibit *S. aureus* Lcp proteins (Ph.D. thesis Fritz 2024), which catalyze the ultimate incorporation of WTAs into the cell wall mesh (Schaefer *et al.* 2017). Combining this results with the cellular effects described in the present work demonstrates, that targeting the final steps of WTA biosynthesis is an integral part of moenomycins antibacterial activity, which manifests on a cellular level in an interference with cell splitting. Importantly, these effects can be observed at comparably low concentrations of moenomycin (see chapter 4.3.1). Thus, they constitute key cellular consequences of treatment and not secondary effects emerging from very high antibiotic concentrations. However, the impact of moenomycin on the cell cycle was less pronounced than those described for compounds, that primarily act by WTA biosynthesis inhibition (Hammond *et al.* 2022). Furthermore, there is no reasonable doubt, that the high-affinity binding to TGase donor sites and subsequent PGS inhibition is moenomycins dominant molecular mechanism of action. Inhibition of TGase activity has been demonstrated numerous times and the interaction with of moenomycin with the active site of the key *S. aureus* TGase PBP2 as well as the monofunctional TGase MtgA has been elucidated to the structural level (Lovering *et al.* 2007; Yuan *et al.* 2008; Heaslet *et al.* 2009; Gampe *et al.* 2011, 2013; Boes *et al.* 2020). Considering this, interference with WTA biosynthesis may be regarded not as the sufficient cause, but as an important additional aspect of moenomycins mechanism of action, which contributes to its activity and may also decrease resistance development against the antibiotic. In this regard, mutation of a single amino acid at the donor site of PBP2 was found to be omnipresent in lab-generated moenomycin-resistant strains, demonstrating a crucial relevance of the TGase target site for the antibiotics activity (Rebets *et al.* 2014). Unfortunately, the authors did not screen for mutations in genes associated with WTA biosynthesis. Newer results by Lloyd *et al.* (2020) also showed several mutations of the PBP2 donor region in moenomycin resistant mutants. Interestingly, they further showed that all their moenomycin resistant mutants harbored a specific point mutation in SagB (Lloyd *et al.* 2020), a glucosaminidase and with key roles in controlling peptidoglycan strand length, autolysis and cell division[17] (Y. G. Y. Chan *et al.* 2016; Schaefer *et al.* 2020; Willing *et al.* 2021). Importantly, its deletion was observed to cause cell separation defects with aberrant formation of new septa in non-

[17] Of note, SagB was recently described as virulence factor involved in murine model and human macrophage survival of *S. aureus* (Sutton *et al.* 2021).

separated daughter cells (Y. G. Y. Chan *et al.* 2016), which has considerable resemblance to the effect of moenomycin described in the present work. Currently, the regulatory mechanisms governing SagB activity are not comprehensively understood. Interaction of SagB with the integral membrane protein SpdC was shown to influence the length of glycan strands produced by SagB cleavage (Schaefer *et al.* 2020). However, the structural basis of this interaction does not include the moenomycin-resistance mutation site described by Chan *et al.* (2016). The observed mutation of SagB in moenomycin-resistant *S. aureus* suggests, that resistance development does not exclusively rely on PBP2 mutation, but additionally requires modification of autolysis (via SagB mutation), potentially due to the antibiotic's interference with WTA biosynthesis. Exclusive introduction of the respective PBP2 or SagB point mutation into naïve *S. aureus* populations could help to clarify the individual role of each mutation in moenomycin resistance and thereby further elucidate the relevance of Lcp targeting in moenomycins mechanism of action. Furthermore, characterization of mutant SagB activity and its impact on *S. aureus* autolysis and cell division would yield advances in understanding the cellular role of SagB and how it contributes to antibiotic activity and resistance. Recently, both SagB and SpdC were found to be regulated by the antibiotic resistance-associated VraSR system and involved in susceptibility towards the corbomycin and complestatin (Gómez-Arrebola *et al.* 2023), antibiotics which interfere with autolytic activity by binding to peptidoglycan (Culp *et al.* 2020, see also chapter 5.1.9). SagB was also shown to be involved in vancomycin killing of *S. aureus* (Salamaga *et al.* 2021, see also chapter 5.1.3). These examples further highlight the role of SagB in antibacterial activity. Investigating the functional integration of SagB in the *S. aureus* CWBM, cell division and autolytic homeostasis promises to elucidate the enzymes' role in *S. aureus* cellular biology and antibiotic treatment. Understanding its involvement in moenomycin activity and resistance might be a useful approach to this end.

5.3.2. Cell division disruption precedes ultimate inhibition of peptidoglycan synthesis

To further investigate how impairment of cell separation relates to TGase inhibition on a temporal scale, the impact of moenomycin on PGS activity was analyzed by quantifying HADA incorporation into nascent peptidoglycan of individual *S. aureus* cells (see chapter 4.3.3). Thereby, it was shown that loss of PGS activity was not achieved after 30 min of moenomycin treatment, the timeframe in which the impact on cell separation and new divisome formation was already clearly established (see chapters 4.3.2 and 5.3.1). In line with this, the incorporated HADA was significantly more focused to midcell, corroborating that moenomycin causes cell division defects while PGS is still active. Still, after 90 min of treatment, total loss of cell wall biosynthesis was observed, verifying that moenomycin ultimately inhibits TGase activity completely. Thus, while binding to TGase donor sites clearly constitutes the major part of moenomycins mechanism of action, inhibition of WTA incorporation by Lcp binding was proven to play a significant role in the antibiotics action. Remarkably, the visualization of HADA incorporation demonstrated that the effect on cell splitting was more immediate than and independent from ultimate inhibition of the cell wall biosynthesis. The first observable effects on *S. aureus* cell cycle and divisome organization very likely emerge from WTA biosynthesis interference. This may contribute to moenomycin activity by already interfering with cellular growth until ultimate PGS inhibition is established. Why PGS inhibition is delayed so substantially compared to vancomycin and fosfomycin

remains unclear. As moenomycin binds to the donor site of TGases (see chapter 1.3), its interaction with TGases already engaged in processive glycan strand polymerization might be hampered or even impossible. In such a case, the lipid II accumulation caused by moenomycin (W. Lee *et al.* 2016; Qiao *et al.* 2017; Srisuknimit *et al.* 2017) treatment would further delay establishment of a moenomycin:TGase interaction, as more substrates for initiation of processive strand polymerization are available under such conditions. Analysis of the temporal relationship between WTA biosynthesis inhibition, TGase inhibition and lipid II accumulation could help to answer this question.

5.3.3. Model of how moenomycin interferes with cell division in *S. aureus*

Ultimately, the results of this work suggest a following model for the impact of moenomycin on cell division of *S. aureus* (Figure 60). By binding to Lcp proteins, the antibiotic inhibits the final stages of WTA biosynthesis. This impairs cell separation and leads to the formation of non-divided daughter cells, that aberrantly progress to early-divisome recruitment. By binding to TGase donor sites, moenomycin further inhibits the final stages of PGS, which stops septum constriction. On a temporal scale, WTA biosynthesis is inhibited first, while PGS is still occurring. However, after both pathways are inhibited, a full arrest of the cell division cycle featuring a subpopulation of aberrated cell phenotypes is established.

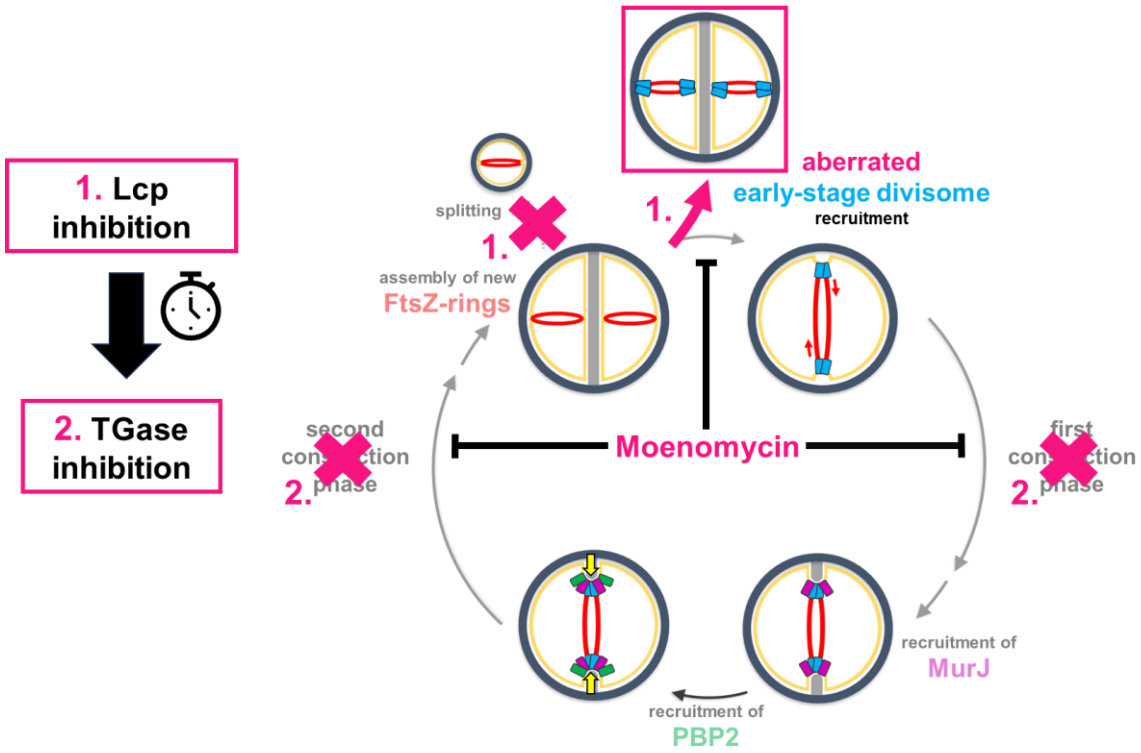

Figure 60: Model for cell cycle inhibition by moenomycin. In a first phase, cell splitting is impaired via binding to Lcp proteins, thus inhibiting WTA biosynthesis. This leads to the formation of aberrated early-stage divisome recruitment in non-divided daughter cells. In a second phase, PGS is inhibited by binding to TGase donor sites, which stops all septum constriction.

5.4. DCAP disrupts the organization of cell division and cell wall biosynthesis machineries

The synthetic small molecule DCAP was identified in an *in vitro* high-throughput screening for cell division inhibitors. It shows activity against several gram-positive and gram-negative species, including biofilms of *Caulobacter crescentus* and *S. aureus* (Eun *et al.* 2012; Hurley *et al.* 2015) and furthermore *E. coli* in a cell culture model for uropathogenic infections (Allavena *et al.* 2018). Previous work on the mechanism of action of DCAP revealed a membrane-targeting mechanism of action, inducing transmembrane depolarization, increase of membrane permeability, and mislocalization of essential membrane-associated proteins. The authors hypothesized, that DCAPs antibacterial activity likely involves a specific target interaction and speculated that the compound interacts with lipids or proteins in the bacterial membrane. However, no molecular target was identified (Eun *et al.* 2012). Therefore, the cellular impact of DCAP treatment on *S. aureus* was investigated to further elucidate the distinctive features of the molecules antibiotic activity and to contribute to the discovery of a molecular target.

The results of this work show, that the antibiotic activity of DCAP is not limited to membrane interaction, but extents to substantial impairment of *S. aureus* cell division and cell wall biosynthesis organization. Induction of heavily aberrated septum phenotypes were distinct to DCAP and not caused by the membrane-depolarizing compound CCCP (see chapter 4.4.2). This was validated by the observation, that DCAP had less impact on Z-ring integrity than CCCP, while it heavily impaired divisome placement even at 1 x MIC (see chapter 4.4.2). Z-ring disintegration is caused by a loss of FtsZ-GTPase activity due to decreased GTP levels after collapse of the transmembrane potential dependent respiratory chain (Strahl *et al.* 2010). In contrast, aberrant divisome placement and septum formation is closely associated with disruptions in CWBM activity (Atilano *et al.* 2010; Farha *et al.* 2013; Grein *et al.* 2020; Hill *et al.* 2019; Lund *et al.* 2018; Monteiro *et al.* 2019, 2018; Pinho and Errington 2005; Reed *et al.* 2015; Reichmann *et al.* 2019; Salamaga *et al.* 2021; Steele *et al.* 2011; Tinajero-Trejo *et al.* 2022; Turner *et al.* 2010; Veiga *et al.* 2023; Wacnik *et al.* 2022). Additionally, DCAP treatment lead to dislocation of PGS activity and a loss of PBP2 septal focus (see chapter 4.4.3), akin to effects described for CWBM targeting antibiotics in the present work and others (see chapters 4.1 and 5.1.4). These observations suggest a direct interference of DCAP with the CWBM of *S. aureus*, which results in inhibition and disorganization of key PGS proteins. This induces failure in septum formation and division site placements and ultimately contributes to killing. In line with this, DCAP was shown to bind to C_{55}PP-containing PGS precursors, thereby inhibiting various steps in cell wall biosynthesis *in vitro* (Ph.D. thesis Ludwig 2023). Likewise, DCAP-induced cell wall stress response in *B. subtilis* was antagonized by the addition of C_{55}PP-containing lipids. Treatment of *B. subtilis* with DCAP also induces membrane blebbing (thesis (Ludwig 2023), which is characteristic for cell wall damage (Reithuber *et al.* 2021; T. Schneider Kruse *et al.* 2010; Wirtz *et al.* 2021; Z. Yao *et al.* 2012). Furthermore, DCAP treatment induced accumulation of the soluble peptidoglycan precursor UDP-MurNAc-PP in *S. aureus* (thesis (Ludwig 2023), which is a typical effect of CWBM inhibiting antibiotics (Ling *et al.* 2015; Reithuber *et al.* 2021; T. Schneider Kruse *et al.* 2010; Shukla *et al.* 2023; Wirtz *et al.* 2021). Combining these various results with the observations and reasoning presented in this work, it can be concluded that DCAP directly targets the CWBM. By binding

to various C_{55}PP-containing precursors including lipid II, the synthetic small molecule induces striking cellular effects impairing septum construction and cell division of *S. aureus*. These effects likely emerge from PGS inhibition, as the structural-functional coordination of cell division and CWBM with active PGS have been demonstrated numerous times (see chapters 1.3, 4.1 and 5.1). Interestingly, the effects of DCAP towards spatial organization of divisome and CWBM were distinct from that observed for the exclusively PGS-targeting antibiotics. This may be caused by the dual and putatively independent targeting of both CWBM and membrane function. Since DCAP furthermore interacted with the WTA precursor lipid III_{WTA} *in vitro* (Ph.D. thesis Ludwig 2023), it may be possible that the distinctive cellular effects of the synthetic molecule are caused by impacting PGS, WTA biosynthesis and transmembrane potential in unique proportions.

The complex mechanism of action of DCAP illustrates the potentials of fully synthetic antimicrobial scaffolds. The results of this work combined with other results (see above) demonstrate that the mode of action of small synthetic molecules such as DCAP can be multifaceted and lead to complex cellular consequences despite their small size. Furthermore, the synthetic character of these molecules allows for comparably easy investigation into their structure-actvity-relationship (SAR), which enables further improvement of antibacterial activity and fosters in-depth understanding of the chemical building blocks required for different aspects of their molecular action. For DCAP, such an SAR study already showed, that the carbazole moiety is essential for antibiotic activity, thus likely constituting the pharmacophore of the molecule (Hurley *et al.* 2015). To this end, the (also fully synthetic) THCz were recently found to interact with C_{55}PP-containing lipids via a diamino motif consisting of a carbazole amino group and an adjacent linker amino group (Reithuber *et al.* 2021). A highly similar constellation is found in DCAP, suggesting that both classes bind to the pyrophosphate by coordinating the two positive amino groups with the corresponding negative phosphate moieties of PGS and WTA precursors. The recently described trypyricins show very similar structures and were already shown to impact the *S. aureus* membrane (Podoll *et al.* 2023), suggesting that these compounds might exert a comparable multi-targeting mechanism of action. However, there is no information on their interaction with C_{55}PP-containing lipids available as of now. Still, the apparent antibiotic activity of all these different classes (DCAP, THCz, trypyricins) clearly demonstrates the potential of the carbazole scaffold for further development of synthetic compounds, especially in connection with an adjacent amino-linked hydrophobic appendage to elevate both PGS precursor and hydrophobic membrane interaction.

5.5. FloA is required for correct localization of the heme-acquisition system component IsdF

Recent advances in the biological understanding of microbiota, host-pathogen interactions, pathogenesis and virulence have enabled the development of numerous anti-infective approaches orthogonal to antibiotic-based chemotherapy. Instead of directly killing the bacteria, these ideas focus on weakening the pathogenic potential of a bacterium, reducing its in-host survival capabilities and/or supporting the immune system. One promising approach is to limit essential resource availability, which in turn hinders growth of the pathogen and complements the hosts nutritional immunity systems in

infection containment and eradication (Murdoch *et al.* 2022). In *S. aureus*, the heme-acquisition iron-regulated surface determinant (Isd) system constitutes a central target of such an approach to inhibit the iron uptake and thus reduce in-host survival of the opportunistic pathogen (see chapter 1.4). IsdF is membrane-integrated permease and essential component of the Isd system, which transfers the captured heme from outside into the cytoplasm, where it is then further processed (Mazmanian *et al.* 2002, 2003; Muryoi *et al.* 2008; Sheldon *et al.* 2015; Skaar and Schneewind 2004). Recent observations showed an association of IsdF to fluid membrane microdomains (FMMs) and the FMM scaffolding protein FloA (Adolf *et al.* 2023). Thus, the role of FloA for localization of IsdF was investigated in the present work.

The results show, that IsdF and FloA co-localize to some degree in *S. aureus* (see chapter 4.5), but interestingly do not exhibit an interaction as strong as expected from typical FMM cargo (García-Fernández *et al.* 2017; Koch *et al.* 2017; Mielich-Süss *et al.* 2017; J. Schneider *et al.* 2015). This suggests that FloA only transiently interacts with FMMs. Additionally, FloA (and likely its scaffolding activity to form FMMs) are clearly critical for production of functional IsdF (see chapter 4.5), suggesting a key role of the FloA:FMM interaction for proper IsdF maturation. This is in line with earlier works, which describe FMMs as important regions for membrane protein processing, which have a scaffolding function for multiple chaperones and are crucial for functional oligomerization of membrane proteins (García-Fernández *et al.* 2017; Koch *et al.* 2017; Mielich-Süss *et al.* 2017; J. Schneider *et al.* 2015). IsdF functions as a homodimer in the *S. aureus* membrane (Grigg *et al.* 2010; Mazmanian *et al.* 2003), which contextualizes the results of the present work with the role of FMMs in membrane protein processing. The transient interaction with FMMs may facilitate the folding and/or dimerization of individual IsdF proteins. Further investigations validated, that FloA is indeed crucial for functionality of the Isd system heme uptake (Adolf *et al.* 2023), corroborating the results of the present work.

Given the relevance of FloA/FMMs for functional Isd-governed heme uptake, targeting the integrity of FMMs promises to diminish *S. aureus* virulence in iron-limiting conditions during infection. The human immune system already harbors multiple systems to prevent the iron-scavenging of bacterial pathogens (see chapter 1.4, Murdoch *et al.* 2022). Additional interference of *S. aureus* heme uptake could assist this so-called nutritional immunity and limit the virulence of the opportunistic pathogen. Furthermore, it could reduce proliferation, especially in life-threatening bloodstream infections, where heme naturally constitutes the main iron source of the invading bacteria. Approaches for targeting FMM integrity via inhibition of the biosynthesis of the *S. aureus* special lipid staphyloxanthin were already proven to be successful in disrupting FMM formation in *S. aureus*, including MRSA (García-Fernández *et al.* 2017; Koch *et al.* 2017). According to the crucial role of FMMs in protein oligomerization and maturation, a significant decrease in virulence was observed in infection mouse models after treatment with staphyloxanthin biosynthesis inhibitors (García-Fernández *et al.* 2017; Koch *et al.* 2017). The results of the present work further substantiate this result by giving an illustrative example for a key virulence pathway, which is dependent on functional FMM organization. Interestingly, the MRSA resistance factor PBP2a (see chapter 1.2) also depends on FMM functionality. Therefore, disruption of FMMs not only reduces virulence, but also re-senzitizes MRSA to beta-lactams. Accordingly, inhibition of

staphyloxanthin enabled effective beta-lactam treatment of MRSA in mice (García-Fernández *et al.* 2017). Thus, targeting of FMMs represents a promising approach to combat *S. aureus* virulence and simultaneously enable successful beta-lactam treatment of resistant MRSA infections.

5.6. A37 production contributes to competitiveness of *S. epidermidis* against corynebacteria

The by now clearly established role of the human microbiota in health and infection (see chapter 1.5) demonstrates the need for a comprehensive understanding of the factors and mechanisms, that govern microbiome composition. To this end, bacteriocins (see chapter 1.6) play an important role in shaping the microbiome to the advantage of the producer (Heilbronner *et al.* 2021). Still, the mechanisms of action and cellular effects of many of these compounds is unknown, as is their impact on microbiome ecology and composition. This also applies to the epilancins, which constitute a subgroup of the lantibiotic group of bacteriocins (see chapter 1.6). Until now, only three members of the epilancin group were described with only little to no information on ecological relevance (Bierbaum 1996; Ekkelenkamp *et al.* 2005; Knerr *et al.* 2012; J. Petersen *et al.* 2009; Van De Kamp *et al.* 1995; Velásquez *et al.* 2011). Phylogenetic analysis of public databases revealed numerous epilancin biosynthetic gene clusters present in staphylococci (Puls *et al.* 2024). This illustrates an ecological relevance of epilancins to the staphylococcus genus, which comprises multiple key players in human microbiome health and infection, such as *S. epidermidis* and *S. aureus* (Jenul *et al.* 2019; Krismer *et al.* 2017; Laux *et al.* 2019; C. M. Liu *et al.* 2015; Severn *et al.* 2023). Thus, the ability of the newly identified epilancin A37 (see chapter 4.6) in conferring competitional growth advantage to the producer was assessed and the mechanism of action investigated.

The results of direct competition of *S. epidermidis* A37 with *C. glutamicum* in liquid medium (see chapter 4.6) demonstrated, that the production of A37 conveyed a gain in competitive fitness of *S. epidermidis* against corynebacteria. This is in line with observations of notable growth inhibition zones of *S. epidermidis* A37 against various nasal corynebacterial isolates as well as potent activity and low MICs of the purified compound against several corynebacteria (Puls *et al.* 2024). These approaches further showed that activity of A37 is very specific to corynebacteria, with notably less effect on other genera.

Staphylococci and corynebacteria both constitute key genera of human nasal and skin microbiota and are closely associated with health and disease (Flowers *et al.* 2020; Grice *et al.* 2009; Hardy *et al.* 2020; C. M. Liu *et al.* 2015). In the hostile environments of human skin and nose, they naturally compete for limited space and nutrients within a complex bacterial interaction network governing microbiome composition and metabolism (Byrd *et al.* 2018; Flowers *et al.* 2020; Grice *et al.* 2009; Hardy *et al.* 2019, 2020; Q. Liu *et al.* 2020). While corynebacteria evolved various strategies to inhibit the expansion of staphylococci, e.g., via siderophore secretion, bacteriocin production appears to be the main staphylococcal strategy in this inter-species competition (Bomar *et al.* 2016; Hardy *et al.* 2019, 2020; Heilbronner *et al.* 2021; Janek *et al.* 2016; Stubbendieck *et al.* 2019). Colonization of either genus has been shown to impact the pathogenic potential and/or abundance of pathogens in the nasal microbiome.

Importantly, the range of effects on other bacteria ranges from growth inhibition, over modulating expression of key virulence factors, to direct growth promotion and also potential enhancement of pathogenesis (Flowers *et al.* 2020; Hardy *et al.* 2020). Additionally, members of both genera show notable pathogenic potential themselves and can cause severe infections (Blaise *et al.* 2008; Díez-Aguilar *et al.* 2013; Kleinschmidt *et al.* 2015; Severn *et al.* 2023). This illustrates the complexity of the various relationships and highlights, how delicate and multi-factor-dependent the balance between beneficial and detrimental impact on the microbiome and, thus, host health can be. Accordingly, understanding the roles of key commensal and opportunistic pathogenic species, the factors influencing their behaviour and abundance and the interaction network of them is key for a comprehensive knowledge of the nasal microbiome ecology. The competitional relationship between staphylococci and corynebacteria is an integral part of this network. The results of this work indicate, that epilancins play an important role in this competition and thus suggest, that epilancin A37 has considerable microbiome-shaping impact on the nasal microbiome. This might impact other nasal colonizers important for human health such as *S. aureus*, *S. pneumoniae*, *Moraxella catarrhalis* and others. The apparent benefit of A37 production for *S. epidermidis* indicates a pronounced inter-species competition specifically between *S. epidermidis* and nasal corynebacteria. Previous reports seem to corroborate this, as they describe a distinct negative correlation between *S. epidermidis* and corynebacterial abundance in nasal microbiome composition (C. M. Liu *et al.* 2015; Q. Liu *et al.* 2020). A specific reason for this competition is not known. Analysis of spatial distribution of both genera in the different nasal microenvironments and factors that determine colonization and proliferation success of either genus (e.g., by metabolic profiling) might shine a light on the nature of this competition. Furthermore, it would help to elucidate general principles underlying nasal microbiome composition and could foster rational approaches to shape this important microbiome in a beneficial way. Bacteriocins such as A37 could eventually play an important role in this endeavor.

5.7. A37 has a unique mechanism of action

The mode of action of many lantibiotics is still unknown. Of those with a characterized mode of action, almost all kill by disruption of cytoplasmic membrane functionality (e.g., via formation of pores) or inhibition of peptidoglycan biosynthesis (Cao *et al.* 2021; Ongpipattanakul *et al.* 2022; van Staden *et al.* 2021; X. Wang *et al.* 2020). The most prominent lantibiotic nisin acts via a mechanism of pore-formation, that is based on interaction of the nisin N-terminus with lipid II pyrophosphate (Bonelli *et al.* 2006; Brötz Josten *et al.* 1998; Driessen *et al.* 1995; S. T. D. Hsu *et al.* 2004; Medeiros-Silva *et al.* 2018; K. Scherer *et al.* 2013; K. M. Scherer *et al.* 2015). Due to the high structurally similarity of epilancins to the C-terminus of nisin, The mechanism of action of epilancins was initially thought to involve pore-formation without lipid II-binding (see chapter 1.6, Bierbaum 1996; Driessen *et al.* 1995). However, the inability to disrupt liposomes (Brötz, Bierbaum *et al.* 1998; Brötz Josten *et al.* 1998), and reports of very moderate effects on membrane integrity, observed only at higher concentrations (Knerr *et al.* 2012; X. Wang *et al.* 2023) made it difficult to precisely define the mode of action (X. Wang *et al.* 2020, 2023). Observations of $DiSC_3(5)$ efflux added further uncertainty (Knerr *et al.* 2012; X. Wang *et al.* 2023), as this is often a result of membrane depolarization (te Winkel *et al.* 2016).

5.7.1. A37 enters the cytoplasm without membrane disruption

Antibiotics with a membrane disruptive mechanism of action, e.g., via pore-formation, typically localize in the cell membrane (Bierbaum and Sahl 2009; X. Wang *et al.* 2020; Cao *et al.* 2021; van Staden *et al.* 2021; Ongpipattanakul *et al.* 2022). The primarily cytoplasmic localization of A37 observed in this work differs remarkably from this localization pattern. In line with this, no impact of A37 on membrane potential [$DiBAC_4(3)$] or integrity (propidium iodide) of *C. glutamicum* was found (Figure 61, see chapter 4.7.1). Instead, results of a moderate and concentration dependent $DiSC_3(5)$ efflux as well as the significant role of the transmembrane potential in A37 uptake show, that the epilancin is able to pass the membrane without severely impairing its function, and accumulates in the cytoplasm due to its polycationic and amphiphilic nature. The moderate concentration-dependent $DiSC_3(5)$ efflux is linked to this transmembrane-dependent influx of the polycationic epilancin, which in turn disrupts the localization equilibrium of the cationic $DiSC_3(5)$. Thus, the finding of intracellular localization of the polycationic A37 contextualize earlier results, which observed DiSC-dye efflux during epilancin treatment and suggested membrane depolarization as a cause of this effect (Knerr *et al.* 2012; X. Wang *et al.* 2023). However, the more detailed investigations of this work demonstrated, that $DiSC_3(5)$ efflux is rather caused by the concentration dependent ion exchange of the cationic dye with the cationic epilancin. This is illustrated by two results:

1. The cytoplasmic localization of A37, which is at least partially dependent on the negative transmembrane potential to drive uptake of the cationic dye. This was demonstrated by the effect of pre-treatment with the ionophore CCCP, which reduced the intracellular accumulation of A37 substantially.

2. The failure of A37 to induce $DiBAC_4(3)$ fluorescence, which quantifies membrane depolarization via a different chemical mechanism. Fluorescence development of $DiBAC_4(3)$ relies on intracellular accumulation of the anionic dye, which is directly dependent on the net charge inside the cell and thus not affected by an ion exchange of intracellular cations with the cationic A37 during uptake.

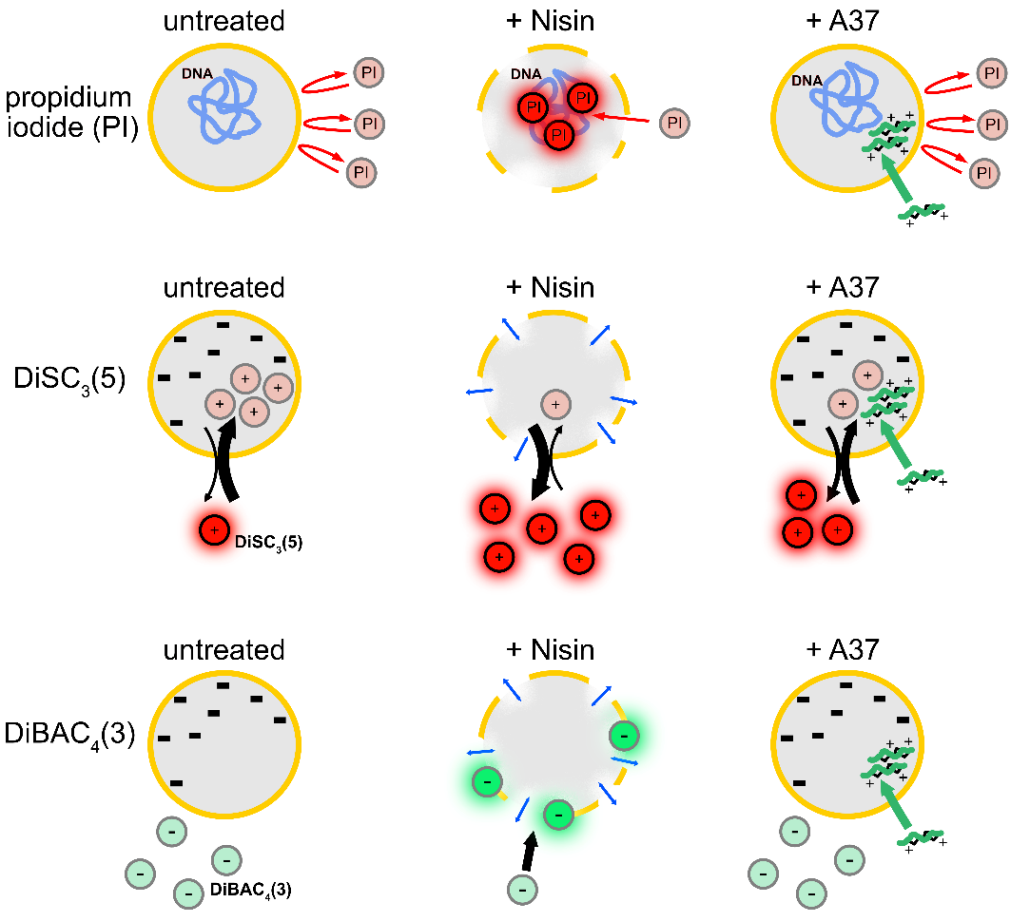

Figure 61: Schematic illustration of the mechanisms of Propidium iodide, $DiSC_3(5)$ and $DiBAC_4(3)$ fluorescence behaviour and how nisin and A37 modulate fluorescence of the dyes. Membrane-binding and vesicle formation of A37 not included for clarity.

Further investigations verified, that A37 binds to and traverses *in vitro* GUV membranes (Puls *et al.* 2024), which shows that the amphiphilic nature of the epilancin enables association and disassociation from membranes. Interestingly, the *in vitro* model further suggests that this mechanism does not require a specific target molecule in the membrane. It may be conferred by the C-terminal region of A37, which is highly similar to that of nisin (see chapters 1.6 and 4.6). For nisin, it has been proven that this region is spanning the cytoplasmic membrane and is critical for modulating activity (Medeiros-Silva *et al.* 2018). The flexible C-terminus was shown to reach into the cytoplasm (Medeiros-Silva *et al.* 2018), which in case of A37 might enable the membrane dissociation. *In vivo*, this dissociation into the cytoplasm may be further enhanced by the negative transmembrane potential, thus driving the accumulation to high intracellular concentrations of the cationic A37. This would explain, why substantial intra-GUV accumulation of A37 was not observed in contrast to the *in vivo* situation, as no transmembrane potential was applied to the GUVs (Puls *et al.* 2024). The finding that *in vivo* A37 uptake significantly depends on the transmembrane potential corroborates this hypothesis.

5.7.2. A37 induces formation of intracellular vesicles that correspond with antibiotic activity

Additional to the cytoplasmic localization, aggregation of A37 in distinct spots along the cell boundaries was observed. Thesehese spots were identified as intracellular membrane vesicles through superresolution microscopy. This was further verified via cryo electron tomography, which visualized diverse features ranging from heteromorph protrusions to circular unilamellar and double membrane vesicles (Puls *et al.* 2024). Notably, a likely intermediate step in the formation of these double membrane vesicles was observed, where cytoplasmic membrane invaginations contained a single membrane vesicle. Additionally, a detachment of the mycolic outer membrane layer was observed in cryo electron tomography. However, the implications of this detachment for antibacterial activity remain unclear.

The formation of the intracellular vesicles clearly corresponds to antibacterial activity, as the comparison between *C. glutamicum* wild type and strain A37/8 revealed. Accordingly, intracellular localization alone is not sufficient for antibacterial activity. This shows that vesicle formation is closely associated with killing of the bacteria and further demonstrates that intracellular accumulation is not the result of a lethally damaged membrane. Importantly, reduction of cytoplasmic localization via CCCP pre-treatment also significantly reduced vesicle formation in the wild type. This strongly suggests that intracellular accumulation is a prerequisite for effective formation of vesicles. Interaction with anionic membrane components may drive the formation of these vesicles via hydrophobic and/or charge interaction. This corresponds well with the septal and polar focus of vesicle formation, since multiple anionic lipid species are known to localize in these regions due to local curvature (e.g., cardiolipin; Bansal-Mutalik *et al.* 2011; Beltrán-Heredia *et al.* 2019; F. Kawai *et al.* 2004; Klatt *et al.* 2018; Renner *et al.* 2011) and/or cell wall biosynthesis activity (C_{55}PP-containing lipids; Sher *et al.* 2021; Valbuena *et al.* 2007; Zhou *et al.* 2019).

5.7.3. Model of A37 mechanism of action

Virtually all lantibiotics with a known antibiotic activity kill bacteria either by disrupting the cytoplasmic membrane or by inhibiting cell wall biosynthesis (Brotz 2000; Cao *et al.* 2021; Ongpipattanakul *et al.* 2022; Willey *et al.* 2007). The results shown in this work unequivocally demonstrate, that the primary cellular effect of A37 is not directed to impairing membrane integrity or potential. In contrast, binding of the epilancin relies to significant extent on an intact transmembrane potential facilitating an uptake of the lantibiotic into the cytoplasm. Interaction of A37 with the CWBM is highly unlikely as primary mechanism of action, as the distinguishing feature of epilancins from nisin is the explicit lack of the lipid II-binding motif (X. Wang *et al.* 2020). The absence of a specific lipid II interaction governing the epilancin mechanism of action was previously validated experimentally for K7 (Brötz Josten *et al.* 1998)and 15X (X. Wang *et al.* 2020) as well as for A37 (unpublished data, personal communication Benjamin Winnerling). Furthermore, the cytoplasmic localization and intracellular vesicle formation of A37 do not suggest a CWBM component as primary interaction target.

The results of this work congregate to a model of the mechanism of action of A37 against corynebacteria (Figure 62). First, the cationic peptide attaches to the cell surface due to charge attraction, which is a well-known mechanism described for numerous cationic antimicrobial peptides (Dathe *et al.* 2001;

Demel *et al.* 1996; Driessen *et al.* 1995; Ernst *et al.* 2009; Peschel *et al.* 1999; Yin *et al.* 2012; L. Zhang *et al.* 2001). A37 then inserts into the cytoplasmic membrane via hydrophobic interaction, presumably via its C-terminus that is highly similar to the membrane-interacting part of nisin (Medeiros-Silva *et al.* 2018). Subsequently, the cationic epilancin is translocated into the cytoplasm, in a process which is at least partially driven by the negative transmembrane potential. Conceptiually, this is similar to the uptake of aminoglycosides, which are structurally unrelated, cationic, small molecule antibiotics. The mechanism of intracellular accumulation of these clinically relevant antibiotics has been studied in great detail and was found to rely on ionic binding to the cell surface, followed by a transmembrane potential dependent uptake facilitated by the polycationic nature of the aminoglycosides (Lang *et al.* 2023; Taber *et al.* 1987). Upon intracellular accumulation, the high local concentration of A37 enforces the formation of vesicles, likely via interaction with anionic membrane components. The continuous aggregation of membrane components within these intracellular vesicles leads to cell death, as the clear correlation between vesicle formation and antimicrobial activity shows. This likely involves trapping of essential proteins and/or detrimental changes in lipid distribution. Consequently, this leads to a lethal collapse of membrane bound biosynthetic machineries and core metabolic processes. Again, this is conceptually similar to another, structurally unrelated compound. The small, uncharged, plant natural product rhodomyrtone was shown to induce the formation of fluid intracellular membrane vesicles, which trap proteins essential for cell division, cell wall biosynthesis and respiration (Saeloh *et al.* 2018). Notably, the molecular mechanisms, by which the intracellular vesicles are formed, differ substantially between A37 and rhodomyrtone. In this regard, both compounds are individually unique.

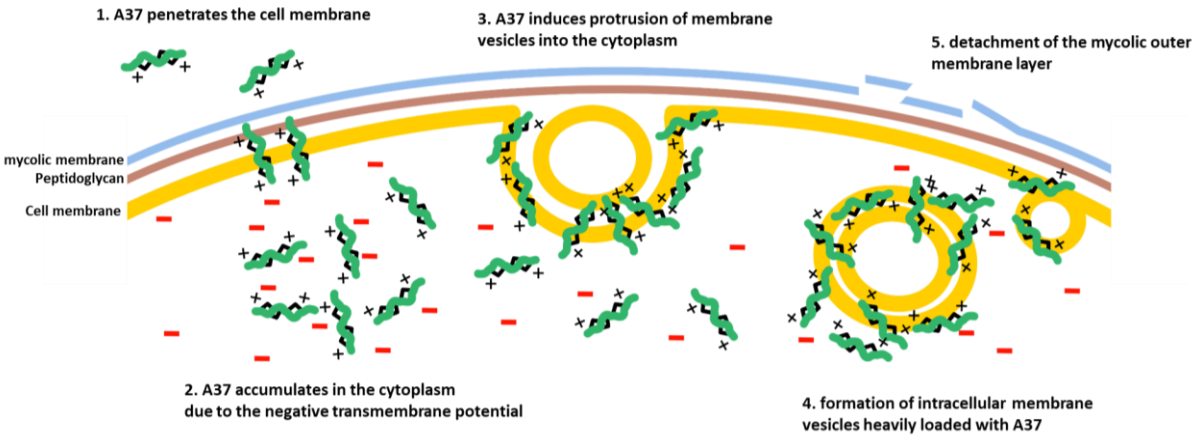

Figure 62: Model of epilancin A37 mechanism of action in corynebacteria.

This constitutes a hitherto undescribed mode of action for lantibiotics (see Cao *et al.* 2021; Ongpipattanakul *et al.* 2022; van Staden *et al.* 2021; X. Wang *et al.* 2020). Notably, the modes of action of the structurally related lantibiotics Pep5 and epicidin 280 (van Staden *et al.* 2021) have not been resolved so far (Brötz, Bierbaum *et al.* 1998; Brötz Josten *et al.* 1998; Heidrich *et al.* 1998; Kordel *et al.* 1988; Sahl 1985; Sahl *et al.* 1981). It is possible that these and other peptides act by a comparable mechanism.

5.7.4. Implications for epilancins as antibiotic compounds

The results of this work help to resolve the ambiguities of epilancin mechanism of action by providing a comprehensive model of how epilancin A37 acts against corynebacteria. A37 seems to be optimized for the specific composition of corynebacterial membranes, given the extraordinary activity against members of this genus. This may be achieved by an optimization of the epilancin structure to interact with the corynebacterial membrane composition to balance membrane binding with cytoplasmic dissociation and intracellular vesicle formation. Interestingly, reports of the antibiotic spectrum of the different epilancins vary considerably (Bierbaum 1996; Ekkelenkamp *et al.* 2005; J. Petersen *et al.* 2009). E.g., epilancin 15X was reported to show high activity against staphylococci such as *S. epidermidis*, *S. carnosus* and *S. aureus* (Ekkelenkamp *et al.* 2005; Knerr *et al.* 2012; X. Wang *et al.* 2023; C. Wu *et al.* 2023), which was not observed for A37 and K7 (unpublished data, personal communication Benjamin Winnerling, Fabian Grein and Simon Heilbronner). This suggests that the epilancin scaffold may allow for specific tailoring towards different target bacteria (X. Wang *et al.* 2023). Investigating the structural-functional relationship between different permutations of the epilancin scaffold and membrane compositions may yield insights into the biophysical mechanisms responsible for the unique mechanism of action. Furthermore, it may provide an understanding of how the epilancin scaffold can be modulated to act against specific bacterial targets. The high specificity of A37 against corynebacterial colonizers of the human microbiome suggests a potential use of A37 for targeted microbiome shaping and/or the treatment of corynebacterial infections. However, since both corynebacteria and *S. epidermidis* have multiple roles in health and infection and are part of the human functional core microbiome (see chapter 5.6), potential risks and benefits of such strategies should be carefully elucidated.

Appendices

Appendix 1

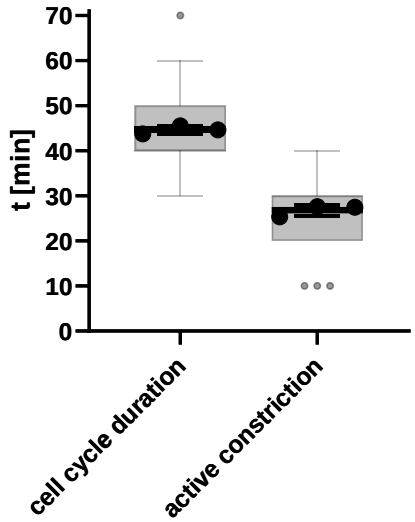

Appendix Figure 1: Quantification of cell division dynamics of *S. aureus* RN4220 pCQ11-FtsZ-SNAP from analysis of Z-ring diameter over time on the individual cell level (see chapter 4.1.3). Quantification of time needed to complete a full division cycle from Z-ring assembly until septum closure (cell cycle duration) and the time of active septum constriction. Semi-transparent boxplots show the distribution of individual cell data with 95% confidence interval. Semitransparent small points represent outlier of individual cell data. Large Points correspond to values of individual replicates, thick line shows the mean of three independent biological experiments ± SD. n ≥ 30 cells per replicate.

Appendix 2

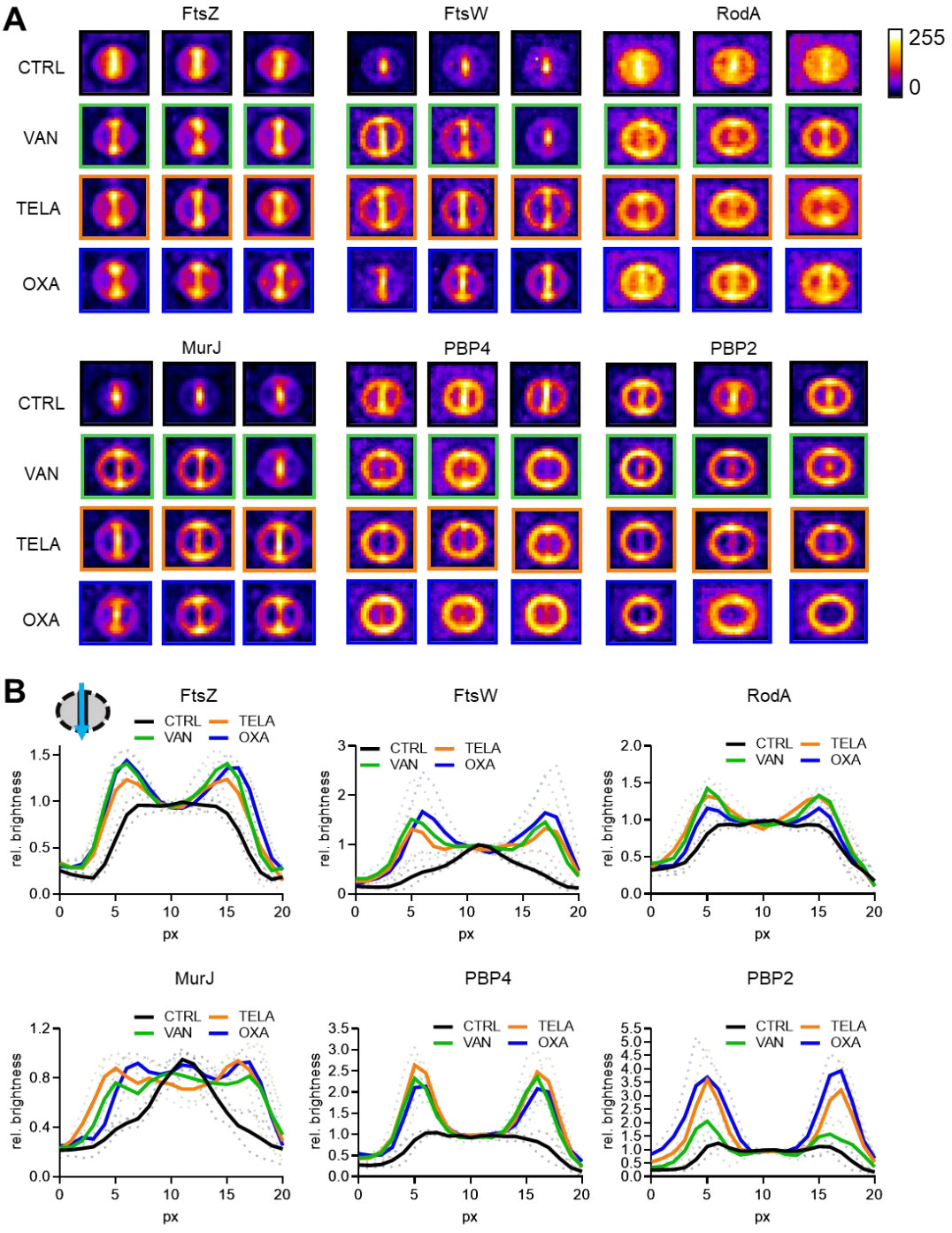

Appendix Figure 2: (A) CAPs of FtsZ, FtsW, RodA, MurJ, PBP4 and PBP2 used for data analysis shown in chapter 4.1.6 and Figure 27. **(B)** Quantification of CAP brightness for all CAPs shown in (A) along the septal axis, plotted relative to the medial brightness value. For each condition, the mean of three independent biological experiments is shown as thick, full line. The respective standard deviations are given as dotted, semi-transparent lines. n ≥ 94 cells per replicate and condition.

Appendix 3

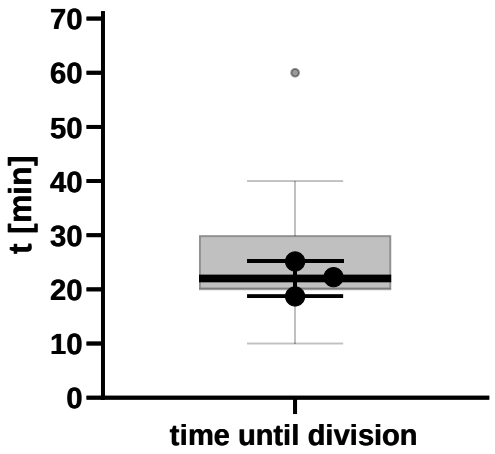

Appendix Figure 3: Quantification of time until cell division from the first imaging of septal PBP2 localization in individual cells of *S. aureus* RN4220 RNpPBP2-31 (see chapter 4.1.7). Semi-transparent boxplots show the distribution of individual cell data with 95% confidence interval. Semitransparent small points represent outlier of individual cell data. Large Points correspond to mean values of individual replicates, thick line shows the mean of three independent biological experiments ± SD. n = 30 cells per replicate and condition.

Appendix 4

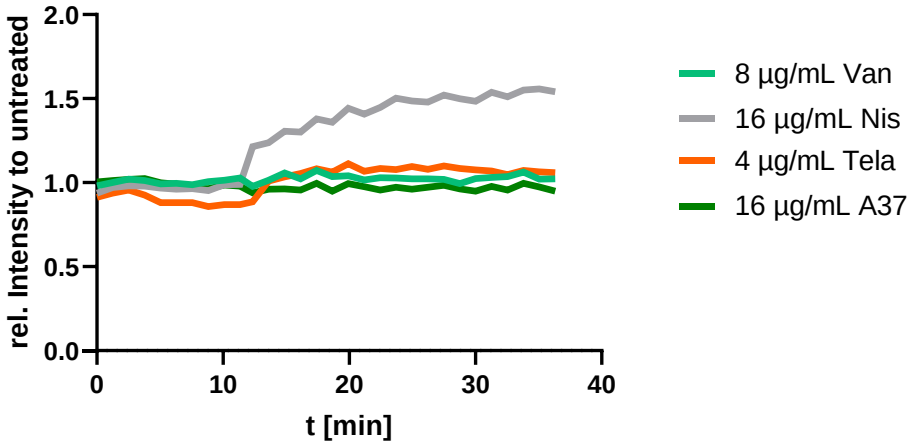

Appendix Figure 4: Interaction control of all compounds used with $DiSC_3(5)$ in this work. Compounds were added at t = 10 min. Change in $DiSC_3(5)$ fluorescence after addition of the compound given relative to the untreated control.

Appendix 5

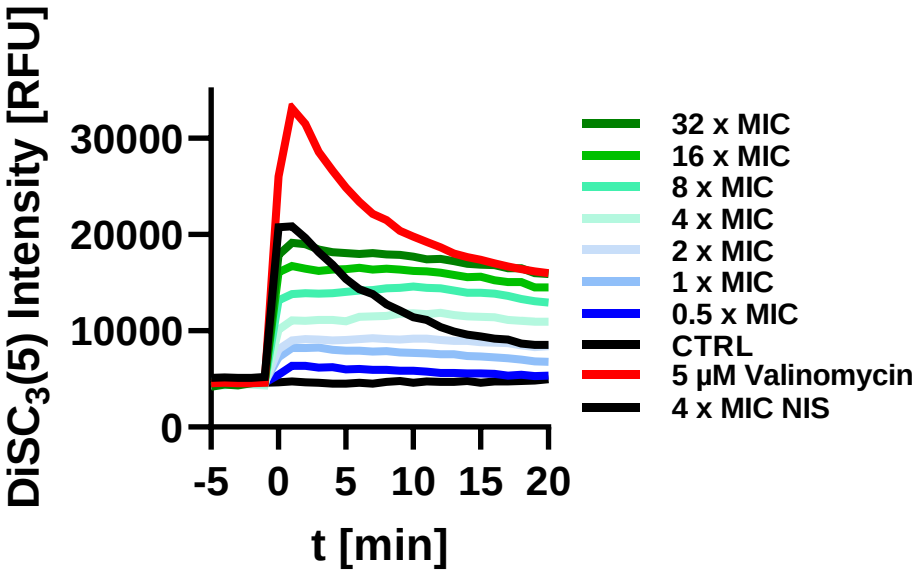

Appendix Figure 5: Quantification of $DiSC_3(5)$ fluorescence during treatment with 0.5 – 16 MIC A37, 4 x MIC nisin (NIS) and an untreated control (CTRL). 5 µM valinomycin + 300 mM KCl was used as positive control. Mean of three independent biological experiments. See chapter 4.7.1 and Figure 54B. RFU: Relative Fluorescence Unit.

Appendix 6

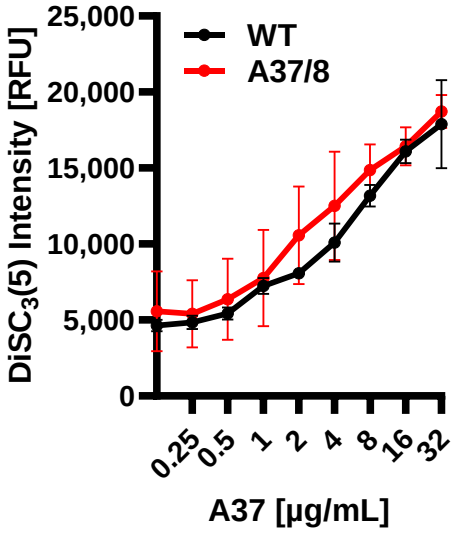

Appendix Figure 6: Comparison of $DiSC_3(5)$ release from cells of *C. glutamicum* wild type and *C. glutamicum* A37/8 after 2 min of treatment with 0.25 - 32 µg/mL A37, measured as $DiSC_3(5)$ fluorescence intensity (see chapter 4.7.1). Mean of three independent biological experiments ± SD. RFU: Relative Fluorescence Unit.

References

Adams, Wu, Czaplewski and Errington (2011): Multiple effects of benzamide antibiotics on FtsZ function. *Molecular Microbiology*, **80 (1)**: 68–84.

Adolf, Müller-Jochim, Kricks, Puls, Lopez, Grein, and Heilbronner (2023): Functional membrane microdomains and the hydroxamate siderophore transporter ATPase FhuC govern Isd-dependent heme acquisition in *Staphylococcus aureus*. *eLife*, **12**: e85304.

Alexander, Chatterjee, Hamilton, Eltis, Chambers and Strynadka (2018): Structural and kinetic analyses of penicillin-binding protein 4 (PBP4)-mediated antibiotic resistance in *Staphylococcus aureus. Journal of Biological Chemistry*, **293 (51)**: 19854–19865.

Allavena, Debellis, Marotta, Joshi, Mysorekar and Grimaldi (2018): A broad-spectrum antibiotic, DCAP, reduces uropathogenic *Escherichia coli* infection and enhances vorinostat anticancer activity by modulating autophagy. *Cell Death and Disease*, **9 (7)**: 780.

Allen, Letourneau, and Hobbs (1997): The role of hydrophobic side chains as determinants of antibacterial activity of semisynthetic glycopeptide antibiotics. *The Journal of Antibiotics*, **50 (8)**: 677–684.

Aly, Shinefield, Litz, and Maibach (1980): Role of teichoic acid in the binding of *Staphylococcus aureus* to nasal epithelial cells. *Journal of Infectious Diseases*, **141 (4)**: 463–465.

Anderson, Matsuhashi, Haskin and Strominger (1965): Lipid-phosphoacetylmuramyl-pentapeptide and lipid-phosphodisaccharide-pentapeptide: presumed membrane transport intermediates in cell wall synthesis. *Proceedings of the National Academy of Sciences of the United States of America*, **53 (4)**: 881–889.

Anderson, Matsuhashi, Haskin and Strominger (1967): Biosynthesis of the peptidoglycan of bacterial cell walls: II. phospholipid carriers in the reaction sequence. *Journal of Biological Chemistry*, **242 (13)**: 3180–3190.

Anderson and Strominger (1965): Isolation and utilization of phospholipid intermediates in cell wall glycopeptide synthesis. *Biochemical and Biophysical Research Communications*, **21 (5)**: 516–521.

Andreu, Schaffner-Barbero, Huecas, Alonso, Lopez-Rodriguez, Ruiz-Avila, Núñez-Ramírez, Llorca and Martín-Galiano (2010): The antibacterial cell division inhibitor PC190723 is an FtsZ polymer-stabilizing agent that induces filament assembly and condensation. *Journal of Biological Chemistry*, **285 (19)**: P14239-14246.

Appelbaum (2006): The emergence of vancomycin-intermediate and vancomycin-resistant *Staphylococcus aureus. Clinical Microbiology and Infection*, **12 (Suppl. 1)**: 16–23.

Arbeloa, Segal, Hugonnet, Josseaume, Dubost, Brouard, Gutmann, Mengin-Lecreulx and Arthur (2004): Role of class a penicillin-binding proteins in PBP5-mediated β-lactam resistance in *Enterococcus faecalis. Journal of Bacteriology*, **186 (5)**: 1221–1228.

Arndt-Jovin and Jovin (1989): Chapter 16: Fluorescence labeling and microscopy of DNA. *Methods in Cell Biology*, **30 (C)**: 417–448.

Askarova, Umbayev, Masoud, Kaiyrlykyzy, Safarova, Tsoy, Olzhayev and Kushugulova (2020): The links between the gut microbiome, aging, modern lifestyle and alzheimer's disease. *Frontiers in Cellular and Infection Microbiology*, **10**: 491270.

Asli, Brouillette, Krause, Nichols and Malouin (2016): Distinctive binding of avibactam to penicillin-binding proteins of gram-negative and gram-positive bacteria. *Antimicrobial Agents and Chemotherapy*, **60 (2)**: 752–756.

Atilano, Pereira, Yates, Reed, Veiga, Pinho and Filipe (2010): Teichoic acids are temporal and spatial regulators of peptidoglycan cross-linking in *Staphylococcus aureus. Proceedings of the National Academy of Sciences of the United States of America*, **107 (44)**: 18991–18996.

Atkins, Burman, Chamberlain, Cooper, Poutrel, Bagby, Jenkins, Feil and van den Elsen (2008): *S. aureus* IgG-binding proteins SpA and Sbi: Host specificity and mechanisms of immune complex formation. *Molecular Immunology*, **45 (6)**: 1600–1611.

Auty, Gardiner, McBrearty, O'Sullivan, Mulvihill, Collins, Fitzgerald, Stanton and Ross (2001): Direct in situ viability assessment of bacteria in probiotic dairy products using viability staining in conjunction with confocal scanning laser microscopy. *Applied and Environmental Microbiology*, **67 (1)**: 420–425.

Awasthi, Kumar, Knudson, Slayden and Ojima (2013): SAR studies on trisubstituted benzimidazoles as inhibitors of *Mtb* FtsZ for the development of novel antitubercular agents. *Journal of Medicinal Chemistry*, **56 (23)**: 9756–9770.

Bach and Bramkamp (2013): Flotillins functionally organize the bacterial membrane. *Molecular Microbiology*, **88 (6)**: 1205–1217.

Balaban, Helaine, Lewis, Ackermann, Aldridge, Andersson, Brynildsen, Bumann, Camilli, Collins, Dehio, Fortune, Ghigo, Hardt, Harms, Heinemann, Hung, Jenal, Levin, … Zinkernagel (2019): Definitions and guidelines for research on antibiotic persistence. *Nature Reviews Microbiology*, **17 (7)**: 441–448.

Bansal-Mutalik and Nikaido (2011): Quantitative lipid composition of cell envelopes of *Corynebacterium glutamicum* elucidated through reverse micelle extraction. *Proceedings of the National Academy of Sciences of the United States of America*, **108 (37)**: 15360–15365.

Baquero and Levin (2021): Proximate and ultimate causes of the bactericidal action of antibiotics. *Nature Reviews Microbiology*, **19 (2)**: 123–132.

Baranova, Radler, Hernández-Rocamora, Alfonso, López-Pelegrín, Rivas, Vollmer and Loose (2020): Diffusion and capture permits dynamic coupling between treadmilling FtsZ filaments and cell division proteins. *Nature Microbiology*, **5 (3)**: 407.

Barcia-Macay, Lemaire, Mingeot-Leclercq, Tulkens and Van Bambeke (2006): Evaluation of the extracellular and intracellular activities (human THP-1 macrophages) of telavancin versus vancomycin against methicillin-susceptible, methicillin-resistant, vancomycin-intermediate and vancomycin-resistant *Staphylococcus aureus*. *Journal of Antimicrobial Chemotherapy*, **58 (6)**: 1177–1184.

Barlow, Yu and Mathur (2015): Role of the gut microbiome in obesity and diabetes mellitus. *Nutrition in Clinical Practice*, **30 (6)**: 787–797.
Barna, Williams, Stone, Leung and Doddrell (1984): Structure elucidation of the teicoplanin antibiotics. *Journal of the American Chemical Society*, **106 (17)**: 4895–4902.
Barrett, Leimkuhler, Chen, Walker, Kahne and Walker (2005): Kinetic characterization of the glycosyltransferase module of *staphylococcus aureus* PBP2. *Journal of Bacteriology*, **187 (6)**: 2215–2217.
Barrows and Goley (2021): FtsZ dynamics in bacterial division: what, how, and why? *Current Opinion in Cell Biology*, **68**: 163.
Basuino, Jousselin, Andrew, Strynadka, Pinho, Chambers and Chatterjee (2018): PBP4 activity and its overexpression are necessary for PBP4-mediated high-level β-lactam resistance. *Journal of Antimicrobial Chemotherapy*, **73 (5)**: 1177–1180.
Beauregard, Williams, Gwynn and Knowles (1995): Dimerization and membrane anchors in extracellular targeting of vancomycin group antibiotics. *Antimicrobial Agents and Chemotherapy*, **39 (3)**: 781–785.
Belenky, Ye, Porter, Cohen, Lobritz, Ferrante, Jain, Korry, Schwarz, Walker and Collins (2015): Bactericidal antibiotics induce toxic metabolic perturbations that lead to cellular damage. *Cell Reports*, **13 (5)**: 968–980.
Belley, McKay, Arhin, Sarmiento, Beaulieu, Fadhil, Parr and Moeck (2010): Oritavancin disrupts membrane integrity of *Staphylococcus aureus* and vancomycin-resistant enterococci to effect rapid bacterial killing. *Antimicrobial Agents and Chemotherapy*, **54 (12)**: 5369–5371.
Belley, Neesham-Grenon, McKay, Arhin, Harris, Beveridge, Parr and Moeck (2009): Oritavancin kills stationary-phase and biofilm *Staphylococcus aureus* cells *in vitro. Antimicrobial Agents and Chemotherapy*, **53 (3)**: 918–925.
Beltramini, Mukhopadhyay and Pancholi (2009): Modulation of cell wall structure and antimicrobial susceptibility by a *staphylococcus aureus* eukaryote-like serine/threonine kinase and phosphatase. *Infection and Immunity*, **77 (4)**: 1406–1416.
Beltrán-Heredia, Tsai, Salinas-Almaguer, Cao, Bassereau and Monroy (2019): Membrane curvature induces cardiolipin sorting. *Communications Biology*, **2 (1)**: 225.
Benarroch and Asally (2020): The microbiologist's guide to membrane potential dynamics. *Trends in Microbiology*, **28 (4)**: 304–314.
Bertsche, Weidenmaier, Kuehner, Yang, Baur, Wanner, Francois, Schrenzel, Yeaman and Bayer (2011): Correlation of daptomycin resistance in a clinical *Staphylococcus aureus* strain with increased cell wall teichoic acid production and D-alanylation. *Antimicrobial Agents and Chemotherapy*, **55 (8)**: 3922–3928.
Bertsche, Yang, Kuehner, Wanner, Mishra, Roth, Nega, Schneider, Mayer, Grau, Bayer and Weidenmaier (2013): Increased cell wall teichoic acid production and D-alanylation are common phenotypes among daptomycin-resistant methicillin-resistant *Staphylococcus aureus* (MRSA) clinical isolates. *PLOS ONE*, **8 (6)**: e67398.
Bierbaum (1996): The biosynthesis of the lantibiotics epidermin, gallidermin, Pep5 and epilancin K7. *Antonie van Leeuwenhoek, International Journal of General and Molecular Microbiology*, **69 (2)**: 119–127.
Bierbaum and Sahl (2009): Lantibiotics: mode of action, biosynthesis and bioengineering. *Current Pharmaceutical Biotechnology*, **10 (1)**: 2–18.
Billot-Klein, Blanot, Gutmann and Van Heijenoort (1994): Association constants for the binding of vancomycin and teicoplanin to N-acetyl-D-alanyl-D-alanine and N-acetyl-D-alanyl-D-serine. *Biochemical Journal*, **304 (3)**: 1021–1022.
Bisson-Filho, Hsu, Squyres, Kuru, Wu, Jukes, Sun, Dekker, Holden, VanNieuwenhze, Brun and Garner (2017): Treadmilling by FtsZ filaments drives peptidoglycan synthesis and bacterial cell division. *Science*, **355 (6326)**: 739–743.
Biswas, Martinez, Göhring, Schlag, Josten, Xia, Hegler, Gekeler, Gleske, Götz, Sahl, Kappler and Peschel (2012): proton-binding capacity of *Staphylococcus aureus* wall teichoic acid and its role in controlling autolysin activity. *PLOS ONE*, **7 (7)**: e41415.
Biswas, Voggu, Simon, Hentschel, Thumm and Götz (2006): Activity of the major staphylococcal autolysin Atl. *FEMS Microbiology Letters*, **259 (2)**: 260–268.
Bitschar, Sauer, Focken, Dehmer, Moos, Konnerth, Schilling, Grond, Kalbacher, Kurschus, Götz, Krismer, Peschel and Schittek (2019): Lugdunin amplifies innate immune responses in the skin in synergy with host- and microbiota-derived factors. *Nature Communications*, **10 (1)**: 2730.
Blaise, Nikkels, Hermanns-Lê, Nikkels-Tassoudji and Piérard (2008): *Corynebacterium*-associated skin infections. *International Journal of Dermatology*, **47 (9)**: 884–890.
Blaskovich, Hansford, Butler, Jia, Mark and Cooper (2018): Developments in glycopeptide antibiotics. *ACS Infectious Diseases*, **4 (5)**: 715–735.
Blumberg and Strominger (1971): Inactivation of D-alanine carboxypeptidase by penicillins and cephalosporins is not lethal in *Bacillus subtilis*. *Proceedings of the National Academy of Sciences of the United States of America*, **68 (11)**: 2814–2817.
Boberek, Stach and Good (2010): Genetic evidence for inhibition of bacterial division protein FtsZ by berberine. *PLoS ONE*, **5 (10)**: e13745.
Boes, Olatunji, Mohammadi, Breukink and Terrak (2020): Fluorescence anisotropy assays for high throughput screening of compounds binding to lipid II, PBP1b, FtsW and MurJ. *Scientific Reports*, **10 (1)**: 1–8.
Bolla, Sauer, Wu, Mehmood, Allison and Robinson (2018): Direct observation of the influence of cardiolipin and antibiotics on lipid II binding to MurJ. *Nature Chemistry*, **10 (3)**: 363–371.
Bomar, Brugger, Yost, Davies and Lemon (2016): *Corynebacterium accolens* releases antipneumococcal free fatty acids from human nostril and skin surface triacylglycerols. *mBio*, **7 (1)** e01725-15.

Bonelli, Schneider, Sahl and Wiedemann (2006): Insights into in vivo activities of lantibiotics from gallidermin and epidermin mode-of-action studies. *Antimicrobial Agents and Chemotherapy*, **50 (4)**: 1449–1457.
Bordet and Perkins (1970): Iodinated vancomycin and mucopeptide biosynthesis by cell-free preparations from *Micrococcus lysodeikticus. Biochemical Journal*, **119 (5)**: 877–883.
Bose, Lehman, Fey and Bayles (2012): Contribution of the *Staphylococcus aureus* Atl AM and GL murein hydrolase activities in cell division, autolysis, and biofilm formation. *PLoS ONE*, **7 (7)**: e42244.
Böttiger, Schneider, Martínez, Sahl and Wiedemann (2009:) Influence of Ca^{2+} ions on the activity of lantibiotics containing a mersacidin-like lipid II binding motif. *Applied and Environmental Microbiology*, **75 (13)**: 4427–4434.
Bouhss, Crouvoisier, Blanot and Mengin-Lecreulx (2004): Purification and characterization of the bacterial MraY translocase catalyzing the first membrane step of peptidoglycan biosynthesis. *Journal of Biological Chemistry*, **279 (29)**: 29974–29980.
Boyd, Willey, Fawcett, Gillani and Mulvey (2008): Molecular characterization of *Enterococcus faecalis* N06-0364 with low-level vancomycin resistance harboring a novel D-Ala-D-Ser gene cluster, *vanL*. *Antimicrobial Agents and Chemotherapy*, **52 (7)**: 2667–2672.
Bramkamp and Lopez (2015): Exploring the existence of lipid rafts in bacteria. *Microbiology and Molecular Biology Reviews*, **79 (1)**: 81–100.
Breukink and de Kruijff (2006): Lipid II as a target for antibiotics. *Nature Reviews Drug Discovery*, **5 (4)**: 321–323.
Brötz (2000): New insights into the mechanism of action of lantibiotics - diverse biological effects by binding to the same molecular target. *Journal of Antimicrobial Chemotherapy*, **46 (1)**: 1–6.
Brötz, Bierbaum, Leopold, Reynolds and Sahl (1998): The lantibiotic mersacidin inhibits peptidoglycan synthesis by targeting lipid II. *Antimicrobial Agents and Chemotherapy*, **42 (1)**: 154–160.
Brötz, Bierbaum, Reynolds and Sahl (1997): The Lantibiotic Mersacidin Inhibits Peptidoglycan Biosynthesis at the Level of Transglycosylation. *European Journal of Biochemistry*, **246 (1)**: 193–199.
Brötz, Josten, Wiedemann, Schneider, Götz, Bierbaum and Sahl (1998): Role of lipid-bound peptidoglycan precursors in the formation of pores by nisin, epidermin and other lantibiotics. *Molecular Microbiology*, **30 (2)**: 317–327.
Brown, D. A. (2002): Isolation and Use of Rafts. *Current Protocols in Immunology*, **51 (1)**
Brown, E. D. and Wright (2016): Antibacterial drug discovery in the resistance era. *Nature*, **529 (7586)**: 336–343.
Brown, S., Xia, Luhachack, Campbell, Meredith, Chen, Winstel, Gekeler, Irazoqui, Peschel and Walker (2012): Methicillin resistance in *Staphylococcus aureus* requires glycosylated wall teichoic acids. *Proceedings of the National Academy of Sciences*, **109 (46)**: 18909–18914.
Bryson and Demerec (1955): Bacterial resistance. *The American Journal of Medicine*, **18 (5)**: 723–737.
Bugg, Wright, Walsh, Dutka-Malen, Arthur and Courvalin (1991): Molecular Basis for Vancomycin Resistance in *Enterococcus faecium* BM4147: biosynthesis of a depsipeptide peptidoglycan precursor by vancomycin resistance proteins VanH and VanA. *Biochemistry*, **30 (43)**: 10408–10415.
Bury, Dahmane, Derouaux, Dumbre, Herdewijn, Matagne, Breukink, Mueller-Seitz, Petz and Terrak (2014): Positive cooperativity between acceptor and donor sites of the peptidoglycan glycosyltransferase. *Biochemical Pharmacology,* **93 (2)**: 141-150.
Butler, Hansford, Blaskovich, Halai and Cooper (2014): Glycopeptide antibiotics: back to the future. *Journal of Antibiotics*, **67 (9)**: 631–644.
Büttner, Zoll, Nega, Götz and Stehle (2014): Structure-function analysis of *Staphylococcus aureus* amidase reveals the determinants of peptidoglycan recognition and cleavage. *Journal of Biological Chemistry*, **289 (16)**: 11083–11094.
Byrd, Belkaid and Segre (2018): The human skin microbiome. *Nature Reviews Microbiology*, **16 (3)**: 143–155.
Cafiso, Bertuccio, Spina, Purrello, Campanile, Di Pietro, Purrello and Stefani (2012): Modulating activity of vancomycin and daptomycin on the expression of autolysis cell-wall turnover and membrane charge genes in hVISA and VISA strains. *PLOS ONE*, **7 (1)**: e29573.
Campbell, Singh, Santa Maria, Kim, Brown, Swoboda, Mylonakis, Wilkinson and Walker (2011): Synthetic lethal compound combinations reveal a fundamental connection between wall teichoic acid and peptidoglycan biosyntheses in *Staphylococcus aureus. ACS Chemical Biology*, **6 (1)**: 106–116.
Campbell, Singh, Swoboda, Gilmore, Wilkinson and Walker (2012): An antibiotic that inhibits a late step in wall teichoic acid biosynthesis induces the cell wall stress stimulon in *Staphylococcus aureus. Antimicrobial Agents and Chemotherapy*, **56 (4)**: 1810–1820.
Cao, Do and Link (2021): Mechanisms of action of ribosomally synthesized and posttranslationally modified peptides (RiPPs). *Journal of Industrial Microbiology and Biotechnology*, **48 (3–4)**: kuab005.
Cars, Chandy, Mpundu, Peralta, Zorzet and So (2021): Resetting the agenda for antibiotic resistance through a health systems perspective. *The Lancet Global Health*, **9 (7)**: e1022–e1027.
Chambers and DeLeo (2009): Waves of resistance: *Staphylococcus aureus* in the antibiotic era. *Nature Reviews Microbiology*, **7 (9)**: 629–641.
Chan, L. C., Gilbert, Basuino, da Costa, Hamilton, dos Santos, Chambers and Chatterjee (2016): PBP 4 mediates high-level resistance to new-generation cephalosporins in *Staphylococcus aureus. Antimicrobial Agents and Chemotherapy*, **60 (7)**: 3934–3941.
Chan, Y. G. Y., Frankel, Missiakas and Schneewind (2016): SagB glucosaminidase is a determinant of *Staphylococcus aureus* glycan chain length, antibiotic susceptibility, and protein secretion. *Journal of Bacteriology*, **198 (7)**: 1123–1136.
Chang, Sievert, Hageman, Boulton, Tenover, Downes, Shah, Rudrik, Pupp, Brown, Cardo and Fridkin (2003): Infection with vancomycin-resistant *Staphylococcus aureus* containing the *vanA* resistance gene. *New England Journal of Medicine*, **348 (14)**: 1342–1347.

Chen, Walker, Sun, Hu, Walker and Kahne (2003): Vancomycin analogues active against *vanA*-resistant strains inhibit bacterial transglycosylase without binding substrate. *Proceedings of the National Academy of Sciences*, **100 (10)**: 5658–5663.
Cheng, A. G., McAdow, Kim, Bae, Missiakas and Schneewind (2010): Contribution of coagulases towards *Staphylococcus aureus* disease and protective immunity. *PLoS Pathogens*, **6 (8)**: e1001036.
Cheng, M., Huang, Ramu, Butler and Cooper (2014:) Ramoplanin at bactericidal concentrations induces bacterial membrane depolarization in *Staphylococcus aureus. Antimicrobial Agents and Chemotherapy*, **58 (11)**: 6819–6827.
Cheng, M., Ziora, Hansford, Blaskovich, Butler and Cooper (2014): Anti-cooperative ligand binding and dimerisation in the glycopeptide antibiotic dalbavancin. *Organic & Biomolecular Chemistry*, **12 (16)**: 2568–2575.
Chmara, Ripa, Mignini and Borowski (1991): Bacteriolytic effect of teicoplanin. *Journal of General Microbiology*, **137 (4)**: 913–919.
Cho, Uehara and Bernhardt (2014): Beta-lactam antibiotics induce a lethal malfunctioning of the bacterial cell wall synthesis machinery. *Cell*, **159 (6)**: 1300–1311.
Claesen, Spagnolo, Ramos, Kurita, Byrd, Aksenov, Melnik, Wong, Wang, Hernandez, Donia, Dorrestein, Kong, Segre, Linington, Fischbach and Lemon (2020): A *Cutibacterium acnes* antibiotic modulates human skin microbiota composition in hair follicles. *Science Translational Medicine*, **12 (570)**: 5445.
Clauditz, Resch, Wieland, Peschel and Götz (2006): Staphyloxanthin plays a role in the fitness of *Staphylococcus aureus* and its ability to cope with oxidative stress. *Infection and Immunity*, **74 (8)**: 4950–4953.
Coltharp, Buss, Plumer and Xiao (2016): Defining the rate-limiting processes of bacterial cytokinesis. *Proceedings of the National Academy of Sciences of the United States of America*, **113 (8)**: 1044–1053.
Conlon, Nakayasu, Fleck, LaFleur, Isabella, Coleman, Leonard, Smith, Adkins and Lewis (2013): Activated ClpP kills persisters and eradicates a chronic biofilm infection. *Nature*, **503 (7476)**: 365–370.
Conlon, Rowe, Gandt, Nuxoll, Donegan, Zalis, Clair, Adkins, Cheung and Lewis (2016): Persister formation in *Staphylococcus aureus* is associated with ATP depletion. *Nature Microbiology*, **1 (5)**: 16051.
Conway and Cohen (2015): Commensal and pathogenic *Escherichia coli* metabolism in the gut. *Microbiology Spectrum*, **3 (3)**: MBP-0006-2014.
Costello, Stagaman, Dethlefsen, Bohannan and Relman (2012): The application of ecological theory toward an understanding of the human microbiome. *Science*, **336 (6086)**: 1255–1262.
Cui, Iwamoto, Lian, Neoh, Maruyama, Horikawa and Hiramatsu (2006): Novel mechanism of antibiotic resistance originating in vancomycin-intermediate *Staphylococcus aureus. Antimicrobial Agents and Chemotherapy*, **50 (2)**: 428–438.
Cui, Ma, Sato, Okuma, Tenover, Mamizuka, Gemmell, Kim, Ploy, El Solh, Ferraz and Hiramatsu (2003): Cell wall thickening is a common feature of vancomycin resistance in *Staphylococcus aureus. Journal of Clinical Microbiology*, **41 (1)**: 5–14.
Cui, Murakami, Kuwahara-Arai, Hanaki and Hiramatsu (2000): Contribution of a thickened cell wall and its glutamine nonamidated component to the vancomycin resistance expressed by *Staphylococcus aureus* Mu50. *Antimicrobial Agents and Chemotherapy*, **44 (9)**: 2276–2285.
Culp, Waglechner, Wang, Fiebig-Comyn, Hsu, Koteva, Sychantha, Coombes, Van Nieuwenhze, Brun and Wright (2020): Evolution-guided discovery of antibiotics that inhibit peptidoglycan remodelling. *Nature*, **578 (7796)**: 582–587.
Dargis and Malouin (1994): Use of biotinylated beta-lactams and chemiluminescence for study and purification of penicillin-binding proteins in bacteria. *Antimicrobial Agents and Chemotherapy*, **38 (5)**: 973–980.
Dathe, Nikolenko, Meyer, Beyermann and Bienert (2001): Optimization of the antimicrobial activity of magainin peptides by modification of charge. *FEBS Letters*, **501 (2–3)**: 146–150.
Davies and Davies (2010): Origins and evolution of antibiotic resistance. *Microbiology and Molecular Biology Reviews*, **74 (3)**: 417–433.
De Filippo, Cavalieri, Di Paola, Ramazzotti, Poullet, Massart, Collini, Pieraccini and Lionetti (2010): Impact of diet in shaping gut microbiota revealed by a comparative study in children from Europe and rural Africa. *Proceedings of the National Academy of Sciences of the United States of America*, **107 (33)**: 14691–14696.
Debray, Herbert, Jaffe, Crits-Christoph, Power and Koskella (2021): Priority effects in microbiome assembly. *Nature Reviews Microbiology*, **20 (2)**: 109–121.
Deisinger, Arts, Kotsogianni, Puls, Grein, Ortiz-López, Martin, Müller, Genilloud and Schneider (2023): Dual targeting of the class V lanthipeptide antibiotic cacaoidin. *iScience*, **26 (4)**: 106394.
Demel, Peelen, Siezen, Kruijff and Kuipers (1996): Nisin Z, Mutant Nisin Z and Lacticin 481 Interactions with Anionic Lipids Correlate with Antimicrobial Activity. A Monolayer Study. *European Journal of Biochemistry*, **235 (1–2)**: 267–274.
Deo and Deshmukh (2019): Oral microbiome: Unveiling the fundamentals. *Journal of Oral and Maxillofacial Pathology*, **23 (1)**: 122.
Dickson, Kumar, Jacques, Malmirchegini, Spirig, Mackay, Clubb, Guss and Gell (2014): Structure of the hemoglobin-IsdH complex reveals the molecular basis of iron capture by *Staphylococcus aureus. Journal of Biological Chemistry*, **289 (10)**: 6728–6738.
Dietrich, Steffens, Sass and Bierbaum (2021): The hypersusceptible antibiotic screening strain *Staphylococcus aureus* SG511-Berlin harbors multiple mutations in regulatory genes. *International Journal of Medical Microbiology*, **311 (8)**: 151545.
Díez-Aguilar, Ruiz-Garbajosa, Fernández-Olmos, Guisado, Campo, Quereda, Cantón and Meseguer (2013): Non-diphtheriae *Corynebacterium species*: an emerging respiratory pathogen. *European Journal of Clinical Microbiology & Infectious Diseases*, **32 (6)**: 769–772.

DiGiulio, Callahan, McMurdie, Costello, Lyell, Robaczewska, Sun, Goltsman, Wong, Shawa, Stevenson, Holmes and Relman (2015): Temporal and spatial variation of the human microbiota during pregnancy. *Proceedings of the National Academy of Sciences of the United States of America*, **112 (35)**: 11060–11065.

Dinges, Orwin and Schlievert (2000): Exotoxins of *Staphylococcus aureus. Clinical Microbiology Reviews*, **13 (1)**: 16–34.

Do, Schaefer, Santiago, Coe, Fernandes, Kahne, Pinho and Walker (2020): *Staphylococcus aureus* cell growth and division are regulated by an amidase that trims peptides from uncrosslinked peptidoglycan. *Nature Microbiology*, **5 (2)**: 291–303.

Domadia, Bhunia, Sivaraman, Swarup and Dasgupta (2008): Berberine targets assembly of *Escherichia coli* cell division protein FtsZ. *Biochemistry*, **47 (10)**: 3225–3234.

Dombrowski and Winston (2008) Clinical failures of appropriately-treated methicillin-resistant *Staphylococcus aureus* infections *Journal of Infection*, **57 (2)**: 110–115.

Domenech, Dufrêne, Van Bambeke, Tukens and Mingeot-Leclercq (2010): Interactions of oritavancin, a new semi-synthetic lipoglycopeptide, with lipids extracted from *Staphylococcus aureus. Biochimica et Biophysica Acta (BBA) - Biomembranes*, **1798 (10)**: 1876–1885.

Domenech, Francius, Tulkens, Van Bambeke, Dufrêne and Mingeot-Leclercq (2009): Interactions of oritavancin, a new lipoglycopeptide derived from vancomycin, with phospholipid bilayers: effect on membrane permeability and nanoscale lipid membrane organization. *Biochimica et Biophysica Acta (BBA) - Biomembranes*, **1788 (9)**: 1832–1840.

Donovan and Bramkamp (2009): Characterization and subcellular localization of a bacterial flotillin homologue. *Microbiology*, **155 (6)**: 1786–1799.

Dörries, Schlueter and Lalk (2014): Impact of antibiotics with various target sites on the metabolome of *Staphylococcus aureus. Antimicrobial Agents and Chemotherapy*, **58 (12)**: 7151–7163.

Draper, Cotter, Hill and Ross (2015): Lantibiotic resistance. *Microbiology and Molecular Biology Reviews*, **79 (2)**: 171–191.

Driessen, van den Hooven, Kuiper, Van de Camp, Sahl, Konings and Konings (1995): Mechanistic studies of lantibiotic-induced permeabilization of phospholipid vesicles. *Biochemistry*, **34 (5)**: 1606–1614.

Dubrac, Boneca, Poupel and Msadek (2007): New insights into the WalK/WalR (YycG/YycF) essential signal transduction pathway reveal a major role in controlling cell wall metabolism and biofilm formation in *Staphylococcus aureus. Journal of Bacteriology*, **189 (22)**: 8257–8269.

Ducret, Quardokus and Brun (2016): MicrobeJ, a tool for high throughput bacterial cell detection and quantitative analysis. *Nature Microbiology*, **1 (7)**, 16077.

Duncan, Louis, Thomson and Flint (2009): The role of pH in determining the species composition of the human colonic microbiota. *Environmental Microbiology*, **11 (8)**: 2112–2122.

Eagle (1954): The binding of penicillin in relation to its cytotoxic action I. correlation between the penicillin sensitivity and combining activity of intact bacteria and cell-free extracts. *Journal of Experimental Medicine*, **99 (3)**: 207–226.

Economou, Cocklin and Loll (2013): High-resolution crystal structure reveals molecular details of target recognition by bacitracin. *Proceedings of the National Academy of Sciences of the United States of America*, **110 (35)**: 14207–14212.

Egan, Cleverley, Peters, Lewis and Vollmer (2017): Regulation of bacterial cell wall growth. *The FEBS Journal*, **284 (6)**: 851–867.

Ekkelenkamp, Hanssen, Hsu, De Jong, Milatovic, Verhoef and Van Nuland (2005): Isolation and structural characterization of epilancin 15X, a novel lantibiotic from a clinical strain of *Staphylococcus epidermidis. FEBS Letters*, **579 (9)**: 1917–1922.

Groussin, Poyet, Sistiaga, Kearney, Moniz, Noel, Hooker, Gibbons, Segurel, Froment, Mohamed, Fezeu, Juimo, Lafosse, Tabe, Girard, Iqaluk, Nguyen, Shapiro, Lehtimäki and Alm (2021): Elevated rates of horizontal gene transfer in the industrialized human microbiome. *Cell,* **184 (8)**: 2053-2067.

Elsen, Lu, Parthasarathy, Reid, Sharma, Soisson and Lumb (2012): Mechanism of action of the cell-division inhibitor PC190723: modulation of FtsZ assembly cooperativity. *Journal of the American Chemical Society*, **134 (30)**: 12342–12345.

Emami, Guyet, Kawai, Devi, Wu, Allenby, Daniel and Errington (2017): RodA as the missing glycosyltransferase in Bacillus subtilis and antibiotic discovery for the peptidoglycan polymerase pathway. *Nature Microbiology 2017 2:3*, **2 (3)**: 1–9.

Erickson, Anderson and Osawa (2010): FtsZ in bacterial cytokinesis: cytoskeleton and force generator all in one. *Microbiology and Molecular Biology Reviews*, **74 (4)**: 504–528.

Ernst, Staubitz, Mishra, Yang, Hornig, Kalbacher, Bayer, Kraus and Peschel (2009): The bacterial defensin resistance protein MprF consists of separable domains for lipid lysinylation and antimicrobial peptide repulsion. *PLoS Pathogens*, **5 (11)**: e1000660.

Ersoy, Gonçalves, Cavaco, Manna, Sobral, Nast, Proctor, Chambers, Cheung and Bayer (2022): Influence of sodium bicarbonate on wall teichoic acid synthesis and β-lactam sensitization in $NaHCO_3$-responsive and nonresponsive methicillin-resistant *Staphylococcus aureus. Microbiology Spectrum*, **10 (6)**: e03422-22.

Essig, Hofmann, Münch, Gayathri, Künzler, Kallio, Sahl, Wider, Schneider and Aebi (2014): Copsin, a novel peptide-based fungal antibiotic interfering with the peptidoglycan synthesis. *Journal of Biological Chemistry*, **289 (50)**: 34953–34964.

Eun, Foss, Kiekebusch, Pauw, Westler, Thanbichler and Weibel (2012): DCAP: a broad-spectrum antibiotic that targets the cytoplasmic membrane of bacteria. *Journal of the American Chemical Society*, **134 (28)**: 11322–11325.
Falony, Joossens, Vieira-Silva, Wang, Darzi, Faust, Kurilshikov, Bonder, Valles-Colomer, Vandeputte, Tito, Chaffron, Rymenans, Verspecht, Sutter, Lima-Mendez, D'hoe, Jonckheere, Homola, … Raes (2016): Population-level analysis of gut microbiome variation. *Science*, **352 (6285)**: 560–564.
Fang, X., Tiyanont, Zhang, Wanner, Boger and Walker (2006): The mechanism of action of ramoplanin and enduracidin. *Molecular BioSystems*, **2 (1)**: 69–76.
Fang, Z., Ban, Li, Yuan, Liu, Liu, Li, Wong, Lu, Sun and Yao (2018): A quinoline-based FtsZ inhibitor for the study of antimicrobial activity and synergistic effects with β-lactam antibiotics. *Journal of Pharmacological Sciences*, **137 (3)**: 283–289.
Farha, Leung, Sewell, D'Elia, Allison, Ejim, Pereira, Pinho, Wright and Brown (2013): Inhibition of WTA synthesis blocks the cooperative action of PBPs and sensitizes MRSA to β-lactams. *ACS Chemical Biology*, **8 (1)**: 226–233.
Farrand, Reniere, Ingmer, Frees and Skaar (2013): Regulation of host hemoglobin binding by the *Staphylococcus aureus* Clp Proteolytic system. *Journal of Bacteriology*, **195 (22)**: 5041–5050.
Ferrer-González, Huh, Al-Tameemi, Boyd, Lee and Pilch (2021): Impact of FtsZ inhibition on the localization of the penicillin binding proteins in methicillin-resistant *Staphylococcus aureus. Journal of Bacteriology*, **203 (16)**: e00204-21.
Ferrer-González, Kaul, Parhi, LaVoie and Pilch (2017): β-Lactam antibiotics with a high affinity for PBP2 act synergistically with the FtsZ-targeting agent TXA707 against methicillin-resistant *Staphylococcus aureus. Antimicrobial Agents and Chemotherapy*, **61 (9)**: e00863-1.
Fishkin (2015): Maytansinoid-BODIPY conjugates: application to microscale determination of drug extinction coefficients and for quantification of maytansinoid analytes. *Molecular Pharmaceutics*, **12 (6)**: 1745–1751.
Flowers and Grice (2020): The skin microbiota: balancing risk and reward. *Cell Host & Microbe*, **28 (2)**: 190–200.
Foster, J. A. and McVey Neufeld (2013): Gut-brain axis: How the microbiome influences anxiety and depression. *Trends in Neurosciences*, **36 (5)**: 305–312.
Foster, T. J. (2019): Surface Proteins of *Staphylococcus aureus. Microbiology Spectrum*, **7 (4)**: GPP3-0046-2018.
Foster, T. J., Geoghegan, Ganesh and Höök (2014): Adhesion, invasion and evasion: the many functions of the surface proteins of *Staphylococcus aureus. Nature Reviews Microbiology*, **12 (1)**: 49–62.
Foxley, Wright, Lam, Friedline, Strange, Xiao, Moen and Rice (2017): Targeting wall teichoic acid *in situ* with branched polyethylenimine potentiates β-lactam efficacy against MRSA. *ACS Medicinal Chemistry Letters*, **8 (10)**: 1083–1088.
Frankel and Schneewind (2012): Determinants of murein hydrolase targeting to cross-wall of *Staphylococcus aureus* peptidoglycan. *Journal of Biological Chemistry*, **287 (13)**: 10460–10471.
Fritz (2024): The elucidation of the modes of action of moenomycin and corallorazine A. *Ph. D. Thesis, Rheinische Friedrich-Wilhelms-Universität Bonn.*
Gajer, Brotman, Bai, Sakamoto, Schütte, Zhong, Koenig, Fu, Ma, Zhou, Abdo, Forney and Ravel (2012): Temporal dynamics of the human vaginal microbiota. *Science Translational Medicine*, **4 (132)**: 132ra52.
Gampe, Tsukamoto, Doud, Walker and Kahne (2013): Tuning the moenomycin pharmacophore to enable discovery of bacterial cell wall synthesis inhibitors. *Journal of the American Chemical Society*, **135 (10)**: 3776–3779.
Gampe, Tsukamoto, Wang, Walker and Kahne (2011): Modular synthesis of diphospholipid oligosaccharide fragments of the bacterial cell wall and their use to study the mechanism of moenomycin and other antibiotics. *Tetrahedron*, **67 (51)**: 9771–9778.
García-Fernández, Koch, Wagner, Fekete, Stengel, Schneider, Mielich-Süss, Geibel, Markert, Stigloher and Lopez (2017): membrane microdomain disassembly inhibits MRSA antibiotic resistance. *Cell*, **171 (6)**: 1354-1367.e20.
Gardete, Wu, Gill and Tomasz (2006): Role of VraSR in antibiotic resistance and antibiotic-induced stress response in *Staphylococcus aureus. Antimicrobial Agents and Chemotherapy*, **50 (10)**: 3424–3434.
Garrett (2015): Cancer and the microbiota. *Science*, **348 (6230)**: 80–86.
Gautam, Kim, Shoda, Sen, Deep, Luthra, Ferreira, Pinho and Spiegel (2015): An activity-based probe for studying crosslinking in live bacteria. *Angewandte Chemie International Edition*, **127 (36)**: 10638–10642.
Georgopapadakou, Dix and Mauriz (1986): Possible physiological functions of penicillin-binding proteins in *Staphylococcus aureus. Antimicrobial Agents and Chemotherapy*, **29 (2)**: 333–336.
Georgopapadakou and Liu (1980): Binding of beta-lactam antibiotics to penicillin-binding proteins of *Staphylococcus aureus* and *Streptococcus faecalis*: relation to antibacterial activity. *Antimicrobial Agents and Chemotherapy*, **18 (5)**: 834–836.
Georgopapadakou, Smith and Bonner (1982): Penicillin-binding proteins in a *Staphylococcus aureus* strain resistant to specific beta-lactam antibiotics. *Antimicrobial Agents and Chemotherapy*, **22 (1)**: 172–175.
Geriak, Haddad, Rizvi, Rose, Kullar, LaPlante, Yu, Vasina, Ouellette, Zervos, Nizet and Sakoulas (2019): Clinical data on daptomycin plus ceftaroline versus standard of care monotherapy in the treatment of methicillin-resistant *Staphylococcus aureus* bacteremia. *Antimicrobial Agents and Chemotherapy*, **63 (5)**: e02483-18.
Ghuysen, J. M. (1991): Serine beta-lactamases and penicillin-binding proteins. *Annual Review of Microbiology*, **45**: 37–67.
Ghuysen, J.-M. (1994): Molecular mechanisms: molecular structures of penicillin-binding proteins and β-lactamases. *Trends in Microbiology,* **2 (10)**: 372-380.
Giesbrecht, Kersten, Maidhof and Wecke (1998): Staphylococcal cell wall: morphogenesis and fatal variations in the presence of penicillin. *Microbiology and Molecular Biology Reviews*, **62 (4)**: 1371–1414.
Gilbert, Blaser, Caporaso, Jansson, Lynch and Knight (2018): Current understanding of the human microbiome. *Nature Medicine*, **24 (4)**: 392–400.

Goh and Klaenhammer (2015): Genetic mechanisms of prebiotic oligosaccharide metabolism in probiotic microbes *Annual Review of Food Science and Technology*, **6**: 137–156.

Gómez-Arrebola, Hernandez, Culp, Wright, Solano, Cava and Lasa (2023): *Staphylococcus aureus* susceptibility to complestatin and corbomycin depends on the VraSR two-component system. *Microbiology Spectrum*, **11 (5)**: e00370-23.

Goto, Li, Claesen, Shi, Bibb and van der Donk (2010): Discovery of unique lanthionine synthetases reveals new mechanistic and evolutionary insights. *PLOS Biology*, **8 (3)**: e1000339.

Grein, Müller, Scherer, Liu, Ludwig, Klöckner, Strach, Sahl, Kubitscheck and Schneider (2020): Ca^{2+}-Daptomycin targets cell wall biosynthesis by forming a tripartite complex with undecaprenyl-coupled intermediates and membrane lipids. *Nature Communications,* **11 (1)**: 1455.

Grein, Schneider and Sahl (2019): Docking on lipid II - a widespread mechanism for potent bactericidal activities of antibiotic peptides. *Journal of Molecular Biology*, **431 (18)**: 3520–3530.

Greninger, Chatterjee, Chan, Hamilton, Chambers and Chiu (2016): Whole-genome sequencing of methicillin-resistant *Staphylococcus aureus* resistant to fifth-generation cephalosporins reveals potential non-*mecA* mechanisms of resistance. *PLOS ONE*, **11 (2)**: e0149541.

Grice, Kong, Conlan, Deming, Davis, Young, Bouffard, Blakesley, Murray, Green, Turner and Segre (2009): Topographical and temporal diversity of the human skin microbiome. *Science*, **324 (5931)**: 1190–1192.

Grigg, Ukpabi, Gaudin and Murphy (2010); Structural biology of heme binding in the *Staphylococcus aureus* Isd system. *Journal of Inorganic Biochemistry*, **104 (3)**: 341–348.

Grigg, Vermeiren, Heinrichs and Murphy (2007): Heme coordination by *Staphylococcus aureus* IsdE. *Journal of Biological Chemistry*, **282 (39)**: 28815–28822.

Gueguen, Herpin, Aumelas, Garnier, Fievet, Escoubas, Bulet, Gonzalez, Lelong, Favrel and Bachère (2006): Characterization of a defensin from the oyster *Crassostrea gigas*: recombinant production, folding, solution structure, antimicrobial activities, and gene expression. *Journal of Biological Chemistry*, **281 (1)**: 313–323.

Gunetileke and Anwar (1966): Biosynthesis of uridine diphospho-N-acetyl muramic acid. *Journal of Biological Chemistry*, **241 (23)**: 5740–5743.

Haaber, Penadés and Ingmer (2017): Transfer of antibiotic resistance in *Staphylococcus aureus. Trends in Microbiology*, **25 (11)**: 893–905.

Hamburger, Hoertz, Lee, Senturia, Mccafferty and Loll (2009): A crystal structure of a dimer of the antibiotic ramoplanin illustrates membrane positioning and a potential Lipid II docking interface. *Proceedings of the National Academy of Sciences of the United States of America*, **106 (33)**: 13759-13764.

Hamilton, Alexander, Choo, Basuino, Da Costa, Severin, Chung, Aedo, Strynadka, Tomasz, Chatterjee and Chambers (2017): High-level resistance of *Staphylococcus aureus* to β-Lactam antibiotics mediated by penicillin-binding protein 4 (PBP4). *Antimicrobial Agents and Chemotherapy*, **61 (6)**: e02727-16.

Hammond, Sacco, Khan, Spanoudis, Hough-Neidig, Chen and Eswara (2022): GpsB coordinates cell division and cell surface decoration by wall teichoic acids in *Staphylococcus aureus*. *Microbiology Spectrum*, **10 (3)**: e01413-22.

Hanaki (1998): Activated cell-wall synthesis is associated with vancomycin resistance in methicillin-resistant *Staphylococcus aureus* clinical strains Mu3 and Mu50. *Journal of Antimicrobial Chemotherapy*, **42 (2)**: 199–209.

Hardt, Engels, Rausch, Gajdiss, Ulm, Sass, Ohlsen, Sahl, Bierbaum, Schneider and Grein (2017): The cell wall precursor lipid II acts as a molecular signal for the Ser/Thr kinase PknB of *Staphylococcus aureus. International Journal of Medical Microbiology*, **307 (1)**: 1–10.

Hardy, Dickey, Plaut, Riggins, Stibitz, Otto and Merrell (2019): *Corynebacterium pseudodiphtheriticum* exploits *Staphylococcus aureus* virulence components in a novel polymicrobial defense strategy. *mBio*, **10 (1)**: e02491-18.

Hardy and Merrell (2020): Friend or foe: interbacterial competition in the nasal cavity. *Journal of Bacteriology*, **203 (5)**: e00480-20.

Hartstra, Bouter, Bäckhed and Nieuwdorp (2015): Insights into the role of the microbiome in obesity and type 2 diabetes. *Diabetes Care*, **38 (1)**: 159–165.

Hashizume, Sawa, Harada, Igarashi, Adachi, Nishimura and Nomoto (2011): Tripropeptin C blocks the lipid cycle of cell wall biosynthesis by complex formation with undecaprenyl pyrophosphate. *Antimicrobial Agents and Chemotherapy*, **55 (8)**: 3821.

Hayden, Rezai, Hayes, Lolans, Quinn and Weinstein (2005): Development of daptomycin resistance *in vivo* in methicillin-resistant *Staphylococcus aureus. Journal of Clinical Microbiology*, **43 (10)**: 5285–5287.

Haydon, Stokes, Ure, Galbraith, Bennett, Brown, Baker, Barynin, Rice, Sedelnikova, Heal, Sheridan, Aiwale, Chauhan, Srivastava, Taneja, Collins, Errington and Czaplewski (2008): An inhibitor of FtsZ with potent and selective anti-staphylococcal activity. *Science*, **321 (5896)**: 1673–1675.

Hayes, Curtis, Wyke and Ward (1981): Decreased affinity of a penicillin-binding protein for β-lactam antibiotics in a clinical isolate of *Staphylococcus aureus* resistant to methicillin. *FEMS Microbiology Letters*, **10**: 119–122.

Hazmanian, Skaar, Gaspar, Humayun, Gornicki, Jelenska, Joachmiak, Missiakas and Schneewind (2003): Passage of heme-iron across the envelope of *Staphylococcus aureus. Science*, **299 (5608)**: 906–909.

Healy, Lessard, Roper, Knox and Walsh (2000): Vancomycin resistance in enterococci: reprogramming of the D-Ala–D-Ala ligases in bacterial peptidoglycan biosynthesis. *Chemistry & Biology*, **7 (5)**: 109–119.

Heaslet, Shaw, Mistry and Miller (2009): Characterization of the active site of *S. aureus* monofunctional glycosyltransferase (Mtg) by site-directed mutation and structural analysis of the protein complexed with moenomycin. *Journal of Structural Biology*, **167 (2)**: 129–135.

Hegde, Skinner, Lewis, Krause, Blais and Benton (2010): Activity of telavancin against heterogeneous vancomycin-intermediate *Staphylococcus aureus* (hVISA) *in vitro* and in an *in vivo* mouse model of bacteraemia. *Journal of Antimicrobial Chemotherapy*, **65 (4)**: 725–728.

Hegemann and Süssmuth (2020): Matters of class: coming of age of class III and IV lanthipeptides. *RSC Chemical Biology*, **1 (3)**: 110–127.
Heidrich, Pag, Josten, Metzger, Jack, Bierbaum, Jung and Sahl (1998): Isolation, characterization, and heterologous expression of the novel lantibiotic epicidin 280 and analysis of its biosynthetic gene cluster. *Applied and Environmental Microbiology*, **64 (9)**: 3140–3146.
Heilbronner, Krismer, Brötz-Oesterhelt and Peschel (2021): The microbiome-shaping roles of bacteriocins. *Nature Reviews Microbiology*, **19 (11)**: 726–739.
Henze and Berger-Bächi (1995): *Staphylococcus aureus* penicillin-binding protein 4 and intrinsic beta-lactam resistance. *Antimicrobial Agents and Chemotherapy*, **39 (11)**: 2415–2422.
Henze and Berger-Bächi (1996): Penicillin-binding protein 4 overproduction increases beta-lactam resistance in *Staphylococcus aureus. Antimicrobial Agents and Chemotherapy*, **40 (9)**: 2121–2125.
Heptinstall, Archibald and Baddiley (1970): Teichoic acids and membrane function in bacteria. *Nature*, **225 (5232)**: 519–521.
Herbert, Ziebandt, Ohlsen, Schäfer, Hecker, Albrecht, Novick and Götz (2010): Repair of global regulators in *Staphylococcus aureus* 8325 and comparative analysis with other clinical isolates. *Infection and Immunity*, **78 (6)**: 2877–2889.
Higashi, Strominger and Sweeley (1967): Structure of a lipid intermediate in cell wall peptidoglycan synthesis: a derivative of a C55 isoprenoid alcohol. *Proceedings of the National Academy of Sciences of the United States of America*, **57 (6)**: 1878–1884.
Higgins, Chang, Debabov, Leung, Wu, Krause, Sandvik, Hubbard, Kaniga, Schmidt, Gao, Cass, Karr, Benton and Humphrey (2005): Telavancin, a multifunctional lipoglycopeptide, disrupts both cell wall synthesis and cell membrane integrity in methicillin-resistant *Staphylococcus aureus. Antimicrobial Agents and Chemotherapy*, **49 (3)**: 1127–1134.
Hill, C. M., Krause, Lewis, Blais, Benton, Mammen, Humphrey, Kinana and Janc (2010): Specificity of induction of the *vanA* and *vanB* operons in vancomycin-resistant enterococci by telavancin. *Antimicrobial Agents and Chemotherapy*, **54 (7)**: 2814–2818.
Hill, M. A., Lam, Reed, Harney, Wilson, Moen, Wright, Pinho and Rice (2019): BPEI-Induced delocalization of PBP4 potentiates β-lactams against MRSA. *Biochemistry*, **58 (36)**: 3813–3822.
Hirschwerk, Ginocchio, Bythrow and Condon (2006): Diminished susceptibility to daptomycin accompanied by clinical failure in a patient with methicillin-resistant *Staphylococcus aureus* bacteremia. *Infection Control & Hospital Epidemiology*, **27 (3)**: 315–317.
Homma, Nuxoll, Gandt, Ebner, Engels, Schneider, Götz, Lewis and Conlon (2016): Dual targeting of cell wall precursors by teixobactin leads to cell lysis. *Antimicrobial Agents and Chemotherapy,* **60 (11)**: 6510–6517.
Hort, Bertsche, Nozinovic, Dietrich, Schrötter, Mildenberger, Axtmann, Berscheid and Bierbaum (2021): The role of β-glycosylated wall teichoic acids in the reduction of vancomycin susceptibility in vancomycin-intermediate *Staphylococcus aureus*. *Microbiology Spectrum*, **9 (2)**: e00528-21.
Howden, McEvoy, Allen, Chua, Gao, Harrison, Bell, Coombs, Bennett-Wood, Porter, Robins-Browne, Davies, Seemann and Stinear (2011): Evolution of multidrug resistance during *Staphylococcus aureus* infection involves mutation of the essential two component regulator WalKR. *PLoS Pathogens*, **7 (11)**: e1002359.
Hsu, S. T. D., Breukink, Tischenko, Lutters, De Kruijff, Kaptein, Bonvin and Van Nuland (2004): The nisin–lipid II complex reveals a pyrophosphate cage that provides a blueprint for novel antibiotics. *Nature Structural & Molecular Biology*, **11 (10)**: 963–967.
Hsu, S.-T. D., Breukink, Bierbaum, Sahl, de Kruijff, Kaptein, van Nuland and Bonvin (2003): NMR study of mersacidin and lipid II interaction in dodecylphosphocholine micelles. *Journal of Biological Chemistry*, **278 (15)**: 13110–13117.
Hu, Helm, Chen, Ye and Walker (2003): Ramoplanin inhibits bacterial transglycosylases by binding as a dimer to lipid II. *Journal of the American Chemical Society*, **125 (29)**: 8736–8737.
Huang, Shih, Lin, Tien, Cheng, Cheng, Wong and Ma (2012): Crystal structure of *Staphylococcus aureus* transglycosylase in complex with a lipid II analog and elucidation of peptidoglycan synthesis mechanism. *Proceedings of the National Academy of Sciences of the United States of America*, **109 (17)**: 6496–6501.
Huemer, Mairpady Shambat, Bergada-Pijuan, Söderholm, Boumasmoud, Vulin, Gómez-Mejia, Antelo Varela, Tripathi, Götschi, Marques Maggio, Hasse, Brugger, Bumann, Schuepbach and Zinkernagel (2021): Molecular reprogramming and phenotype switching in *Staphylococcus aureus* lead to high antibiotic persistence and affect therapy success. *Proceedings of the National Academy of Sciences of the United States of America*, **118 (7)**: e2014920118.
Huemer, Mairpady Shambat, Brugger and Zinkernagel (2020): Antibiotic resistance and persistence - Implications for human health and treatment perspectives. *EMBO Reports*, **21 (12)**: e51034.
Huemer, Mairpady Shambat, Hertegonne, Bergada-Pijuan, Chang, Pereira, Gómez-Mejia, Van Gestel, Bär, Vulin, Pfammatter, Stinear, Monk, Dworkin and Zinkernagel (2023): Serine-threonine phosphoregulation by PknB and Stp contributes to quiescence and antibiotic tolerance in *Staphylococcus aureus. Science Signaling*, **16 (766):** eabj8194.
Hummels, Berry, Li, Taguchi, Min, Walker, Marks and Bernhardt (2023): Coordination of bacterial cell wall and outer membrane biosynthesis. *Nature*, **615 (7951)**: 300–304.
Hurley, Heinrich, Hershfield, Demons and Weibel (2015): Membrane-targeting DCAP Analogues with broad-spectrum antibiotic activity against pathogenic bacteria. *ACS Medicinal Chemistry Letters*, **6 (4)**: 466–471.
Hutchings, Truman and Wilkinson (2019): Antibiotics: past, present and future. *Current Opinion in Microbiology* **51**: 72–80.

Ikuta, Swetschinski, Robles Aguilar, Sharara, Mestrovic, Gray, Davis Weaver, Wool, Han, Gershberg Hayoon, Aali, Abate, Abbasi-Kangevari, Abbasi-Kangevari, Abd-Elsalam, Abebe, Abedi, Abhari, Abidi, … Naghavi (2022): Global mortality associated with 33 bacterial pathogens in 2019: a systematic analysis for the Global Burden of Disease Study 2019. *The Lancet*, **400 (10369)**: 2221–2248.

Ito and Strominger (1973): Enzymatic synthesis of the peptide in bacterial uridine nucleotides. *Journal of Biological Chemistry*, **248 (9)**: 3131–3136.

Janek, Zipperer, Kulik, Krismer and Peschel (2016): High frequency and diversity of antimicrobial activities produced by nasal staphylococcus strains against bacterial competitors. *PLOS Pathogens*, **12 (8)**: e1005812.

Jensen, Li, Vestergaard, Dalsgaard, Frees and Leisner (2020): nisin damages the septal membrane and triggers DNA condensation in methicillin-resistant *Staphylococcus aureus. Frontiers in Microbiology*, **11**: 524279.

Jenul and Horswill (2019): Regulation of *Staphylococcus aureus* virulence. *Microbiology Spectrum*, **7 (2)**: GPP3-0031-2018.

Weng, You, Luan, Yang, Bae, Yu, Jiang and He (2016): Structure and mechanism of the essential two-component signal-transduction system WalKR in *Staphylococcus aureus. Nature Communications*, **7 (1)**: 11000.

Jia, O'Mara, Zuegg, Cooper and Mark (2013): Vancomycin: ligand recognition, dimerization and super-complex formation. *The FEBS Journal*, **280 (5)**: 1294–1307.

Jones, E. W., Carlson, Sivak and Ludington (2022): Stochastic microbiome assembly depends on context. *Proceedings of the National Academy of Sciences of the United States of America*, **119 (7)**: e2115877119.

Jones, R. N., Sader and Flamm (2013): Update of dalbavancin spectrum and potency in the USA: report from the SENTRY Antimicrobial Surveillance Program (2011). *Diagnostic Microbiology and Infectious Disease*, **75 (3)**: 304–307.

Jorgensen, Zasowski, Trinh, Lagnf, Bhatia, Sabagha, Abdul-Mutakabbir, Alosaimy, Mynatt, Davis and Rybak (2020): Daptomycin plus β-lactam combination therapy for methicillin-resistant *Staphylococcus aureus* bloodstream infections: a retrospective, comparative cohort study. *Clinical Infectious Diseases*, **71 (1)**: 1–10.

Kahan, Kahan, Cassidy and Kropp (1974): The mechanism of action of fosfomycin (phosphonomycin). *Annals of the New York Academy of Sciences*, **235 (1)**: 364–386.

Kajimura, Fujiwara, Yamada, Suzawa, Nishida, Oyamada, Hayashi, Yamagishi, Komatsuzawa and Sugai (2005): Identification and molecular characterization of an N-acetylmuramyl-L-alanine amidase Sle1 involved in cell separation of *Staphylococcus aureus. Molecular Microbiology*, **58 (4)**: 1087–1101.

Karlowsky, Nichol and Zhanel (2015): Telavancin: mechanisms of action, *in vitro* activity, and mechanisms of resistance. *Clinical Infectious Diseases*, **61 (S2)**: S58–S68.

Käshammer, van den Ent, Jeffery, Jean, Hale and Löwe (2023): Cryo-EM structure of the bacterial divisome core complex and antibiotic target FtsWIQBL. *Nature Microbiology*, **8 (6)**: 1149–1159.

Kasianowicz, Benz and McLaughlin (1984): The kinetic mechanism by which CCCP (carbonyl cyanidem-chlorophenylhydrazone) transports protons across membranes. *The Journal of Membrane Biology*, **82 (2)**: 179–190.

Kaul, Mark, Parhi, LaVoie and Pilch (2016): Combining the FtsZ-targeting prodrug TXA709 and the cephalosporin cefdinir confers synergy and reduces the frequency of resistance in methicillin-resistant *Staphylococcus aureus. Antimicrobial Agents and Chemotherapy*, **60 (7)**: 4290–4296.

Kaul, Mark, Zhang, Parhi, Lyu, Pawlak, Saravolatz, Saravolatz, Weinstein, LaVoie and Pilch (2015): TXA709, an FtsZ-targeting benzamide prodrug with improved pharmacokinetics and enhanced *in vivo* efficacy against methicillin-resistant *Staphylococcus aureus. Antimicrobial Agents and Chemotherapy*, **59 (8)**: 4845–4855.

Kaur, Rausch, Malakar, Watson, Damle, Chawla, Srinivasan, Sharma, Schneider, Jhingan, Saini, Mohanty, Grein and Nandicoori (2019): LipidII interaction with specific residues of *Mycobacterium tuberculosis* PknB extracytoplasmic domain governs its optimal activation. *Nature Communications*, **10 (1)**: 1231.

Kawai, F., Shoda, Harashima, Sadaie, Hara and Matsumoto (2004): Cardiolipin domains in *Bacillus subtilis* marburg membranes. *Journal of Bacteriology*, **186 (5)**: 1475–1483.

Kawai, Y., Kawai, Mackenzie, Dashti, Kepplinger, Waldron and Errington (2023): On the mechanisms of lysis triggered by perturbations of bacterial cell wall biosynthesis. *Nature Communications*, **14 (1)**: 4123.

Kawai, Y., Mercier, Mickiewicz, Serafini, Sório de Carvalho and Errington (2019): Crucial role for central carbon metabolism in the bacterial L-form switch and killing by β-lactam antibiotics. *Nature Microbiology*, **4 (10)**: 1716–1726.

Kim, S. G., Becattini, Moody, Shliaha, Littmann, Seok, Gjonbalaj, Eaton, Fontana, Amoretti, Wright, Caballero, Wang, Jung, Morjaria, Leiner, Qin, Ramos, Cross, … Pamer (2019): Microbiota-derived lantibiotic restores resistance against vancomycin-resistant Enterococcus. *Nature*, **572 (7771)**: 665–669.

Kim, S. J., Cegelski, Stueber, Singh, Dietrich, Tanaka, Parr, Far and Schaefer (2008): Oritavancin exhibits dual mode of action to inhibit cell-wall biosynthesis in *Staphylococcus aureus*. *Journal of Molecular Biology*, **377 (1)**: 281–293.

Kim, S. J., Singh and Schaefer (2009): Oritavancin binds to isolated protoplast membranes but not intact protoplasts of *Staphylococcus aureus*. *Journal of Molecular Biology*, **391 (2)**: 414–425.

Kim, S. J., Singh, Wohlrab, Yu, Patti, O'Connor, Vannieuwenhze and Schaefer (2013): Isotridecanyl side chain of plusbacin-A3 is essential for the transglycosylase inhibition of peptidoglycan biosynthesis. *Biochemistry*, **52 (11)**: 1973.

Kim, S. J., Tanaka, Dietrich, Rafai Far and Schaefer (2013): Locations of the hydrophobic side chains of lipoglycopeptides bound to the peptidoglycan of *Staphylococcus aureus*. *Biochemistry*, **52 (20)**: 3405–3414.

Kimi, Cegelski, Preobrazhenskaya and Schaefer (2006): Structures of *Staphylococcus aureus* cell-wall complexes with vancomycin, eremomycin, and chloroeremomycin derivatives by13C{19F} and15N{19F} rotational-echo double resonance. *Biochemistry*, **45 (16)**: 5235–5250.

Kirshner, Aguet, Sage and Unser (2013): 3-D PSF fitting for fluorescence microscopy: implementation and localization application. *Journal of Microscopy*, **249 (1)**: 13–25.
Klatt, Brammananth, O'Callaghan, Kouremenos, Tull, Crellin, Coppel and McConville (2018): Identification of novel lipid modifications and intermembrane dynamics in *Corynebacterium glutamicum* using high-resolution mass spectrometry. *Journal of Lipid Research*, **59 (7)**: 1190–1204.
Klein, Van Boeckel, Martinez, Pant, Gandra, Levin, Goossens and Laxminarayan (2018): Global increase and geographic convergence in antibiotic consumption between 2000 and 2015. *Proceedings of the National Academy of Sciences of the United States of America*, **115 (15)**: 3463–3470.
Kleinschmidt, Huygens, Faoagali, Rathnayake and Hafner (2015): *Staphylococcus epidermidis* as a cause of bacteremia. *Future Microbiology*, **10 (11)**: 1859–1879.
Kluytmans and Wertheim (2005): Nasal carriage of *Staphylococcus aureus* and prevention of nosocomial infections. *Infection*, **33 (1)**: 3–8.
Knerr and van der Donk (2012): Chemical synthesis and biological activity of analogues of the lantibiotic epilancin 15X *Journal of the American Chemical Society*, **134 (18)**: 7648–7651.
Koch, Wermser, Acosta, Kricks, Stengel, Yepes and Lopez (2017): Attenuating *Staphylococcus aureus* virulence by targeting flotillin protein scaffold activity. *Cell Chemical Biology*, **24 (7)**: 845-857.e6.
Kohanski, Dwyer and Collins (2010): How antibiotics kill bacteria: From targets to networks. *Nature Reviews Microbiology*, **8 (6)**: 423–435.
Kohanski, Dwyer, Hayete, Lawrence and Collins (2007): A common mechanism of cellular death induced by bactericidal antibiotics. *Cell*, **130 (5)**: 797–810.
Kohga, Mori, Tanaka, Yoshikaie, Taniguchi, Fujimoto, Fritz, Schneider and Tsukazaki (2022): Crystal structure of the lipid flippase MurJ in a "squeezed" form distinct from its inward- and outward-facing forms. *Structure*, **30 (8)**: 1088-1097.e3.
Kohler, Weidenmaier and Peschel (2009): Wall teichoic acid protects *Staphylococcus aureus* against antimicrobial fatty acids from human skin. *Journal of Bacteriology*, **191 (13)**: 4482–4484.
Kommineni, Bretl, Lam, Chakraborty, Hayward, Simpson, Cao, Bousounis, Kristich and Salzman (2015): Bacteriocin production augments niche competition by enterococci in the mammalian gastrointestinal tract. *Nature*, **526 (7575)**: 719–722.
Koopman (2004): Modeling infection transmission. *Annual Review of Public Health,* **25**: 303–326.
Kordel, Benz and Sahl (1988): Mode of action of the staphylococcinlike peptide Pep 5: voltage-dependent depolarization of bacterial and artificial membranes. *Journal of Bacteriology*, **170 (1)**: 84–88.
Kosowska-Shick, Clark, Pankuch, McGhee, Dewasse, Beachel and Appelbaum (2009): Activity of telavancin against staphylococci and enterococci determined by MIC and resistance selection studies. *Antimicrobial Agents and Chemotherapy*, **53 (10)**: 4217–4224.
Kosowska-Shick, McGhee and Appelbaum (2010): Affinity of ceftaroline and other β-lactams for penicillin-binding proteins from *Staphylococcus aureus* and *Streptococcus pneumoniae. Antimicrobial Agents and Chemotherapy*, **54 (5)**: 1670–1677.
Krause, Blais, Lewis, Lunde, Barriere, Friedland, Kitt and Benton (2012): In vitro activity of telavancin and occurrence of vancomycin heteroresistance in isolates from patients enrolled in phase 3 clinical trials of hospital-acquired pneumonia. *Diagnostic Microbiology and Infectious Disease*, **74 (4)**: 429–431.
Krismer, Weidenmaier, Zipperer and Peschel (2017): The commensal lifestyle of *Staphylococcus aureus* and its interactions with the nasal microbiota. *Nature Reviews Microbiology 2017 15:11*, **15 (11)**: 675–687.
Kuehl, Morata, Meylan, Mensa and Soriano (2020): When antibiotics fail: a clinical and microbiological perspective on antibiotic tolerance and persistence of *Staphylococcus aureus*. *Journal of Antimicrobial Chemotherapy*, **75 (5)**: 1071–1086.
Kuipers, Stapels, Weerwind, Ko, Ruyken, Lee, van Kessel and Rooijakkers (2016): The *Staphylococcus aureus* polysaccharide capsule and Efb-dependent fibrinogen shield act in concert to protect against phagocytosis. *Microbiology*, **162 (7)**: 1185–1194.
Kuk, Hao, Guan and Lee (2019): Visualizing conformation transitions of the Lipid II flippase MurJ. *Nature Communications*, **10 (1)**: 1736.
Kuk, Mashalidis and Lee (2017): Crystal structure of the MOP flippase MurJ in an inward-facing conformation. *Nature Structural & Molecular Biology*, **24 (2)**: 171–176.
Kumar, K., Awasthi, Lee, Zanardi, Ruzsicska, Knudson, Tonge, Slayden and Ojima (2011): Novel trisubstituted benzimidazoles, targeting *Mtb* FtsZ, as a new class of antitubercular agents. *Journal of Medicinal Chemistry*, **54 (1)**: 374–381.
Kumar, S., Mollo, Kahne and Ruiz (2022): The bacterial cell wall: from lipid II flipping to polymerization. *Chemical Reviews*, **122 (9)**: 8884–8910.
Kuru, Hughes, Brown, Hall, Tekkam, Cava, De Pedro, Brun and Vannieuwenhze (2012): *In situ* probing of newly synthesized peptidoglycan in live bacteria with fluorescent D-amino acids. *Angewandte Chemie International Edition*, **51 (50)**: 12519.
Kuru, Radkov, Meng, Egan, Alvarez, Dowson, Booher, Breukink, Roper, Cava, Vollmer, Brun and VanNieuwenhze (2019): Mechanisms of incorporation for D-amino acid probes that target peptidoglycan biosynthesis. *ACS Chemical Biology,* **14 (12)**: 2745–2756.
Kuzin, Liu, Kelly and Knox (1995): Binding of cephalothin and cefotaxime to D-ala-D-ala-peptidase reveals a functional basis of a natural mutation in a low-affinity penicillin-binding protein and in extended-spectrum β-lactamases. *Biochemistry*, **34 (29)**: 9532–9540.

Lahiri and Alm (2016): Identification of non-PBP2a resistance mechanisms in *Staphylococcus aureus* after serial passage with ceftaroline: involvement of other PBPs. *Journal of Antimicrobial Chemotherapy*, **71 (11)**: 3050–3057.
Lambert and Neuhaus (1972): Mechanism of D-cycloserine action: alanine racemase from *Escherichia coli* W. *Journal of Bacteriology*, **110 (3)**: 978–987.
Lang, Carvalho, Baharoglu, & Mazel (2023): Aminoglycoside uptake, stress, and potentiation in Gram-negative bacteria: new therapies with old molecules. *Microbiology and Molecular Biology Reviews*, **87 (4)**
Laux, Peschel and Krismer (2019): *Staphylococcus aureus* colonization of the human nose and interaction with other microbiome members. *Microbiology Spectrum*, **7 (2)**: GPP3-0029-2018.
Laxminarayan (2022): The overlooked pandemic of antimicrobial resistance. *The Lancet*, **399 (10325)**: 606–607.
Laxminarayan, Duse, Wattal, Zaidi, Wertheim, Sumpradit, Vlieghe, Hara, Gould, Goossens, Greko, So, Bigdeli, Tomson, Woodhouse, Ombaka, Peralta, Qamar, Mir, … Cars (2013): Antibiotic resistance - the need for global solutions. *The Lancet Infectious Diseases*, **13 (12)**: 1057–1098.
Lázár, Snitser, Barkan and Kishony (2022): Antibiotic combinations reduce *Staphylococcus aureus* clearance. *Nature*, **610 (7932)**: 540–546.
Le Maréchal, Seyffert, Jardin, Hernandez, Jan, Rault, Azevedo, François, Schrenzel, van de Guchte, Even, Berkova, Thiéry, Fitzgerald, Vauto and Le Loir (2011): Molecular basis of virulence in *Staphylococcus aureus* mastitis. *PLOS ONE*, **6 (11)**: e27354.
Ledala, Wilkinson And Jayaswal (2006): Effects of oxacillin and tetracycline on autolysis, autolysin processing and atl transcription in *Staphylococcus aureus*. *International Journal of Antimicrobial Agents*, **27 (6)**: 518–524.
Ledger, Mesnage and Edwards (2022): Human serum triggers antibiotic tolerance in *Staphylococcus aureus. Nature Communications*, **13 (1)**: 2041.
Lee, B.-G., Park, Lee, Jeon, Sung, Paulsen, Rübsamen-Schaeff, Brötz-Oesterhelt and Song (2010): Structures of ClpP in complex with acyldepsipeptide antibiotics reveal its activation mechanism. *Nature Structural & Molecular Biology*, **17 (4)**: 471–478.
Lee, W., Schaefer, Qiao, Srisuknimit, Steinmetz, Müller, Kahne and Walker (2016): The mechanism of action of lysobactin. *Journal of the American Chemical Society*, **138 (1)**: 100–103.
Leeuw, Li, Zeng, Li, Buin, Lu, Breukink and Lu (2010): Functional interaction of human neutrophil peptide-1 with the cell wall precursor lipid II. *FEBS Letters*, **584 (8)**: 1543–1548.
Leimkuhler, Chen, Barrett, Panzone, Sun, Falcone, Oberthür, Donadio, Walker and Kahne (2005): Differential inhibition of *Staphylococcus aureus* PBP2 by glycopeptide antibiotics. *Journal of the American Chemical Society*, **127 (10)**: 3250–3251.
Łęski and Tomasz (2005): Role of penicillin-binding protein 2 (PBP2) in the antibiotic susceptibility and cell wall cross-linking of *Staphylococcus aureus*: Evidence for the cooperative functioning of PBP2, PBP4, and PBP2a. *Journal of Bacteriology*, **187 (5)**: 1815–1824.
Leuko, Legat, Fendrihan and Stan-Lotter (2004): Evaluation of the LIVE/DEAD BacLight kit for detection of extremophilic archaea and visualization of microorganisms in environmental hypersaline samples. *Applied and Environmental Microbiology*, **70 (11)**: 6884–6886.
Levin-Reisman, Ronin, Gefen, Braniss, Shoresh and Balaban (2017): Antibiotic tolerance facilitates the evolution of resistance. *Science*, **355 (6327)**: 826–830.
Lewis (2013): Platforms for antibiotic discovery. *Nature Reviews Drug Discovery*, **12 (5)**: 371–387.
Lim and Strynadka (2002): Structural basis for the β-lactam resistance of PBP2a from methicillin-resistant *Staphylococcus aureus. Nature Structural Biology,* **9 (11)**: 870–876.
Lima, Silva, Barbosa and Barreiro (2020): β-lactam antibiotics: an overview from a medicinal chemistry perspective. *European Journal of Medicinal Chemistry*, **208 (15)**: 112829.
Ling, Schneider, Peoples, Spoering, Engels, Conlon, Mueller, Schäberle, Hughes, Epstein, Jones, Lazarides, Steadman, Cohen, Felix, Fetterman, Millett, Nitti, Zullo, … Lewis (2015): A new antibiotic kills pathogens without detectable resistance. *Nature*, **517 (7535)**: 455–459.
Liu, C. M., Price, Hungate, Abraham, Larsen, Christensen, Stegger, Skov and Andersen (2015): *Staphylococcus aureus* and the ecology of the nasal microbiome. *Science Advances*, **1 (5)**: e1400216.
Liu, J., Gefen, Ronin, Bar-Meir and Balaban (2020): Effect of tolerance on the evolution of antibiotic resistance under drug combinations. *Science*, **367 (6474)**: 200–204.
Liu, L., Chen, Skogerbø, Zhang, Chen, He and Huang (2012): The human microbiome: A hot spot of microbial horizontal gene transfer. *Genomics*, **100 (5)**: 265–270.
Liu, Q., Liu, Meng, Lv, Liu, Liu, Wang, He, Qin, Wang, Dai, Otto and Li (2020): *Staphylococcus epidermidis* contributes to healthy maturation of the nasal microbiome by stimulating antimicrobial peptide production. *Cell Host & Microbe*, **27 (1)**: 68-78.e5.
Lloyd, Schofield, Goddard and Taylor (2020): *De novo* resistance to Arg_{10}-teixobactin occurs slowly and is costly. *Antimicrobial Agents and Chemotherapy*, **65 (1)**: e01152-20.
Lloyd-Price, Abu-Ali and Huttenhower (2016): The healthy human microbiome. *Genome Medicine*, **8 (1)**: 1–11.
Lloyd-Price, Mahurkar, Rahnavard, Crabtree, Orvis, Hall, Brady, Creasy, McCracken, Giglio, McDonald, Franzosa, Knight, White and Huttenhower (2017): Strains, functions and dynamics in the expanded human microbiome project. *Nature*, **550 (7674)**: 61–66.
Lo, Men, Branstrom, Helm, Yao, Goldman and Walker (2000): A new mechanism of action proposed for ramoplanin. *Journal of the American Chemical Society*, **122 (14)**: 3540–3541.
Lopatkin, Stokes, Zheng, Yang, Takahashi, You and Collins (2019): Bacterial metabolic state more accurately predicts antibiotic lethality than growth rate. *Nature Microbiology*, **4 (12)**: 2109–2117.

Lord, Velle, Dyche Mullins and Fritz-Laylin (2020): SuperPlots: Communicating reproducibility and variability in cell biology. *The Journal of Cell Biology*, **219 (6)**: e202001064.
Lovering, De Castro, Lim and Strynadka (2007): Structural insight into the transglycosylation step of bacterial cell-wall biosynthesis. *Science*, **315 (5817)**: 1402–1405.
Lowy (1998): *Staphylococcus aureus* infections. *New England Journal of Medicine*, **339 (8)**: 520–532.
Lu, X., Wang, Guo, Zhang, Hu, Nie, Yang, Li, Wang, Li, Lu, Li, Zhang, Sun, Pang and You (2023): Antibacterial activity of an FtsZ inhibitor celastrol and its synergistic effect with vancomycin against enterococci *in vitro* and *in vivo. Microbiology Spectrum*, **11 (1)**: e03699-22.
Lu, Y., Chen, Zhao, Cao, Chen, Pan, Wang, Huang, Huang, Liu, Li, Bae, Liang and Lan (2023): Modulation of MRSA virulence gene expression by the wall teichoic acid enzyme TarO. *Nature Communications*, **14 (1)**: 1594.
Ludwig (2023): Lipid II-binding antibiotics – differential antibiotic activities beyond sequestration of the central peptidoglycan precursor. *Ph. D. Thesis, Rheinische Friedrich-Wilhelms-Universität Bonn.*
Lui, Gao, Cheung, Jin, Sun, Kan, Wong, Chiou, Lin, Chan, Leung, Chan, Chen, Chan and Wong (2019): Boosting the efficacy of anti-MRSA β-lactam antibiotics via an easily accessible, non-cytotoxic and orally bioavailable FtsZ inhibitor. *European Journal of Medicinal Chemistry*, **163 (1)**: 95–115.
Lund, Wacnik, Turner, Cotterell, Walther, Fenn, Grein, Wollman, Leake, Olivier, Cadby, Mesnage, Jones and Foster (2018): Molecular coordination of *Staphylococcus aureus* cell division. *eLife*, **7**: e32057.
Lunde, Hartouni, Janc, Mammen, Humphrey and Benton (2009): Telavancin disrupts the functional integrity of the bacterial membrane through targeted interaction with the cell wall precursor lipid II. *Antimicrobial Agents and Chemotherapy*, **53 (8)**: 3375–3383.
Lunde, Rexer, Hartouni, Axt and Benton (2010): Fluorescence microscopy demonstrates enhanced targeting of telavancin to the division septum of *Staphylococcus aureus*. *Antimicrobial Agents and Chemotherapy*, **54 (5)**: 2198–2200.
Madrigal, Basuino and Chambers (2005): Efficacy of telavancin in a rabbit model of aortic valve endocarditis due to methicillin-resistant *Staphylococcus aureus* or vancomycin-intermediate *Staphylococcus aureus. Antimicrobial Agents and Chemotherapy*, **49 (8)**: 3163–3165.
Mahasenan, Molina, Bouley, Batuecas, Fisher, Hermoso, Chang and Mobashery (2017): Conformational dynamics in penicillin-binding protein 2a of methicillin-resistant *Staphylococcus aureus*, allosteric communication network and enablement of catalysis. *Journal of the American Chemical Society*, **139 (5)**: 2102–2110.
Mainous (2006): Nasal carriage of *Staphylococcus aureus* and methicillin-resistant *S. aureus* in the United States, 2001-2002. *The Annals of Family Medicine*, **4 (2)**: 132–137.
Maki, Miura and Yamano (2001): Katanosin B and Plusbacin A3, inhibitors of peptidoglycan synthesis in methicillin-resistant *Staphylococcus aureus. Antimicrobial Agents and Chemotherapy*, **45 (6)**: 1823.
Maki, Yamaguchi and Murakami (1994): Cloning and characterization of a gene affecting the methicillin resistance level and the autolysis rate in *Staphylococcus aureus. Journal of Bacteriology*, **176 (16)**: 4993–5000.
Mangili, Bica, Snydman and Hamer (2005) Daptomycin-resistant, methicillin-resistant *Staphylococcus aureus* bacteremia. *Clinical Infectious Diseases*, **40 (7)**: 1058–1060.
Mann, Müller, Xiao, Pereira, Yang, Ho Lee, Wang, Trzeciak, Schneeweis, dos Santos, Murgolo, She, Gill, Balibar, Labroli, Su, Flattery, Sherborne, Maier, … Roemer (2013): Murgocil is a highly bioactive staphylococcal-specific inhibitor of the peptidoglycan glycosyltransferase enzyme MurG. *ACS Chemical Biology*, **8 (11)**: 2442–2451.
Marcos and Camins (2010): Successful treatment of vancomycin-intermediate *Staphylococcus aureus* pacemaker lead infective endocarditis with telavancin. *Antimicrobial Agents and Chemotherapy*, **54 (12)**: 5376–5378.
Marmont, Orta, Corey, Sychantha, Galliano, Li, Baileeves, Greene, Stansfeld, William M. Clemons and Bernhardt (2023): A feedback control mechanism governs the synthesis of lipid-linked precursors of the bacterial cell wall *BioRxiv*, 2023.08.01.551478.
Marraffini, Ton-That, Zong, Narayana and Schneewind (2004): Anchoring of surface proteins to the cell wall of *Staphylococcus aureus*: a conserved arginine residue is required for efficient catalysis of sortase A. *Journal of Biological Chemistry*, **279 (36)**: 37763–37770.
Martínez, Böttiger, Schneider, Rodriguez, Sahl and Wiedemann (2008): Specific interaction of the unmodified bacteriocin lactococcin 972 with the cell wall precursor lipid II. *Applied and Environmental Microbiology*, **74 (15)**: 4666–4670.
Martínez-Caballero, Mahasenan, Kim, Molina, Feltzer, Lee, Bouley, Hesek, Fisher, Muñoz, Chang, Mobashery and Hermoso (2021): Integrative structural biology of the penicillin-binding protein-1 from *Staphylococcus aureus*, an essential component of the divisome machinery. *Computational and Structural Biotechnology Journal*, **19**: 5392–5405.
Mascio, Alder and Silverman (2007): Bactericidal action of daptomycin against stationary-phase and nondividing *Staphylococcus aureus* cells. *Antimicrobial Agents and Chemotherapy*, **51 (12)**: 4255–4260.
Maya-Martinez, Alexander, Otten, Ayala, Vollmer, Gray, Bougault, Burt, Laguri, Fonvielle, Arthur, Strynadka, Vollmer and Simorre (2019): Recognition of peptidoglycan fragments by the transpeptidase PBP4 from *Staphylococcus aureus*. *Frontiers in Microbiology*, **9**: 426432.
Mazmanian, Skaar, Gaspar, Humayun, Gornicki, Jelenska, Joachmiak, Missiakas and Schneewind (2003): Passage of heme-iron across the envelope of *Staphylococcus aureus. Science*, **299 (5608)**: 906–909.
Mazmanian, Ton-That, Su and Schneewind (2002): An iron-regulated sortase anchors a class of surface protein during *Staphylococcus aureus* pathogenesis. *Proceedings of the National Academy of Sciences of the United States of America*, **99 (4)**: 2293–2298.
McCormick, McGuire, Pittenger, Pittenger and Stark (1955): Vancomycin, a new antibiotic. I. Chemical and biologic properties. *Antibiotics Annual*, **3**: 606–611.

McEvoy, Tsuji, Gao, Seemann, Porter, Doig, Ngo, Howden and Stinear (2013): Decreased vancomycin susceptibility in *Staphylococcus aureus* caused by IS *256* tempering of WalKR expression. *Antimicrobial Agents and Chemotherapy*, **57 (7)**: 3240–3249.
McPherson and Popham (2003): Peptidoglycan synthesis in the absence of class A penicillin-binding proteins in *Bacillus subtilis. Journal of Bacteriology*, **185 (4)**: 1423–1431.
McQuillen and Xiao (2020): Insights into the structure, function, and dynamics of the bacterial cytokinetic FtsZ-ring. *Annual Review of Biophysics*, **49**: 309–341.
Medeiros-Silva, Jekhmane, Breukink and Weingarth (2019): Towards the native binding modes of antibiotics that target lipid II. *ChemBioChem*, **20 (14)**: 1731–1738.
Medeiros-Silva, Jekhmane, Paioni, Gawarecka, Baldus, Swiezewska, Breukink and Weingarth (2018): High-resolution NMR studies of antibiotics in cellular membranes. *Nature Communications*, **9 (1)**: 3963.
Meeske, Riley, Robins, Uehara, Mekalanos, Kahne, Walker, Kruse, Bernhardt and Rudner (2016): SEDS proteins are a widespread family of bacterial cell wall polymerases. *Nature,* **537 (7622)**: 634–638.
Memmi, Filipe, Pinho, Fu and Cheung (2008): *Staphylococcus aureus* PBP4 Is essential for β-Lactam resistance in community-acquired methicillin-resistant strains. *Antimicrobial Agents and Chemotherapy*, **52 (11)**: 3955–3966.
Mengin-Lecreulx and Van Heijenoort (1990): Correlation between the effects of fosfomycin and chloramphenicol on *Escherichia coli* cells. *FEMS Microbiology Letters*, **66** : 129–163.
Messelink, Meyer, Bramkamp and Broedersz (2021): Single-cell growth inference of *Corynebacterium glutamicum* reveals asymptotically linear growth. *eLife*, **10**: e70106.
Mielich-Süss, Wagner, Mietrach, Hertlein, Marincola, Ohlsen, Geibel and Lopez (2017): Flotillin scaffold activity contributes to type VII secretion system assembly in *Staphylococcus aureus. PLOS Pathogens*, **13 (11)**: e1006728.
Misawa, Kelley, Wang, Wang, Park, Birtel, Saslowsky and Lee (2015): *Staphylococcus aureus* colonization of the mouse gastrointestinal tract is modulated by wall teichoic acid, capsule, and surface proteins. *PLOS Pathogens*, **11 (7)**: e1005061.
Mitchell and Moyle (1957): Autolytic release and osmotic properties of “protoplasts” from *Staphylococcus aureus*. *Journal of General Microbiology*, **16 (1)**: 184–194.
Münch, Müller, Schneider, Kohl, Wenzel, Bandow, Maffioli, Sosio, Donadio, Wimmer and Sahl (2014): The lantibiotic NAI-107 binds to bactoprenol-bound cell wall precursors and impairs membrane functions. *Journal of Biological Chemistry*, **289 (17)**: 12063–12076.
Mohammadi, van Dam, Sijbrandi, Vernet, Zapun, Bouhss, Diepeveen-de Bruin, Nguyen-Distèche, de Kruijff and Breukink (2011): Identification of FtsW as a transporter of lipid-linked cell wall precursors across the membrane. *The EMBO Journal*, **30 (8)**: 1425–1432.
Moks, Abrahmsen, Nilsson, Hellman, Sjoquist and Uhlen (1986): Staphylococcal protein A consists of five IgG-binding domains. *European Journal of Biochemistry*, **156 (3)**: 637–643.
Monteiro, Covas, Rausch, Filipe, Schneider, Sahl and Pinho (2019): The pentaglycine bridges of *Staphylococcus aureus* peptidoglycan are essential for cell integrity. *Scientific Reports*, **9 (1)**: 5010.
Monteiro, Fernandes, Vaz, Pereira, Tavares, Ferreira, Pereira, Veiga, Kuru, Vannieuwenhze, Brun, Filipe and Pinho (2015): Cell shape dynamics during the staphylococcal cell cycle. *Nature Communications*, **6**: 8055.
Monteiro, Pereira, Reichmann, Saraiva, Fernandes, Veiga, Tavares, Santos, Ferreira, Macário, VanNieuwenhze, Filipe and Pinho (2018): Peptidoglycan synthesis drives an FtsZ-treadmilling-independent step of cytokinesis. *Nature*, **554 (7693)**: 528–532.
Moreillon, Entenza, Francioli, McDevitt, Foster, François and Vaudaux (1995): Role of *Staphylococcus aureus* coagulase and clumping factor in pathogenesis of experimental endocarditis. *Infection and Immunity*, **63 (12)**: 4738–4743.
Motulsky and Brown (2006): Detecting outliers when fitting data with nonlinear regression - A new method based on robust nonlinear regression and the false discovery rate. *BMC Bioinformatics*, **7 (1)**: 1–20.
Müller, Grein, Otto, Gries, Orlov, Zarubaev, Girard, Sher, Shamova, Roemer, François, Becher, Schneider and Sahl (2018): Differential daptomycin resistance development in *Staphylococcus aureus* strains with active and mutated *gra* regulatory systems. *International Journal of Medical Microbiology*, **308 (3)**: 335–348.
Müller, Münch, Schmidt, Reder-Christ, Schiffer, Bendas, Gross, Sahl, Schneider and Brötz-Oesterhelt (2012): Lipodepsipeptide empedopeptin inhibits cell wall biosynthesis through Ca^{2+}-dependent complex formation with peptidoglycan precursors. *Journal of Biological Chemistry*, **287 (24)**: 20270–20280.
Müller, Wenzel, Strahl, Grein, Saaki, Kohl, Siersma, Bandow, Sahl, Schneider and Hamoen (2016): Daptomycin inhibits cell envelope synthesis by interfering with fluid membrane microdomains. *Proceedings of the National Academy of Sciences of the United States of America*, **113 (45)**: 7077–7086.
Münch, Engels, Müller, Reder-Christ, Falkenstein-Paul, Bierbaum, Grein, Bendas, Sahl and Schneider (2015): Structural variations of the cell wall precursor lipid II and their influence on binding and activity of the lipoglycopeptide antibiotic oritavancin. *Antimicrobial Agents and Chemotherapy*, **59 (2)**: 772–781.
Münch, Roemer, Lee, Engeser, Sahl and Schneider (2012): Identification and *in vitro* analysis of the GatD/MurT enzyme-complex catalyzing lipid II amidation in *Staphylococcus aureus. PLoS Pathogens*, **8 (1)**: e1002509.
Murdoch and Skaar (2022): Nutritional immunity: the battle for nutrient metals at the host–pathogen interface. *Nature Reviews Microbiology*, **20 (11)**: 657–670.
Murray, Ikuta, Sharara, Swetschinski, Robles Aguilar, Gray, Han, Bisignano, Rao, Wool, Johnson, Browne, Chipeta, Fell, Hackett, Haines-Woodhouse, Kashef Hamadani, Kumaran, McManigal, … Naghavi (2022): Global burden of bacterial antimicrobial resistance in 2019: a systematic analysis. *The Lancet*, **399 (10325)**: 629-655.
Muryoi, Tiedemann, Pluym, Cheung, Heinrichs and Stillman (2008): Demonstration of the iron-regulated surface determinant (Isd) heme transfer pathway in *Staphylococcus aureus. Journal of Biological Chemistry*, **283 (42)**: 28125–28136.

Myrbråten, Stamsås, Chan, Angeles, Knutsen, Salehian, Shapaval, Straume and Kjos (2022): SmdA is a novel cell morphology determinant in *Staphylococcus aureus. mBio*, **13 (2)**: e03404-21.
Nakatsuji, Chen, Narala, Chun, Two, Yun, Shafiq, Kotol, Bouslimani, Melnik, Latif, Kim, Lockhart, Artis, David, Taylor, Streib, Dorrestein, Grier, … Gallo (2017): Antimicrobials from human skin commensal bacteria protect against *Staphylococcus aureus* and are deficient in atopic dermatitis. *Science Translational Medicine*, **9 (378)**: eaah4680.
Nakaya, Yabe, Mashalidis, Sato, Yamamoto, Hikiji, Katsuyama, Shinohara, Minato, Takahashi, Horiuchi, Yokota, Lee and Ichikawa (2022): Synthesis of macrocyclic nucleoside antibacterials and their interactions with MraY. *Nature Communications*, **13 (1)**: 7575.
Navarro, Vettiger, Ananda, Llopis, Allolio, Bernhardt and Chao (2022): Cell wall synthesis and remodelling dynamics determine division site architecture and cell shape in *Escherichia coli*. *Nature Microbiology*, **7 (10)**: 1621–1634.
Nega, Tribelli, Hipp, Stahl and Götz (2020): New insights in the coordinated amidase and glucosaminidase activity of the major autolysin (Atl) in *Staphylococcus aureus. Communications Biology*, **3 (1)**: 695.
Neuhaus (1960): The enzymatic synthesis of D-alanyl-D-alanine. *Biochemical and Biophysical Research Communications*, **3 (4)**: 401–405.
Neuhaus (1962): The Enzymatic synthesis of D-Alanyl-D-alanine. *Journal of Biological Chemistry*, **237 (3)**: 778–786.
Neuhaus and Lynch (1964): Enzymatic synthesis of N-alanyl-D-alanine. III. on the inhibition of D-Alanyl-D-alanine synthetase by the antibiotic D-cycloserine. *Biochemistry,* **3 (4)**: 471-480.
Neuhaus and Struve (1965): Enzymatic synthesis of analogs of the cell-wall precursor. I. kinetics and specificity of uridine diphospho-N-acetylmuramyl-L-alanyl-D-glutamyl-L-lysine:D-Alanyl-D-alanine ligase (adenosine diphosphate) from *Streptococcus faecalis* R. *Biochemistry*, **4 (1)**: 120–131.
Nguyen, Oikonomou, Ding, Kaplan, Yao, Chang, Beeby and Jensen (2019): Simulations suggest a constrictive force is required for Gram-negative bacterial cell division. *Nature Communications*, **10 (1)**: 1259.
Nguyen, Oikonomou and Jensen (2021): Simulations of proposed mechanisms of FtsZ-driven cell constriction. *Journal of Bacteriology*, **203 (3)**: :e00576-2.
Nilsson, Lee, Bremell, Rydén and Tarkowski (1997): The role of staphylococcal polysaccharide microcapsule expression in septicemia and septic arthritis. *Infection and Immunity*, **65 (10)**: 4216–4221.
Nitanai, Kikuchi, Kakoi, Hanamaki, Fujisawa and Aoki (2009): Crystal structures of the complexes between vancomycin and cell-wall precursor analogs. *Journal of Molecular Biology*, **385 (5)**: 1422–1432.
O'Connor, Singh, Chang, Kim, VanNieuwenhze and Schaefer (2017): Dual mode of action for plusbacin A3 in *Staphylococcus aureus. Journal of Physical Chemistry B*, **121 (7)**: 1499–1505.
Oeemig, Lynggaard, Knudsen, Hansen, Nørgaard, Schneider, Vad, Sandvang, Nielsen, Neve, Kristensen, Sahl, Otzen and Wimmer (2012): Eurocin, a new fungal defensin: structure, lipid binding, and its mode of action. *Journal of Biological Chemistry*, **287 (50)**: 42361–42372.
Oman and van der Donk (2009): Insights into the mode of action of the two-peptide lantibiotic haloduracin. *ACS Chemical Biology*, **4 (10)**: 865–874.
Omardien, Drijfhout, Vaz, Wenzel, Hamoen, Zaat and Brul (2018): Bactericidal activity of amphipathic cationic antimicrobial peptides involves altering the membrane fluidity when interacting with the phospholipid bilayer. *Biochimica et Biophysica Acta (BBA) - Biomembranes*, **1860 (11)**: 2404–2415.
O'Neill (2014): Antimicrobial resistance: tackling a crisis for the health and wealth of nations. *The Review on Antimicrobial Resistance. Wellcome collection.*
Ongpipattanakul, Desormeaux, DiCaprio, van der Donk, Mitchell and Nair (2022): Mechanism of action of ribosomally synthesized and post-translationally modified peptides. *Chemical Reviews*, **122 (18)**: 14722–14814.
Ono, Muratani and Matsumoto (2005): Mechanisms of resistance to imipenem and ampicillin in *Enterococcus faecalis*. *Antimicrobial Agents and Chemotherapy*, **49 (7)**: 2954–2958.
Ortiz-López, Carretero-Molina, Sánchez-Hidalgo, Martín, González, Román-Hurtado, de la Cruz, García-Fernández, Reyes, Deisinger, Müller, Schneider and Genilloud (2020): Cacaoidin, first member of the new lanthidin RiPP family. *Angewandte Chemie International Edition*, **59 (31)**: 12654–12658.
Osawa and Erickson (2013): Liposome division by a simple bacterial division machinery. *Proceedings of the National Academy of Sciences of the United States of America*, **110 (27)**: 11000–11004.
Ostash and Walker (2010): Moenomycin family antibiotics: Chemical synthesis, biosynthesis, and biological activity. *Natural Product Reports,* **27 (11)**: 1594-1617.
Otero, Rojas-Altuve, Llarrull, Carrasco-López, Kumarasiri, Lastochkin, Fishovitz, Dawley, Hesek, Lee, Johnson, Fisher, Chang, Mobashery and Hermoso (2013): How allosteric control of *Staphylococcus aureus* penicillin binding protein 2a enables methicillin resistance and physiological function. *Proceedings of the National Academy of Sciences of the United States of America*, **110 (42)**: 16808–16813.
Ottonello, Wyllie, Yahiaoui, Sun, Koelln, Homer, Johnson, Murray, Williams, Bolla, Robinson, Fallon, Soares da Costa and Moses (2023): Shapeshifting bullvalene-linked vancomycin dimers as effective antibiotics against multidrug-resistant gram-positive bacteria. *Proceedings of the National Academy of Sciences of the United States of America*, **120 (15)**
Paiva, Breukink and Mantovani (2011): Role of lipid II and membrane thickness in the mechanism of action of the lantibiotic bovicin HC5. *Antimicrobial Agents and Chemotherapy*, **55 (11)**: 5284–5293.
Parisot, Carey, Breukink, Chan, Narbad and Bonev (2008): Molecular mechanism of target recognition by subtilin, a class I lanthionine antibiotic. *Antimicrobial Agents and Chemotherapy*, **52 (2)**: 612–618.
Park, Gedi, Cho, Hyun, Lee, Kang, So and Yoon (2014): Characterization and *in vitro* inhibition studies of *Bacillus anthracis* FtsZ: a potential antibacterial target. *Applied Biochemistry and Biotechnology*, **172 (6)**: 3263–3270.
Parsons, Yao, Frank, Jackson and Rock (2012): Membrane disruption by antimicrobial fatty acids releases low-molecular-weight proteins from *Staphylococcus aureus*. *Journal of Bacteriology*, **194 (19)**: 5294–5304.

Patel (2015): Performance standards for antimicrobial susceptibility testing: twenty-fourth informational supplement. *CLSI M100 Performance Standards for Antimicrobial Susceptibility Testing,* **24**.
Patti, Kim, Yu, Dietrich, Tanaka, Parr, Far and Schaefer (2009): Vancomycin and oritavancin have different modes of action in *Enterococcus faecium. Journal of Molecular Biology*, **392 (5)**: 1178–1191.
Payne, Miller, Findlay, Anderson and Marks (2015): Time for a change: addressing R&D and commercialization challenges for antibacterials. *Philosophical Transactions of the Royal Society B: Biological Sciences*, **370 (1670)**: 20140086.
Pazos, Peters, Casanova, Palacios, VanNieuwenhze, Breukink, Vicente and Vollmer (2018): Z-ring membrane anchors associate with cell wall synthases to initiate bacterial cell division. *Nature Communications*, **9 (1)**: 5090.
Peirce and Alviña (2019): The role of inflammation and the gut microbiome in depression and anxiety. *Journal of Neuroscience Research*, **97 (10)**: 1223–1241.
Pereira, P. M., Filipe, Tomasz and Pinho (2007): Fluorescence ratio imaging microscopy shows decreased access of vancomycin to cell wall synthetic sites in vancomycin-resistant *Staphylococcus aureus. Antimicrobial Agents and Chemotherapy*, **51 (10)**: 3627–3633.
Pereira, S. F. F., Henriques, Pinho, De Lencastre and Tomasz (2007): Role of PBP1 in cell division of *Staphylococcus aureus. Journal of Bacteriology*, **189 (9)**: 3525–3531.
Pereira, S. F. F., Henriques, Pinho, De Lencastre and Tomasz (2009): Evidence for a dual role of PBP1 in the cell division and cell separation of *Staphylococcus aureus. Molecular Microbiology*, **72 (4)**: 895–904.
Perez, Cesbron, Shaw, Villicana, Tsui, Boersma, Ye, Tovpeko, Dekker, Holden and Winkler (2019): Movement dynamics of divisome proteins and PBP2x: FtsW in cells of *Streptococcus pneumoniae. Proceedings of the National Academy of Sciences of the United States of America*, **116 (8)**: 3211–3220.
Peschel, Otto, Jack, Kalbacher, Jung and Götz (1999): Inactivation of the *dlt* operon in *Staphylococcus aureus* confers sensitivity to defensins, protegrins, and other antimicrobial peptides. *Journal of Biological Chemistry*, **274 (13)**: 8405–8410.
Peschel, Vuong, Otto and Götz (2000): The D-alanine residues of *Staphylococcus aureus* teichoic acids alter the susceptibility to vancomycin and the activity of autolytic enzymes. *Antimicrobial Agents and Chemotherapy*, **44 (10)**: 2845–2847.
Petersen, C. and Round (2014): Defining dysbiosis and its influence on host immunity and disease. *Cellular Microbiology*, **16 (7)**: 1024–1033.
Petersen, J., Boysen, Fogh, Tabermann, Kofoed, King, Schrotz-King and Hansen (2009): Identification and characterization of a bioactive lantibiotic produced by *Staphylococcus warneri*. *Biological Chemistry*, **390 (5–6)**: 437–444.
Pfaller, Mendes, Sader and Jones (2010): Telavancin activity against Gram-positive bacteria isolated from respiratory tract specimens of patients with nosocomial pneumonia. *Journal of Antimicrobial Chemotherapy*, **65 (11)**: 2396–2404.
Piepenbreier, Diehl and Fritz (2019): Minimal exposure of lipid II cycle intermediates triggers cell wall antibiotic resistance. *Nature Communications*, **10 (1)**: 2733.
Pinho, De Lencastre and Tomasz (2000): Cloning, characterization, and inactivation of the Gene *pbpC*, encoding penicillin-binding protein 3 of *Staphylococcus aureus. Journal of Bacteriology*, **182 (4)**: 1074–1079.
Pinho, De Lencastre and Tomasz (2001): An acquired and a native penicillin-binding protein cooperate in building the cell wall of drug-resistant staphylococci. *Proceedings of the National Academy of Sciences of the United States of America*, **98 (19)**: 10886–10891.
Pinho and Errington (2005): Recruitment of penicillin-binding protein PBP2 to the division site of *Staphylococcus aureus* is dependent on its transpeptidation substrates. *Molecular Microbiology*, **55 (3)**: 799–807.
Pinho, Filipe, De Lencastre and Tomasz (2001): Complementation of the essential peptidoglycan transpeptidase function of penicillin-binding protein 2 (PBP2) by the drug resistance protein PBP2a in *Staphylococcus aureus. Journal of Bacteriology*, **183 (22)**: 6525–6531.
Pinho, Kjos and Veening (2013): How to get (a)round: Mechanisms controlling growth and division of coccoid bacteria. *Nature Reviews Microbiology,* **11 (9)**: 601–614.
Pishchany, Sheldon, Dickson, Alam, Read, Gell, Heinrichs and Skaar (2014): IsdB-dependent hemoglobin binding is required for acquisition of heme by *Staphylococcus aureus. The Journal of Infectious Diseases*, **209 (11)**: 1764–1772.
Pluym, Vermeiren, Mack, Heinrichs and Stillman (2007): Heme binding properties of *Staphylococcus aureus* IsdE. *Biochemistry*, **46 (44)**: 12777–12787.
Podoll, Rosen, Wang, Gao, Zhang and Wang (2023): A small-molecule membrane fluidizer re-sensitizes methicillin-resistant *Staphylococcus aureus* (MRSA) to β-lactam antibiotics. *Antimicrobial Agents and Chemotherapy*, **67 (10)**: e00051-23.
Portolés, Kiser, Bhasin, Chan and Lee (2001): *Staphylococcus aureus* Cap5O has UDP-ManNAc dehydrogenase activity and is essential for capsule expression. *Infection and Immunity*, **69 (2)**: 917–923.
Poupel, Moyat, Groizeleau, Antunes, Gribaldo, Msadek and Dubrac (2016): Transcriptional analysis and subcellular protein localization reveal specific features of the essential WalKR system in *Staphylococcus aureus. PLOS ONE*, **11 (3)**: e0151449.
Proctor, Creasy, Fettweis, Lloyd-Price, Mahurkar, Zhou, Buck, Snyder, Strauss, Weinstock, White and Huttenhower (2019): The integrative human microbiome project. *Nature*, **569 (7758)**: 641–648.
Puls, Brajtenbach, Schneider, Kubitscheck and Grein (2023): Inhibition of peptidoglycan synthesis is sufficient for total arrest of staphylococcal cell division. *Science Advances*, **9 (12)**: eade9023.

Puls, Winnerling, Power, Krüger, Brajtenbach, Johnson, Bilici, Camus, Fließwasser, Schneider, Sahl, Ghosal, Kubitscheck, Heilbronner, Grein, (2024): *Staphylococcus epidermidis* bacteriocin A37 kills natural competitors with a unique mechanism of action. *The ISME Journal*, wrae044

Qiao, Lebar, Schirner, Schaefer, Tsukamoto, Kahne and Walker (2014): Detection of lipid-linked peptidoglycan precursors by exploiting an unexpected transpeptidase reaction. *Journal of the American Chemical Society*, **136 (42)**: 14678–14681.

Qiao, Srisuknimit, Rubino, Schaefer, Ruiz, Walker and Kahne (2017): Lipid II overproduction allows direct assay of transpeptidase inhibition by β-lactams. *Nature Chemical Biology*, **13 (7)**: 793–798.

Qin, Yang, Li, Prifti, Chen, Shao, Guo, Le Chatelier, Yao, Wu, Zhou, Ni, Liu, Pons, Batto, Kennedy, Leonard, Yuan, Ding, … Li (2014): Alterations of the human gut microbiome in liver cirrhosis. *Nature*, **513 (7516)**: 59–64.

Que, Haefliger, Piroth, François, Widmer, Entenza, Sinha, Herrmann, Francioli, Vaudaux and Moreillon (2005): Fibrinogen and fibronectin binding cooperate for valve infection and invasion in *Staphylococcus aureus* experimental endocarditis. *Journal of Experimental Medicine*, **201 (10)**: 1627–1635.

Rausch, Deisinger, Ulm, Müller, Li, Hardt, Wang, Li, Sylvester, Engeser, Vollmer, Müller, Sahl, Lee and Schneider (2019): Coordination of capsule assembly and cell wall biosynthesis in *Staphylococcus aureus. Nature Communications*, **10 (1)**: 1404.

Ray, Jindal, Kunal, Surolia and Panda (2015): BT-benzo-29 inhibits bacterial cell proliferation by perturbing FtsZ assembly. *The FEBS Journal*, **282 (20)**: 4015–4033.

Rebets, Lupoli, Qiao, Schirner, Villet, Hooper, Kahne and Walker (2014): Moenomycin resistance mutations in *Staphylococcus aureus* reduce peptidoglycan chain length and cause aberrant cell division. *ACS Chemical Biology*, **9 (2)**: 459–467.

Reed, Atilano, Alves, Hoiczyk, Sher, Reichmann, Pereira, Roemer, Filipe, Pereira-Leal, Ligoxygakis and Pinho (2015): *Staphylococcus aureus* survives with a minimal peptidoglycan synthesis machine but sacrifices virulence and antibiotic resistance. *PLOS Pathogens*, **11 (5)**: e1004891.

Reed, Veiga, Jorge, Terrak and Pinho (2011): Monofunctional transglycosylases are not essential for *Staphylococcus aureus* cell wall synthesis. *Journal of Bacteriology*, **193 (10)**: 2549–2556.

Reichmann, Cassona and Gründling (2013): Revised mechanism of D-alanine incorporation into cell wall polymers in gram-positive bacteria. *Microbiology*, **159 (Pt_9)**: 1868–1877.

Reichmann, Tavares, Saraiva, Jousselin, Reed, Pereira, Monteiro, Sobral, VanNieuwenhze, Fernandes and Pinho (2019): SEDS–bPBP pairs direct lateral and septal peptidoglycan synthesis in *Staphylococcus aureus. Nature Microbiology*, **4 (8)**: 1368–1377.

Reithuber, Wixe, Ludwig, Muller, Uvell, Grein, Lindgren, Muschiol, Nannapaneni, Eriksson, Schneider, Normark, Henriques-Normark, Almqvist and Mellroth (2021): THCz: Small molecules with antimicrobial activity that block cell wall lipid intermediates. *Proceedings of the National Academy of Sciences of the United States of America*, **118 (47)**: e2108244118.

Renner and Weibel (2011): Cardiolipin microdomains localize to negatively curved regions of *Escherichia coli* membranes. *Proceedings of the National Academy of Sciences of the United States of America*, **108 (15)**: 6264–6269.

Repka, Chekan, Nair and van der Donk (2017): Mechanistic understanding of lanthipeptide biosynthetic enzymes. *Chemical Reviews*, **117 (8)**: 5457–5520.

Reynolds (1989): Structure, biochemistry and mechanism of action of glycopeptide antibiotics. *European Journal of Clinical Microbiology & Infectious Diseases,* **8 (11)**: 943-950.

Reynolds, Snaith, Maguire, Dutka-Malen and Courvalin (1994): Analysis of peptidoglycan precursors in vancomycin-resistant *Enterococcus gallinarum* BM4174. *Biochemical Journal*, **301 (1)**: 5–8.

Richmond (1969): Extrachromosomal elements and the spread of antibiotic resistance in bacteria. *Biochemical Journal*, **113 (2)**: 225–234.

Rieg, Joost, Weiß, Peyerl-Hoffmann, Schneider, Hellmich, Seifert, Kern and Kaasch (2017): Combination antimicrobial therapy in patients with *Staphylococcus aureus* bacteraemia - a post hoc analysis in 964 prospectively evaluated patients. *Clinical Microbiology and Infection*, **23 (6)**: 406.e1-406.e8.

Roberts, Sulaiman and Rybak (2015): Dalbavancin and oritavancin: an innovative approach to the treatment of gram-positive infections. *Pharmacotherapy: The Journal of Human Pharmacology and Drug Therapy*, **35 (10)**: 935–948.

Ronneau, Hill and Helaine (2021): Antibiotic persistence and tolerance: not just one and the same. *Current Opinion in Microbiology*, **64**: 76–81.

Rubino, Kumar, Ruiz, Walker and Kahne (2018): Membrane potential is required for MurJ function. *Journal of the American Chemical Society*, **140 (13)**: 4481–4484.

Rubino, Mollo, Kumar, Butler, Ruiz, Walker and Kahne (2020): Detection of transport intermediates in the peptidoglycan flippase MurJ identifies residues essential for conformational cycling. *Journal of the American Chemical Society*, **142 (12)**: 5482–5486.

Saeloh, Tipmanee, Jim, Dekker, Bitter, Voravuthikunchai, Wenzel, & Hamoen (2018): The novel antibiotic rhodomyrtone traps membrane proteins in vesicles with increased fluidity. *PLOS Pathogens*, **14 (2)**: e1006876.

Sage, Donati, Soulez, Fortun, Schmit, Seitz, Guiet, Vonesch and Unser (2017): DeconvolutionLab2: An open-source software for deconvolution microscopy. *Methods*, **115**: 28–41.

Sahl (1985): Influence of the staphylococcinlike peptide Pep 5 on membrane potential of bacterial cells and cytoplasmic membrane vesicles. *Journal of Bacteriology*, **162 (2)**: 833–836.

Sahl and Brandis (1981): Production, purification and chemical properties of an antistaphylococcal agent produced by *Staphylococcus epidermidis. Microbiology*, **127 (2)**: 377–384.

Sakoulas, Eliopoulos, Fowler, Moellering, Novick, Lucindo, Yeaman and Bayer (2005): Reduced susceptibility of *Staphylococcus aureus* to vancomycin and platelet microbicidal protein correlates with defective autolysis and loss of accessory gene regulator (*agr*) function. *Antimicrobial Agents and Chemotherapy*, **49 (7)**: 2687–2692.

Salamaga, Kong, Pasquina-Lemonche, Lafage, Von Und Zur Muhlen, Gibson, Grybchuk, Tooke, Panchal, Culp, Tatham, O'Kane, Catley, Renshaw, Wright, Plevka, Bullough, Han, Hobbs and Foster (2021): Demonstration of the role of cell wall homeostasis in *Staphylococcus aureus* growth and the action of bactericidal antibiotics. *Proceedings of the National Academy of Sciences of the United States of America*, **118 (44)**: e2106022118.

Santiago, Lee, Fayad, Coe, Rajagopal, Do, Hennessen, Srisuknimit, Müller, Meredith and Walker (2018): Genome-wide mutant profiling predicts the mechanism of a Lipid II binding antibiotic. *Nature Chemical Biology*, **14 (6)**: 601.

Saraiva, Sorg, Pereira, Ferreira, Caulat, Reichmann and Pinho (2020): Reassessment of the distinctive geometry of *Staphylococcus aureus* cell division. *Nature Communications*, **11 (1)**: 4097.

Sass, P., Jansen, Szekat, Sass, Sahl and Bierbaum (2008): The lantibiotic mersacidin is a strong inducer of the cell wall stress response of *Staphylococcus aureus*. *BMC Microbiology*, **8 (1)**: 186.

Sass, P., Josten, Famulla, Schiffer, Sahl, Hamoen and Brötz-Oesterhelt (2011): Antibiotic acyldepsipeptides activate ClpP peptidase to degrade the cell division protein FtsZ. *Proceedings of the National Academy of Sciences of the United States of America*, **108 (42)**: 17474–17479.

Sass, V., Schneider, Wilmes, Körner, Tossi, Novikova, Shamova and Sahl (2010): Human-Defensin 3 inhibits cell wall biosynthesis in staphylococci. *Infection and Immunity*, **78 (6)**: 2793–2800.

Sassone-Corsi, Nuccio, Liu, Hernandez, Vu, Takahashi, Edwards and Raffatellu (2016): Microcins mediate competition among Enterobacteriaceae in the inflamed gut. *Nature*, **540 (7632)**: 280–283.

Sauvage, Kerff, Terrak, Ayala and Charlier (2008): The penicillin-binding proteins: structure and role in peptidoglycan biosynthesis. *FEMS Microbiology Reviews*, **32 (2)**: 234–258.

Schaefer, Matano, Qiao, Kahne and Walker (2017): *In vitro* reconstitution demonstrates the cell wall ligase activity of LCP proteins. *Nature Chemical Biology*, **13 (4)**: 396–401.

Schaefer, Owens, Page, Santiago, Kahne and Walker (2020): Structure and reconstitution of a hydrolase complex that may release peptidoglycan from the membrane after polymerization. *Nature Microbiology*, **6 (1)**: 34–43.

Schäper, Brito, Saraiva, Squyres, Holmes, Garner, Hensel, Henriques and Pinho (2023): Processive movement of *Staphylococcus aureus* essential septal peptidoglycan synthases is independent of FtsZ treadmilling and drives cell constriction *BioRxiv*, 2023.06.29.547026.

Scheffers and Pinho (2005): Bacterial cell wall synthesis: new insights from localization studies. *Microbiology and Molecular Biology Reviews*, **69 (4)**: 585–607.

Schelli, Zhong and Zhu (2017): Comparative metabolomics revealing *Staphylococcus aureus* metabolic response to different antibiotics. *Microbial Biotechnology*, **10 (6)**: 1764–1774.

Scherer, K. M., Spille, Sahl, Grein and Kubitscheck (2015): The lantibiotic nisin induces lipid II aggregation, causing membrane instability and vesicle budding. *Biophysical Journal*, **108 (5)**: 1114–1124.

Scherer, K., Wiedemann, Ciobanasu, Sahl and Kubitscheck (2013): Aggregates of nisin with various bactoprenol-containing cell wall precursors differ in size and membrane permeation capacity. *Biochimica et Biophysica Acta (BBA) - Biomembranes*, **1828 (11)**: 2628–2636.

Schlag, Biswas, Krismer, Kohler, Zoll, Yu, Schwarz, Peschel and Götz (2010): Role of staphylococcal wall teichoic acid in targeting the major autolysin Atl. *Molecular Microbiology*, **75 (4)**: 864–873.

Schloissnig, Arumugam, Sunagawa, Mitreva, Tap, Zhu, Waller, Mende, Kultima, Martin, Kota, Sunyaev, Weinstock and Bork (2012): Genomic variation landscape of the human gut microbiome. *Nature*, **493 (7430)**: 45–50.

Schmitt, Wilmes, Pugnière, Aumelas, Bachère, Sahl, Schneider and Destoumieux-Garzón (2010): Insight into invertebrate defensin mechanism of action. *Journal of Biological Chemistry*, **285 (38)**: 29208–29216.

Schneider, C. A., Rasband and Eliceiri (2012): NIH Image to ImageJ: 25 years of image analysis. *Nature Methods*, **9 (7)**: 671–675.

Schneider, J., Klein, Mielich-Süss, Koch, Franke, Kuipers, Kovács, Sauer and Lopez (2015): Spatio-temporal remodeling of functional membrane microdomains organizes the signaling networks of a bacterium. *PLOS Genetics*, **11 (4)**: e1005140.

Schneider, T., Gries, Josten, Wiedemann, Pelzer, Labischinski and Sahl (2009): The lipopeptide antibiotic friulimicin B inhibits cell wall biosynthesis through complex formation with bactoprenol phosphate. *Antimicrobial Agents and Chemotherapy*, **53 (4)**: 1610–1618.

Schneider, T., Kruse, Wimmer, Wiedemann, Sass, Pag, Jansen, Nielsen, Mygind, Raventós, Neve, Ravn, Bonvin, De Maria, Andersen, Gammelgaard, Sahl and Kristensen (2010): Plectasin, a fungal defensin, targets the bacterial cell wall precursor lipid II. *Science*, **328 (5982)**: 1168–1172.

Schneider, T. and Sahl (2010): An oldie but a goodie - cell wall biosynthesis as antibiotic target pathway. *International Journal of Medical Microbiology,* **300 (2-3)**: 161–169.

Schneider, T., Senn, Berger-Bächi, Tossi, Sahl and Wiedemann (2004): In vitro assembly of a complete, pentaglycine interpeptide bridge containing cell wall precursor (lipid II-Gly5) of *Staphylococcus aureus. Molecular Microbiology*, **53 (2)**: 675–685.

Schnell, Entian, Schneider, Götz, Zähner, Kellner and Jung (1988): Prepeptide sequence of epidermin, a ribosomally synthesized antibiotic with four sulphide-rings. *Nature*, **333 (6170)**: 276–278.

Segura Munoz, Mantz, Martínez, Li, Schmaltz, Pudlo, Urs, Martens, Walter and Ramer-Tait (2022): Experimental evaluation of ecological principles to understand and modulate the outcome of bacterial strain competition in gut microbiomes. *The ISME Journal*, **16 (6)**: 1594–1604.

Sekirov and Finlay (2009): The role of the intestinal microbiota in enteric infection. *The Journal of Physiology*, **587 (17)**: 4159–4167.

Severn and Horswill (2022): *Staphylococcus epidermidis* and its dual lifestyle in skin health and infection. *Nature Reviews Microbiology*, **21 (2)**: 97–111.
Shahid, Sobia, Singh, Malik, Khan, Jonas and Hawkey (2009): Beta-lactams and beta-lactamase inhibitors in current- or potential-clinical practice: a comprehensive update. *Critical Reviews in Microbiology,* **35 (2)**: 81–108.
Sham, Butler, Lebar, Kahne, Bernhardt and Ruiz (2014): MurJ is the flippase of lipid-linked precursors for peptidoglycan biogenesis. *Science*, **345 (6193)**: 220–222.
Shan, Brown Gandt, Rowe, Deisinger, Conlon and Lewis (2017): ATP-dependent persister formation in *Escherichia coli mBio*, **8 (1)**: e02267-16.
Sharkey, Guerillot, Walsh, Turner, Lee, Neville, Klatt, Baines, Pidot, Rossello, Seemann, McWilliam, Cho, Carter, Howden, McDevitt, Hachani, Stinear and Monk (2023): The two-component system WalKR provides an essential link between cell wall homeostasis and DNA replication in *Staphylococcus aureus. mBio* **14 (6)**: e02262-23.
Sheldon and Heinrichs (2015): Recent developments in understanding the iron acquisition strategies of gram positive pathogens. *FEMS Microbiology Reviews*, **39 (4)**: 592–630.
Sher, Lim and Bernhardt (2021): Polar growth in *Corynebacterium glutamicum* has a flexible cell wall synthase requirement. *mBio*, **12 (3)**: e00682-21.
Shukla, Lavore, Maity, Derks, Jones, Vermeulen, Melcrová, Morris, Becker, Wang, Kumar, Medeiros-Silva, van Beekveld, Bonvin, Lorent, Lelli, Nowick, MacGillavry, Peoples, … Weingarth: (2022) Teixobactin kills bacteria by a two-pronged attack on the cell envelope. *Nature*, **608 (7922)**: 390–396.
Shukla, Medeiros-Silva, Parmar, Vermeulen, Das, Paioni, Jekhmane, Lorent, Bonvin, Baldus, Lelli, Veldhuizen, Breukink, Singh and Weingarth (2020): Mode of action of teixobactins in cellular membranes. *Nature Communications*, **11 (1)**: 2848.
Shukla, Peoples, Ludwig, Maity, Derks, De Benedetti, Krueger, Vermeulen, Harbig, Lavore, Kumar, Honorato, Grein, Nieselt, Liu, Bonvin, Baldus, Kubitscheck, Breukink, … Weingarth (2023): An antibiotic from an uncultured bacterium binds to an immutable target. *Cell*, **186 (19)**: 4059-4073.e27.
Sidders, Kedziora, Arts, Daniel, de Benedetti, Beam, Bui, Parsons, Schneider, Rowe and Conlon (2023): Antibiotic-induced accumulation of lipid II synergizes with antimicrobial fatty acids to eradicate bacterial populations. *eLife*, **12**: e80246.
Sieradzki, Pinho and Tomasz (1999): Inactivated PBP4 in highly glycopeptide-resistant laboratory mutants of *Staphylococcus aureus*. *Journal of Biological Chemistry*, **274 (27)**: 18942–18946.
Sieradzki and Tomasz (1997): Inhibition of cell wall turnover and autolysis by vancomycin in a highly vancomycin-resistant mutant of *Staphylococcus aureus*. *Journal of Bacteriology*, **179 (8)**: 2557–2566.
Sieradzki and Tomasz (2003): Alterations of cell wall structure and metabolism accompany reduced susceptibility to vancomycin in an isogenic series of clinical isolates of *Staphylococcus aureus. Journal of Bacteriology*, **185 (24)**: 7103–7110.
Silber, Matos de Opitz, Mayer and Sass (2020): Cell division protein FtsZ: from structure and mechanism to antibiotic target. *Future Microbiology*, **15 (9)**: 801–831.
Silhavy, Kahne and Walker (2010): The bacterial cell envelope. *Cold Spring Harbor Perspectives in Biology*, **2 (5)**: a000414.
Singh, D., Bhattacharya, Rai, Dhaked, Awasthi, Ojima and Panda (2014): SB-RA-2001 inhibits bacterial proliferation by targeting FtsZ assembly. *Biochemistry*, **53 (18)**: 2979–2992.
Singh, P., Jindal, Surolia and Panda (2012): A rhodanine derivative CCR-11 inhibits bacterial proliferation by inhibiting the assembly and GTPase activity of FtsZ. *Biochemistry*, **51 (27)**: 5434–5442.
Sitaraman (2018): Prokaryotic horizontal gene transfer within the human holobiont: ecological-evolutionary inferences, implications and possibilities. *Microbiome*, **6 (1)**: 1–14.
Skaar, Gaspar and Schneewind (2004): IsdG and IsdI, heme-degrading enzymes in the cytoplasm of *Staphylococcus aureus. Journal of Biological Chemistry*, **279 (1)**: 436–443.
Skaar and Schneewind (2004): Iron-regulated surface determinants (Isd) of *Staphylococcus aureus*: stealing iron from heme. *Microbes and Infection*, **6 (4)**: 390–397.
Smith, E. J., Visai, Kerrigan, Speziale and Foster (2011): The Sbi protein is a multifunctional immune evasion factor of *Staphylococcus aureus. Infection and Immunity*, **79 (9)**: 3801–3809.
Smith, K., Gemmell and Lang (2013): Telavancin shows superior activity to vancomycin with multidrug-resistant *Staphylococcus aureus* in a range of in vitro biofilm models. *European Journal of Clinical Microbiology & Infectious Diseases*, **32 (10)**: 1327–1332.
Smith, L., Hasper, Breukink, Novak, Čerkasov, Hillman, Wilson-Stanford and Orugunty (2008): Elucidation of the antimicrobial mechanism of mutacin 1140. *Biochemistry*, **47 (10)**: 3308–3314.
Sollid, Furberg, Hanssen and Johannessen (2014): *Staphylococcus aureus*: determinants of human carriage. *Infection, Genetics and Evolution*, **21**: 531–541.
Somner and Reynolds (1990): Inhibition of peptidoglycan biosynthesis by ramoplanin. *Antimicrobial Agents and Chemotherapy*, **34 (3)**: 413–419.
Song, Lunde, Benton and Wilkinson (2012): Further insights into the mode of action of the lipoglycopeptide telavancin through global gene expression studies. *Antimicrobial Agents and Chemotherapy*, **56 (6)**: 3157–3164.
Squyres, Holmes, Barger, Pennycook, Ryan, Yan and Garner (2021): Single-molecule imaging reveals that Z-ring condensation is essential for cell division in *Bacillus subtilis. Nature Microbiology*, **6 (5)**: 553–562.
Srisuknimit, Qiao, Schaefer, Kahne and Walker (2017): Peptidoglycan cross-linking preferences of *Staphylococcus aureus* penicillin-binding proteins have implications for treating MRSA infections. *Journal of the American Chemical Society*, **139 (29)**: 9791–9794.

Steele, Bottomley, Garcia-Lara, Kasturiarachchi and Foster (2011): Multiple essential roles for EzrA in cell division of *Staphylococcus aureus. Molecular Microbiology*, **80 (2)**: 542–555.
Stennett, Back and Race (2022): Derivation of a precise and consistent timeline for antibiotic development. *Antibiotics*, **11 (9)**: 1237.
Stiefel, Schmidt-Emrich, Maniura-Weber and Ren (2015): Critical aspects of using bacterial cell viability assays with the fluorophores SYTO9 and propidium iodide. *BMC Microbiology*, **15 (1)**: 1–9.
Stocks (2004): Mechanism and use of the commercially available viability stain, BacLight. *Cytometry Part A*, **61A (2)**: 189–195.
Stokes, Lopatkin, Lobritz and Collins (2019): Bacterial metabolism and antibiotic efficacy. *Cell Metabolism*, **30 (2)**: 251–259.
Stone and Strominger (1971): Mechanism of action of bacitracin: complexation with metal ion and C55-isoprenyl pyrophosphate. *Proceedings of the National Academy of Sciences of the United States of America*, **68 (12)**: 3223–3227.
Strahl and Hamoen (2010): Membrane potential is important for bacterial cell division. *Proceedings of the National Academy of Sciences of the United States of America*, **107 (27)**: 12281–12286.
Stubbendieck, May, Chevrette, Temkin, Wendt-Pienkowski, Cagnazzo, Carlson, Gern and Currie (2019): Competition among nasal bacteria suggests a role for siderophore-mediated interactions in shaping the human nasal microbiota. *Applied and Environmental Microbiology*, **85 (10)**: e02406-18.
Sun, N., Chan, Lu, Neves, Lui, Wang, Chow, Chan, Yan, Leung, Abagyan, Chan and Wong (2014): rational design of berberine-based FtsZ inhibitors with broad-spectrum antibacterial activity. *PLoS ONE*, **9 (5)**: e97514.
Sun, Y., Hürlimann and Garner (2023): Growth rate is modulated by monitoring cell wall precursors in *Bacillus subtilis*. *Nature Microbiology*, **8 (3)**: 469–480.
Sutton, Carnell, Lafage, Gray, Biboy, Gibson, Pollitt, Tazoll, Turnbull, Hajdamowicz, Salamaga, Pidwill, Condliffe, Renshaw, Vollmer and Foster (2021): *Staphylococcus aureus* cell wall structure and dynamics during host-pathogen interaction. *PLOS Pathogens*, **17 (3)**: e1009468.
Szwedziak, Wang, Bharat, Tsim and Löwe (2014): Architecture of the ring formed by the tubulin homologue FtsZ in bacterial cell division. *eLife*, **3**: e04601.
'T Hart, Oppedijk, Breukink and Martin (2016): New insights into nisin's antibacterial mechanism revealed by binding studies with synthetic lipid II analogues. *Biochemistry*, **55 (1)**: 232–237.
Taber, Mueller, Miller and Arrow (1987): Bacterial uptake of aminoglycoside antibiotics. *Microbiological Reviews*, **51 (4)**: 439–457.
Taguchi, Welsh, Marmont, Lee, Sjodt, Kruse, Kahne, Bernhardt and Walker (2019): FtsW is a peptidoglycan polymerase that is functional only in complex with its cognate penicillin-binding protein. *Nature Microbiology*, **4 (4)**: 587–594.
Tamber, Schwartzman and Cheung (2010): Role of PknB kinase in antibiotic resistance and virulence in community-acquired methicillin-resistant *Staphylococcus aureus* strain USA300. *Infection and Immunity*, **78 (8)**: 3637–3646.
Tan, C. M., Therien, Lu, Lee, Caron, Gill, Lebeau-Jacob, Benton-Perdomo, Monteiro, Pereira, Elsen, Wu, Deschamps, Petcu, Wong, Daigneault, Kramer, Liang, Maxwell, … Roemer (2012): Restoring methicillin-resistant *Staphylococcus aureus* susceptibility to β-lactam antibiotics. *Science Translational Medicine*, **4 (126)**: 126ra35.
Tan, S., Cho and Nodwell (2022): A defect in cell wall recycling confers antibiotic resistance and sensitivity in *Staphylococcus aureus. Journal of Biological Chemistry*, **298 (10)**: 102473.
Tan, S., Ludwig, Müller, Schneider and Nodwell (2019): The lasso peptide siamycin-I targets Lipid II at the gram-positive cell surface. *ACS Chemical Biology*, **14 (5)**: 966–974.
Tap, Lejzerowicz, Cotillard, Pichaud, McDonald, Song, Knight, Veiga and Derrien (2023): Global branches and local states of the human gut microbiome define associations with environmental and intrinsic factors. *Nature Communications*, **14 (1)**: 3310.
te Winkel, Gray, Seistrup, Hamoen and Strahl (2016): Analysis of antimicrobial-triggered membrane depolarization using voltage sensitive dyes. *Frontiers in Cell and Developmental Biology*, **4 (APR)**: 192007.
Thakker, Park, Carey and Lee (1998): *Staphylococcus aureus* serotype 5 capsular polysaccharide is antiphagocytic and enhances bacterial virulence in a murine bacteremia model. *Infection and Immunity*, **66 (11)**: 5183–5189.
Thalsø-Madsen, Torrubia, Xu, Petersen, Jensen and Frees (2019): The Sle1 cell wall amidase is essential for β-lactam resistance in community-acquired methicillin-resistant *Staphylococcus aureus* USA300. *Antimicrobial Agents and Chemotherapy*, **64 (1)**: e01931-19.
Tiedemann, Heinrichs and Stillman (2012): Multiprotein heme shuttle pathway in *Staphylococcus aureus*: Iron-regulated surface determinant cog-wheel kinetics. *Journal of the American Chemical Society*, **134 (40)**: 16578–16585.
Tinajero-Trejo, Carnell, Kabli, Pasquina-Lemonche, Lafage, Han, Hobbs and Foster (2022): *The Staphylococcus aureus* cell division protein, DivIC, interacts with the cell wall and controls its biosynthesis. *Communications Biology*, **5 (1)**: 1–13.
Tiwari, Gatto, Walker and Wilkinson (2018): Exposure of *Staphylococcus aureus* to targocil blocks translocation of the major autolysin Atl across the membrane, resulting in a significant decrease in autolysis. *Antimicrobial Agents and Chemotherapy*, **62 (7)**: e00323-18.
Tol, Angeles and Scheffers (2015): *In vivo* cluster formation of nisin and lipid II is correlated with membrane depolarization. *Antimicrobial Agents and Chemotherapy*, **59 (6)**: 3683–3686.
Tommasi, Brown, Walkup, Manchester and Miller (2015): ESKAPEing the labyrinth of antibacterial discovery. *Nature Reviews Drug Discovery*, **14 (8)**: 529–542.
Torres, Pishchany, Humayun, Schneewind and Skaar (2006): *Staphylococcus aureus* IsdB is a hemoglobin receptor required for heme iron utilization. *Journal of Bacteriology*, **188 (24)**: 8421–8429.

Treviño, Bayõn, Ardá, Marinelli, Gandolfi, Molinari, Jimenez-Barbero and Hernáiz (2014): new insights into glycopeptide antibiotic binding to cell wall precursors using SPR and NMR spectroscopy. *Chemistry – A European Journal*, **20 (24)**: 7363–7372.
Trompette, Gollwitzer, Yadava, Sichelstiel, Sprenger, Ngom-Bru, Blanchard, Junt, Nicod, Harris and Marsland (2014): Gut microbiota metabolism of dietary fiber influences allergic airway disease and hematopoiesis. *Nature Medicine*, **20 (2)**: 159–166.
Turner, Ratcliffe, Wheeler, Golestanian, Hobbs and Foster (2010): Peptidoglycan architecture can specify division planes in *Staphylococcus aureus. Nature Communications*, **1 (1)**: 26.
Ulm and Schneider (2016): Targeting bactoprenol-coupled cell envelope precursors. *Applied Microbiology and Biotechnology*, **100 (18)**: 7815–7825.
Valbuena, Letek, Ordóñez, Ayala, Daniel, Gil and Mateos (2007): Characterization of HMW-PBPs from the rod-shaped actinomycete *Corynebacterium glutamicum*: peptidoglycan synthesis in cells lacking actin-like cytoskeletal structures. *Molecular Microbiology*, **66 (3)**: 643–657.
Van Boeckel, Gandra, Ashok, Caudron, Grenfell, Levin and Laxminarayan (2014): Global antibiotic consumption 2000 to 2010: An analysis of national pharmaceutical sales data. *The Lancet Infectious Diseases*, **14 (8)**: 742–750.
van Dalen, Peschel and van Sorge (2020): Wall teichoic acid in *Staphylococcus aureus* host interaction. *Trends in Microbiology*, **28 (12)**: 985–998.
Van De Kamp, Van Den Hooven, Konings, Bierbaum, Sahl, Kuipers, Siezen, De Vos, Hilbers and Van De Ven (1995): Elucidation of the primary structure of the lantibiotic epilancin K7 from *Staphylococcus epidermidis* K7. *European Journal of Biochemistry*, **230 (2)**: 587–600.
Van Heijenoort and Van Heijenoort (1980): Biosynthesis of the peptidoglycan of *Escherichia coli* K-12. Properties of the in vitro polymerization by Transglycosylation. *FEBS Letters*, **110 (2)**: 241–244.
van Staden, van Zyl, Trindade, Dicks and Smith (2021): Therapeutic application of lantibiotics and other lanthipeptides: old and new findings. *Applied and Environmental Microbiology*, **87 (14)**: e00186-21.
Varghese and Veeraraghavan (2021): Decoding the penicillin resistance of *Streptococcus pneumoniae* for invasive and noninvasive infections. *Microbial Drug Resistance,* **27 (7)**: 942-950.
Veiga, Jousselin, Schäper, Saraiva, Marques, Reed, Wilton, Pereira, Filipe and Pinho (2023): Cell division protein FtsK coordinates bacterial chromosome segregation and daughter cell separation in *Staphylococcus aureus. The EMBO Journal*, **42 (11)**: e112140.
Velásquez, Zhang and van der Donk (2011): Biosynthesis of the antimicrobial peptide epilancin 15X and its N-terminal lactate. *Chemistry and Biology*, **18 (7)**: 857–867.
Visai, Yanagisawa, Josefsson, Tarkowski, Pezzali, Rooijakkers, Foster and Speziale (2009): Immune evasion by *Staphylococcus aureus* conferred by iron-regulated surface determinant protein IsdH. *Microbiology*, **155 (3)**: 667–679.
Vollmer, Blanot and De Pedro (2008): Peptidoglycan structure and architecture. *FEMS Microbiology Reviews*, **32 (2)**: 149–167.
Vollmer and Seligman (2010): Architecture of peptidoglycan: more data and more models. *Trends in Microbiology*, **18 (2)**: 59–66.
Wacnik, Rao, Chen, Lafage, Pazos, Booth, Vollmer, Hobbs, Lewis and Foster (2022): Penicillin-binding protein 1 (PBP1) of *Staphylococcus aureus* has multiple essential functions in cell division. *mBio*, **13 (4)**: e00669-22.
Wade (2013): The oral microbiome in health and disease. *Pharmacological Research*, **69 (1)**: 137–143.
Waksman, Schatz and Reynolds (1946): Production of antibiotic substances by actinomycetes. *Annals of the New York Academy of Sciences*, **48 (2)**: 73–86.
Walesch, Birkelbach, Jézéquel, Haeckl, Hegemann, Hesterkamp, Hirsch, Hammann and Müller (2023): Fighting antibiotic resistance - strategies and (pre)clinical developments to find new antibacterials. *EMBO Reports*, **24 (1)**: e56033.
Walsh (1989): Enzymes in the D-alanine branch of bacterial cell wall peptidoglycan assembly. *Journal of Biological Chemistry*, **264 (5)**: 2393–2396.
Wang, B., Yao, Lv, Ling and Li (2017): The Human Microbiota in Health and Disease. *Engineering*, **3 (1)**: 71–82.
Wang, Q. M., Peery, Johnson, Alborn, Yeh and Skatrud (2001): Identification and characterization of a monofunctional glycosyltransferase from *Staphylococcus aureus*. *Journal of Bacteriology*, **183 (16)**: 4779–4785.
Wang, X., Gu and Breukink (2020): Non-lipid II targeting lantibiotics. *Biochimica et Biophysica Acta (BBA) – Biomembranes.* **1862 (8)**: 183244.
Wang, X., van Beekveld, Xu, Parmar, Das, Singh and Breukink (2023): Analyzing mechanisms of action of antimicrobial peptides on bacterial membranes requires multiple complimentary assays and different bacterial strains. *Biochimica et Biophysica Acta (BBA) - Biomembranes*, **1865 (6)**: 184160.
Wang, Y., Bojer, George, Wang, Jensen, Wolz and Ingmer (2018): Inactivation of TCA cycle enhances *Staphylococcus aureus* persister cell formation in stationary phase. *Scientific Reports*, **8 (1)**: 10849.
Wang, Z., Koirala, Hernandez, Zimmerman and Brady (2022): Bioinformatic prospecting and synthesis of a bifunctional lipopeptide antibiotic that evades resistance. *Science*, **376 (6596)**: 991–996.
Warren, Fukuma, Mikkelsen, Flanagan, Williams, Lisle, Cuív, Morrison and Gidley (2018): Food starch structure impacts gut microbiome composition. *mSphere,* **3 (3)**: e00086-18.
Weidenmaier, Kokai-Kun, Kristian, Chanturiya, Kalbacher, Gross, Nicholson, Neumeister, Mond and Peschel (2004): Role of teichoic acids in *Staphylococcus aureus* nasal colonization, a major risk factor in nosocomial infections. *Nature Medicine*, **10 (3)**: 243–245.
Weidenmaier, Kokai-Kun, Kulauzovic, Kohler, Thumm, Stoll, Götz and Peschel (2008): Differential roles of sortase-anchored surface proteins and wall teichoic acid in *Staphylococcus aureus* nasal colonization. *International Journal of Medical Microbiology*, **298 (5–6)**: 505–513.

Weidenmaier, Peschel, Xiong, Kristian, Dieiz, Yeaman and Bayer (2005): Lack of wall teichoic acids in *Staphylococcus aureus* leads to reduced interactions with endothelial cells and to attenuated virulence in a rabbit model of endocarditis. *The Journal of Infectious Diseases*, **191 (10)**: 1771–1777.
Weil, Beck-Sickinger, Metzger, Stevanovic, Jung, Josten and Sahl (1990): Biosynthesis of the lantibiotic Pep5. *European Journal of Biochemistry*, **194 (1)**: 217–223.
Wenzel, Chiriac, Otto, Zweytick, May, Schumacher, Gust, Albada, Penkova, Krämer, Erdmann, Metzler-Nolte, Straus, Bremer, Becher, Brötz-Oesterhelt, Sahl and Bandow (2014): Small cationic antimicrobial peptides delocalize peripheral membrane proteins. *Proceedings of the National Academy of Sciences of the United States of America*, **111 (14)**: E1409-E1418.
Wenzel, Rautenbach, Vosloo, Siersma, Aisenbrey, Zaitseva, Laubscher, van Rensburg, Behrends, Bechinger and Hamoen (2018): The multifaceted antibacterial mechanisms of the pioneering peptide antibiotics tyrocidine and gramicidin S. *mBio*, **9 (5)**: e00802-18.
Westblade, Errington and Dörr (2020): Antibiotic tolerance. *PLOS Pathogens*, **16 (10)**: e1008892.
Weyrich, Dixit, Farrer, Cooper and Cooper (2015): The skin microbiome: Associations between altered microbial communities and disease. *Australasian Journal of Dermatology*, **56 (4)**: 268–274.
Whitley, Jukes, Tregidgo, Karinou, Almada, Cesbron, Henriques, Dekker and Holden (2021): FtsZ treadmilling is essential for Z-ring condensation and septal constriction initiation in *Bacillus subtilis* cell division. *Nature Communications*, **12 (1)**: 2448.
WHO (2021): WHO Model List of Essential Medicines – 22nd List. *WHO*, **(22)**: WHO/MHP/HPS/EML/2021.02
WHO (2022a): Antibacterial products in clinical development for priority pathogens. *WHO*, https://www.who.int/observatories/global-observatory-on-health-research-and-development/monitoring/antibacterial-products-in-clinical-development-for-priority-pathogens, (accessed 2023-07-21)
WHO (2022b): WHO antibacterial preclinical pipeline review. *WHO*, https://www.who.int/observatories/global-observatory-on-health-research-and-development/monitoring/who-antibacterial-preclinical-pipeline-review (accessed 2023-07-21)
Wiedemann, Böttiger, Bonelli, Schneider, Sahl and Martínez (2006): Lipid II-based antimicrobial activity of the lantibiotic plantaricin C. *Applied and Environmental Microbiology*, **72 (4)**: 2809–2814.
Wiedemann, Böttiger, Bonelli, Wiese, Hagge, Gutsmann, Seydel, Deegan, Hill, Ross and Sahl (2006): The mode of action of the lantibiotic lacticin 3147 – a complex mechanism involving specific interaction of two peptides and the cell wall precursor lipid II. *Molecular Microbiology*, **61 (2)**: 285–296.
Willey and van der Donk (2007): Lantibiotics: peptides of diverse structure and function. *Annual Review of Microbiology*, **61 (1)**: 477–501.
Willing, Schneewind and Missiakas (2021): Regulated cleavage of glycan strands by the murein hydrolase SagB in *Staphylococcus aureus* involves a direct interaction with LyrA (SpdC). *Journal of Bacteriology*, **203 (9)**: :e00014-2.
Wilson (2003): Linezolid resistance in clinical isolates of *Staphylococcus aureus. Journal of Antimicrobial Chemotherapy*, **51 (1)**: 186–188.
Windels, Michiels, Van den Bergh, Fauvart and Michiels (2019): Antibiotics: Combatting Tolerance To Stop Resistance *mBio*, **10 (5)**: e02095-19.
Wirtz, Ludwig, Arts, Marx, Krannich, Barac, Kehraus, Josten, Henrichfreise, Müller, König, Peoples, Nitti, Spoering, Ling, Lewis, Crüsemann and Schneider (2021): Biosynthesis and mechanism of action of the cell wall targeting antibiotic hypeptin. *Angewandte Chemie International Edition*, **60 (24)**: 13579–13586.
Wong, Wilson, Helbig, Hegde, Aftenieva, Zheng, Liu, Pilizota, Garner, Amir and Renner (2021): Understanding Beta-Lactam-Induced Lysis at the Single-Cell Level. *Frontiers in Microbiology*, **12**: 712007.
Wu, C., Lower, Moreira, Dorantes, Le, Giurgiu, Shi and van der Donk (2023): Investigation into the mechanism of action of the antimicrobial peptide epilancin 15X. *Frontiers in Microbiology*, **14**: 1247222.
Wu, R., Skaar, Zhang, Joachimiak, Gornicki, Schneewind and Joachimiak (2005): *Staphylococcus aureus* IsdG and IsdI, Heme-degrading Enzymes with Structural Similarity to Monooxygenases. *Journal of Biological Chemistry*, **280 (4)**: 2840–2846.
Wu, Z., Wright and Walsh (1995): Overexpression, Purification, and Characterization of VanX, a D-, D-Dipeptidase which Is Essential for Vancomycin Resistance in *Enterococcus faecium* BM4147. *Biochemistry*, **34 (8)**: 2455–2463.
Xing, Wang, Dai, Liu, Tan, Qu, Li, Ling, Liu, Fu and Chen (2014): Daptomycin exerts rapid bactericidal activity against *Bacillus anthracis* without disrupting membrane integrity. *Acta Pharmacologica Sinica*, **35 (2)**: 211–218.
Xu, Henriksen, Mebus, Guérillot, Petersen, Jacques, Jiang, Derks, Sánchez-López, Giera, Leeten, Stinear, Oury, Howden, Peleg and Frees (2023): A clinically selected *Staphylococcus aureus clpP* mutant survives daptomycin treatment by reducing binding of the antibiotic and adapting a rod-shaped morphology. *Antimicrobial Agents and Chemotherapy*, **67 (6)**: e00328-23.
Yamada, Sugai, Komatsuzawa, Nakashima, Oshida, Matsumoto and Suginaka (1996): An autolysin ring associated with cell separation of *Staphylococcus aureus. Journal of Bacteriology*, **178 (6)**: 1565–1571.
Yang, Lyu, Miguel, Mcquillen, Huang and Xiao (2017): GTPase activity-coupled treadmilling of the bacterial tubulin FtsZ organizes septal cell wall synthesis. *Science,* **355 (6326)**: 744–747.
Yang, McQuillen, Lyu, Phillips-Mason, De La Cruz, McCausland, Liang, DeMeester, Santiago, Grimes, de Boer and Xiao (2021): A two-track model for the spatiotemporal coordination of bacterial septal cell wall synthesis revealed by single-molecule imaging of FtsW. *Nature Microbiology*, **6 (5)**: 584–593.
Yao, X., Jericho, Pink and Beveridge (1999): Thickness and elasticity of gram-negative murein sacculi measured by atomic force microscopy. *Journal of Bacteriology*, **181 (22)**: 6865–6875.

Yao, Z., Kahne and Kishony (2012): Distinct single-cell morphological dynamics under beta-lactam antibiotics. *Molecular Cell*, **48 (5)**: 705–712.
Yatsunenko, Rey, Manary, Trehan, Dominguez-Bello, Contreras, Magris, Hidalgo, Baldassano, Anokhin, Heath, Warner, Reeder, Kuczynski, Caporaso, Lozupone, Lauber, Clemente, Knights, … Gordon (2012): Human gut microbiome viewed across age and geography. *Nature*, **486 (7402)**: 222–227.
Yeung, Foletti, Deng, Abdiche, Strop, Glanville, Pitts, Lindquist, Sundar, Sirota, Hasa-Moreno, Pham, Melton Witt, Ni, Pons, Shelton, Rajpal and Chaparro-Riggers (2016): Germline-encoded neutralization of a *Staphylococcus aureus* virulence factor by the human antibody repertoire. *Nature Communications*, **7 (1)**: 13376.
Yin, Edwards, Li, Yip and Deber (2012): Roles of hydrophobicity and charge distribution of cationic antimicrobial peptides in peptide-membrane interactions. *Journal of Biological Chemistry*, **287 (10)**: 7738–7745.
Yuan, Barrett, Zhang, Kahne, Sliz and Walker (2007): Crystal structure of a peptidoglycan glycosyltransferase suggests a model for processive glycan chain synthesis. *Proceedings of the National Academy of Sciences of the United States of America*, **104 (13)**: 5348–5353.
Zapun, Contreras-Martel and Vernet (2008): Penicillin-binding proteins and β-lactam resistance. *FEMS Microbiology Reviews*, **32 (2)**: 361–385.
Zhanel, Calic, Schweizer, Zelenitsky, Adam, Lagac-Wiens, Rubinstein, Gin, Hoban and Karlowsky (2010): New lipoglycopeptides: a comparative review of dalbavancin, oritavancin and telavancin. *Drugs*, **70 (7)**: 859–886.
Zhang, H.-M., Li, Tsudome, Ito, Takami and Horikoshi (2005): An alkali-inducible flotillin-like protein from *Bacillus halodurans* C-125. *The Protein Journal*, **24 (2)**: 125–131.
Zhang, L., Rozek and Hancock (2001): Interaction of Cationic Antimicrobial Peptides with Model Membranes. *Journal of Biological Chemistry*, **276 (38)**: 35714–35722.
Zheng, Andrews, Grote, Manson, Alcantar, Earl and Collins (2022): Modulating the evolutionary trajectory of tolerance using antibiotics with different metabolic dependencies. *Nature Communications*, **13 (1)**: 2525.
Zheng, Stokes and Collins (2020): Eradicating bacterial persisters with combinations of strongly and weakly metabolism-dependent antibiotics. *Cell Chemical Biology*, **27 (12)**: 1544-1552.e3.
Zhou, Rodriguez-Rivera, Lim, Bell, Bernhardt, Bertozzi and Theriot (2019): Sequential assembly of the septal cell envelope prior to V snapping in *Corynebacterium glutamicum. Nature Chemical Biology*, **15 (3)**: 221–231.
Zhu, Liu, Singh, Drolia, Bai, Tenguria and Bhunia (2018): Tunicamycin mediated inhibition of wall teichoic acid affects *Staphylococcus aureus* and *Listeria monocytogenes* cell morphology, biofilm formation and virulence. *Frontiers in Microbiology*, **9**: 1352.
Zipperer, Konnerth, Laux, Berscheid, Janek, Weidenmaier, Burian, Schilling, Slavetinsky, Marschal, Willmann, Kalbacher, Schittek, Brötz-Oesterhelt, Grond, Peschel and Krismer (2016): Human commensals producing a novel antibiotic impair pathogen colonization. *Nature*, **535 (7613)**: 511–516.
Zlotnick, Lee, Bourne, Johnson, Domanico and Stray (2007): In vitro screening for molecules that affect virus capsid assembly (and other protein association reactions). *Nature Protocols*, **2 (3)**: 490–498.
Zong, Mazmanian, Schneewind and Narayana (2004): The structure of sortase B, a cysteine transpeptidase that tethers surface protein to the *Staphylococcus aureus* cell wall. *Structure*, **12 (1)**: 105–112.

List of Figures

List of Tables